

Functional analysis of
arbuscular mycorrhiza-related
membrane transporter and defensin genes
of *Medicago truncatula*

Von der Naturwissenschaftlichen Fakultät der
Gottfried Wilhelm Leibniz Universität Hannover

zur Erlangung des Grades
Doktor der Naturwissenschaften (Dr. rer. nat.)

genehmigte Dissertation

von

Marian Uhe, M. Sc.

2018

Referent: Prof. Dr. rer. nat. Helge Küster

Korreferent: Prof. Dr. rer. hort. Manfred K. Schenk

Tag der Promotion: 13.08.2018

ZUSAMMENFASSUNG

Die Arbuskuläre Mykorrhiza (AM) Symbiose, eine Interaktion die ~80% der Landpflanzen mit Pilzen der Ordnung Glomeromycota eingehen, reicht ~450 Millionen Jahre, bis zur Kolonisierung des Landes durch Pflanzen, zurück. Durch die Interaktion beider Organismen wird die Nährstoffversorgung der Wirtspflanze verbessert. Die Nährstoffverfügbarkeit ändert hierbei das *cost-benefit-ratio*. Aus diesem Grund wurde die Expression AM-induzierter Membrantransporter- und Markergene in Wurzeln von *Medicago truncatula* nach der Inokulation mit *Rhizophagus irregularis* in verschiedenen Phosphatregimes (P) und Stickstoff- (N) untersucht. Durch P-Verarmung wurde hierbei die Mykorrhizierungs- und die Arbuskelrate gesteigert, was auf einen größeren Einfluss der Nährstoffversorgung durch die Symbiose hinweist. Mehr als 100 Membrantransportergene wurden bereits in den ersten zwei Wochen der Symbiose induziert und stiegen in der Expression bis sechs Wochen nach der Inokulation der Pflanzen mit dem AM-Pilz weiter an. Fünf Kandidatengene aus stark AM-induzierten Genfamilien, die Kupfer- (*MtCopMd1*), Oligopeptid- (*MtOliMd1*), ABC- (*MtABCG3*) und Stickstoff- (*MtAMT2;4*) Membrantransporter sowie ein AM-induziertes Defensin (*MtDefMd1*) kodieren, wurden funktionell untersucht, um Prozesse am Pflanze-Pilz Interface besser zu verstehen. Räumlich und zeitlich gesehen zeigten Zellen, die Arbuskeln beherbergten, verschiedene Level von *MtCopMd1*-, *MtOliMd1*- und *MtABCG3* Promotoraktivitäten, das auf eine unterschiedliche Regulation von AM-bezogenen Membrantransportergenen hindeutet. In diesem Zusammenhang wurden die Promotoren von *MtCopMd1* und *MtAMT2;4* auch durch Stickstoffmangel aktiviert, wohingegen die *MtOliMd1*- und *MtABCG3*-Promotoren nur bei Phosphatverarmung induziert wurden. Diese Membrantransportergene wurden in Mutanten- oder RNAi-Wurzeln, denen funktionelle Schlüsselregulatoren der Symbiose fehlen, differentiell reprimiert. In *Medicago truncatula* Wurzeln, die RNAi-Konstrukte gegen *MtOliMd1* und *MtABCG3* exprimieren, wurde mit *MtRam1* ein Schlüsseltranskriptionsfaktor-Gen, dessen Aktivität die Verzweigung von Arbuskeln reguliert, weniger transkribiert. Ein starker *Knockdown* der *MtAMT2;4*-Expression durch RNAi, veränderte die Expression von ausgewählten AM-Markergenen hingegen nicht. Die heterologe Expression von *MtAMT2;4* in Froschoozyten deutete darauf hin, dass nicht das geladene Ammonium, sondern eher Ammoniak über die periarbuskuläre Membran transportiert wird. Abschließend wurde die Expression von *MtDefMd*-Genen, die Defensine mit speziellen strukturellen Eigenschaften kodieren, untersucht. Hierbei wurde ein Set von fünf Defensin-Genen, die im Verlauf der Kolonisierung von *M. truncatula* Wurzeln durch den Pilz induziert werden, identifiziert. Diese wurden durch Studien an Mutanten von AM-Schlüsselregulatorgenen zeitlich der Arbuskelbildung oder -degradation zugeordnet. Hierbei wiesen Zellen mit voll entwickelten Arbuskeln verschiedene *MtDefMd1* und *MtDefMd2* Promotoraktivitäten auf, was auf eine Induktion der Gene in späteren Phasen der Arbuskelbildung hindeutet. Die Kolo-kalisation einer *MtDefMd1*-mGFP6 Fusion mit subzellularen Fluoreszenz-Markern zeigte, dass das Defensin mit kollabierenden Arbuskeln assoziiert und final in Vakuolen zu finden ist. Im Weiteren wurden zwei *EXO70*-Gene in Wurzeln, die *MtDefMd1* überexprimieren, weniger stark transkribiert. *EXO70*-Proteine haben eine Funktion für die gerichtete Sekretion von Vesikeln. Zusammenfassend betrachtet, liefert diese Arbeit neue Einsichten in Prozesse, die in aktiven und degradierenden Arbuskeln stattfinden, indem die Expression und Lokalisation von AM-induzierten Membrantransportergenen, beziehungsweise deren Produkten, betrachtet wurden. Diese sind Startpunkte für weitere Studien des zellulären *targeting* während Auf- und insbesondere Abbauprozessen der periarbuskulären Membran.

Schlüsselwörter: Arbuskuläre Mykorrhiza, Symbiose, Zellorganellmarker, zelluläre Restrukturierung, Konfokale Mikroskopie, *EXO70*, Membranlipide, Membrantransportergene, *MtDefMd*

ABSTRACT

The arbuscular mycorrhiza (AM) symbiosis, an interaction of ~80% of terrestrial plants and Glomeromycota fungi, dating back ~450 million years and promoting the colonization of land by plants, improves the nutrient supply of the host. *Vice versa* the mutualistic interaction itself is influenced by nutrient availability, which alters the cost-benefit-ratio. Thus, the expression of AM-related membrane transporter and selected marker genes was studied in *Medicago truncatula* roots, mycorrhized with *Rhizophagus irregularis*, supplied with different phosphate (P) and nitrogen (N) amounts. Here, the root colonization, as well as the rate of arbuscule formation, were enhanced by P depletion, implying a high impact of nutrient allocation on the symbiosis. More than 100 membrane transporter genes were induced in the first two weeks of the AM-interaction and their accumulated induction increased further during the next four weeks. Five representative candidate genes from highly AM-induced gene families, encoding copper (*MtCopMd1*), oligopeptide (*MtOliMd1*), ABC (*MtABCG3*), and nitrogen (*MtAMT2;4*) membrane transporters as well as a defensin (*MtDefMd1*) were investigated to study processes at the plant-fungal interface. Arbuscule-harboring cells displayed different spacio-temporal levels of *MtCopMd1*-, *MtOliMd1*-, and *MtABCG3* promoter activities, indicating a diverging regulation during AM. In this context, *MtCopMd1* and *MtAMT2;4* promoters were also activated by a strong nitrogen depletion, whereas *MtOliMd1* and *MtABCG3* were solely expressed in a P-dependent manner. Furthermore, the selected membrane transporter genes were differentially repressed in mutant or RNAi knockdown roots, lacking key regulators of AM symbioses. In *Medicago truncatula* roots expressing artificial micro-RNAs that target *MtOliMd1* and *MtABCG3*, *MtRam1*, encoding a key transcription factor regulating arbuscular branching was significantly less expressed. Contrasting this, a strong knock-down of *MtAMT2;4* expression by RNA-interference did not change the transcription of selected AM marker genes. Nevertheless, *MtAMT2;4* localization correlated with arbuscule structures. The heterologous expression of *MtAMT2;4* in frog oocytes indicated that ammonia, rather than ammonium, might be the transported substrate. Finally, the expression of *MtDefMd* genes, encoding defensins with specific structural properties, were studied. Here, a core set of five defensin genes was induced over the time of fungal colonization of *Medicago truncatula* roots. *MtDefMd1* and *MtDefMd2* activation was placed relative to arbuscule formation and degradation, using mutants in key AM-activated regulator genes. Since cells with fully developed arbuscules displayed different levels of *MtDefMd1* and *MtDefMd2* promoter activities, they indicated an up-regulation towards later stages of arbuscule formation. Co-localization of an *MtDefMd1*-mGFP6 fusion with subcellular fluorescence markers revealed that this defensin is associated with arbuscules about to collapse, and ultimately is located in vacuolar compartments. Consecutively, two *EXO70* genes, associated with vesicle targeting, were found to be repressed in *MtDefMd1*-overexpressing roots. By monitoring the expression and localization of different AM-related membrane transporter genes and their encoded gene products, this thesis provides novel insights on processes that occur in either active or degrading arbuscules. These are starting points for further studies of the cellular targeting towards symbiotic membranes during the biogenesis and in particular during the degradation of arbuscule structures.

Keywords: arbuscular mycorrhiza, symbiosis, cell organelle markers, cellular restructuring, confocal microscopy, *EXO70*, membrane lipids, membrane transporter genes, *MtDefMd*

GENERAL INTRODUCTION	1
The peak of phosphorus mining.....	1
The arbuscular mycorrhiza symbiosis	1
<i>Medicago truncatula</i> and <i>Rhizophagus irregularis</i> as model organisms to study	
arbuscular mycorrhizal symbiosis	5
Functional analysis of arbuscular mycorrhiza-related membrane transporter genes of	
<i>M. truncatula</i>	6
Aims of the Thesis	8
CHAPTER I	
Determination of optimal nutrient supply for studies on the arbuscular mycorrhiza	
symbiosis and identification of AM-related membrane transporter genes	15
Abstract	17
Introduction	19
Plant cultivars and fungal strains.....	20
Cultivation of <i>M. truncatula</i> plants	20
Inoculation of <i>M. truncatula</i> with AM fungi.....	20
Digestion of plant shoots.....	20
Measurement of pH	21
Measurement of NO ₃ ⁻	21
Measurement of the phosphorus contents of the soil	21
Staining of fungal structures	21
Evaluation of the root colonization	21
Real-time RT-PCR.....	21
Affymetrix GeneChip hybridizations.....	22
Results and Discussion	23
Selection of appropriate phosphate and nitrogen regimes for the cultivation of	
mycorrhized <i>M. truncatula</i> plants	23
Using sterile <i>R. irregularis</i> spores as inoculant for colonization of <i>M. truncatula</i> roots.....	26
Several large gene families encoding membrane transporters are induced by	
AMF colonization of <i>M. truncatula</i> roots	31
Conclusion.....	33
CHAPTER II	
Functional analysis of AM-induced membrane transporter genes	39
Abstract	41
Introduction	42
Materials and Methods	44
Bioinformatic analyses	44

Plant cultivars, fungal and bacterial strains	44
Cultivation of <i>M. truncatula</i> plants	44
Induction of transgenic <i>M. truncatula</i> roots and inoculation of <i>M. truncatula</i> with AM fungi.....	45
Cloning of promoter- <i>gusA</i> int fusions	45
Cloning of knockdown constructs aiming selected AM-related membrane transporter genes of <i>M. truncatula</i>	46
Cloning of MtAMT2;4 mGFP6 fusion constructs for subcellular localizations	48
Isolation of plant RNA from <i>M. truncatula</i> roots	48
Real-time RT-PCR.....	49
Affymetrix GeneChip hybridizations	49
Histological studies.....	49
Detection of reporter proteins via fluorescence microscopy	50
Heterologous translation of <i>M. truncatula</i> membrane-transporter genes in oocytes of <i>X. laevis</i>	50
Results.....	54
The expression of AM-induced membrane transporter genes is dependent on phosphate and nitrogen supply	54
Functional analysis of the copper, oligopeptide and ABC transporter genes <i>MtCopMd1</i> , <i>MtOliMd1</i> , and <i>MtABCG3</i> in arbuscular mycorrhiza	55
Expression and <i>in silico</i> analyses of the <i>MtCopMd1</i> , <i>MtOliMd1</i> , and <i>MtABCG3</i> genes.....	55
The AM-induced copper, oligopeptide, and ABC transporter genes <i>MtCopMd1</i> , <i>MtOliMd1</i> , and <i>MtABCG3</i> display a different spacio-temporal expression	58
Knockdown of the oligopeptide and ABC transporter genes <i>MtOliMd1</i> and <i>MtABCG3</i> affects AM marker gene expression.....	62
Functional analysis of the ammonium transporter gene <i>MtAMT2;4</i> in arbuscular mycorrhiza	65
Knock-down of <i>MtAMT2;4</i> under nitrogen limitation does not affect AM marker gene expression	65
Heterologous translation of <i>MtAMT2;4</i> in oocytes of <i>X. laevis</i> indicates ammonia as potential substrate	68
Localization of <i>MtAMT2;4</i> -GFP and subcellular markers in AM roots	69
The expression of symbiosis-related membrane transporter genes is differentially affected in <i>ram1-1</i> - and <i>pt4-1</i> mutants, known for aberrant arbuscule morphology.....	74
Discussion.....	76
The copper transporter gene <i>MtCopMd1</i> is primarily induced during the active stage of AM symbiosis.....	76
The proton-dependent oligopeptide transporter <i>MtOliMd1</i> probably functions in the PAM.....	77
The ATP-binding cassette (ABC) transporter <i>MtABCG3</i> could function during PAM biogenesis.....	78

The ammonium transporter MtAMT2;4 probably transports a non-electrogenic substrate across the PAM.....	79
--	----

CHAPTER III

The mycorrhiza-dependent defensin MtDefMd1 of *Medicago truncatula* acts during the late restructuring stages of arbuscule-containing cells 89

Abstract	91
-----------------------	-----------

Introduction	92
---------------------------	-----------

Materials and Methods	94
------------------------------------	-----------

Bioinformatic analyses	94
------------------------------	----

Plant cultivars, fungal, and bacterial strains	94
--	----

Cloning of promoter- <i>gusA</i> int fusions	94
--	----

Cloning of knock-down and overexpression constructs.....	95
--	----

Cloning of constructs for subcellular localizations	95
---	----

Cultivation of <i>M. truncatula</i> plants	95
--	----

Induction of transgenic <i>M. truncatula</i> roots and inoculation of <i>M. truncatula</i> with AM fungi or Rhizobia	96
--	----

Isolation of plant RNA from <i>M. truncatula</i> roots	96
--	----

Real-time RT-PCR.....	97
-----------------------	----

Affymetrix GeneChip hybridizations.....	97
---	----

Histological studies.....	98
---------------------------	----

Detection of reporter proteins via fluorescence microscopy	98
--	----

Heterologous expression of <i>MtDefMd1</i> in <i>S. cerevisiae</i>	99
--	----

Results	100
----------------------	------------

Arbuscular mycorrhiza-related defensins differ from defense-related defensins.....	100
--	-----

Heterologous translation in <i>S. cerevisiae</i> underlines the impact of hydrophobic amino acids for the AM-related defensin MtDefMd1	102
--	-----

<i>MtDefMd</i> transcription is upregulated in the course of mycorrhization and depends on phosphate and nitrogen supply.....	103
---	-----

<i>MtDefMd1</i> and <i>MtDefMd2</i> promoters are active in cells with fully developed arbuscules	105
---	-----

<i>MtDefMd1</i> and <i>MtDefMd2</i> expression is impaired in <i>ram1-1</i> mutants forming birdfoot arbuscules	106
---	-----

Five AM-related MtDefMd and three EXOCYST genes change their expression in dependence of the formation of a functional symbiotic interaction	107
--	-----

Knockdown of <i>MtDefMd1</i> and <i>MtDefMd2</i> does not affect expression of AM marker genes	109
--	-----

Overexpression of <i>MtDefMd1</i> activates <i>MtDefMd3</i> and <i>MtRam1</i>	110
---	-----

Overexpression of <i>MtDefMd1</i> in tendency activates <i>MtABCG3</i> and suppresses <i>EXO70k</i> and <i>EXO70j</i> transcription.....	112
--	-----

Overexpression of <i>MtDefMd1</i> did not alter the global lipid content in AM roots	113
Knockdown of <i>MtDefMd1/2</i> transcription and overexpression of <i>MtDefMd1</i> has no significant impact on the arbuscule size distribution	115
Overexpression of <i>MtDefMd1</i> in root nodules did not significantly alter the fine-structures of bacteroid-harboring cells	118
MtDefMd1 acts during late restructuring stages of arbuscule-containing cells.....	121
Discussion.....	125
GENERAL DISCUSSION	141
Arbuscular mycorrhiza-related <i>M. truncatula</i> membrane transporter genes associated with the active stage of the symbiosis	141
Arbuscular mycorrhiza-related <i>M. truncatula</i> defensin genes are associated with the late stage of the symbiosis.....	144
Perspectives	147
GENERAL MATERIALS AND METHODS	150
Standard Protocols	150
Isolation of genomic DNA from <i>M. truncatula</i>	150
Preparation of plasmid DNA.....	150
Quantification of nucleic acids	151
Agarose gel-electrophoresis.....	151
Polymerase Chain Reaction (PCR).....	151
Transformation and cultivation of bacteria	153
Generation of heat-shock competent <i>E. coli</i> -cells	153
Transformation of <i>E. coli</i> via heat-shock.....	153
Transformation of <i>A. rhizogenes</i> via electroporation	154
Oligonucleotides.....	154
Media for the cultivation of microbes, antibiotics and additives	154
Culture media.....	154
Antibiotics and additives.....	155
Buffers and solutions	155
Buffer and solutions for gel-electrophoresis	155
Buffers for the cultivation of competent bacteria	156
Buffer for bacterial suspensions	156
Buffers for HB-Lyses.....	157
Buffers for enzymatic reactions.....	157
Buffer and solutions for histochemical analyses	158
Enzymes and Buffers.....	159
Kits	159

Chemicals	160
Desposables	161
Technical devices.....	162
Software and internet tools.....	163
APPENDIX.....	164
Plasmid maps	164
Supplemental Tables	165
Supporting information on the Data CD.....	175
List of Figures	177
List of Tables	181
Abbreviations.....	183
<i>Curriculum Vitae</i>	187
Acknowledgements.....	192

GENERAL INTRODUCTION

The peak of phosphorus mining

Phosphorus is an element found in minerals of the Earth's crust. Inorganic phosphorus (Pi) in the form of phosphates is an obligatory compound found in all organisms [1]. It is part of biomolecules, such as DNA, RNA, and phospholipids, the latter forming structural components of lipid bilayers in cell membranes. In the form of adenosine triphosphate (ATP), cells use phosphate to transport energy. In addition, ATP is important for the cellular process of phosphorylation, a key event of metabolic regulation. However, concentrations of inorganic phosphate in the soil solution are often low due to the formation of complexes with aluminum, iron and calcium [2, 3], resulting in the need for an active uptake by plants [4].

The global amount of P-containing fertilizers rose from 9 to 40 million tons between the years 1960 and 2000 [3], underlining its importance in modern agriculture. Estimates for future production vary, depending on the expected extent of the resource. It was initially hypothesized that usable P reserves could be depleted in 50–125 years [3, 5, 1]. Contrasting this scenario, it was suggested that supplies could last for several hundred years [6]. Whereas the actual peak of phosphorus mining thus remains unknown, integrative strategies for improved phosphorus use in agriculture must be developed.

To that end, evolutionary old interactions between land plants and a certain clade of fungi could help to counteract phosphate starvation by increasing the explored soil volume.

The arbuscular mycorrhiza symbiosis

Plant-fungal symbioses are subcategorized by the structural association of the fungus within the plant's roots. Whereas Ectomycorrhizae explore the soil and the intercellular apoplastic space of the host root via their hyphae, Endomycorrhizae additionally traverse plant cell walls within the inner root cortex and form structures within the cell lumen [7]. Most of terrestrial plants form arbuscular mycorrhizal (AM) symbioses with a group of obligate biotrophic fungi designated *Glomeromycota* [8, 9, 10]. Janse [11] and Galland [12] were first to describe this widespread association, whereas Sanders *et al.* [13] were pioneers in developing a concept of the AM symbiosis.

In the early stage of the AM interaction, fungal spores germinate and built extraradical hyphae that branch [14, 15] and explore the soil (Fig 1). This process is stimulated by strigolactones (Fig 1), which are secreted by the host plant [17, 18]. In consecutive symbiotic signaling and root colonization, the arbuscular mycorrhiza shares some aspects with the root nodule symbiosis, a beneficial interaction of plants and nitrogen-fixing soil-bacteria.

General Introduction

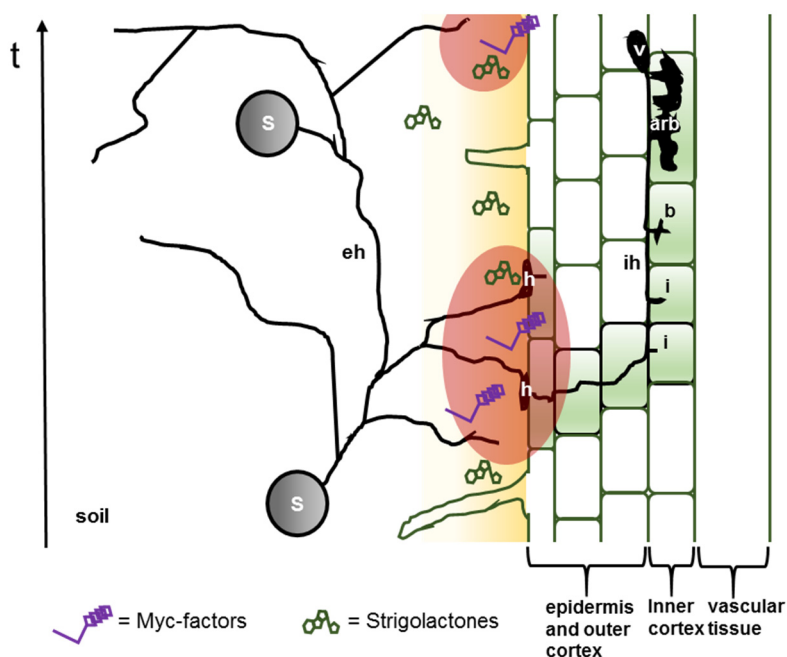


Fig 1: Symbiotic signaling and root colonization in arbuscular mycorrhiza symbioses.

Fungal spores (s) germinate in dependence of phosphates in the soil solution and extraradical hyphae (eh) branch after the perception of strigolactones (yellow gradient), secreted by plant roots. Simultaneously, Myc-factors, composed of COs and LCOs (red area), are released from the fungus and induce calcium-spiking in the nuclei of plant cells. Then, a key signaling cascade is activated. Fungal hyphae form hyphopodia (h), closely connected to the rhizodermal cell layer. Subsequently, a pre-penetration apparatus is formed. From this point, fungal hyphae spread in the outer and inner root cortex. In the inner root cortex, in proximity to the vascular tissue, arbuscules (arb) are established from intraradical spreading hyphae (ih). They develop from invading trunks (i) and birdfoot-like structures (b) to highly branched structures, to facilitate the exchange of molecules between micro- and macrosymbionts. For the storage of lipids, vesicles (v) are built. Abbreviations: t, time; COs, chitooligosaccharides; LCOs, lipo-chitooligosaccharides [16, modified].

Both mycorrhization- and nodulation-related microsymbionts secrete specific signal molecules, Myc- (Fig 1) and Nod-factors, which are either lipo-chitooligosaccharides (LCOs, Nod- and Myc-factors) or chitooligosaccharides (COs, Myc-factors) [19, 20]. In case of LCOs, AM fungi are known to produce sulphated or non-sulphated signaling molecules [20], whereas rhizobial LCO Nod-factors are more diverse [21, 22]. The diffusible molecules are perceived by membrane-bound receptor-kinases of the host plant. Whereas the LysM receptor-kinases MtNFP and MtLYK3 are required for Nod-LCO perception, only MtNFP was shown to be essential for Myc-LCO signaling [23]. Here, additional receptors may exist that also recognize Myc-COs [24, 25]. The leucine-rich repeat (LRR) receptor kinase SMYRK/MtDMI2 is required for the generation of Myc factor-induced calcium-spiking [26] and most likely acts as co-receptor of symbiotic receptors [27].

Ca²⁺-spiking activates the potassium channels MtDMI1/POLLUX and CASTOR [9], as well as a calcium ATPase [28] and cyclic nucleotide gated channels [29], which are located in the nuclear membrane. This results in a flow of potassium into the intermembrane space, which in turn triggers the release of internal calcium stores [30]. The Calmodulin-dependent kinase CCaMK/DMI3 is thought to respond to

the calcium spiking pattern [31, 32]. It interacts with CYCLOPS/IPD3 and phosphorylates this transcription factor [33, 34, 35]. In consequence, signal cascades are activated that modulate gene expression via GRAS transcription factors [36, 20] and finally lead to symbiosis [37]. To support infection and colonization, AM fungi secrete, in dependence of the host plant and fungal structures, a mixture of effectors [38], of which some, like SP7, are known to suppress the plant's immune response [39].

Whereas root nodule bacteria attach to root hairs, which start to swell and curl, thereby enclosing the bacteria [40], fungal hyphae, in contact to the root epidermis, build hyphopodia for infection. As soon as they penetrated epidermal cells, hyphae start to spread from this initial site of infection in the root cortex [41, 42] (Fig 1). Cell entry of both microsymbionts is guided by similar structures, the pre-infection thread (PIT) during root nodule development and the pre-penetration apparatus (PPA) in AM symbiosis [43, 44, 7]. Thus, it was hypothesized that signaling pathways and infection mechanisms from the AM symbiosis, already established 450 million years ago, were recruited for the root nodule symbiosis [7]. Due to these overlaps in signaling, the term common symbiotic signaling (SYM) pathway, was defined [45].

The fungus recruits up to 20 % of the carbon assimilated by the plant, in the form of hexoses and C16 fatty acids [46, 47, 48, 49, 50, 51, 52, 53]. It is thought that plants preserve this energy-consuming interaction, because AM fungal mycelia can recruit different nutrients effectively from soils and transport them to the host plant [54] (Fig 2). The formation of an intraradical mycelium is accompanied by the establishment of arbuscules (Fig 1 and Fig 2). Those highly branched dendritic hyphae, which are invaginated into plant cells of the inner cortex, are characteristic of AM symbioses and are considered to be the major sites of nutrient exchange (Fig 2).

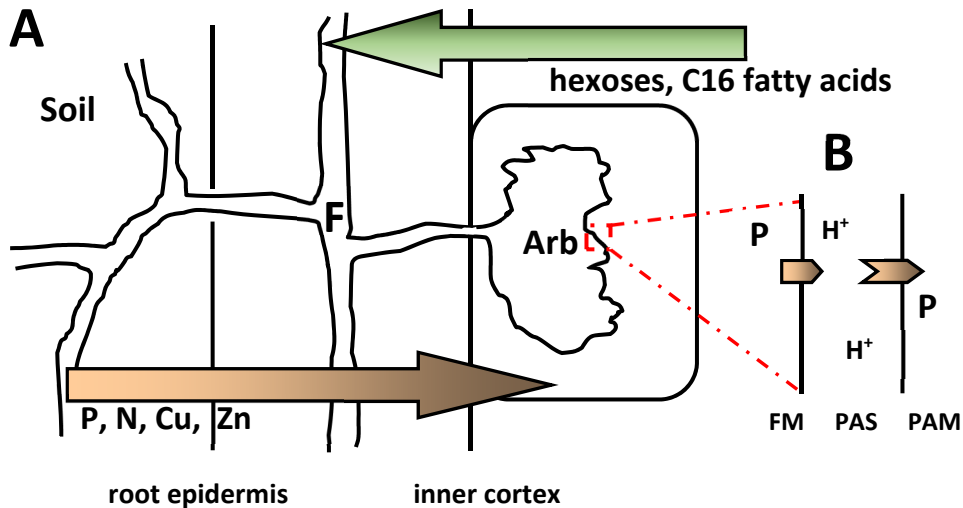


Fig 2: Nutrient exchange during AM symbioses.

The transfer of phosphate (P), nitrogen (N), copper (Cu), zinc (Zn) and other nutrients from the soil to the inner cortex of plant roots via fungal structures (brown arrow) and of plant hexoses and C16 fatty acids to the fungus (green arrow) are shown (A). Specialized transporter proteins of the extraradical mycelium import nutrients that can later be exchanged at the symbiotic interface. During the establishment of the periarbuscular membrane (PAM), the whole secretory apparatus is reoriented towards the arbuscule (Arb). The PAM, being continuously connected to the plasma membrane, is characterized by a unique set of proteins. At the periarbuscular interface, a pH gradient is produced by membrane-bound ATPases from the plant and the fungal side, which support the active exchange of nutrients, such as by a fungal phosphate exporter to the PAS and a plant phosphate importer from the PAS to the cytoplasm (B). Abbreviations: F, fungus; FM, fungal membrane; PAS, periarbuscular space; PAM, periarbuscular membrane; H^+ , proton; P, phosphate

The enhanced supply with nutrients (Fig 2) is probably a selective advantage for AM-forming terrestrial plants [55]. It is thought that 450 million years ago, AM fungi facilitated the colonization of land by early plant species due to the low P availability in terrestrial systems, caused by the low diffusion of phosphate and the formation of a root depletion zone [56, 57].

For this delivery of nutrients towards the host plant, a specific interface is needed (Fig 2, A and B). Cox and Tinker [58] suggested that arbuscules, structures with an extensive surface, are of great importance. Their highly ramified hyphae were hypothesized as main site for nutrient exchange [14, 59]. The transfer of nutrients throughout the AM symbiosis is mediated by the periarbuscular membrane (PAM) (Fig 2, B) which permanently separates micro- and macrosymbionts [60].

Two AM-specific transcription factors are key switches of arbuscule development. With respect to arbuscule build-up, RAM1 (Reduced Arbuscular Mycorrhiza 1), together with other GRAS-transcription factors, controls proper arbuscule branching [61]. During the formation of active arbuscules, a suite of mycorrhiza-specific phosphate transporter and other nutrient transporter genes is activated [62, 63]. The encoded proteins accumulate in the PAM during fine-branching of arbuscules, which is therefore a critical moment in arbuscule development towards effective structures in terms of nutrient uptake [63, 64, 65, 66, 67]. Here, Gutjahr and Parniske [68] deduced stages of the arbuscular life cycle from

mutant phenotypes, such as the formation of the PPA (stage I), arbuscule trunks (stage II), birdfoot arbuscules (stage III), fine-branched mature arbuscules (stage IV), and finally degenerating arbuscules (stage V) (Fig 3).

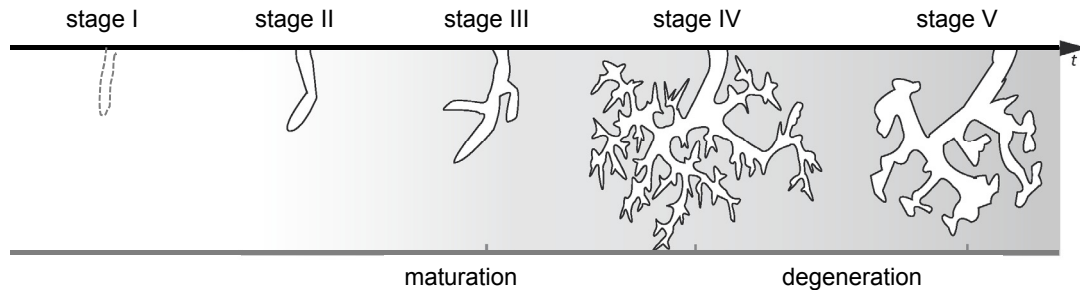


Fig 3: Arbuscule development from trunk to degenerating arbuscules during AM symbioses.

The arbuscule life cycle starts with the formation of a pre-penetration apparatus, which results in the establishment of an arbuscule trunk. During the birdfoot stage a few hyphal branches are established, which then start to branch further at the distal ends during arbuscule maturation. Finally, the arbuscule begins to degenerate, starting by a collapse of distal branches. Abbreviations: stage I, pre-penetration apparatus; stage II, arbuscule trunk; stage III, birdfoot arbuscule; stage IV, mature arbuscule; stage V, degenerating arbuscule; t, time

In addition to benefiting the plant's nutrient status, AM symbioses also result in a higher resistance of host plants towards abiotic stresses, such as drought, salinity and heavy metals, as well as to certain pathogens [69, 70, 71, 72]. Being energy-consuming and depending on a molecular cross-talk as well as structural adaptations of both organisms, root colonization by AM fungi is controlled by the host plant, depending on the physiological and developmental status [73, 74].

During the late stages of arbuscule development, the Myb transcription factor MYB1 activates a transcriptional program associated with arbuscule degeneration, leading to the production of different hydrolases and other arbuscule-degrading enzymes [75]. The life cycle of the AM fungus completes with the biogenesis of intraradical vesicles as lipid storage organs and finally the formation of spores by the extraradical mycelium.

Medicago truncatula and Rhizophagus irregularis as model organisms to study arbuscular mycorrhizal symbiosis

Rhizophagus irregularis, previously named *Glomus intraradices* [76, 77, 78] is a well-known representative of arbuscular mycorrhizal fungi [63]. The AM fungus (AMF) is present in many soils, usually associated with vascular plants [79]. The interaction with crop plants such as tomato [80], onion [81], flax [82] and kidney vetch [83] was investigated. Here, spores of *R. irregularis* were applied to enhance yield. Furthermore, the fungal microsymbiont was characterized via comprehensive transcript and genome sequences [84, 85, 86].

Medicago truncatula, which belongs to the “Galegoid phylum” of the order Fabales (*Fabaceae*), is a model legume for studies of the AM symbiosis [87]. An overview of the key advantages is given in *Brenner’s Genetic Encyclopedia* [88]. Amongst other advantages, a short generation time, self-fertilization and well-established transformation protocols are considerable [89].

The *M. truncatula* genome sequencing project started in 2003, attempting to sequence the euchromatic parts of the genome. The initial approach was based on a bacterial artificial chromosome (BAC)-based assembly, and an in-depth analysis of the genome was published in 2011 [90]. The website (<http://www.medicagogenome.org>) hosts the most recent version of the genome (Mt4.0), which can be explored with many open-source tools [91]. Most of the sequences and genes from previous assemblies have been incorporated into Mt4.0 pseudochromosomes [92]. Recent *M. truncatula* pseudochromosome assemblies thus encompass ~360 Mb of actual sequences, spanning 390 Mb of which ~330 Mb align perfectly with the optical map [92]. In total, more than 50,000 gene models were annotated, covering more than 94% of the gene space [92].

In comparison to other crop plants of the order Fabales, *M. truncatula* has a small genome of ~500 Mb. The genome is organized in a diploid manner ($2n=2x=16$), simplifying genetic analyses. Due to the interaction with N-fixing rhizobia, *M. truncatula* can grow on N-depleted soils. The symbiosis with fungi of the order Glomeromycota, which has an impact on the supply of phosphate and other minerals, extends the range of possible investigations.

Functional analysis of arbuscular mycorrhiza-related membrane transporter genes of *M. truncatula*

In contrast to the quantity of differentially expressed genes in root nodules, the set of genes altered in expression during AM is much smaller [93]. Expression studies, such as from Hohnjec *et al.* [63] and Hogekamp *et al.* [94], indicated the existence of a suite of AM-induced membrane transporter genes, which may have essential functions in the symbiosis. When sorting AM-induced genes from laser microdissection transcriptomics experiments into bins of cellular functions, the category “membrane transporter” was, apart from “signaling” and “transcription factors”, most prominent, and their members were most significantly altered in expression in comparison to others in mycorrhized roots [94]. That way, transcript-profiling techniques, such as *Affymetrix GeneChip* hybridizations or semi-quantitative real time RT-PCRs, could be a starting point to identify candidate genes. Nevertheless, AM studies are complicated by the asynchronous root colonization by AMF, resulting in the presence of younger and older fungal structures at each stage of the symbiosis in parallel. Apart from the arbuscule-specific phosphate transporter gene *MtPt4* [64, 65] and the arbuscule-specific ATPase gene *MtHa1* [95], there is a lack of reliable marker genes to determine the status of plant and fungal interfaces regarding the effectiveness of molecule exchange. Nevertheless, comprehensive gene

expression profiles [94, 96, 97, 63, 64] are available to identify candidate genes for AM-related membrane transporters. Hogekamp *et al.* [94] and Gaude *et al.* [96] showed, using a collection of microdissected cell types, the induction of these transporter genes during growth of intraradical hyphae and especially during arbuscule establishment. However, their impact on the biogenesis and degradation of symbiotic structures is still unknown for many genes.

Based on these studies, a set of membrane transporter genes, which were shown to be upregulated during AM [94, 96], has been chosen and will be the focus of the present work (Table 1), in order to deepen the understanding of bidirectional molecule exchange in the symbiosis.

Table 1: Selected AM-dependent membrane transporter genes.

Gene*	Annotation	GeneChip identifier	Genome ID	Expression**
<i>MtCopMd1</i>	Copper transporter	<i>Mtr.37110.S1_at</i>	<i>Medtr7g066070.1</i>	induced in AM-roots
<i>MtOliMd1</i>	Oligopeptide transporter	<i>Mtr.4863.1.S1_at</i>	<i>Medtr7g098160.1</i>	induced in AM-roots
<i>MtABCG3</i>	ABC transporter	<i>Mtr.52071.1.S1_at</i>	<i>Medtr4g093845.1</i>	induced in AM-roots
<i>MtAMT2;4</i>	Ammonium transporter	<i>Mtr.4243.1.S1_at</i>	<i>Medtr7g115050.1</i>	induced in AM-roots
<i>MtDefMd1</i>	Defensin-like protein	<i>Mtr.35854.1.S1_at</i>	<i>Medtr8g012805.1</i>	induced in AM-roots

*These gene names will be used in the following chapters, the letters “Md” are an abbreviation for “Mycorrhiza-dependent”

**Expression patterns were deduced from transcript studies [94, 95, 96] stored in the *M. truncatula* gene expression atlas [99, 100]

The expression of all five membrane transporter genes rose during root colonization by AMF (Table 1). The ammonium transporter gene *MtAMT2;4* and the defensin gene *MtDefMd1*, which are strongly expressed in arbuscule-containing cells [94], are of special interest as potential regulators of the life cycle of arbuscules. In this context, the copper transporter gene *MtCopMd1*, the oligopeptide transporter gene *MtOliMd1* and the ATP-binding cassette (ABC) transporter gene *MtABCG3*, might encode transporters of either nutrients or for potential effectors.

Establishing a functionally effective protein composition of the PAM interface is critical for the AM symbiosis. Thus, it is the central hypothesis of this thesis that membrane transporter gene expression is connected to a functional morphology and a proper life cycle of the periarbuscular membrane. Gene silencing by RNA interference (RNAi) or artificial miRNAs [98] are well-established techniques to selectively knock down membrane transporter genes. For example, Recorbet *et al.* [101] investigated the function of AM-related membrane transporter genes via gene silencing. Those techniques are based on the function of DCL1 (Dicer Like Protein 1) to cut double stranded RNA in short segments of 21-23 base pairs (bp). Consecutively, one strand of these small RNAs is incorporated into the RNA-

Induced Silencing Complex (RISC) and provides an association with mRNAs of complementary sequence [102, 103]. Subsequently, it cleaves the mRNA or prevents efficient translation, which abolishes the formation of gene products. Since the specific expression of the membrane transporter genes in certain phases of the AM interaction is vital, the promoters used for the post transcriptional gene silencing (PTGS) constructs must reach the correct tissue at a suitable time point. Furthermore, the expression of membrane transporter genes can be analyzed in mutants, which lack certain key regulators of the AM-symbiosis, such as the functional arbuscule-specific phosphate transporter *MtPt4* [65] or the GRAS transcription factor *MtRam1* [61].

Unfortunately, the mode of action of many transporters, including the actual substrate and optimal nutrient status are unknown. To overcome this disadvantage, membrane transporters can be analyzed using oocytes from *Xenopus laevis*. These form a membrane-surrounded space, which is relatively easy accessible for micromanipulators. Feng *et al.* [104] showed that *X. laevis* oocytes can express plant transporter genes at a high level for functional studies. With the two-electrode patch clamp technique, currents between the in- and outside of transfected oocytes can be measured in response to the supply of substrates. Thus, membrane transporters of the plant fungal interface that mediate an electrogenic transport mode can be studied.

There are indications that apart from the encoded n-terminal signal peptide, the time point and tissue of gene expression are of importance for studying protein targeting [105]. Translational fusions with reporter genes, such as the Green Fluorescent Protein (GFP), are a tool to analyze the localization of a transporter in transgenic roots. Using this technique, Hohnjec *et al.* [106] investigated the translocation of *MtNOD25* proteins to the symbiosomes of root nodules via its N terminal signal peptide. Since Pumplin *et al.* [105] proposed related processes of translocation for membrane transporter proteins to the PAM, this technique can be used to monitor the final targeting of AM-related membrane transporters.

Aims of the Thesis

The techniques detailed above shall provide a deeper understanding of the function of the plant-fungal interface during AM symbioses. Central aims of this thesis are the identification of new AM marker genes, which can be related to a certain stage of the AM interaction and the investigation of dynamics of transport-regulating processes at the plant fungal-interface. Five candidate genes that represent major AM-activated families of membrane transporter genes, namely *MtCopMd1*, *MtOliMd1*, *MtABCG3*, *MtAMT2;4* and *MtDefMd1* (Table 1) are investigated. Based on gene annotations, a functional role in the active stage of the symbioses was hypothesized for the first four candidates, whereas *MtDefMd1* might have a function in later stages.

General Introduction

The experimental work of this thesis contains three major steps that are addressed in three Chapters:

- I. In the first Chapter, the experimental set up for studies of AM-related membrane transporter genes of mycorrhized *M. truncatula* plants, especially phosphate and nitrogen supply, is investigated. The presence of structures from the arbuscular mycorrhiza fungus (AMF) and the induction of membrane transporter gene expression during AM are monitored.
- II. In the second Chapter, the activation of the selected membrane transporter genes *MtCopMd1*, *MtOliMd1*, *MtABCG3*, and *MtAMT2; 4* as well as their impact on the plant-fungal-interface in the AM-symbiosis are studied via reporter gene and transcriptional gene silencing constructs.
- III. In the third Chapter, membrane transport-related processes in the late stages of the AM interaction are addressed by studying the function of the mycorrhiza-dependent defensin gene *MtDefMd1*.

References

- [1] Ruttenberg, K.C. Phosphorus Cycle – Terrestrial Phosphorus Cycle, Transport of Phosphorus, from *Continents to the Ocean, The Marine Phosphorus Cycle*. (archived link)
- [2] Bielecki RL. Phosphate Pools, Phosphate Transport, and Phosphate Availability. *Annu. Rev. Plant. Physiol.* 1973; 24(1): 225–52[<https://doi.org/10.1146/annurev.pp.24.060173.001301>]
- [3] Vance CP, Uhde-Stone C, Allan DL. Phosphorus acquisition and use: Critical adaptations by plants for securing a nonrenewable resource. *New Phytol* 2003; 157(3): 423–47 [<https://doi.org/10.1046/j.1469-8137.2003.00695.x>]
- [4] Sakano K, Yazaki Y, Mimura T. Cytoplasmic Acidification Induced by Inorganic Phosphate Uptake in Suspension Cultured *Catharanthus roseus* Cells: Measurement with Fluorescent pH Indicator and ³¹P-Nuclear Magnetic Resonance. *Plant Physiol* 1992; 99(2): 672–80 [<https://doi.org/10.1104/pp.99.2.672>]
- [5] Gilbert J, Gowing D, Wallace H. Available soil phosphorus in semi-natural grasslands: Assessment methods and community tolerances. *Biological Conservation* 2009; 142(5): 1074–83 [<https://doi.org/10.1016/j.biocon.2009.01.018>]
- [6] IFDC.org - IFDC Report Indicates Adequate Phosphorus Resources, Sep-2010
- [7] Parniske M. Arbuscular mycorrhiza: The mother of plant root endosymbioses. *Nat Rev Microbiol* 2008; 6(10): 763–75 [<https://doi.org/10.1038/nrmicro1987>][PMID: 18794914]
- [8] Fitter AH, Moyersoen B. Evolutionary Trends in Root-Microbe Symbioses. *Philosophical Transactions of the Royal Society B: Biological Sciences* 1996; 351(1345): 1367–75 [<https://doi.org/10.1098/rstb.1996.0120>]
- [9] Charpentier M, Bredemeier R, Wanner G, Takeda N, Schleiff E, Parniske M. Lotus japonicus CASTOR and POLLUX are ion channels essential for perinuclear calcium spiking in legume root endosymbiosis. *Plant Cell* 2008; 20(12): 3467–79 [<https://doi.org/10.1105/tpc.108.063255>][PMID: 19106374]
- [10] Schüßler A, Schwarzott D, Walker C (2001). A new fungal phylum, the Glomeromycota: phylogeny and evolution. *Mycol Res* 105: 1413–1421
- [11] Janse JM. 1897. Les endophytes radicaux de quelques plantes Javanaises. *Annales du Jardin Botanique de Buitenzorg* 14:53±201.
- [12] Galland G (1905). fitudes sur les mycorrhizes endotrophes. *Rév. Gén. d. Bot.* 17: 5-48; 66-85; 123-136; 223-239; 313-325; 423-433; 479-490
- [13] Sanders FE, Tinker PB, Black RLB, Palmerley SM. The development of endomycorrhizal root systems: i. Spread of Infection and Growth-Promoting Effects with four species of Vesicular-Arbuscular Endophyte. *New Phytol* 1977; 78(2): 257–68 [<https://doi.org/10.1111/j.1469-8137.1977.tb04829.x>]
- [14] Cox G, Tinker PB. Translocation and transfer of nutrients in Vesicular-Arbuscular Mycorrhizas. I. The arbuscule and phosphorus transfer: A quantitative ultrastructural study. *New Phytol* 1976; 77(2): 371–8 [<https://doi.org/10.1111/j.1469-8137.1976.tb01526.x>]
- [15] Hohnjec N, Czaja-Hasse LF, Hogeckamp C, Küster H. Pre-announcement of symbiotic guests: Transcriptional reprogramming by mycorrhizal lipochitooligosaccharides shows a strict co-dependency on the GRAS transcription factors NSP1 and RAM1. *BMC Genomics* 2015; 16(1): 48 [<https://doi.org/10.1186/s12864-015-2224-7>]
- [16] Bonfante P, Genre A. Mechanisms underlying beneficial plant-fungus interactions in mycorrhizal symbiosis. *Nat Commun* 2010; 1: 48 [<https://doi.org/10.1038/ncomms1046>][PMID: 20975705]
- [17] Akiyama K, Matsuzaki K-i, Hayashi H. Plant sesquiterpenes induce hyphal branching in arbuscular mycorrhizal fungi. *Nature* 2005; 435(7043): 824–7 [<https://doi.org/10.1038/nature03608>][PMID: 15944706]
- [18] Besserer A, Puech-Pagès V, Kiefer P, *et al.* Strigolactones stimulate arbuscular mycorrhizal fungi by activating mitochondria. *PLoS Biol* 2006; 4(7): e226 [<https://doi.org/10.1371/journal.pbio.0040226>][PMID: 16787107]
- [19] Denarie J. Rhizobium Lipo-Chitooligosaccharide Nodulation Factors: Signaling Molecules Mediating Recognition and Morphogenesis. *Annual Review of Biochemistry* 1996; 65(1): 503–35 [<https://doi.org/10.1146/annurev.biochem.65.1.503>]
- [20] Maillet F, Poinot V, André O, *et al.* Fungal lipochitooligosaccharide symbiotic signals in arbuscular mycorrhiza. *Nature* 2011; 469(7328): 58–63 [<https://doi.org/10.1038/nature09622>][PMID: 21209659]
- [21] Lerouge P, Roche P, Faucher C, *et al.* Symbiotic host-specificity of *Rhizobium meliloti* is determined by a sulphated and acylated glucosamine oligosaccharide signal. *Nature* 1990; 344(6268): 781–4 [<https://doi.org/10.1038/344781a0>][PMID: 2330031]
- [22] D'haeze W, Holsters M. Nod factor structures, responses, and perception during initiation of nodule development. *Glycobiology* 2002; 12(6): 79R-105R [PMID: 12107077]

- [23] Czaja, L. F, Hoge Kamp, C, Lamm, P, Maillet, F, et al. Transcriptional responses toward diffusible signals from symbiotic microbes reveal MtNFP-and MtDMI3-dependent reprogramming of host gene expression by arbuscular mycorrhizal fungal lipochitooligosaccharides. *Plant Physiology* 2012, 159(4), 1671-1685.
- [24] Gough C, Cullimore J. Lipo-chitooligosaccharide signaling in endosymbiotic plant-microbe interactions. *Mol Plant Microbe Interact* 2011; 24(8): 867–78 [https://doi.org/10.1094/MPMI-01-11-0019][PMID: 21469937]
- [25] Antolín-Llovera M, Ried MK, Binder A, Parniske M. Receptor kinase signaling pathways in plant-microbe interactions. *Annu Rev Phytopathol* 2012; 50: 451–73 [https://doi.org/10.1146/annurev-phyto-081211-173002][PMID: 22920561]
- [26] Sun J, Miller JB, Granqvist E, et al. Activation of symbiosis signaling by arbuscular mycorrhizal fungi in legumes and rice. *Plant Cell* 2015; 27(3): 823–38 [https://doi.org/10.1105/tpc.114.131326][PMID: 25724637]
- [27] Ried MK, Antolín-Llovera M, Parniske M. Spontaneous symbiotic reprogramming of plant roots triggered by receptor-like kinases. *Elife* 2014; 3 [https://doi.org/10.7554/eLife.03891][PMID: 25422918]
- [28] Capoen W, Sun J, Wysham D, et al. Nuclear membranes control symbiotic calcium signaling of legumes. *Proc Natl Acad Sci U S A* 2011; 108(34): 14348–53 [https://doi.org/10.1073/pnas.1107912108][PMID: 21825141]
- [29] Charpentier, M., Sun, J., Martins, T. V., Radhakrishnan, G. V., Findlay, K., Soumpourou, E., ... & Oldroyd, G. E. (2016). Nuclear-localized cyclic nucleotide-gated channels mediate symbiotic calcium oscillations. *Science*, 352(6289), 1102-1105.
- [30] Venkateshwaran M, Cosme A, Han L, et al. The recent evolution of a symbiotic ion channel in the legume family altered ion conductance and improved functionality in calcium signaling. *Plant Cell* 2012; 24(6): 2528–45 [https://doi.org/10.1105/tpc.112.098475][PMID: 22706284]
- [31] Miller JB, Pratap A, Miyahara A, et al. Calcium/Calmodulin-dependent protein kinase is negatively and positively regulated by calcium, providing a mechanism for decoding calcium responses during symbiosis signaling. *Plant Cell* 2013; 25(12): 5053–66 [https://doi.org/10.1105/tpc.113.116921][PMID: 24368786]
- [32] Lévy J, Bres C, Geurts R, et al. A putative Ca²⁺ and calmodulin-dependent protein kinase required for bacterial and fungal symbioses. *Science* 2004; 303(5662): 1361–4 [https://doi.org/10.1126/science.1093038][PMID: 14963335]
- [33] Messinese E, Mun J-H, Yeun LH, et al. A novel nuclear protein interacts with the symbiotic DMI3 calcium- and calmodulin-dependent protein kinase of *Medicago truncatula*. *Mol Plant Microbe Interact* 2007; 20(8): 912–21 [https://doi.org/10.1094/MPMI-20-8-0912][PMID: 17722695]
- [34] Yano K, Yoshida S, Müller J, et al. CYCLOPS, a mediator of symbiotic intracellular accommodation. *Proc Natl Acad Sci U S A* 2008; 105(51): 20540–5 [https://doi.org/10.1073/pnas.0806858105][PMID: 19074278]
- [35] Singh S, Katzer K, Lambert J, Cerri M, Parniske M. CYCLOPS, a DNA-binding transcriptional activator, orchestrates symbiotic root nodule development. *Cell Host Microbe* 2014; 15(2): 139–52 [https://doi.org/10.1016/j.chom.2014.01.011][PMID: 24528861]
- [36] Hirsch S, Kim J, Muñoz A, Heckmann AB, Downie JA, Oldroyd GED. GRAS proteins form a DNA binding complex to induce gene expression during nodulation signaling in *Medicago truncatula*. *Plant Cell* 2009; 21(2): 545–57 [https://doi.org/10.1105/tpc.108.064501][PMID: 19252081]
- [37] Horváth, B., Yeun, L. H., Domonkos, Á., Halász, G., Gobbato, E., Ayaydin, F., ... & Ratet, P. (2011). *Medicago truncatula* IPD3 is a member of the common symbiotic signaling pathway required for rhizobial and mycorrhizal symbioses. *Molecular plant-microbe interactions*, 24(11), 1345-1358.
- [38] Zeng, T., Holmer, R., Hontelez, J., te Lintel-Hekkert, B., Marufu, L., de Zeeuw, T., ... & Limpens, E. (2018). Host-and stage-dependent secretome of the arbuscular mycorrhizal fungus *Rhizophagus irregularis*. *The Plant Journal*.
- [39] Klopffholz, S., Kuhn, H., & Requena, N. (2011). A secreted fungal effector of *Glomus intraradices* promotes symbiotic biotrophy. *Current Biology*, 21(14), 1204-1209.
- [40] Murray JD. Invasion by invitation: Rhizobial infection in legumes. *Mol Plant Microbe Interact* 2011; 24(6): 631–9 [https://doi.org/10.1094/MPMI-08-10-0181][PMID: 21542766]
- [41] Harrison MJ. The arbuscular mycorrhizal symbiosis: An underground association 1997; 2(2): 54–60 [https://doi.org/10.1016/S1360-1385(97)82563-0]
- [42] Strack D, Fester T, Hause B, Schliemann W, Walter MH. Arbuscular mycorrhiza: Biological, chemical, and molecular aspects. *J Chem Ecol* 2003; 29(9): 1955–79 [PMID: 14584670]

- [43] Timmers AC, Auriac MC, Truchet G. Refined analysis of early symbiotic steps of the Rhizobium-Medicago interaction in relationship with microtubular cytoskeleton rearrangements. *Development* 1999; 126(16): 3617–28 [PMID: 10409507]
- [44] Genre A, Chabaud M, Timmers T, Bonfante P, Barker DG. Arbuscular mycorrhizal fungi elicit a novel intracellular apparatus in *Medicago truncatula* root epidermal cells before infection. *Plant Cell* 2005; 17(12): 3489–99 [https://doi.org/10.1105/tpc.105.035410][PMID: 16284314]
- [45] Oldroyd, G.E. and Downie, J.A. (2006) Nuclear calcium changes at the core of symbiosis signaling. *Curr. Opin. Plant Biol.* 9: 351–357.
- [46] Shachar-Hill Y, Pfeffer PE, Douds D, Osman SF, Doner LW, Ratcliffe RG. Partitioning of Intermediary Carbon Metabolism in Vesicular-Arbuscular Mycorrhizal Leek. *Plant Physiol* 1995; 108(1): 7–15 [PMID: 12228450]
- [47] Pfeffer, Douds DD, JR, Becard, Shachar-Hill. Carbon uptake and the metabolism and transport of lipids in an arbuscular mycorrhiza. *Plant Physiol* 1999; 120(2): 587–98 [PMID: 10364411]
- [48] Bago B, Pfeffer PE, Shachar-Hill Y. Carbon metabolism and transport in arbuscular mycorrhizas. *Plant Physiol* 2000; 124(3): 949–58 [PMID: 11080273]
- [49] Helber N, Wippel K, Sauer N, Schaarschmidt S, Hause B, Requena N. A versatile monosaccharide transporter that operates in the arbuscular mycorrhizal fungus *Glomus* sp is crucial for the symbiotic relationship with plants. *Plant Cell* 2011; 23(10): 3812–23 [https://doi.org/10.1105/tpc.111.089813][PMID: 21972259]
- [50] Bravo A, Brands M, Wewer V, Dörmann P, Harrison MJ. Arbuscular mycorrhiza-specific enzymes FatM and RAM2 fine-tune lipid biosynthesis to promote development of arbuscular mycorrhiza. *New Phytol* 2017; 214(4): 1631–45 [https://doi.org/10.1111/nph.14533][PMID: 28380681]
- [51] Jiang Y, Wang W, Xie Q, *et al.* Plants transfer lipids to sustain colonization by mutualistic mycorrhizal and parasitic fungi. *Science* 2017; 356(6343): 1172–5 [https://doi.org/10.1126/science.aam9970][PMID: 28596307]
- [52] Keymer, A., Pimprakar, P., Wewer, V., Huber, C., Brands, M., Bucerius, S. L., ... & Eisenreich, W. (2017). Lipid transfer from plants to arbuscular mycorrhiza fungi. *Elife*, 6.
- [53] Luginbuehl LH, Menard GN, Kurup S, *et al.* Fatty acids in arbuscular mycorrhizal fungi are synthesized by the host plant. *Science* 2017; 356(6343): 1175–8 [https://doi.org/10.1126/science.aan0081][PMID: 28596311]
- [54] Smith SE, Smith FA. Roles of arbuscular mycorrhizas in plant nutrition and growth: New paradigms from cellular to ecosystem scales. *Annu Rev Plant Biol* 2011; 62: 227–50 [https://doi.org/10.1146/annurev-arplant-042110-103846][PMID: 21391813]
- [55] Fitter AH. What is the link between carbon and phosphorus fluxes in arbuscular mycorrhizas? A null hypothesis for symbiotic function. *New Phytol* 2006; 172(1): 3–6 [https://doi.org/10.1111/j.1469-8137.2006.01861.x][PMID: 16945083]
- [56] Simon L, Bousquet J, Lévesque RC, Lalonde M. Origin and diversification of endomycorrhizal fungi and coincidence with vascular land plants. *Nature* 1993; 363(6424): 67–9 [https://doi.org/10.1038/363067a0]
- [57] Heckman DS, Geiser DM, Eidell BR, Stauffer RL, Kardos NL, Hedges SB. Molecular evidence for the early colonization of land by fungi and plants. *Science* 2001; 293(5532): 1129–33 [https://doi.org/10.1126/science.1061457][PMID: 11498589]
- [58] Bonfante P, Perotto S. Tansley Review No. 82. Strategies of arbuscular mycorrhizal fungi when infecting host plants. *New Phytol* 1995; 130(1): 3–21 [https://doi.org/10.1111/j.1469-8137.1995.tb01810.x]
- [59] Holley JD, Peterson RL. Development of a vesicular-arbuscular mycorrhiza in bean roots. *Can. J. Bot.* 1979; 57(19): 1960–78 [https://doi.org/10.1139/b79-246]
- [60] Provorov NA, Borisov AY, Tikhonovich IA. Developmental Genetics and Evolution of Symbiotic Structures in Nitrogen-fixing Nodules and Arbuscular Mycorrhiza. *Journal of Theoretical Biology* 2002; 214(2): 215–32 [https://doi.org/10.1006/jtbi.2001.2453]
- [61] Park H-J, Floss DS, Levesque-Tremblay V, Bravo A, Harrison MJ. Hyphal branching during arbuscule development requires RAM1. *Plant Physiol.* 2015: pp.01155.2015 [https://doi.org/10.1104/pp.15.01155]
- [62] Hogekamp C, Küster H. A roadmap of cell-type specific gene expression during sequential stages of the arbuscular mycorrhiza symbiosis. *BMC Genomics* 2013; 14: 306 [https://doi.org/10.1186/1471-2164-14-306][PMID: 23647797]
- [63] Hohnjec N, Vieweg MF, Pühler A, Becker A, Küster H. Overlaps in the transcriptional profiles of *Medicago truncatula* roots inoculated with two different *Glomus* fungi provide insights into the

- genetic program activated during arbuscular mycorrhiza. *Plant Physiol* 2005; 137(4): 1283–301 [https://doi.org/10.1104/pp.104.056572][PMID: 15778460]
- [64] Harrison MJ, Dewbre GR, Liu J. A phosphate transporter from *Medicago truncatula* involved in the acquisition of phosphate released by arbuscular mycorrhizal fungi. *Plant Cell* 2002; 14(10): 2413–29 [PMID: 12368495]
- [65] Javot H, Penmetsa RV, Breuillin F, *et al.* *Medicago truncatula* mtpt4 mutants reveal a role for nitrogen in the regulation of arbuscule degeneration in arbuscular mycorrhizal symbiosis. *Plant J* 2011; 68(6): 954–65 [https://doi.org/10.1111/j.1365-313X.2011.04746.x][PMID: 21848683]
- [66] Yang S-Y, Grønlund M, Jakobsen I, *et al.* Nonredundant regulation of rice arbuscular mycorrhizal symbiosis by two members of the phosphate transporter1 gene family. *Plant Cell* 2012; 24(10): 4236–51 [https://doi.org/10.1105/tpc.112.104901][PMID: 23073651]
- [67] Breuillin-Sessoms F, Floss DS, Gomez SK, *et al.* Suppression of Arbuscule Degeneration in *Medicago truncatula* phosphate transporter4 Mutants Is Dependent on the Ammonium Transporter 2 Family Protein AMT2;3. *Plant Cell* 2015; 27(4): 1352–66 [https://doi.org/10.1105/tpc.114.131144]
- [68] Gutjahr, C. and Parniske, M. (2013) Cell and developmental biology of the arbuscular mycorrhiza symbiosis. *Annu. Rev. Cell Dev. Biol.* 29: 593–617
- [69] Augé RM. Water relations, drought and vesicular-arbuscular mycorrhizal symbiosis. *Mycorrhiza* 2001; 11(1): 3–42 [https://doi.org/10.1007/s005720100097]
- [70] Ruiz-Lozano JM. Arbuscular mycorrhizal symbiosis and alleviation of osmotic stress. New perspectives for molecular studies. *Mycorrhiza* 2003; 13(6): 309–17 [https://doi.org/10.1007/s00572-003-0237-6][PMID: 12690537]
- [71] Göhre V, Paszkowski U. Contribution of the arbuscular mycorrhizal symbiosis to heavy metal phytoremediation. *Planta* 2006; 223(6): 1115–22 [https://doi.org/10.1007/s00425-006-0225-0]
- [72] Liu J, Maldonado-Mendoza I, Lopez-Meyer M, Cheung F, Town CD, Harrison MJ. Arbuscular mycorrhizal symbiosis is accompanied by local and systemic alterations in gene expression and an increase in disease resistance in the shoots. *Plant J* 2007; 50(3): 529–44 [https://doi.org/10.1111/j.1365-313X.2007.03069.x][PMID: 17419842]
- [73] Carbonnel S, Gutjahr C. Control of arbuscular mycorrhiza development by nutrient signals. *Front Plant Sci* 2014; 5: 462 [https://doi.org/10.3389/fpls.2014.00462][PMID: 25309561]
- [74] Gutjahr C. Phytohormone signaling in arbuscular mycorrhiza development. *Curr Opin Plant Biol* 2014; 20: 26–34 [https://doi.org/10.1016/j.pbi.2014.04.003][PMID: 24853646]
- [75] Floss DS, Gomez SK, Park H-J, *et al.* A Transcriptional Program for Arbuscule Degeneration during AM Symbiosis Is Regulated by MYB1. *Curr Biol* 2017; 27(8): 1206–12 [https://doi.org/10.1016/j.cub.2017.03.003][PMID: 28392110]
- [76] NC Schenk and G.S.Sm., 1982
- [77] Schüßler, A., & Walker, C. (2010). The Glomeromycota: a species list with new families and new genera. The Royal Botanic Garden Kew, Botanische Staatssammlung Munich, and Oregon State University, 19.
- [78] Krüger M, Krüger C, Walker C, Stockinger H, Schüssler A. Phylogenetic reference data for systematics and phylotaxonomy of arbuscular mycorrhizal fungi from phylum to species level. *New Phytol* 2012; 193(4): 970–84 [https://doi.org/10.1111/j.1469-8137.2011.03962.x][PMID: 22150759]
- [79] Peterson RL, Massicotte HB. Exploring structural definitions of mycorrhizas, with emphasis on nutrient-exchange interfaces. *Can. J. Bot.* 2004; 82(8): 1074–88 [https://doi.org/10.1139/b04-071]
- [80] Cavagnaro T, Jackson L, Six J, Ferris H, Goyal S, Asami D and Scow K (2005a). Arbuscular mycorrhizas, microbial communities, nutrient availability, and soil aggregates in organic tomato production. *Plant and Soil.* 282: 209-225.
- [81] Toro M, Azcon R, Barea J. Improvement of Arbuscular Mycorrhiza Development by Inoculation of Soil with Phosphate-Solubilizing Rhizobacteria To Improve Rock Phosphate Bioavailability ((sup32)P) and Nutrient Cycling. *Appl Environ Microbiol* 1997; 63(11): 4408–12 [PMID: 16535730]
- [82] Cavagnaro TR, Smith FA, Smith SE, Jakobsen I. Functional diversity in arbuscular mycorrhizas: Exploitation of soil patches with different phosphate enrichment differs among fungal species. *Plant Cell Environ* 2005; 28(5): 642–50 [https://doi.org/10.1111/j.1365-3040.2005.01310.x]
- [83] Franken, P., Requena, N., Bütchorn, B., Krajinski, F., Kuhn, G., Lapopin, L., ... & Stommel, M. (2000). Molecular analysis of the arbuscular mycorrhiza symbiosis. *Archives of Agronomy and Soil Science*, 45(4), 271-286.
- [84] Tisserant E, Malbreil M, Kuo A, *et al.* Genome of an arbuscular mycorrhizal fungus provides insight into the oldest plant symbiosis. *Proc Natl Acad Sci U S A* 2013; 110(50): 20117–22 [https://doi.org/10.1073/pnas.1313452110][PMID: 24277808]

- [85] S.E. Smith, D.J. Read. *Mycorrhizal Symbioses*, Academic Press, London, UK (2008)
- [86] Gutjahr, C., & Parniske, M. (2013). Cell and developmental biology of arbuscular mycorrhiza symbiosis. *Annual review of cell and developmental biology*, 29.
- [87] Barker DG, Bianchi S, Blondon F, et al. *Medicago truncatula*, a model plant for studying the molecular genetics of the Rhizobium-legume symbiosis. *Plant Mol Biol Rep* 1990; 8(1): 40–9 [https://doi.org/10.1007/BF02668879]
- [88] Küster, H. (2013). *Medicago truncatula*.
- [89] Trinh TH, Ratet P, Kondorosi E, et al. Rapid and efficient transformation of diploid *Medicago truncatula* and *Medicago sativa* ssp. *falcata* lines improved in somatic embryogenesis. *Plant Cell Reports* 1998; 17(5): 345–55 [https://doi.org/10.1007/s002990050405]
- [90] Young ND, Debellé F, Oldroyd GED, et al. The *Medicago* genome provides insight into the evolution of rhizobial symbioses. *Nature* 2011; 480(7378): 520–4 [https://doi.org/10.1038/nature10625][PMID: 22089132]
- [91] Krishnakumar, V., Kim, M., Rosen, B. D., Karamycheva, S., Bidwell, S. L., Tang, H., & Town, C. D. (2014). MTGD: The *Medicago truncatula* genome database (link is external). *Plant and Cell Physiology*, pcu179.
- [92] Tang H, Krishnakumar V, Bidwell S, et al. An improved genome release (version Mt4.0) for the model legume *Medicago truncatula*. *BMC Genomics* 2014; 15: 312 [https://doi.org/10.1186/1471-2164-15-312][PMID: 24767513]
- [93] Franken P, Requena N. Analysis of gene expression in arbuscular mycorrhizas: New approaches and challenges 2001; 150(3): 517–23 [https://doi.org/10.1046/j.1469-8137.2001.00123.x]
- [94] Hogekamp C, Arndt D, Pereira PA, Becker JD, Hohnjec N, Küster H. Laser microdissection unravels cell-type-specific transcription in arbuscular mycorrhizal roots, including CAAT-box transcription factor gene expression correlating with fungal contact and spread. *Plant Physiol* 2011; 157(4): 2023–43 [https://doi.org/10.1104/pp.111.186635][PMID: 22034628]
- [95] Krajinski F, Courty PE, Sieh D, Franken P, Zhang H, Bucher M, et al. The H⁺-ATPase HA1 of *Medicago truncatula* is essential for phosphate transport and plant growth during arbuscular mycorrhizal symbiosis. *Plant Cell* 2014; 26(4): 1808–1817 [https://doi.org/10.1105/tpc.113.120436]
- [96] Gaude N, Bortfeld S, Duensing N, Lohse M, Krajinski F. Arbuscule-containing and non-colonized cortical cells of mycorrhizal roots undergo extensive and specific reprogramming during arbuscular mycorrhizal development. *Plant J* 2012; 69(3): 510–28 [https://doi.org/10.1111/j.1365-313X.2011.04810.x][PMID: 21978245]
- [97] Uhe, M. Funktionelle Analyse von Membrantransportergenen in der arbuskulären Mykorrhiza von *Medicago truncatula*. MSc-Arbeit (2013), Leibniz Universität Hannover, Hannover
- [98] Devers EA, Teply J, Reinert A, Gaude N, Krajinski F. An endogenous artificial microRNA system for unraveling the function of root endosymbioses related genes in *Medicago truncatula*. *BMC Plant Biol* 2013; 13: 82 [https://doi.org/10.1186/1471-2229-13-82][PMID: 23679580]
- [99] Benedito VA, Torres-Jerez I, Murray JD, et al. A gene expression atlas of the model legume *Medicago truncatula*. *Plant Journal* 2008; 55(3): 504–513 [https://doi.org/10.1111/j.1365-313X.2008.03519.x][PMID: 18410479]
- [100] He J, Benedito VA, Wang M, et al. The *Medicago truncatula* gene expression atlas web server. *BMC bioinformatics* 2009, 10(1), 441.
- [101] Recorbet G, Abdallah C, Renaut J, Wipf D, Dumas-Gaudot E. Protein actors sustaining arbuscular mycorrhizal symbiosis: Underground artists break the silence. *New Phytol* 2013; 199(1): 26–40 [https://doi.org/10.1111/nph.12287][PMID: 23638913]
- [102] Baulcombe D. RNA silencing in plants. *Nature* 2004; 431(7006): 356–63 [https://doi.org/10.1038/nature02874]
- [103] Bartel DP (2004) MicroRNAs: Genomics, biogenesis, mechanism, and function. *Cell* 116: 281–297
- [104] Feng H, Xia X, Fan X, Xu G, Miller AJ. Optimizing plant transporter expression in *Xenopus* oocytes. *Plant Methods* 2013; 9(1): 48 [https://doi.org/10.1186/1746-4811-9-48][PMID: 24359672]
- [105] Pumplin N, Zhang X, Noar RD, Harrison MJ. Polar localization of a symbiosis-specific phosphate transporter is mediated by a transient reorientation of secretion. *Proc Natl Acad Sci U S A* 2012; 109(11): E665–72 [https://doi.org/10.1073/pnas.1110215109][PMID: 22355114]
- [106] Hohnjec N, Lenz F, Fehlberg V, et al. The signal peptide of the *Medicago truncatula* modular nodulin MtNOD25 operates as an address label for the specific targeting of proteins to nitrogen-fixing symbiosomes. *Mol Plant Microbe Interact* 2009; 22(1): 63–72 [https://doi.org/10.1094/MPMI-22-1-0063][PMID: 19061403]

CHAPTER I

Determination of optimal nutrient supply for studies on the arbuscular mycorrhiza symbiosis and identification of AM-related membrane transporter genes

Scope:

The following chapter is a study on mycorrhized plants grown under different phosphate and nitrogen supplies, investigating parameters such as dry mass and soil pH. In parallel, parameters of AM-fungal colonization, such as the arbuscule and vesicle rates were monitored. Based on these, the expression of marker genes for the AM symbiosis and AM-related membrane transporter genes was studied. It was aimed to set up a system for the functional analysis of AM-activated membrane transporter genes that is used in the two later chapters of this thesis.

Experimental contribution:

Marian Uhe: Conceived and designed the experiments, cultivated and mycorrhized plants, analysed shoot and soil nutrient content, monitored fungal structures, interpreted experimental data.

Rico M. Hartmann: Provided unpublished MtGeneChip hybridization data.

Claudia Hogekamp: Provided unpublished MtGeneChip hybridization data.

Anne Herwig: Analysis of shoot and soil nutrient content.

Manfred K. Schenk: Participated in the conception of the PN-vari nutrient solution system

Natalija Hohnjec and Helge Küster: Participated in the interpretation of experimental data.

Abstract

The symbiotic interaction between plants and AM fungi is influenced by a multitude of factors. Here, especially the impact of phosphate (P) and nitrogen (N) delivery are a potential bias for the experimental results. Due to the importance for the cost-benefit-ratio the supply of these nutrients by the fungus could be sufficient to promote and sustain the formation of fungal structures in *Medicago truncatula* roots. Moderate and severe nutrient stress in P and N supply was induced during the cultivation of mycorrhized *Medicago truncatula* plants. A growth retardation due to P or N depletion was evoked and mycorrhization as well as the arbuscule rate were enhanced by P depletion. In this regime of plant cultivation, the impact of the microsymbiont is thus important. A growth response of mycorrhized plants was monitored after 35 dpi and became more substantial until 42 dpi. The expression of marker genes for AM, such as *GiTub α* , *GiPT* and *MtPt4*, was enhanced during the colonization of *Medicago truncatula* roots by *Rhizophagus irregularis*. Here, expression of the latter two genes is an indication for the establishment of functional arbuscules. In early stages of the AM interaction, more than 100 membrane transporter genes, were found induced, and cumulated relative transporter gene expression rose four-fold until 42 dpi. Candidate genes from highly induced gene families, encoding copper- (MtCopMd1), oligopeptide- (MtOliMd1), ABC- (MtABCG3), and ammonium transporters (MtAMT2;4) as well as a defensin (MtDefMd1) were identified as promising candidates to unravel processes of molecule exchange at the plant-fungal interface.

Introduction

The bidirectional transfer of nutrients is the major advantage of AM symbioses. It is realized in a plurality of interaction scenarios, in dependence of the accessibility of nutrients in the soil and the properties of AM fungi [1]. The connection between the presence of mycorrhizal fungi and changes in plant growth had first been described by Asai [2]. In consecutive studies, the enhanced supply of phosphate (P), which in many soils is an element of deficiency, moved in the focus [3, 4]. Since then, several lines of research, e. g. that of Jakobsen [5], Dunne and Fitter [6], and Merryweather and Fitter [7], showed that AM-colonized plant roots are more effectively supplied with nutrients. Especially in situations of biotic or abiotic stress, the supply of the host plant with minerals is enhanced [8]. Under field conditions, it was shown that the yield of soybean and cotton, as well as the effectiveness of fertilizer-usage can be increased by AM-associations [9]. Furthermore, AM fungi improved the zinc uptake in corn [10]. In South Africa, the rhizospheres of cassava were found to be associated with arbuscular mycorrhizal fungi (AMF), displaying higher species diversity at sites with lower soil nitrogen and available phosphate [11]. Concentrations of inorganic phosphate (Pi) in the soil solution are often low due to the formation of complexes with aluminum, iron and calcium [12, 13], resulting in the need of an active uptake by plants [4].

Unlike non-mycorrhizal plants, in addition to the direct uptake of nutrients from soils, AM plants can recruit nutrients via an interface with the microsymbiont. Here, *R. irregularis* is able to adapt the uptake of phosphate in response to its content in the soil [14]. In return, host plants supply the fungus with hexoses [15] and C16 fatty acids [16], resulting from carbon fixation during photosynthesis.

Furthermore, studies with compartmentalized pots highlighted the potential benefits of AM symbioses in the acquisition of N (ammonium and nitrate) [17]. In this context, Tinker and Nye [18] hypothesized that ammonium is a potential factor of deficiency in dry soils. Due to the AM-induction of ammonium transporter genes of *L. japonicus* and *Glycine max* [19, 20], Recorbet *et al.* [21] suggested that ammonium acts as a signal to arbuscules. The exchange of nutrients between fungi and plants throughout the symbiosis is controlled by the perisymbiotic membrane, which separates the micro- and macrosymbiont. Thus, membrane transporters have an essential role in the formation of a functional plant-fungus interface, especially in arbuscule-containing cells. Nevertheless, analyses of those transporters are yet rare. It is necessary to adjust P and N supplies for functional investigations of candidate genes, for example via RNA interference. Comprehensive transcriptomic data sets [22, 23, 24] are available to further investigate AM-related transport processes. To that end, global trends of the transcriptome during root colonization by AMF could provide novel insights.

It is the goal of this chapter to identify suitable conditions for measuring the activation of AM-related membrane transporter genes, and to select candidates for functional studies.

Materials and Methods

Plant cultivars and fungal strains

Medicago truncatula Gaertn. Jemalong A17 (Thierry Huguet, INRA Toulouse, France) was used for all plant experiments. Sterile *Rhizophagus irregularis* DAOM197198 spores (PremierTech, Rivière-du-Loup, Canada) were applied as fungal inoculum.

Cultivation of *M. truncatula* plants

Plants were cultivated in a phytocabinet (Klimaschrank KPS 1700 Weisshaar, Bad Salzflen, Germany) with 16 h/d light (Osram FLUORA L 18WI77 light tubes, 3100-3400 Lux) at 22°C with a relative humidity of 60%. Plants were fertilized with ½ strength Hoagland's solution [25].

For different phosphate (P) and nitrogen (N) supplies, a PN-variation solution was set up as follows: 1 mM KHCO₃, 1.5 mM K₂SO₄, 1 mM MgSO₄, (0.32, 0.16, 0.081, or 0.02) mM NaH₂PO₄, equilibrated by Na₂SO₄, (1.43, 0.71, 0.36, 0.18) mM NH₄NO₃, (5.71, 2.9, 1.43, 0.71) mM Ca(NO₃)₂, equilibrated by CaCl₂, 0.6 mM NaFeEDTA, 0.2 μM Na₂MoO₄ × 2H₂O, 10 μM H₃BO₃, 0.2 μM NiCl₂ × 6 H₂O, 1 μM ZnSO₄ × 7 H₂O, 2 μM MnCl₂ × 2H₂O, 0.5 μM CuSO₄ × 5 H₂O, and 0.2 μM CoCl₂ × 6 H₂O. pH was adjusted to 6.3 with H₂SO₄. The supply of the micronutrients was identical with the amount in the ½ strengths Hoagland's solution [25], to promote a high mycorrhization rate. Plants were watered from the bottom.

Inoculation of *M. truncatula* with AM fungi

In most of the experiments, sterile *R. irregularis* spores were used for the inoculation of *M. truncatula* wild type and transgenic roots. Here, 2000 spores were incubated with the shaded plant root for three hours in liquid. Subsequently, plants were potted in 9×9 cm pots with seramis (Seramis GmbH, Mogendorf, Germany) as substrate. Remaining spores were pipetted on the roots.

For nutrient variation experiments, *R. irregularis* inoculum from a leech preculture was used (Bettina Hause, IPB, Halle, Germany).

Digestion of plant shoots

50 mg dried plant shoots were milled and transferred into glass vessels. The exact weight of the samples was noted. Then, the samples were burned to ashes overnight at 480°C. The ash was colored white to light grey. After cooling down to room temperature, 1 ml 1:3 diluted nitric acid was added to each sample. Samples were incubated for 10 minutes, then 9 ml distilled water were added. The samples were filtrated through Rotilabo(R)-round filters (type 15A). Samples were analyzed with ICP-OES and CNS-analyzer phosphorus-, nitrogen-, carbon-, copper-, and zinc-amounts were measured.

Measurement of pH

50 ml 0.01 M CaCl₂ were added to 20 g air-dried substrate and incubated under rotation for 1.5 h. Consecutively the pH was measured with a pH-electrode, while stirring the filtrated soil extract.

Measurement of NO₃⁻

100 ml 0.1 M KCL-solution was added to 50 g soil and incubated for 60 minutes in a shaker. The samples were then filtered with a folded filter. The first 10 ml filtrate were discarded, then it was filtered through a Rotilabo(R)-round filters (type 15A). The amounts of NO₃⁻ were measured with an Autoanalyzer.

Measurement of the phosphorus contents of the soil

Phosphorus soluble in sodium bicarbonate was measured according to Olsen *et al.* [26]. To that end, 25 g of substrate were analyzed in each measurement.

Staining of fungal structures

To stain fungal structures, 1-2 cm root sections were incubated in 10 % (w/v) KOH at 95 °C for 7 minutes. Consecutively, the roots were washed three times with water and incubated in staining solution with 20 µg/ml WGA-Alexa Fluor 488 in 1x PBS (0.14 M NaCl, 2.7 mM KCl, 1 mM Na₂HPO₄·2H₂O, 1.8 mM KH₂PO₄, pH 7.3) for 12-24 hours. Samples were protected from light. Finally, excessive dye was washed out with water. Alternatively, ink staining was used according to the protocol of Vierheilig *et al.* [27]. Mycorrhized root samples were randomly collected and pooled.

Evaluation of the root colonization

Hyphae, arbuscules and vesicles in root segments were counted using *gridline intersection* [28].

Real-time RT-PCR

Real-time RT-PCR analyses were performed using the SensiFAST™ SYBR® No-ROX One-Step Kit (Qiagen, Hilden, Germany) with primers listed in the S2 Table. Primers were designed to match annealing temperatures of 55 °C and were tested for gene-specific amplifications. 50 ng of total RNA were used as a template in 20 µl. RT-PCR reactions followed a three-step cycling program: reverse transcription at 45 °C for 10 min; polymerase activation at 95 °C for 2 min; PCR amplification with 40 cycles at 95 °C for 5 sec, 55°C for 10 sec, and 72 °C for 8 sec. Biological replicates were measured in three technical replicates. The housekeeping gene *MtTefα* was used for normalization. Average values were used to calculate gene expression levels via the 2^{-ΔCT} method with ΔCT=CT_{Gene}-CT_{MtTefα}. Statistical significances were calculated using a two-tailed Student's t test in *MS Excel 2016* (Microsoft Corp., Redmond,

Washington, USA). The mean and standard error of the mean of all biological replicates was calculated after normalization and was visualized, if not stated differently.

Affymetrix GeneChip hybridizations

Global gene expression data from *Affymetrix GeneChip* hybridizations studying a time course of root colonization by AM fungi from 0 to 42 dpi (Rico M. Hartmann, LUH, Hannover, personal communication), were filtered for ≥ 2 -fold at $p \leq 0.05$ induced gene expression between selected time points. In these experiments, *M. truncatula* plants have been fertilized using $\frac{1}{2}$ strength Hoagland's solution containing 20 μM phosphate.

Results and Discussion

Selection of appropriate phosphate and nitrogen regimes for the cultivation of mycorrhized *M. truncatula* plants

N and P supplies have an influence on the establishment and maintenance of arbuscules [29] and thus must be adjusted in studies of AM symbioses. To determine suitable settings for investigations of AM-related membrane transporter genes, different P and N regimes were tested for the cultivation of AM-inoculated *M. truncatula* plants. The plants were mycorrhized and shoots, roots, and substrate were harvested. The shoots were harvested per pot, dried at 60°C for a week, weighted (Fig 1) and ground for element analysis.

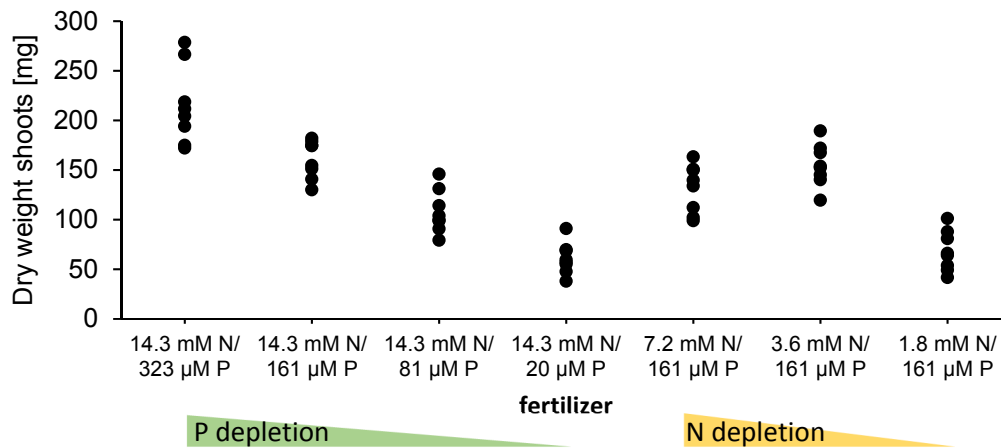


Fig 1: Dry weights of shoots from mycorrhized *M. truncatula* fertilized with different phosphate and nitrogen amounts.

M. truncatula plants were mycorrhized for three weeks and watered eight times with 125 ml nutrient solution per pot. Each black icon represents one plant. n=8 per fertilizer regime, Abbreviations: N, nitrogen; P, phosphate

If the P supply was above 20 μM in the nutrient solution, the plants did respond with a gain of shoot dry mass (Fig 1). Regarding the N-supply, an amount below 3.6 mM in the nutrient solution leads to a decrease in the dry shoot mass (Fig 1). Using Anova- and Tukeys t-Tests, significant differences in dry weight were detected in comparison to the high supply control of both nutrients (S1 Fig, S2-3 Table). Their dry mass reaches a maximum with the highest P-supply. It can be concluded that mild and severe stress in P and N supply can be addressed in the conditions tested (Fig 1, Table S2 and Table S3).

Finally, the pH of the fertilizer solution was adjusted to 6.5 and measured in the substrate after harvesting the plants. The substrate was pooled per batch and air-dried for a week to measure pH (Table 1), nitrate amount, as well as the amount of soluble phosphate (Fig 2). Two separate replicates, containing the substrate of four pooled plants, each, were used. The experimental set up led to an acceptable range of the pH from 6.2 to 7 (Table 1).

Table 1: pH of Seramis® after cultivating *M. truncatula* plants inoculated with *R. irregularis* for three weeks under different phosphate and nitrogen regimes.

PN-vari fertilizer	pH*
14.3 mM N/ 323 µM P	6.5; 6.3
14.3 mM N/ 161 µM P	6.6; 6.3
14.3 mM N/ 81 µM P	6.2; 6.5
14.3 mM N/ 20 µM P	6.5; 6.3
7.2 mM N/ 161 µM P	6.6; 6.8
3.6 mM N/ 161 µM P	6.8; 7.0
1.8 mM N/ 161 µM P	7.0; 6.9

*Two batches, each containing of four pots with two plants, were analyzed. Abbreviations: N, nitrogen; P, phosphate

Subsequently, dry mass, P- and N- content in the substrate were measured (Fig 2, Fig 3). It was aimed to identify suitable nutrient supplies that lead to no, mild, or severe stress (Fig 2).

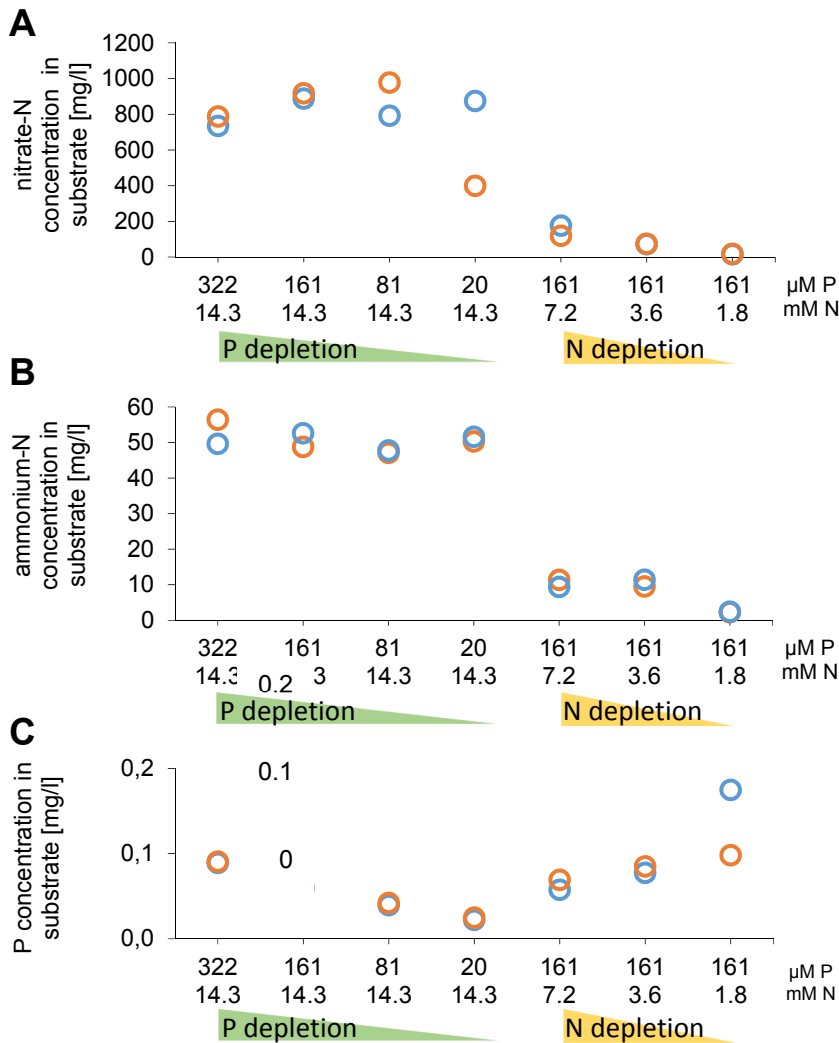


Fig 2: Nitrogen and phosphate concentration in the substrate of mycorrhized *M. truncatula* plants fertilized with different phosphate and nitrogen amounts.

Measurements of nitrogen content in the form of nitrate (A) and ammonium (B) as well as phosphate content (C) are shown. The wild type plants were mycorrhized for three weeks and during that time were watered eight times with 125 ml nutrient solution per pot. n= 2 pools from 4 plants, each, per regime, with circles coloured in orange or blue, respectively, shown. Pi depletion is indicated with a green triangle and N depletion with a yellow triangle. Abbreviations: N, nitrogen; P, phosphate

During P depletion, the residual amounts of N in the substrate were comparable (Fig 2, A and B), indicating that the uptake by the plant was not changed. In N-depleted pots, residual amounts of N in the substrate decreased by a factor of ~10 (Fig 2, A and B). The nitrate-ammonium-ratio was altered

from ~14 to 1 under a regime of higher N supply to ~7 to 1 in the regime of lowest N supply (Fig 2, A and B). *Vice versa*, the leftovers of P also decreased by the factor ~5 in P depleted pots (Fig 2, C). Apparently, the leftovers in nitrogen-depleted pots were again increased (Fig 2, B). This could point towards an N depleted growth depression. Subsequently, the shoots were analyzed via *ICP-OES* and *CNS-analyzer* for their P, Cu, Zn, and N content (Fig 3).

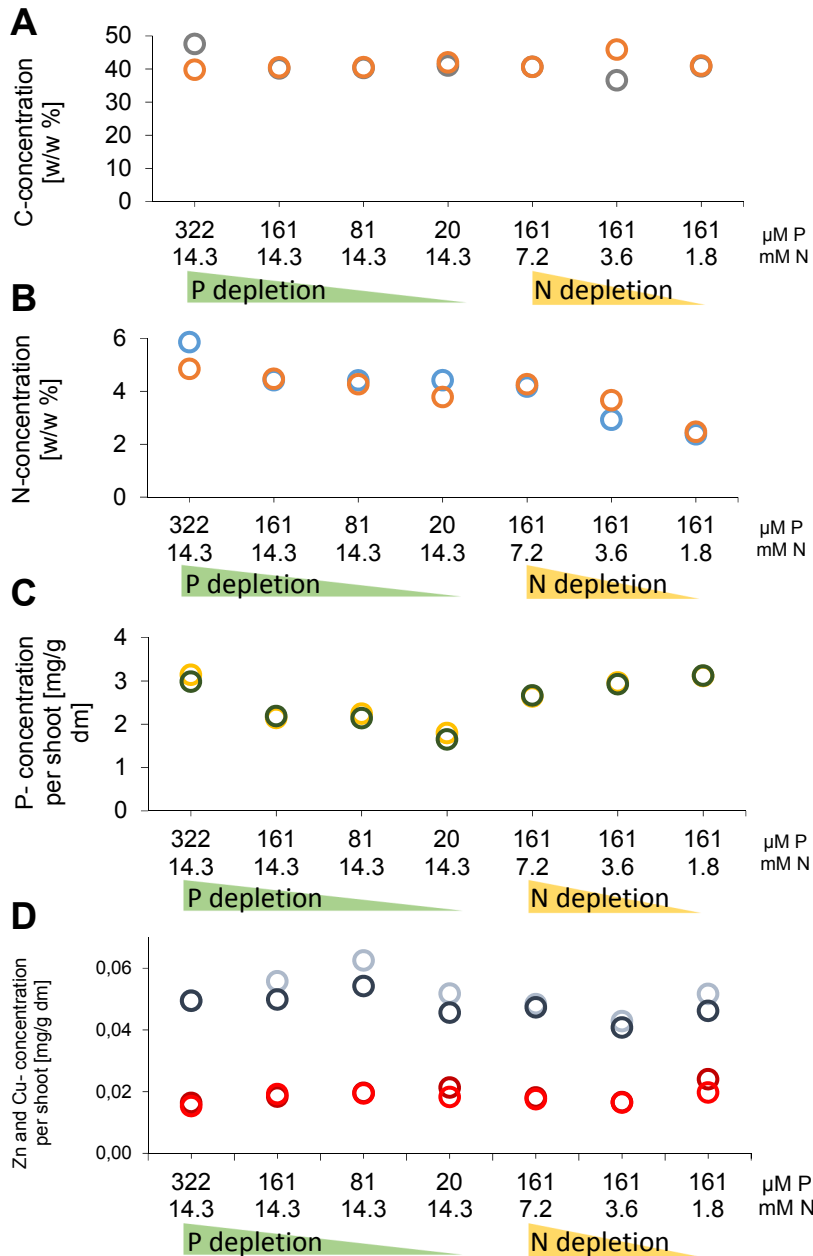


Fig 3: Relative carbon, nitrogen, phosphate, zinc and copper contents in shoot dry matter of mycorrhizal *M. truncatula* plants fertilized with different phosphate or nitrogen amounts.

Measurements of carbon (A), nitrogen (B), phosphate (C), and zinc as well as copper (D) content are shown. The wild type plants were mycorrhizal for three weeks and watered eight times with 125 ml nutrient solution per pot. $n = 2$ pools from 4 plants, each, per regime, indicated by coloured circle. Zn content is depicted in red colours and Cu- content in a grey scale. Pi depletion is indicated with a green triangle and N depletion with a yellow triangle. Abbreviations: dm, dry matter; N, nitrogen; P, phosphate; C, carbon; Zn, zinc; Cu, copper

The concentration of carbon in the shoots was comparable under all conditions for plant cultivation (Fig 2, A). Whereas the N concentration in the shoots was comparable in regimes of P depletion, it apparently decreased in N depletion regimes (Fig 2, B). *Vice versa*, the P-concentration in the shoots decreased in regimes of P depletion but was unaffected in the regime with lowest N-supply and merely

unaffected in the other two regimes of N depletion (Fig 2, C). Finally, the uptake of Cu and Zn was unaffected by the different P and N supplies (Fig 2, D).

In conclusion, both P and N depletion evoked a growth response of *M. truncatula* plants. These regimes can thus be used in investigations of AM-associated transport processes.

Using sterile *R. irregularis* spores as inoculant for colonization of *M. truncatula* roots

To shed light on nutrient transport features at the AM-plant-fungal-interface, it is vital to monitor fungal structures in addition to checking the P and N status in the substrate and the shoots of host plants. To circumvent contaminations and side effects, triggered by other soil-born organisms, it was decided to inoculate the plants with defined fungal material for the analysis of AM-induced membrane transporter genes. Spores in aqueous solution were used. In a first attempt, ~ 20000 spores were diluted in deionized water and filled into a 13x13cm petri dish. The roots of four *M. truncatula* "Jemalong" A17 wild type plants were placed in petri dishes. They were loosely covered with their lid and aluminum foil to protect the root system from light. The plants were then incubated for five days at room temperature. In later experiments, this incubation time was shortened to 3 h. Consecutively, the plants were screened under the binocular (Fig 4) and potted in 200 ml pots filled with seramis®. Roots were then screened at 5, 15 and 21 dpi for AM fungal structures (Fig 4). In total, 60-70% of the spores germinated and the major part of these spores was via hyphae in contact with plant roots (Fig 4; A, a and b). Whether or not infection units have been successfully formed, could not be judged up to this moment. After 15 dpi, one of the four plants was harvested and an ink staining was performed (Fig 4; A, c; B, a and b). The staining confirms the presence of AM fungal spores and highly branched hyphae in many areas all over the root. In conclusion, fungal structures, including arbuscules, structures vital for molecule exchange between micro- and macrosymbiont, were detected.

An additional option for analyses of AM-related membrane transporter genes is the usage of an *M. truncatula* mutant, which lacks the functional arbuscule-specific phosphate transporter MtPt4 [30]. Via immuno staining, this transporter was shown to be specifically present in the periarbuscular membrane and its absence was connected to arbuscule degeneration [30]. Therefore, those plants allow a characterization and validation of AM-related molecule exchange processes independent of the fungal P-support. The screening of mycorrhized MtPt4-mutants for fungal structures documented that under the conditions investigated, there are still areas in AM roots that appear functional (Fig 4, B, a). Those areas did contain intra- and extraradical hyphae as well arbuscules, which appeared to be mature. They were often accompanied by propagation units or early sites of AMF infection (Fig 4, B, b). In other areas, the intensity of root colonization was lower and there were in tendency small arbuscules, which sometimes appeared to be condensed, which could be a hint for premature

arbuscule degradation (PAD) as reported by [29, 30]. MtPt4 mutants could thus be used to study *M. truncatula* gene function in P-transport deficient interactions.

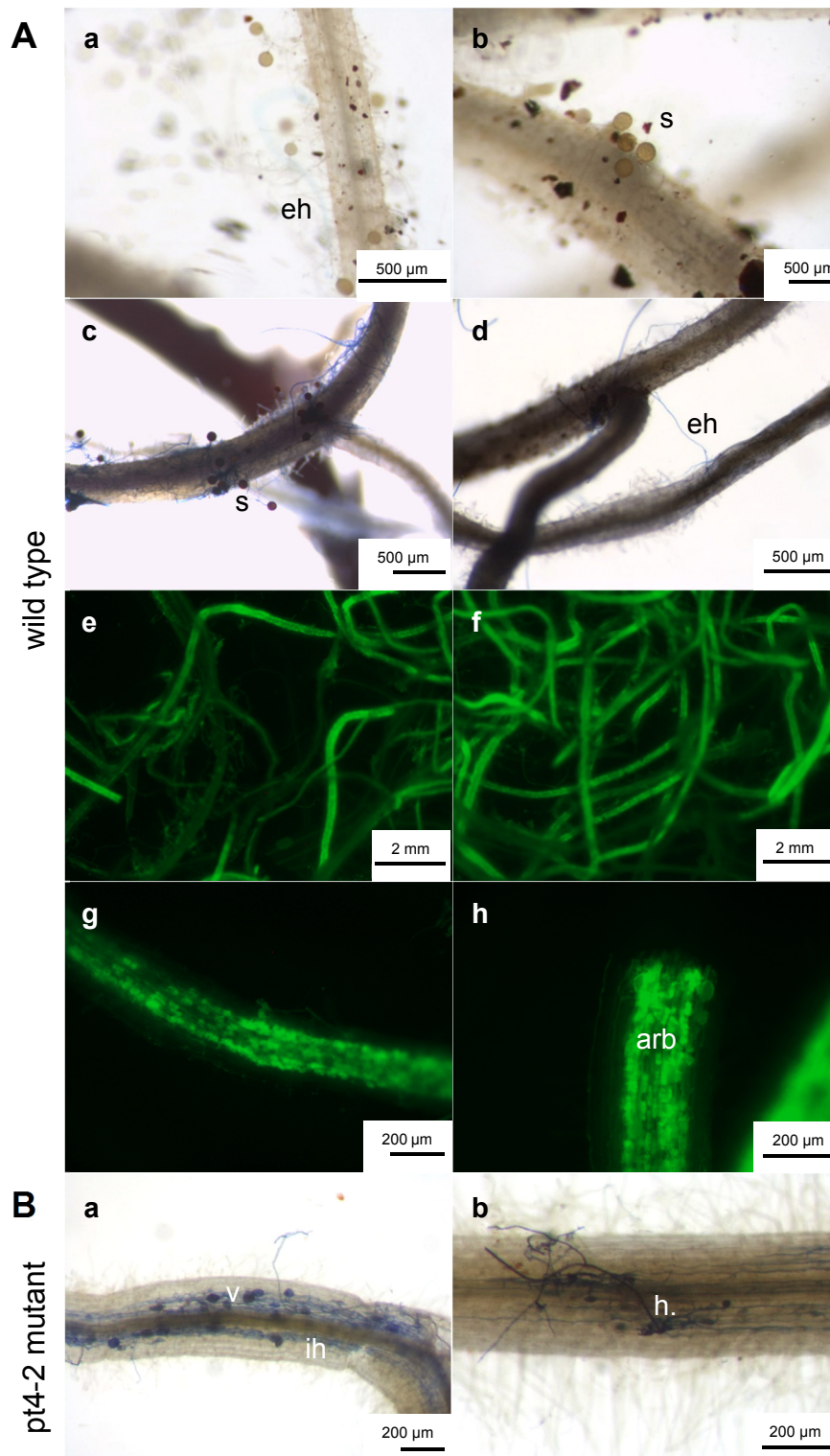


Fig 4: Monitoring of fungal structures in mycorrhizal *M. truncatula* wild type and *pt4-2* mutant roots. Unstained (A, a and b), ink stained (A, c and d; B a and b), and Alexa-WGA Fluor⁴⁸⁸ stained (A, e-h) mycorrhizal *M. truncatula* wild type (A) and *pt4-2* mutant roots (B) are shown. Roots were mycorrhizal for 5 dpi (A, a and b), 15 dpi (A, c-h) and 21 dpi (B, a and b). Abbreviations: s, spore; eh, extraradical hyphae; ih, intraradical hyphae; h., hyphopodium; arb, arbuscule; v, vesicle

After studying fungal structures, the expression of AM-marker genes was measured. In this setup, plants were mycorrhized with only ~1000 *R. irregularis* spores for up to 42 days. The plants were co-incubated with fungal spores for 3 hours, then potted. After cultivation, the expression of selected AM marker genes was measured at 7 dpi and 42 dpi to monitor the process of root colonization by AMF (Fig 5).

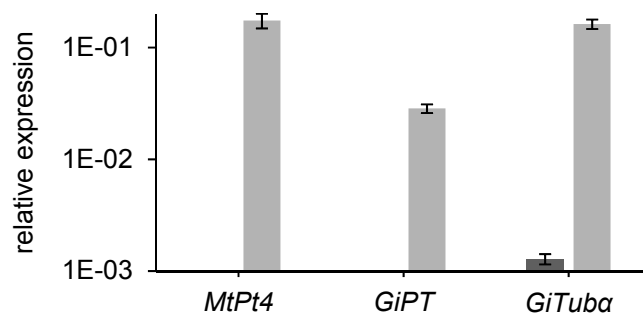


Fig 5: Relative expression of selected AM marker genes in mycorrhized *M. truncatula* roots at 7 and 42 days post inoculation with *R. irregularis*.

Roots harvested at 7 dpi are depicted in dark grey, whereas roots harvested at 42 dpi are colored in light grey. n=14

At 7 dpi, the arbuscule marker genes *MtPt4* [30] and *GiPT* [31], which encode the symbiotic phosphate transporter of plant and fungus, respectively, were not yet expressed. The expression of *GiTuba* α , encoding the fungal α -tubulin gene, which can be used as marker for fungal biomass [32], was substantially reduced. Ink staining and quantifying of fungal structures sheds light on a plausible reason. From 7-21 dpi, solely spores and extraradical hyphae, which were attached to the plant roots were monitored (Fig 4, A, a, b). At 28 dpi, infection units and single infected root areas were present. In the next two weeks, the colonization of the *M. truncatula* roots by *R. irregularis* became more intense (Table 2), so that after 42 dpi most of plant roots were mycorrhized and the relative differences in the rate of mycorrhization became smaller (Table 2). The change in gene expression shown in Fig 5 thus resulted from the ongoing establishment of structures for the exchange of molecules between plant and fungus, the arbuscules. As these symbiotic structures are referred to as the main interface of molecule exchange in AM [33], later stages of root colonization by *R. irregularis* at 35 and 42 dpi were monitored after ink staining of fungal structures via gridline intersection (Table 2). Here, 60-70% of the roots were colonized by fungal structures (Table 2).

Table 2: AMF root colonization of *M. truncatula* inoculated with 1000 *R. irregularis* spores.

dpi	% Fungal Structures	% Arbuscules	% Vesicles
35	42 (20)	33 (16)	32 (16)
42	69 (15)	54 (15)	49 (14)

n=14, standard deviation is shown in brackets

In conclusion, the technique used for mycorrhization led to the formation of typical AMF structures, such as vesicles and arbuscules. Due to the expression of phosphate transport-associated AM marker genes, these structures are presumably active. However, the standard deviation of mycorrhization-, arbuscule- and vesicle rates was high (Table 2). Although not totally unavoidable, a too unsynchronous root colonization would be a major drawback for further experiments. Therefore, a higher spore concentration of 2000 spores per pot was used, which has been applied as a 500 μ l solution directly on the plant root. Additionally, a phosphate boost of 75 μ M in the fertilizer solution was given once, directly after spore application. This should result in more infection events already in the first week after inoculation. A growth response of AM plants became obvious after 35 dpi and more substantial until 42 dpi (Fig 6, A). This fitted well within the range of expected plant growth, first monitored in the experiment studying the impact of a varying P and N concentration (Fig 6, B).

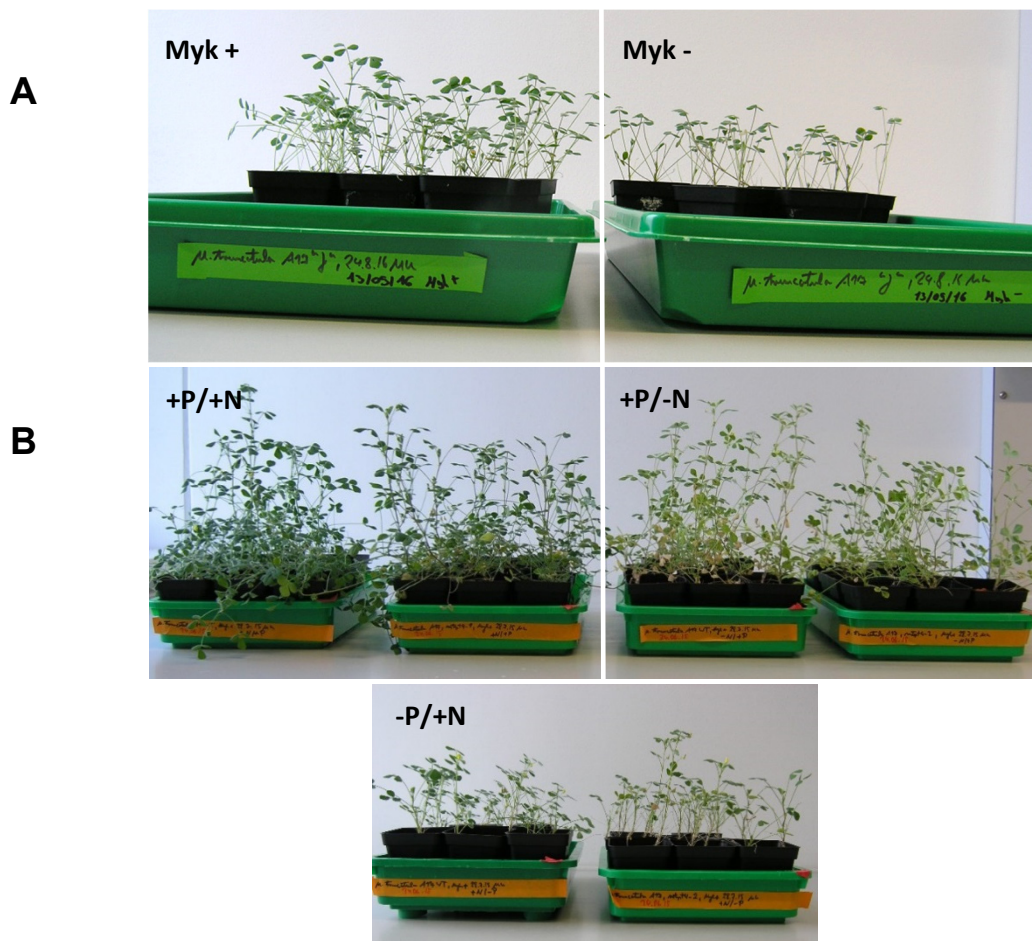


Fig 6: Growth response of mycorrhized *M. truncatula* plants and habitus under different nutrient regimes.

AM plants were compared to non AM plants under a regime of low P supply in A. The habitus of AM plants under different nutrient regimes was monitored in B. Plants were documented 42 days post inoculation with *R. irregularis*. Abbreviations: Myk+, mycorrhized; Myk-, not mycorrhized; P, phosphate; N, nitrogen; +, high supply; -, low supply

As expected, plant biomass strongly increased from low to high nitrogen supply (Fig 6, B). Furthermore, shoots and leaves were of a dark green with high N supply and turned yellowish in case plants were grown in an N-depleted regime (Fig 6, B). The “AM-phenotype” of plants thus differs in dependence on the growth-limiting nutrient and the presence of AMF structures. To assess the microsymbiont, fungal structures were stained and monitored in plants supplied with different amounts of P and N (Fig 7).

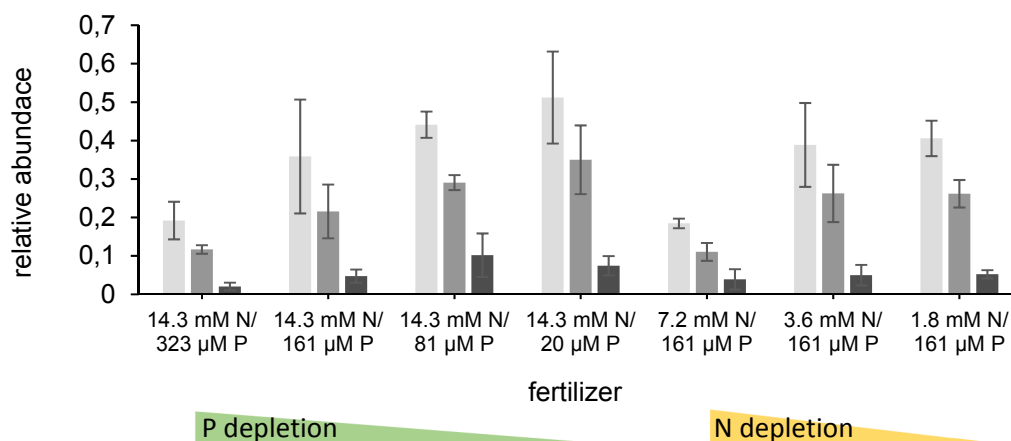


Fig 7: Relative abundance of fungal structures, arbuscules, and vesicles in *M. truncatula* roots supplied with different phosphate and nitrogen amounts.

The quantification of ink stained *M. truncatula* roots sections is shown. Relative amounts of roots with fungal structures are colored in light grey, of segments with arbuscules in medium grey, and vesicle harboring areas in dark grey. P depletion is indicated with a green triangle and N depletion with a yellow triangle. Roots were harvested at 28 days post inoculation with *R. irregularis*. $n=3$ pools of four biological replicates, each, depicted is the standard error of the mean. Abbreviations: N, nitrogen; P, phosphate

Apparently, the mycorrhization-, as well as the arbuscule rate rose with phosphate or nitrogen depletion, whereas high or medium amounts of both nutrients decreased the colonization rate of the plant roots (Fig 7). In the regime with lowest P-supply, the mycorrhization- as well as the arbuscule rate reached their maximum. This is in line with results presented in literature, such as an enhancing mycorrhization of hyacinthoides occurring with an increasing phosphate depletion zone [7]. Under these conditions, the impact of the microsymbiont could thus be most important. Nevertheless, regimes of nitrogen depletion were shown to be suitable for the investigation of nitrogen-transport related processes [29]. In numbers, the amount of phosphate supplied via the nutrient solution could be increased by a factor of ~15 until the number of fungal hyphae, arbuscules and vesicles decreased (Fig 7). Due to the highest rate of arbuscules, the P-depleted regime in combination with a sufficient amount of nitrogen is most suitable for studies on AM-dependent membrane transporter genes, as such a regime is known to correspond with downregulation of AM-unrelated phosphate transporters of *M. truncatula* [34].

In conclusion, phosphate and nitrogen regimes that lead to a positive growth response and maximal amount of AMF structures in *M. truncatula* host plants were identified.

Several large gene families encoding membrane transporters are induced by AMF colonization of *M. truncatula* roots

A mycorrhization time course from 0 to 42 dpi was monitored to define the temporal regulation of membrane transporter gene expression, using *Affymetrix GeneChip* hybridizations (Rico M. Hartmann, LUH, unpublished). To obtain a general overview, genes that were ≥ 2 -fold induced at $p \leq 0.05$ in wild type roots colonized with AM fungi from 7 dpi up to 42 dpi, in comparison to roots at 0 dpi, were identified and sorted in different subgroups (Fig 8).

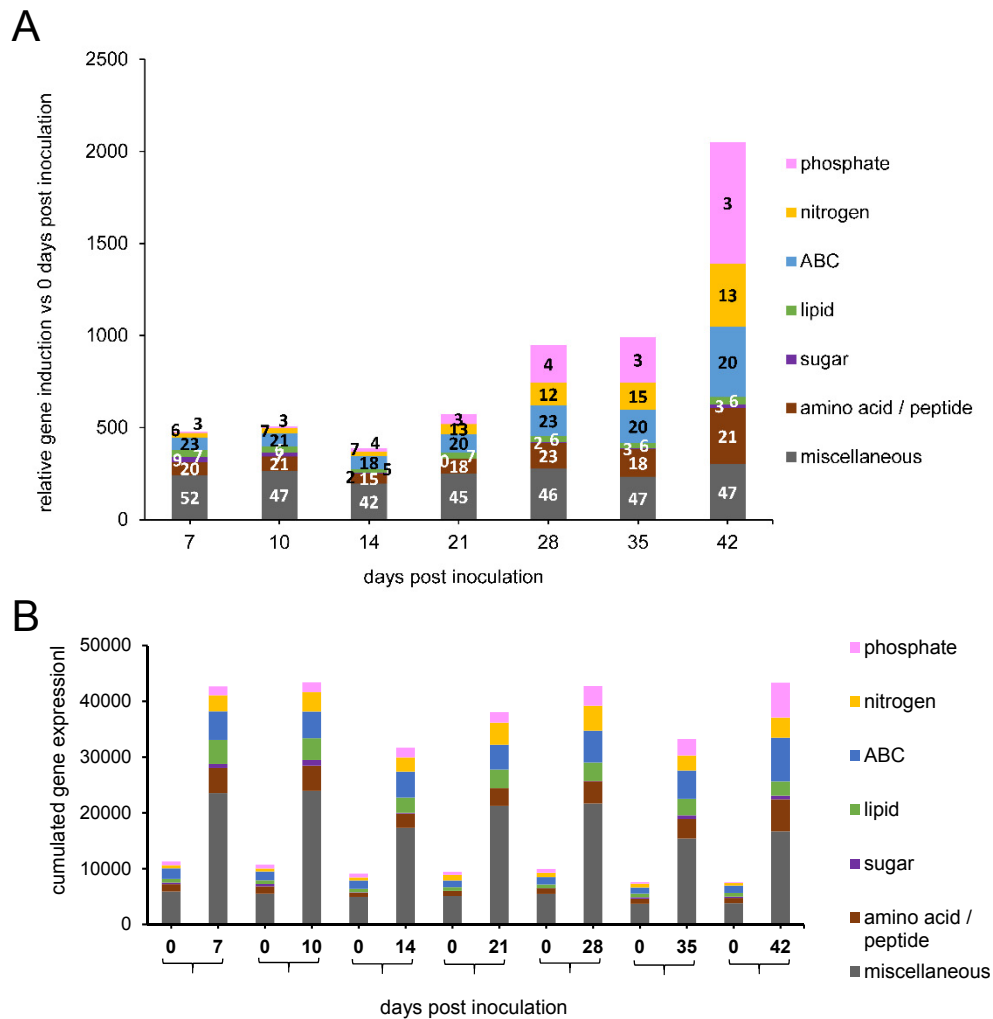


Fig 8: Activation of membrane transporter genes during root colonization of *M. truncatula* by *R. irregularis*.

Data from *Affymetrix GeneChip* hybridizations (Rico M. Hartmann, LUH, unpublished) are depicted in A and B. In A, the cumulated induction of membrane transporter gene expression is shown. It was computed by summing up the gene expression fold changes for this group of genes for each time point post inoculation. Only genes that were ≥ 2 fold at $p \leq 0.05$ induced in comparison to 0 dpi were depicted at 7, 10, 14, 21, 28, 35 and 42 dpi after inoculation of plants with *R. irregularis*. These were sorted in seven subgroups, including genes coding for phosphate, nitrogen, ABC, lipid, sugar, amino acid/peptide and miscellaneous transporters. The total number of induced genes is depicted in A, in the bars of each subgroup. In B, cumulated membrane transporter gene expression levels are shown from 7 to 42 dpi. For each time point, the genes from A are shown in comparison to 0 dpi. Biological replicates were three pools of 6 plant roots each per time point, respectively.

More than 100 membrane transporter genes were induced in the early stage of the AM interaction at 7 dpi (Fig 8, A). Here, and during the whole time of root colonization by AMF, a three to four-fold enhanced cumulated membrane transporter gene expression in comparison to 0 dpi was observed (Fig 8, B). Whereas processes in young symbiotic interactions, can be monitored from 7-10 dpi, many P-, N-, ABC- and amino acid transporter genes are highly activated at 42 dpi (Fig 8, A). The largest group of AM-induced genes, in terms of relative gene induction, are phosphate transporters (Fig 8), which indicates the importance of this element in the symbiotic nutrient allocation [2, 5, 14, 29, 30, 34]. Whereas three to four genes were grouped in the subgroup phosphate transport, up to 15 genes were connected to nitrogen (nitrate and ammonium) transport (Fig 8). Apart from genes that encode nitrogen, amino acid-or peptide transporters, more than 20 ABC-transporter genes were induced (Fig 8, A). In total, their accumulated gene expression levels are even higher than that of phosphate transporter genes (Fig 8, B). Furthermore, the selection of accumulated nitrogen and phosphate transporter gene expression levels also changed during the symbiosis (Fig 8, B). Whereas initially the cumulated nitrogen transporter gene transcription was higher, at 35 and 42 dpi the cumulated phosphate transporter gene expression was even stronger (Fig 8, B).

On a general level, the relative cumulated membrane transporter gene induction increase to two-fold at 35 dpi and four-fold at 42 dpi (Fig 8, A). Since the cumulated gene expression levels did not mirror this trend (Fig 8, B), it is suggestive that the induction of distinct AM-related key members of monitored membrane transporter gene families are decisive for this extensive induction step. It can be concluded that data from this global AM time course can be used as tool to identify transport-related candidate genes. To select candidates of prominent AM-related gene families, the expression was cross-checked with data from the *Medicago* Gene Expression Atlas [35] (Fig 9).

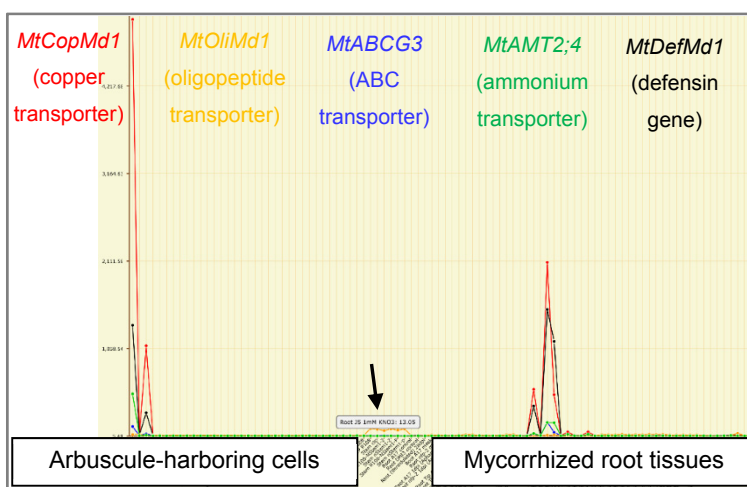


Fig 9: AM-depending transcription of selected membrane transporter and defensin genes in *M. truncatula*.

Relative amounts of transcripts of a copper transporter gene *MtCopMd1* (red), an oligo peptide transporter gene *MtOliMd1* (orange), an ABC transporter gene *MtABCG3* (blue), an ammonium transporter gene *MTAMT2;4* (green), and a defensin gene *MtDefMd1* (black) are shown in mycorrhized root tissues and arbuscule harboring cells. (<http://mtgea.noble.org/v3/>). The black arrow indicates an induction of *MtOliMd1* at by KNO_3 -treatment.

Based on these expression data, the copper transporter gene *MtCopMd1* (*Mtr.37110.1.S1.at*), the oligopeptide transporter gene *MtOliMd1* (*Mtr.4863.1.S1.at*), the ABC transporter gene *MtABCG3*

(*Mtr.52071.1.S1.at*), and the ammonium transporter gene *MtAMT2;4* (*Mtr.4243.1.S1.at*), as well as the defensin gene *MtDefMd1* (*Mtr.35854.1.S1.at*) were chosen as candidate genes for this thesis, since they were specifically induced during the colonization of roots by different AM-fungi (Fig 9). Solely *MtOliMd1*, a gene encoding an oligopeptide transporter gene, was induced by a KNO₃-treatment as well (Fig 9, see black arrow). Furthermore, all membrane transporter genes were found to be highly induced in arbuscule harboring cells [see also 35], supporting the hypothesis of a function during the AM-symbiosis.

Conclusion

In conclusion, more than 100 membrane transporter genes apparently contribute to AM-related transport processes. Since their overall expression level remained, after being strongly enhanced one week post inoculation, relatively constant over time, the ongoing induction of the five *M. truncatula* candidate genes encoding AM-related membrane transporters could be functionally important for nutrient exchange during the process of AM symbiosis.

The experimental setup chosen led to an acceptable substrate pH, and mycorrhization as well as arbuscule rates were enhanced by P depletion. Marker genes for mycorrhization such as *GiTubα*, *GiPT*, and *MtPt4* were strongly induced during root colonization by AMF applied as spore inoculum. A growth response of mycorrhized AM plants was evident after 35 dpi and became more substantial at 42 dpi. Candidates from highly AM-induced membrane transporter gene families, encoding copper- (*MtCopMd1*), oligopeptide- (*MtOliMd1*), ABC- (*MtABCG3*), and ammonium transporter genes (*MtAMT2;4*) as well as a defensin gene (*MtDefMd1*) were selected for functional studies in Chapter II and III.

Acknowledgements

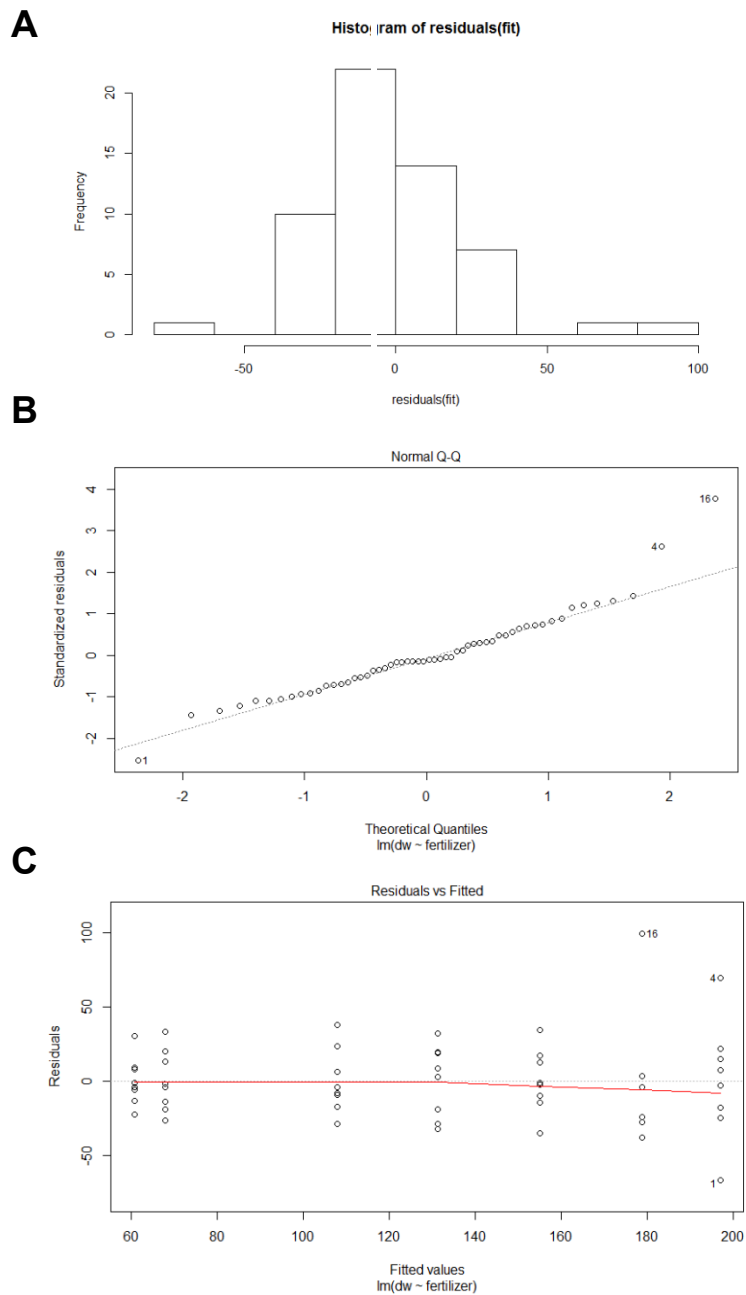
GeneChip hybridisations were carried out by João Sobral and Jörg D. Becker (Plant Genomics Lab and Gene Expression Unit, Instituto Gulbenkian de Ciência, Oeiras, Portugal).

References

- [1] Johnson NC, Graham JH, Smith FA (1997). Functioning of mycorrhizal associations along the mutualism-parasitism continuum. *New Phytol* 135: 575–585; 1997.
- [2] Asai T (1944). Über die Mykorrhizenbildung der Leguminosen-Pflanzen. *Jap. J. Bot.* 13: 463; 1944.
- [3] Gleditsia JW (1975). Vesicular-arbuscular mycorrhizae. *The Development and Function of Roots*: 575-591.; 1975.
- [4] Mosse B (1973). Advances in the study of vesicular-arbuscular mycorrhiza. *Ann. Rev. Phytopathol* 11: 171-96; 1973.
- [5] Jakobsen I (1986). Vesicular-Arbuscular Mycorrhiza in Field-Grown Crops. III. Mycorrhizal Infection and Rates of Phosphorus Inflow in Pea Plants. *New Phytologist* Vol. 104, No. 4 (pp. 573-581); 1986.
- [6] Dunne MJ and Fitter AH (1989). The phosphorus budget of a fieldgrown strawberry (*Fragaria x ananassa* cv. Hapil) crop: Evidence for a mycorrhizal contribution. *Ann Appl Biol* 114:185-193; 1989.
- [7] Merryweather J and Fitter A (1995). Arbuscular mycorrhiza and phosphorus as controlling factors in the life history of the obligately mycorrhizal *Hyacinthoides non-scripta* (L.) Chouard ex Rothm. *New Phytol.* 129: 629-636; 1995.
- [8] Smith SE and Read DJ (1997). *Mycorrhizal Symbiosis*. Academic Press, San Diego, CA.; 1997.
- [9] Cely MVT, Oliveira AG de, Freitas VF de, *et al.* Inoculant of Arbuscular Mycorrhizal Fungi (*Rhizophagus clarus*) Increase Yield of Soybean and Cotton under Field Conditions. *Front. Microbiol.* 2016; 7(e70633): 271 [https://doi.org/10.3389/fmicb.2016.00720]
- [10] Faber BA, Zasoski RJ, Burau RG, Uriu K. Zinc uptake by corn as affected by vesicular-arbuscular mycorrhizae. *Plant Soil* 1990; 129(2): 121–30 [https://doi.org/10.1007/BF00032404]
- [11] Straker CJ, Hilditch AJ, Rey MEC. Arbuscular mycorrhizal fungi associated with cassava (*Manihot esculenta* Crantz) in South Africa. *South African Journal of Botany* 2010; 76(1): 102–11 [https://doi.org/10.1016/j.sajb.2009.09.005]
- [12] Bielecki RL. Phosphate Pools, Phosphate Transport, and Phosphate Availability. *Annu. Rev. Plant. Physiol.* 1973; 24(1): 225–52 [https://doi.org/10.1146/annurev.pp.24.060173.001301]
- [13] Vance CP, Uhde-Stone C, Allan DL. Phosphorus acquisition and use: Critical adaptations by plants for securing a nonrenewable resource. *New Phytol* 2003; 157(3): 423–47 [https://doi.org/10.1046/j.1469-8137.2003.00695.x]
- [14] Cavagnaro T, Jackson L, Six J, Ferris H, Goyal S, Asami D and Scow K (2005a). Arbuscular mycorrhizas, microbial communities, nutrient availability, and soil aggregates in organic tomato production. *Plant and Soil.* 282: 209-225.; 2005.
- [15] Bago B, Pfeffer PE, Abubaker J, *et al.* Carbon export from arbuscular mycorrhizal roots involves the translocation of carbohydrate as well as lipid. *PLANT PHYSIOLOGY* 2003; 131(3): 1496–507 [https://doi.org/10.1104/pp.102.007765][PMID: 12644699]
- [16] Luginbuehl LH, Menard GN, Kurup S, *et al.* Fatty acids in arbuscular mycorrhizal fungi are synthesized by the host plant. *Science* 2017; 356(6343): 1175–8 [https://doi.org/10.1126/science.aan0081][PMID: 28596311]
- [17] Johansen A, Jakobsen I and Jensen ES (1992). Hyphal transport of ¹⁵N-labelled nitrogen by a vesicular-arbuscular mycorrhizal fungus and its effect on depletion of inorganic soil N. *New Phytol.* 122, 281–288.; 1992.
- [18] Tinker PB, Nye PH (2000). *Solute Movement in the Rhizosphere*. Oxford University Press, New York; 2000.
- [19] Guether M, Neuhauser B, Balestrini R, Dynowski M, Ludewig U, Bonfante P. A Mycorrhizal-Specific Ammonium Transporter from *Lotus japonicus* Acquires Nitrogen Released by Arbuscular Mycorrhizal Fungi. *Plant Physiology* 2009; 150(1): 73–83 [https://doi.org/10.1104/pp.109.136390]
- [20] Kobae Y, Tamura Y, Takai S, Banba M, *et al.* (2010). Localized expression of arbuscular mycorrhiza-inducible ammonium transporters in soybean. *Plant Cell Physiol* 51: 1411– 5; 2010.
- [21] Recorbet G, Abdallah C, Renaut J, Wipf D, Dumas-Gaudot E. Protein actors sustaining arbuscular mycorrhizal symbiosis: Underground artists break the silence. *New Phytol* 2013; 199(1): 26–40 [https://doi.org/10.1111/nph.12287]
- [22] Hogekamp C, Arndt D, Pereira PA, Becker JD, Hohnjec N, and Küster H. Laser microdissection unravels cell-type-specific transcription in arbuscular mycorrhizal roots, including CAAT-Box transcription factor gene

- expression correlating with fungal contact and spread. *Plant Physiol* 2011; 157(4): 2023–2043 [https://doi.org/10.1104/pp.111.186635]; 2011.
- [23] Hogekamp C and Küster H. A roadmap of cell-type specific gene expression during sequential stages of the arbuscular mycorrhizal symbiosis. *BMC Gen* 2013; 14(1): 306 [https://doi.org/10.1186/1471-2164-14-306]; 2013.
- [24] Gaude, N, Bortfeld, S, Duensing, N, Lohse M, and Krajinski F. Arbuscule-containing and non-colonized cortical cells of mycorrhizal roots undergo extensive and specific reprogramming during arbuscular mycorrhizal development. *Plant Journal* 2012; 69(3): 510-528 [http://dx.doi.org/10.1111/j.1365-313X.2011.04810.x]25; 2012. Available from: URL: http://dx.doi.org/10.1111/j.1365-313X.2011.04810.
- [25] Arnon, D.I., and Hoagland, D.R. (1940). Crop production in artificial culture solutions and in soils with special reference to factors influencing yields and absorption of inorganic nutrients. *Soil Sci.* 50, 463–483.; 1940.
- [26] S.R. Olsen, C.V. Cole, W.S. Watanabe, L.A. Dean. Estimation of available phosphorus in soils by extraction with sodium bicarbonate United States Department of Agriculture Circular No. 939 (1954), p. 19; 1954.
- [27] Vierheilig H, Coughlan AP, Wyss U, Piche Y (1998) Ink and vinegar, a simple staining technique for arbuscular-mycorrhizal fungi. *Appl Environ Microbiol* 64: 5004–5007; 1998.
- [28] Brundrett M, Bougher N, Dell B, Grove T, and Malajczuk N. Working with mycorrhizas in forestry and agriculture. ACIAR monograph 1996; ACIAR: Canberra [Publication Code: MN032][ISBN: 1 86320 181 5]; 1996.
- [29] Javot H, Penmetsa RV, Breuillin F, *et al.* *Medicago truncatula* mtpt4 mutants reveal a role for nitrogen in the regulation of arbuscule degeneration in arbuscular mycorrhizal symbiosis. *Plant J* 2011; 68(6): 954–65 [https://doi.org/10.1111/j.1365-313X.2011.04746.x][PMID: 21848683]
- [30] Harrison MJ, Dewbre GR, Liu J. A phosphate transporter from *Medicago truncatula* involved in the acquisition of phosphate released by arbuscular mycorrhizal fungi. *Plant Cell* 2002; 14(10): 2413–29 [PMID: 12368495]
- [31] Fiorilli, V., Lanfranco, L., & Bonfante, P. (2013). The expression of GintPT, the phosphate transporter of *Rhizophagus irregularis*, depends on the symbiotic status and phosphate availability. *Planta*, 237(5), 1267-1277.
- [32] Gobbato E, Marsh JF, Vernié T, *et al.* A GRAS-type transcription factor with a specific function in mycorrhizal signaling. *Curr Biol* 2012; 22(23): 2236–41 [https://doi.org/10.1016/j.cub.2012.09.044][PMID: 23122845]
- [33] Provorov NA, Borisov AY, Tikhonovich IA (2002). Developmental genetics and evolution of symbiotic structures in nitrogen-fixing nodules and arbuscular mycorrhiza. *J Theor Biol* 214: 215–232; 2002.
- [34] Liu, H., Trieu, A. T., Blaylock, L. A., & Harrison, M. J. (1998). Cloning and characterization of two phosphate transporters from *Medicago truncatula* roots: regulation in response to phosphate and to colonization by arbuscular mycorrhizal (AM) fungi. *Molecular Plant-Microbe Interactions*, 11(1), 14-22.
- [35] Young ND, Debelle F, Oldroyd GED, *et al.* The *Medicago* genome provides insight into the evolution of rhizobial symbioses. *Nature* 2011; 480(7378): 520–4 [https://doi.org/10.1038/nature10625][PMID: 22089132]

Supporting Information



S1 Fig: Statistical parameters of dry mass distribution of mycorrhized *M. truncatula* plants supplied with different phosphate and nitrogen amounts.

A histogram of residuals (A), the residuals in theoretical regimes (B) and residuals in fitted values (C) of plant dry matter variations in seven nutrient regimes, differing in nitrogen and phosphate supplies, are shown.

S1 Table: Monitoring of plant dry mass from mycorrhized plants fertilized with different P and N amounts.

fertilizer	lsmean	SE	df	lower.CL	upper.CL
323 μ M P 14.3 mM N	196.95	9.99	49	176.87	217.03
161 μ M P 14.3 mM N	178.86	9.99	49	158.78	198.94
81 μ M P 14.3 mM N	107.91	9.99	49	87.83	127.99
20 μ M P 14.3 mM N	60.80	9.99	49	40.72	80.88
161 μ M P 7.2 mM N	131.30	9.99	49	111.22	151.38
161 μ M P 3.6 mM N	154.99	9.99	49	134.91	175.07
161 μ M P 1.8 mM N	68.03	9.99	49	47.95	88.10

Confidence level used: 0.95

S2 Table: All to all comparison of plant dry mass from mycorrhized plants fertilized with different P and N amounts.

contrast	estimate	SE	df	t.ratio	p.value
1 - 2	18.09	14.13	49	1.28	0.8577
1 - 3	89.04	14.13	49	6.30	<.0001
1 - 4	136.15	14.13	49	9.64	<.0001
1 - 5	65.65	14.13	49	4.65	0.0005
1 - 6	41.96	14.13	49	2.97	0.0646
1 - 7	128.93	14.13	49	9.12	<.0001
2 - 3	70.95	14.13	49	5.02	0.0001
2 - 4	118.06	14.13	49	8.36	<.0001
2 - 5	47.56	14.13	49	3.37	0.0234
2 - 6	23.88	14.13	49	1.69	0.6260
2 - 7	110.84	14.13	49	7.844	<.0001
3 - 4	47.11	14.13	49	3.33	0.0255
3 - 5	-23.39	14.13	49	-1.66	0.6481
3 - 6	-47.08	14.13	49	-3.33	0.0257
3 - 7	39.89	14.13	49	2.82	0.0912
4 - 5	-70.50	14.13	49	-4.99	0.0002
4 - 6	-94.19	14.13	49	-6.67	<.0001
4 - 7	-7.23	14.13	49	-0.51	0.9986
5 - 6	-23.69	14.13	49	-1.68	0.6345
5 - 7	63.28	14.13	49	4.48	0.0008
6 - 7	86.96	14.13	49	6.15	<.0001

P value adjustment: Tukey method for comparing a family of 7 estimates, Abbreviations: 1, 323 μ M P/ 14.3 mM N; 2, 161 μ M P/ 14.3 mM N; 3, 81 μ M P/ 14.3 mM N; 4, 20 μ M P/ 14.3 mM N; 5, 161 μ M P/ 7.2 mM N; 6, 161 μ M P/ 3.6 mM N; 7, 161 μ M P/ 1.8 mM N

S3 Table: Primers used in real-time RT-PCR experiments.

Gene	Identifier*	Primers
<i>MtTefa</i>	Medtr6g021805.1	AAGCTAGGAGGTATTGACAAG/ACTGTGCAGTAGTACTTGGTG
<i>MtPt4</i>	Medtr1g028600.1	TCGCGCGCCATGTTTGTGT/GCGAAGAAGAATGTTAGCCC
<i>GiPt</i>	AY037894.1	AACACGATGTCAACAAAGCAAC/AAGACCGATTCCATAAAAAAGCA
<i>GiTuba</i>	GW088233.1	TGTCCAACCGTTTTAAAGT/AAAGCACGTTTGGCGTACAT

* From the *Medicago truncatula* genome 4.0 or GenBank accession numbers, respectively.

CHAPTER II

Functional analysis of AM-induced membrane transporter genes

Scope:

Although it is known that the cellular targeting of AM-related membrane transporters is primarily dependent on the time point of expression of the corresponding genes, the fine-tuning of the composition of symbiotic membranes is not fully understood. Using a combination of different techniques, such as transcriptional and translational fusions and knockdown approaches in transgenic roots, it was aimed in this Chapter to shed light on the function of the AM-induced membrane transporter genes *MtCopMd1*, *MtOliMd1*, *MtABCG3* and *MtAMT2;4*, expressing a copper, an oligopeptide, an ABC, and a putative ammonium transporter, respectively.

Contributor roles:

Marian Uhe: Conceived and designed the experiments, cultivated and mycorrhized plants, *in silico* analyses, gene expression, knockdown experiments, subcellular localization experiments, interpreted experimental data.

Rico M. Hartmann: Provided unpublished MtGeneChip hybridization data.

Claudia Hogekamp: Provided unpublished MtGeneChip hybridization data.

Ingrid Buchwald: Harvesting of *Xenopus laevis* oocytes.

Patrik Schadzek and Anaclet Ngezahayo: Gave helpful advice in the setup of oocyte-media and two-electrode-voltage clamp measurements.

Natalija Hohnjec and Helge Küster: Participated in the interpretation of experimental data.

Abstract

Different nutrient regimes during mycorrhizal symbioses alter the cost-benefit-ratio and therefore the outcome of the plant-microbe interaction. In *Medicago truncatula*, the expression of four genes, encoding arbuscular mycorrhiza-dependent membrane transporters, varied in different phosphate (P) and nitrogen (N) regimes during AM-fungal colonization. Whereas the promoters of *MtCopMd1* and *MtAMT2;4* were induced by phosphate, as well as strong nitrogen depletion, *MtOliMd1* and *MtABCG3* were solely expressed in a phosphate-dependent manner. *Affymetrix GeneChip* hybridizations indicated that all selected membrane transporter genes are less expressed in mycorrhized *ram1-1* mutant roots, defective in MtRAM1, a central regulator of arbuscule branching. In addition, *MtCopMd1* and *MtABCG3* were repressed in *pt4-1* mutants, defective in the AM-specific phosphate transporter MtPT4. In RNAi-roots displaying reduced expression of *MtMyb1*, a regulator of arbuscule degeneration, none of the investigated membrane transporter genes was repressed. This supports a function for these in the active stages of symbiosis. Cells containing arbuscules displayed different spacio-temporal levels of promoter activities, indicating alternative signal pathways for fine-tuning of AM-dependent membrane transporter gene expression. An amiRNA construct targeting *MtABCG3* expression resulted in an enhanced transcription of *MtRAM2*, encoding a glycerolphosphate-O-acyltransferase (GPAT) enzyme involved in the biosynthesis of fatty acids, supporting the model for a plastid-derived fatty acid-support of oleogenic, fatty acid-auxotrophic AMF. In N-starved mycorrhizal RNAi-roots, a ~92% knock-down of *MtAMT2;4* expression was achieved, but no changes in the expression patterns of selected AM-marker genes were evident. Also, the expression of other membrane transporter genes of interest was not altered, indicating that the functional composition of the PAM was not disturbed. Fungal genes that might have a function in nitrogen flux during AM were not altered in expression as well. Since there was no significant electrogenic transport in transgenic *Xenopus laevis* oocytes, expressing *MtAMT2;4* and being supplied with ammonium, the true membrane-transported substrate of *MtAMT2;4* might be ammonia instead. The localization of a p:35S:MtAMT2;4-mGFP6 fusion as well as the analysis of cellular structures, using a combination of subcellular fluorophore markers, indicated that the level of mGFP6 fluorophores rises in arbuscule-containing cells, indicating a PAM-localization of *MtAMT2;4* and a function during nutrient exchange at the active stage of AM.

Introduction

The enhanced supply with plant growth-limiting nutrients via AM-fungal mycelia [1] is a selective advantage for mycorrhized plants. In addition, it also facilitated the colonization of land by early plants more than 400 million years ago [1, 2, 3]. In AM symbiosis, a perisymbiotic membrane permanently separates micro- and macrosymbiont [4] and mediates the exchange of nutrients between fungal hyphae and plant cells. Thus, membrane transporters have a crucial role for the functioning of the symbiotic plant-fungus interface in AM interactions.

Cox and Tinker [5] suggested that arbuscules, fungal structures with a large surface area relative to their volume, are the major spot for the exchange of nutrients and other molecules. Later it was described by Pumplin *et al.* [6] that a unique set of proteins is generated during the formation of the periarbuscular membrane (PAM), which results from a reorientation of the secretory pathway. Several research groups demonstrated that transcripts of *PHT1* genes, belonging to a family of phosphate transporter genes in *M. truncatula*, *Oryza sativa* and *Lotus japonicus* (*MtPt4*, *OsPt11* and *LjPt3*), are specifically expressed in cortical cells that contain one of the two known arbuscule morphotypes, *Arum*-type arbuscules or *Paris*-type coils [7, 8]. In addition to phosphate, an enhanced uptake of nitrogen (N) and sulfur (S) is possible [9, 10]. Studies with compartmentalized plant pots highlighted the potential benefits of AM symbioses for the acquisition of N (ammonium and nitrate) [11]. Due to the presence of AM-inducible ammonium transporter genes in *L. japonicus* and *Glycine max* [12, 13], Recorbet *et al.* [14] suggested that ammonium acts as a signal to the arbuscules. In addition, putative sulfate transporters in *Lotus* and *Medicago* were induced during the AM symbiosis in sulfate-depleted or sufficiently supplied roots [15, 16, 17, 18]. Apart from P, N, and S, also other AM-supplied nutrients are essential for growth and productivity of plants. For example, it was shown that already a moderate level of mycorrhization enhanced the uptake of N, P, K, Ca, Mg, Fe, Mn, Cu, and Zn in chickpea, with a simultaneous increase in plant biomass [19].

Nutrient transfer between both partners involves a tight control of the microsymbiont's life cycle by the host. Fungal arbuscules regularly degrade after several days, and previously infected cells have to be restructured for subsequent re-infection [20]. Harrison *et al.* [7] found that the phosphate transporter *MtPt4* is incorporated in the periarbuscular membrane and that the protein is no longer detectable in cells with degenerated arbuscules. Also, Maeda *et al.* [21] were able to show that the knockdown of the *PHT1* transporter gene *LjPT3* in *Lotus japonicus* led to a retarded development of arbuscules and was associated with a reduced phosphate uptake. By demonstrating an increased activity of H⁺-ATPases in the periarbuscular membrane [22, 23], the role of arbuscules in active P transfer via membrane transporters during symbiosis was validated. Nevertheless, functional analyses of the transporters themselves, as done by Güther *et al.* [12] for the AM-induced *LjAMT2* gene, are still rare.

The experiments presented in this chapter are aiming at a contribution to the understanding of the function of four selected AM-related membrane transporter genes, designated *MtCopMd1*, *MtOliMd1*, *MtABCG3*, and *MtAMT2;4*, using different molecular and phenotypic techniques. Their impact was investigated by transcriptional fusions to monitor promoter activity or by selectively turning off gene expression. Using different phosphate (P) and nitrogen (N) regimes, the interference of these nutrients for gene transcription was displayed. Translational fusions with mGFP were used for the subcellular localization of *MtAMT2;4* *in planta*. In addition, the heterologous expression of an electrogenic membrane transporter in *Xenopus laevis* oocytes was used to shed light on the substrate of *MtAMT2;4*. Taken together, functions related to the AM symbiosis, such as a processing of lipids or a support of the nitrogen flux at the periarbuscular membrane, can be proposed for some AM-related membrane transporters.

Materials and Methods

Bioinformatic analyses

Amino acid sequences of MtOliMd1, MtCopMd1, and MtABCG3 were analyzed with *InterProScan* [24] using standard settings.

Plant cultivars, fungal and bacterial strains

Medicago truncatula Gaertn. Jemalong A17 (Thierry Huguet, INRA Toulouse, France) was used for all plant experiments. Sterile *Rhizophagus irregularis* DAOM197198 spores (PremierTech, Rivière-du-Loup, Canada) were applied as fungal inoculum. *Escherichia coli* DH5 α mcr' [25] was used for cloning and the propagation of plasmids. Transgenic roots were induced by *Agrobacterium rhizogenes* Arqua1 [26].

Cultivation of *M. truncatula* plants

M. truncatula-seeds were covered by three volumes of 95-98% (v/v) sulphuric acid. The vessel with the seeds was constitutively inverted for approximately 10 minutes, until small brown dots on the testa appeared. The volume was three times replaced by sterile tap water and inverted 3 times for 1 minute. This was followed by an incubation with 2% (w/v) sodium hypochloride for 1 min. The washing steps were repeated with a prolonged incubation time of two minutes. Consecutively, the seed were soaked in water for 2-4 hour, were exposed to the light of the phytocabinet. Finally, they were placed on phyto-agar plates and incubated for four days at 6°C in the dark and then for one day at 22°C in the dark. Then they were exposed to the light of the phytocabinet. As soon as the germlings showed longitudinal growth and a thickened, hypocotyl, their roots were transformed via agrobacteria. Plants were then cultivated in a phytocabinet (Klimaschrank KPS 1700 Weisshaar, Bad Salzuflen, Germany) with 16 h/d light (Osram FLUORA L 18WI77 light tubes, 3100-3400 Lux) at 22°C with a relative humidity of 60%. Plants were fertilized with ½ strength Hoagland's solution [27]. For different phosphate (P) and nitrogen (N) supplies, a PN-variation solution was set up as follows: 1 mM KHCO₃, 1.5 mM K₂SO₄, 1 mM MgSO₄, (0.32, 0.16, 0.081, or 0.02) mM NaH₂PO₄, equilibrated by Na₂SO₄, (1.43, 0.71, 0.36, 0.18) mM NH₄NO₃, (5.71, 2.9, 1.43, 0.71) mM Ca(NO₃)₂, equilibrated by CaCl₂, 0.6 mM NaFeEDTA, 0.2 μ M Na₂MoO₄ x 2H₂O, 10 μ M H₃BO₃, 0.2 μ M NiCl₂ x 6 H₂O, 1 μ M ZnSO₄ x 7 H₂O, 2 μ M MnCl₂ x 2H₂O, 0.5 μ M CuSO₄ x 5 H₂O, and 0.2 μ M CoCl₂ x 6 H₂O. The solution was prepared with deionized water, the pH was adjusted to 6.3 with H₂SO₄. Plants were watered from the bottom.

Induction of transgenic *M. truncatula* roots and inoculation of *M. truncatula* with AM fungi

Transgenic *M. truncatula* roots were generated as described elsewhere [28]. *A. rhizogenes* Arqua1 strains were grown for two days at 30 °C on selective TY (0.5 g/l tryptone; 0.3 g/l yeast extract; 0.07 g/l CaCl₂×2H₂O) agar plates. Cells were resuspended in 4 ml PS buffer (40 mM Na₂HPO₄×2H₂O, 85 mM NaCl, 17 mM KH₂PO₄; pH 7 adjusted with HCl). The testa of the *M. truncatula* seedlings was removed and they were moisturized. The bacterial resuspension was injected in the hypocotyl of the seedlings with a sterile syringe. Consecutively, they were planted in sterile seramis and incubated over night at 18 °C in the dark. Finally, the seedlings were transferred to the phytocabinet climate chamber. Transgenic hairy roots were screened and mycorrhized four to five weeks after germination. For most experiments, sterile *R. irregularis* spores were used for the inoculation of *M. truncatula* wild type and transgenic roots. 2000 spores were incubated with the shaded plant root for three hours in liquid. Subsequently, plants were potted in 9×9 cm pots with seramis (Seramis GmbH, Mogendorf, Germany) as a substrate. Remaining spores were pipetted on the roots. For nutrient variation experiments, *R. irregularis* inoculum from a leech preculture was used (Bettina Hause, IPB, Halle, Germany).

Cloning of promoter-*gusAint* fusions

From genomic DNA of *M. truncatula* leaves, the promoters of *MtOliMd1* (Medtr7g098160.1), *MtCopMd1* (Medtr7g066070.1), and *MtABCG3* (Medtr4g093845.1) were PCR-amplified using the primers detailed in Table 1.

Table 1: PCR primers for the amplification of promoter sequences from the *M. truncatula* genome.

Primer	Sequence (5'-3') ¹	Cloning site
pMtOliMd1 (f)	aaaa gcatgc CGACTTTGGTTCAACAAGTGTG	<i>SphI</i>
pMtOliMd1 (r)	aaaa cccggg GATGCTGGAAAGAAGAACTACG	<i>XmaI</i>
pMtCopMd1 (f)	aaaa gaattc GCATAGGAATGTAGGATATGTTTCAC	<i>EcoRI</i>
pMtCopMd1 (r)	aaa aagctt CTGTATTGGTTTCTTTTTCCAAAACC	<i>HindIII</i>
pMtABCG3 (f)	aaaa gaattc CCAACAATTATAGCCCTCCA	<i>EcoRI</i>
pMtABCG3 (r)	aaa aagctt GTTGCTCTGATACCAAATGTTTCAC	<i>HindIII</i>
pMtABCG3 (f) NEU	aaaa gaattc GGTCTATTAATTACCGATGACAAA	<i>EcoRI</i>
pMtABCG3 (r) NEU	aaa aagctt GTCAGTGAACAAATTGGTGATCATC	<i>HindIII</i>

¹the native sequence is written in capital letters, restriction sites and primer extensions in lower case; g= genomic CDS, f=forward, r=reverse; NEU= due to a new genome-based annotation of the gene, primers had to be changed

Fragments were cleaved as indicated in Table 1 and were cloned into pk18 [29]. The promoters were then subcloned into pGUS-INT [30], containing the *gusAint* reporter gene. Using *SpeI*, the transcriptional fusion was cleaved out, *Klenow*-blunted, and ligated into the *SmaI*-digested binary vector pRedRoot [31]. Promoter-*gusAint* fusions cloned in pRedRoot were transferred via electroporation into *A. rhizogenes* Arqua1.

Cloning of knockdown constructs aiming selected AM-related membrane transporter genes of *M. truncatula*

Cloning steps for the generation of the RNAi:MtAMT2;4 -construct have been described elsewhere [32]. The strategy for the generation of amiRNA constructs was performed in accordance to the protocol established by Rico Hartmann (Leibniz Universität Hannover, Germany) via overlapping mutation PCR [33]. Gene specific 21mers were designed based on *Affymetrix GeneChip* probe sets. They were fitted into the *miR159b*-precursor (Fig 8, A), which was reported to produce high amounts of functional micro RNAs [34]. To estimate if the fitting of the 21mers into the backbone was successful, a simulation with the software CLC cloner was performed under standard settings (Table 2).

Table 2: CLC cloner settings to calculate the secondary structure of RNA sequences.

parameter	setting
Calculate partition function and base pair probabilities	No
Avoid isolated base pairs	No
Apply different energy rules for Grossly Asymmetric Interior Loops (GAIL)	Yes
Include coaxial stacking energy rules	No
Apply base pairing constraints	No
Maximum distance between paired bases	No limit
Add best structure as annotation	Yes

The secondary structures of the RNA sequence of the precursors including the changed 21mers were calculated with CLC workbench and muted until the secondary structure was the same (Fig 1).

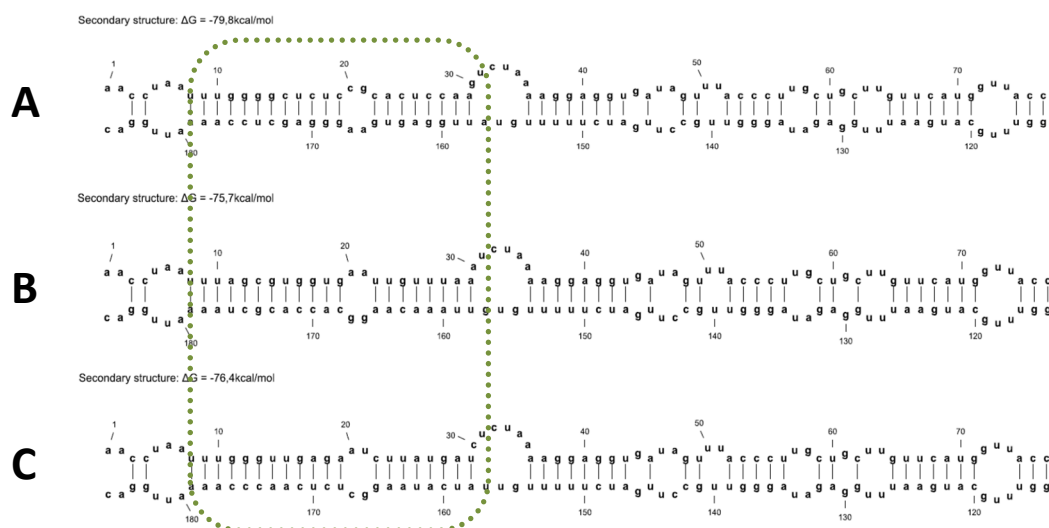


Fig 1: Native, *MtOliMd1*, and *MtABCG3* amiRNA precursors.

miR159b precursors, containing the native 21mer (A), a 21mer directed against oligopeptide transporter *MtOliMd1* (B) and ABC transporter *MtABCG3* (C) genes is shown. The region of the effective micro RNA is marked with a green dotted box, where the upper strand is reported to be the more likely one to be incorporated by the RISC complex by a factor of >1000 [34].

Consecutively, the native 21mer was replaced by oligonucleotides of the new 21mer in three PCR reactions and finally integrated into the backbone via a PCR with the primers A (GATTCATTAATGCAGCTGGCA) and B (GCGGTCACGCTGCGCGTAACC) (Table 3).

Table 3: Strategy for the creation of amiRNAs via overlapping mutation PCR.

Reaction	Reaction a	Reaction b	Reaction c	Reaction d
Primers	A + IV	II + III	B + I	A + B

Template for the PCR a, b, and c (Table 3) was the vector sequence pBlISK:mir159b, whereas the generated amplicons from these reactions were consecutively used as template for reaction d (Table 3). PCRs were performed using the primers listed in Table 4.

Table 4: amiRNA Primers for overlapping mutation PCR.

A				
Primer	5'	miRNA: MtABC <i>G3</i>	3'	
I	CA	TATCATAAGGCTCTCAACCCA	AAATTGGACACGCGTCT	
II	AA	TGGGTTGAGAGCCTTATGATA	ACAAAAAGATCAAGGCA	
III	AA	TGGGTTGAGAATCTTATGATC	TCTAAAAGGAGGTGATA	
IV	CT	CATCATAAGATTCTCAACCCT	AATTAGGTTACTAGTTC	

B				
Primer	5'	miRNA: MtOliMd1	3'	
I	GT	GTAAACAAGGCACCACGCTA	AAATTGGACACGCGTCT	
II	TT	TAGCGTGGTGCCTTGTTTAAC	ACAAAAAGATCAAGGCA	
III	TT	TAGCGTGGTGATTGTTTAA	TCTAAAAGGAGGTGATA	
IV	GA	ATTAAACAACAACCACGCTA	AATTAGGTTACTAGTTC	

A= MtABC*G3* primers; B= MtOliMd1 primers; integrated mismatches are colored red

The PCR products from the first step were purified and assembled using the *Pfu* DNA polymerase into new amplicons, targeting either MtOliMd1 or MtABC*G3*.

These amplicons were cleaved with *Eco*RI and *Bam*HI and after the ends have been filled up with the *Klenow* polymerase and were ligated into the *Sma*I cleaved 918p9RFP-ubi3-Expr. vector. Heat shock transformations in *E. coli* DH5 α -mcr' have been performed. Bacterial clones containing the plasmid have been selected via Streptomycin, the plasmid was purified and finally sequenced.

Table 5: Primers used in real-time RT-PCR experiments.

Gene	Identifier*	Primers
MtDefMd1	Medtr8g012805.1	GGGACATTAAGCAAGCATG/TGTTGCCGGTGGTTCCTTAC
MtDefMd2	Medtr8g012835.1	AAAGGAAAAGCACAACATGG/CAGAAGCAAGCAAATCCAAA
MtDefMd3	Medtr8g012875.1	TGCTCGTAAATTCCTCACAA/CTTCGCCATTGACAACTTT
MtDefMd4	Medtr8g012885.1	TTGTAGAGGGAGAAGCAAAC/CCAGTGTTATCAAGGTGACA
MtTefa	Medtr6g021805.1	AAGCTAGGAGGTATTGACAAG/ACTGTGCAGTAGTACTTGGTG
MtPt4	Medtr1g028600.1	TCGCGGCCATGTTTGTGT/GCGAAGAAGAATGTTAGCCC
MtMyb1	Medtr7g068600.1	TACTGCCAAATTTCTGTTCTA/GGATTGTGTTTTAAAGGATTC
MtRam1	Medtr7g027190.1	CATTACTACTCCGAATTTTC/CAACAAACAACCTTTATCCTC

Gene	Identifier*	Primers
<i>MtHa1</i>	Medtr8g006790.1	AGGTTCTAACATCTATTGGGA/GACAACCTATGTGAACCAATG
<i>GiHa5</i>	GQ205019.1	AAATTACGGTTTCTTCTGCAC/TGGAACATCTTCCTTCATTCA
<i>GiPt</i>	AY037894.1	AACACGATGTCAACAAAGCAAC/AAGACCGATTCCATAAAAAGCA
<i>GiTubα</i>	GW088233.1	TGTCCAACCGGTTTTAAAGT/AAAGCACGTTTGGCGTACAT
<i>MtPHO2</i>	[35]	GGAGCCTCCAGAGTCTTCAAG/AAGGACAAGAGCCTGCAGAGAG
<i>GiUAP</i>	[36]	TTCCGCAGTCGTTGAATTGA/CCTTCGACAATGCTTAAAAATTATCA
<i>GiOAT</i>	[36]	AGGGCTCAAGGTGCGTATGT/ACTGCCGAATAGGCACACAAA
<i>MtNaRd10604</i>	XM_003614772.3	GATACTTTGGCATTGGCTTGT/TTGCCCTAGAACACAAGCAA
<i>MtGS10422</i>	XM_003619821.3	ACTTTGAGGATAGAAGGCCTTCTT/ AATTGTCCAAGTGGTCTTTAAGC

*From the *Medicago truncatula* genome 4.0 or GenBank accession numbers, respectively.

Cloning of MtAMT2;4 mGFP6 fusion constructs for subcellular localizations

Promoter and CDS of the ammonium transporter were PCR-amplified using the primers depicted in Table 6.

Table 6: Primers for the cloning of mGFP6 fusion constructs.

Primer name	Sequence (5'-3') ¹	cutting restriction enzyme
MtAMT2;4 (f)	aaa ggtacc aaaa ATGGAGCTACCTTCAAACCT	<i>KpnI</i>
MtAMT2;4 (r)	aaa agatct tcc tcc TACCATTTGAAGTTCACC	<i>BglII</i>

¹the native sequence is written in capital letters, restriction sites and primer extensions in lower case
Abbreviations: f, forward; r, reverse

Therefore the vectors created for a GFP-based localization of Amtr.4243 were cleaved using *EcoRI* and *HindIII* out of the vector backbone p35S-mGFP6neu. The ends have been filled up using the *Klenow*-polymerase and after gel-purification the fragments were ligated into the *SmaI*-digested and dephosphorylated vector pBIN:ER-rk. The coding sequence of *MTAMT2;4* (~2.3 kb) was cloned into vector p35S-OLI-mGFP6 [37]. This vector encodes an N-terminal GGRSPGGS oligopeptide (OLI) extension of mGFP6 that serves as a flexible linker to the protein of interest. The following cloning strategy were used: *KpnI* and *BglII* were used for the coding sequence (), allowing the translation of an *MTAMT2;4*-OLI-mGFP6 fusion protein under the control of p:35S. All primers were extended by 3 additional adenosine bases. The *MTAMT2;4*-OLI-mGFP6 fusion was released using *KpnI* and *BglII*. It was integrated into the vector pRedRoot [31]. In parallel, the fragment was blunted using *Klenow* polymerase and ligated in between the *HindIII* and *SpeI* site of binary vector pBIN:ER-rk [38] expressing an ER-RFP marker.

Isolation of plant RNA from *M. truncatula* roots

RNA isolations were carried out using the RNeasy Plant Mini Kit (Qiagen, Hilden, Germany). β -mercaptoethanol was added to the RLT buffer and 600 μ l of this mix were added to each sample. Tissues were disrupted using the FastPrep[®]-24 (MP Biomedicals, Santa Ana, USA) for 5 times 30 s (6.5

m/s). The RNA concentrations were measured using a Nanodrop (Thermo Fisher Scientific, Langenselbold, Germany) and checked on agarose gels.

Real-time RT-PCR

Real-time RT-PCR analyses were performed using the SensiFAST™ SYBR® No-ROX One-Step Kit (Qiagen, Hilden, Germany) with primers listed in the S2 Table. Primers were designed to match annealing temperatures of 55 °C and were tested for gene-specific amplifications. 5 ng of total RNA were used as a template in 20 µl for the mycorrhization time course, the *ram1-1* and the *MtDefMd1* overexpression experiment. Otherwise, 50 ng of total RNA were used. RT-PCR reactions followed a three-step cycling program: reverse transcription at 45 °C for 10 min; polymerase activation at 95 °C for 2 min; PCR amplification with 40 cycles at 95 °C for 5 sec, 55°C for 10 sec, and 72 °C for 8 sec. Biological replicates were measured in three technical replicates. The housekeeping gene *MtTefα* was used for normalization. To relate gene expression to the degree of fungal colonization or the presence of active arbuscules, a ratio with *GiTubα* or *MtPt4* expression was calculated. Average values were used to calculate gene expression levels via the $2^{-\Delta CT}$ method with $\Delta CT = CT_{\text{Gene}} - CT_{\text{MtTef}\alpha}$. The mean and standard error of the mean of all biological replicates was calculated after normalization and was visualized, if not stated differently. Using *MS Excel 2016* (Microsoft Corp., Redmond, Washington, USA), two-tailed Student's t-tests were performed to check differences in gene expression between mutant-, RNAi-, overexpression-, and wild type roots.

Affymetrix GeneChip hybridizations

Global gene expression data from *Affymetrix GeneChip* hybridizations studying a time course of root colonization by AM fungi from 0 to 42 dpi (Rico M. Hartmann, LUH, Hannover, personal communication), were filtered for ≥ 2 -fold at $p \leq 0.05$ induced gene expression between selected time points. In addition, gene expression in the mycorrhized *MtRam1* mutant *ram1-1* (Rico M. Hartmann, LUH, Hannover, personal communication), the mycorrhized *MtPt4* mutant *pt4-1* [39], and mycorrhized *MtMyb1*-RNAi roots (Claudia Hoge Kamp, LUH, Hannover, personal communication) was compared to the corresponding mycorrhized control roots, using the filter settings mentioned above.

Histological studies

To investigate the activity of promoter-*gusA* fusions, transgenic roots were incubated in GUS staining buffer as described before [30]. Cells with the strongest promoter activity were visible after 6-7 hours. After overnight staining, also cells with a weak promoter activity were detected. Finally, roots were rinsed with water.

To detect fungal structures, 1-2 cm root sections were incubated in 10 % (w/v) KOH at 95 °C for 7 minutes. The roots were washed three times with water and incubated in staining solution with 20 µg/ml WGA-Alexa Fluor 488 in 1x PBS (0.14 M NaCl, 2.7 mM KCl, 1 mM Na₂HPO₄·2H₂O, 1.8 mM KH₂PO₄; pH 7.3) over night. Samples were protected from light. Consecutively, excessive dye was washed out with water.

A 1 mM LysoSensor™ Green DND-189-Solution (in DMSO) was diluted to 0,3 mM in 1x PBS-buffer. *M. truncatula* plant roots were incubated in this staining solution for 3 h. Consecutively the roots were foto-documented under the fluorescence binocular (Fig 19) using the brightfield and the GFP-fluorescence channel (ET GFP-MZ10F). Therefore, 1-2 cm sections of mycorrhized roots were pre-screened under the fluorescence binocular. Consecutively, longitudinal thin sections were analyzed. They were generated by hand with a razor-blade and later stored in 1x PBS-buffer. Confocal microscopy was used to locate the dye and RFP in the inner root cortex.

Detection of reporter proteins via fluorescence microscopy

Transgenic *M. truncatula* roots were identified using a stereo microscope (Leica MZ10F, Sohns, Germany). 1-2 cm sections of mycorrhized roots were selected. For the localization of fluorescent reporter proteins, longitudinal root sections were cut by hand with a razor blade. These sections were transferred into a physiological buffer (39 mM Na₂HPO₄·2H₂O, 86 mM NaCl, 22 mM KH₂PO₄; pH 7). GFP (500-540 nm), and mRFP (794-799 nm) were detected in the inner root cortex using a hybrid detector and confocal microscopy (Leica TCS SP8 MP, Sohns, Germany). For promoter-GUS studies, an Eclipse TE2000-E inverse confocal laser scanning microscope (Nikon GmbH, Düsseldorf, Germany) and software EZ-C1 (Nikon GmbH, Düsseldorf, Germany) were used. For time-lapse imaging the same technical devices were used. Plants were transferred into a splitted pot with a microscopic cover glass on the bottom. A prescreened root section was placed in this section, then a cover glass was placed on top. The remaining roots were covered with wet tissue, soaked with half Strength Hoagland's solution and the shoot were fixed with sticky tape at the side of the pot, allowing inverse microscopy.

Heterologous translation of *M. truncatula* membrane-transporter genes in oocytes of *X. laevis*

To investigate the electrogenic transport of AM-dependent membrane transporters, two-electrode voltage clamp experiments were performed in transfected *Xenopus* oocytes.

Primarily, a full-length cDNA of the codon-determining sequence (CDS) without introns was generated and cloned into a vector, used for in vitro transcription. This vector, pGEMHE, has a promotor for the T7-polymerase and precloned *Xenopus laevis* untranslated regions (UTRs), which increase translation efficiency. The cloning started with a reverse transcription using the *SuperScript III* reverse

transcriptase, followed by a regular PCR, to amplify the generated cDNA. Specific primers for the heterologous expression of the ammonium- transporter *MTAMT2;4* and the copper transporter *MtCopMd1* were used (Table 7).

Table 7: Primer for the heterologous expression of *M. truncatula* membrane transporters in *X. laevis* oocytes.

Primer name	Sequence (5'-3') ¹	cutting restriction enzyme
pGEMHE:MtAMT2;4 (f)	cttggatccATGGAGCTACCTCAAACCT	<i>Bam</i> HI
pGEMHE:MtAMT2;4 (r)	aattaagcttTCATACCATTGAAGTTCACC	<i>Hind</i> III
pGEMHE:MtCopMd1 (f)	aaaccgggATGGATCATGACATGGATCATG	<i>Sma</i> I/ <i>Xma</i> I
pGEMHE:MtCopMd1 (r)	aattaagcttTTAACAAGATAACGGAGGAAGATC	<i>Hind</i> III

¹the native sequence is written in capital letters, restriction sites and primer extensions in lower case
Abbreviations: f, forward; r, reverse

1 µl gene specific primer (2,5 µM), 1 µl dNTPs (10 mM), 10 µl RNA (10 ng/µl, RIN 9.9, mycorrhized, 28 dpi) and 1 µl water (DEPC treated) were pipetted together, mixed and centrifuged. The sample incubated for 5 min at 65°C and consecutively for 1 min on ice. Then 4 µl 5x buffer (for *SuperScript III*), 1 µl 0,1 M DTT and 1 µl *SuperScript III* were added. The sample incubated for 5 min at 25°C and consecutively for 60 min at 55°C. Finally, the sample incubated at 70°C for 15 min.

For the PCR (Table 8) 2 µl of the described sample were then mixed with 10 µl 5x Phire buffer, 1µl dNTPs (10mM), 1 µl DMSO, 0,5 µl gene specific primers (100 µM, forward and reverse primer), 34 µl water (DEPC treated) and 1 µl *Phire Hot Start II polymerase*.

Table 8: PCR program for the amplification of the CDS of AM dependent membrane transporter genes of *M. truncatula*.

Temperature [°C]	Time [s]	Number of cycles
98	30	1
98	5	33
55/60/65	10	
72	30	
72	60	
4	hold	1

The following step was the digestion of the vector backbone (and its dephosphorylation) and the PCR product with the restriction enzymes listed in Table 7. Consecutively ligation and heat shock transformation of competent *E. coli* DH5α *mcr'* cells were performed. The fragments were column-purified using the "PCR/gel clean kit" (*Macherey und Nagel*). The CDS of each transporter gene was ligated into the vector pGEMHE and transformed via heat shock into *E. coli* DH5α-*mcr'*.

Consecutively the DNA was in vitro transcribed into an mRNA. The plasmids (1-2µg/6µl) were purified and linearized. A reduced efficiency of in vitro transcription was reported, when restriction enzymes creating a 3' overhang were used. Therefore, enzymes creating a 5' overhang were used for the

linearization. In case of the plasmid with the CDS of the copper transporter *NheI*, cutting relatively close behind the 5'UTR, was used. *SapI* was used for the digestion of CDS of the ammonium transporter.

Consecutively, mRNA was generated using the mMessage mMACHINE® Kit (Life Technologies), followed by a phenol-chloroform-extraction. The RNA stored at -20°C.

Oocyte-containing follicles were harvested from anesthetized frogs (done by Ingrid Buchwald, Institute for Biophysics, Leibniz University Hannover). Consecutively the oocytes were defolliculated by mechanical disruption and treated for 1.5 h with 120-150 U/ml of collagenase type II (Worthington, Berlin, Germany) in modified Barth medium without Ca²⁺ (88 mM NaCl, 1 mM KCl, 0.82 mM MgCl₂, 6 mM H₂O, 5 mM glucose, 2.4 mM NaHCO₃ and 15 mM HEPES at pH 7.4). 23 nl of the artificial *MtAMT2;4*-mRNA (1.3 µg/µl) were injected into each oocyte, sterile water was injected into control oocytes. For expression, oocytes were incubated at 16°C in modified Barth medium, as detailed before, containing 2.4 mM CaCl₂.

Macroscopic currents were recorded from single oocytes, using the two-electrode voltage clamp technique (TEV) two days after RNA-injection. To that end, they were transferred into a perfusion chamber. 2.5 M KCl were used as buffer for the electrodes. A voltage-clamp amplifier Turbo TEC-10 CD (npi electronic, Tamm, Germany) connected to a computer via an ITC-16 interface (Instrutech, Port Washington, USA) were used. The oocytes were floated with buffer solution, similar to that from Sjøgaard *et al.* [40], (Table 9, A or B), containing no ammonium chloride as a control solution, which was replaced consecutively by different dilutions of a 90 mM ammonium chloride solution (Table 9, A and C or B and D). Stepwise 1:50, 1:20, 1:10, 1:5 and 1:1 dilutions (of Table 9, C or D) were measured. Finally, the 1:50 dilution, resulting in a 1.8 mM ammonium chloride solution was used. Between measurements, the new dilution was floated over the oocytes for at least 3 minutes, to completely exchange media. This was tested with an ink solution before. Solutions with a pH value of 7.2 and 5.5 were used.

Table 9: Media for TEV-clamp measurements of *MtAMT2;4* transfected and control oocytes of *X. laevis*.

A	chemical compound	molecular weight [u]	molarity [M]	volume [l]	weight [g]
	nmdg	195.21	0.09	1	17.5689
Mannitol	182.17	0.02	1	3.6434	
KCl	74.55	0	1	0	
CaCl ₂	147.02	0.002	1	0.29404	
MgCl	203.3	0.002	1	0.4066	
Hepes	238.31	0.01	1	2.3831	
adjust pH with HCl to 7.2					
B	chemical compound	molecular weight [u]	molarity [M]	volume [l]	weight [g]
	nmdg	195.21	0.09	1	17.5689
Mannitol	182.17	0.02	1	3.6434	
KCl	74.55	0	1	0	
CaCl ₂	147.02	0.002	1	0.29404	
MgCl	203.3	0.002	1	0.4066	
Hepes	238.31	0.01	1	2.3831	
adjust pH with HCl to 5					
C	chemical compound	molecular weight [u]	molarity [M]	volume [l]	weight [g]
	NH ₄ Cl ₂	53.49	0.09	1	4.8141
Mannitol	182.17	0.02	1	3.6434	
KCl	74.55	0	1	0	
CaCl ₂	147.02	0.002	1	0.29404	
MgCl	203.3	0.002	1	0.4066	
Hepes	238.31	0.01	1	2.3831	
adjust pH with TRIS-base to 7.2					
D	chemical compound	molecular weight [u]	molarity [M]	volume [l]	weight [g]
	NH ₄ Cl ₂	53.49	0.09	1	4.8141
Mannitol	182.17	0.02	1	3.6434	
KCl	74.55	0	1	0	
CaCl ₂	147.02	0.002	1	0.29404	
MgCl	203.3	0.002	1	0.4066	
Hepes	238.31	0.01	1	2.3831	
adjust pH with TRIS-base to 5.5					

Abbreviations: nmdg, N-Methyl-D-glucamine

Voltage-evoked currents were monitored before and during the application of NH₄⁺. From a holding potential of -60 mV, pulses of -150 mV to +40 mV were applied for 500 ms in 10 mV steps (S1 Fig). The voltage-evoked currents were sampled at 10 kHz. Pulse protocols, data acquisition, and analysis were performed using Pulse/PulseFit (HEKA, Lambrecht/Pfalz, Germany) and OriginPro 7.5 (Microcal Software, Inc, Northhampton, USA). 2% of the measurements at upper and lower border were filtered out. Then steady state currents were evaluated.

Results

The expression of AM-induced membrane transporter genes is dependent on phosphate and nitrogen supply

Based on their expression profile in the *Medicago Gene Expression Atlas* [41], indicating a strong up-regulation in mycorrhized roots [42], four membrane transporter genes were selected, as stated in Chapter I. These represent highly induced subgroups of AM-dependent transporter genes (*MtCopMd1*, *MtOliMd1*, *MtABCG3*, and *MtAMT2;4*) [43] and their expression was measured in different AM scenarios, characterized by different P and N supplies (Fig 2).

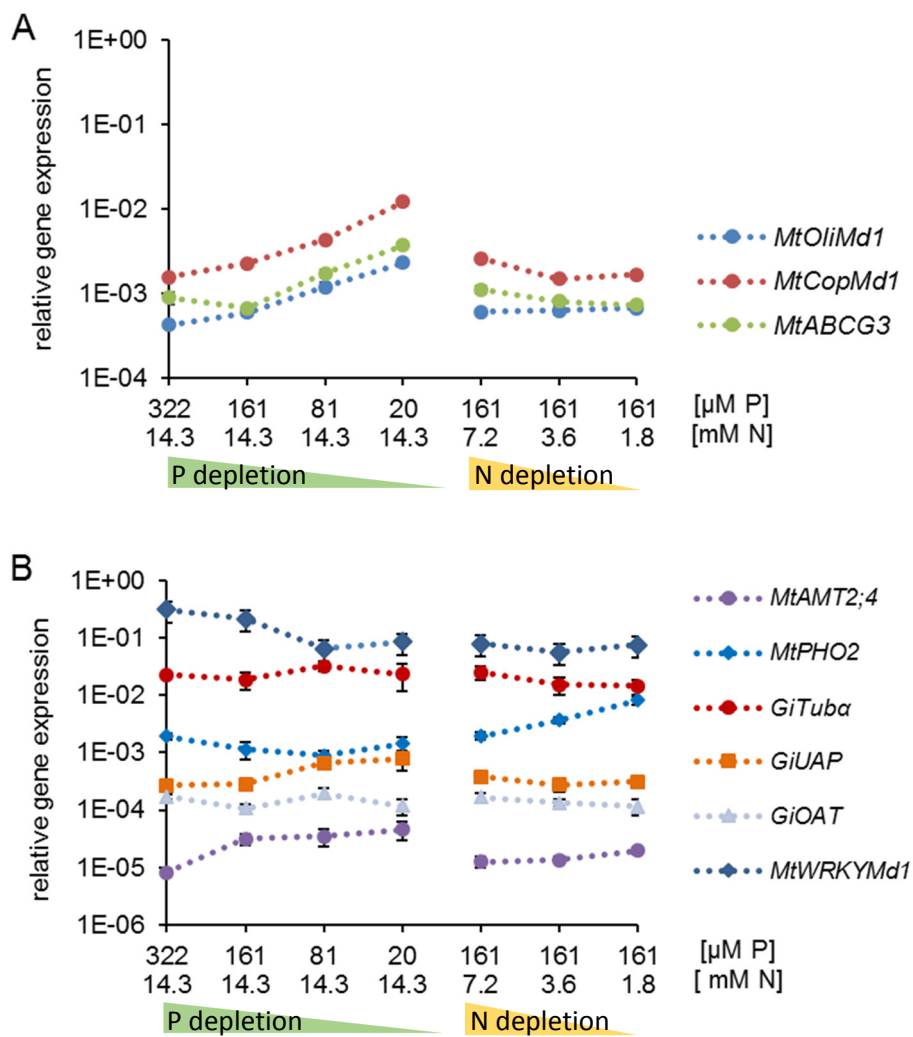


Fig 2: Relative expression of selected AM-related membrane transporter and marker genes in mycorrhized *M. truncatula* roots supplied with phosphate and nitrogen amounts.

Gene expression is given in relation to the expression of *MtTefα*. Pi depletion is indicated with a green triangle and N depletion with a yellow triangle. Plant roots were harvested at 28 days post inoculation with *R. irregularis*. Biological replicates are one pool of six plant roots per treatment. The standard error of the mean of three technical replicates is given. Abbreviations: N, nitrogen; P, phosphate

In general, the transcription of *MtCopMd1*, *MtOliMd1*, and *MtABCG3* was induced with a depletion of phosphate (Fig 2, A). *GiTubα* measurements had a similar expression pattern like *GiOAT*, encoding a fungal ornithyl-acetyl-transferase, being involved in the biogenesis of amino acids, which contribute to fungal nitrogen storage. Whereas the expression of membrane transporters rose with the depletion of P (Fig 2, A and B), the expression of *MtPHO2* and *MtWRKYMd1*, encoding TFs which are possibly involved in phosphate-sensing, as well as the expression of *GiUAP* and *GiOAT* showed another trend. Here, *PHO2* and *MtWRKYMd1* were induced by phosphate excess (Fig 2, B). Since P is no longer the plant growth-limiting factor in a regime of severe N starvation, *MtWRKYMd1* was also strongly induced in this regime (Fig 2, B). *MtAMT2;4* transcript amounts rose with P and N depletion, which matches the expression pattern of *GiUAP*, encoding a fungal protein which supports ureases in converting urea into ammonium and thereby producing a nitrogen source that is transported across fungal and plant membranes at the arbuscule. The experiments further indicated that *MtAMT2;4* as well as *MtOliMd1* in tendency responded to severe N limitation, whereas *MtCopMd1* and *MtABCG3* did not (Fig 2, A). Here, the question of a nitrogen-dependent signaling cascade, which regulates these genes, arises. It can be concluded that on a whole-root level, the expression of four AM-activated membrane transporter genes differentially responds to P and N stresses, induced during the cultivation of the mycorrhized plants.

Functional analysis of the copper, oligopeptide and ABC transporter genes *MtCopMd1*, *MtOliMd1*, and *MtABCG3* in arbuscular mycorrhiza

Expression and *in silico* analyses of the *MtCopMd1*, *MtOliMd1*, and *MtABCG3* genes

The three AM-related membrane transporter genes *MtCopMd1*, *MtOliMd1*, and *MtABCG3* were primarily identified based on their strong up-regulation in mycorrhizal roots [44].

With respect to copper transporters, Senovilla *et al.* [44] recently identified a nodule-specific *M. truncatula* copper transporter gene. Thus, amino acid sequences of *MtCopMd1*, designated MtCOPT2 in [44], and AM-unrelated copper transporters of *M. truncatula* were compared and expression of the gene family during plant root colonization by AMF was monitored (Fig 3).

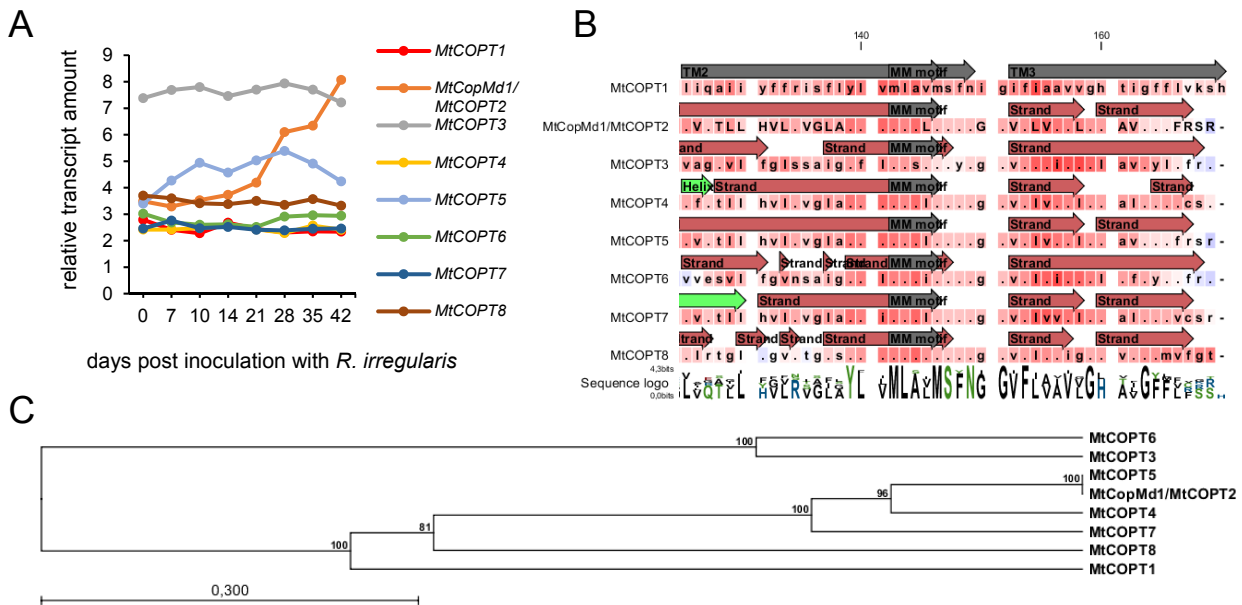


Fig 3: Expression and sequence analyses of MtCopMd1 and AM-unrelated copper transporter genes. Relative gene expression over a time course of root colonization by AMF (A), secondary structures of MtDefMd1-4 and AM-unrelated copper transporters of *M. truncatula* (B), as well as a phylogenetic tree of amino acid sequences (C) are shown. The annotated amino acid sequences were aligned based on their secondary structures. Then, corresponding sequences from the second to the third transmembrane region of MtCOPT1 were shown. Those transmembrane regions as well as the MM motif are marked in grey, whereas as predicted β -strands or α -helices were depicted above the sequences in red and green, respectively. Background colorization of the amino acids (in B) indicate hydrophobicity in a scale from red to blue (red: high hydrophobicity). In A, relative gene expression, as Bi-weight log₂ average signals are shown. Data in A are from an expression time course of *M. truncatula* mycorrhized roots, ranging from 0 to 42 dpi (Rico M. Hartmann, LUH, unpublished). The copper transporters and their genome identifiers are as follows MtCOPT1 (*Medtr4g019870.1*), MtCopMd1/MtCOPT2 (*Medtr7g066070.1*), MtCOPT3 (*Medtr3g105330.1*), MtCOPT4 (*Medtr4g064963.1*), MtCOPT5 (*Medtr4g065660.1*), MtCOPT6 (*Medtr1g015000.1*), MtCOPT7 (*Medtr4g065123.1*), and MtCOPT8 (*Medtr0027s0220.1*). Abbreviation: TM, transmembrane; M, methionine

Whereas *MtCOPT1* expression was shown to be nodule-specific [44], *MtCopMd1* was the only *MtCOPT* gene of *M. truncatula* induced during root colonization by AMF (Fig 3, A). The essential transmembrane domains two and three (Fig 3; B, TM2 and TM3), including the MM motif vital for copper transport, are structurally conserved in MtCopMd1 (Fig 3, B). An alignment, based on amino acid sequences, indicated that in contrast to gene sequences, MtCOPT5 and MtCopMd1 are most similar (Fig 3, C). To further investigate secondary structures of AM-related membrane transporters and identify similarities, such as transmembrane regions and signal peptides, their deduced amino acid sequences were analyzed with *InterProScan* (Fig 4).

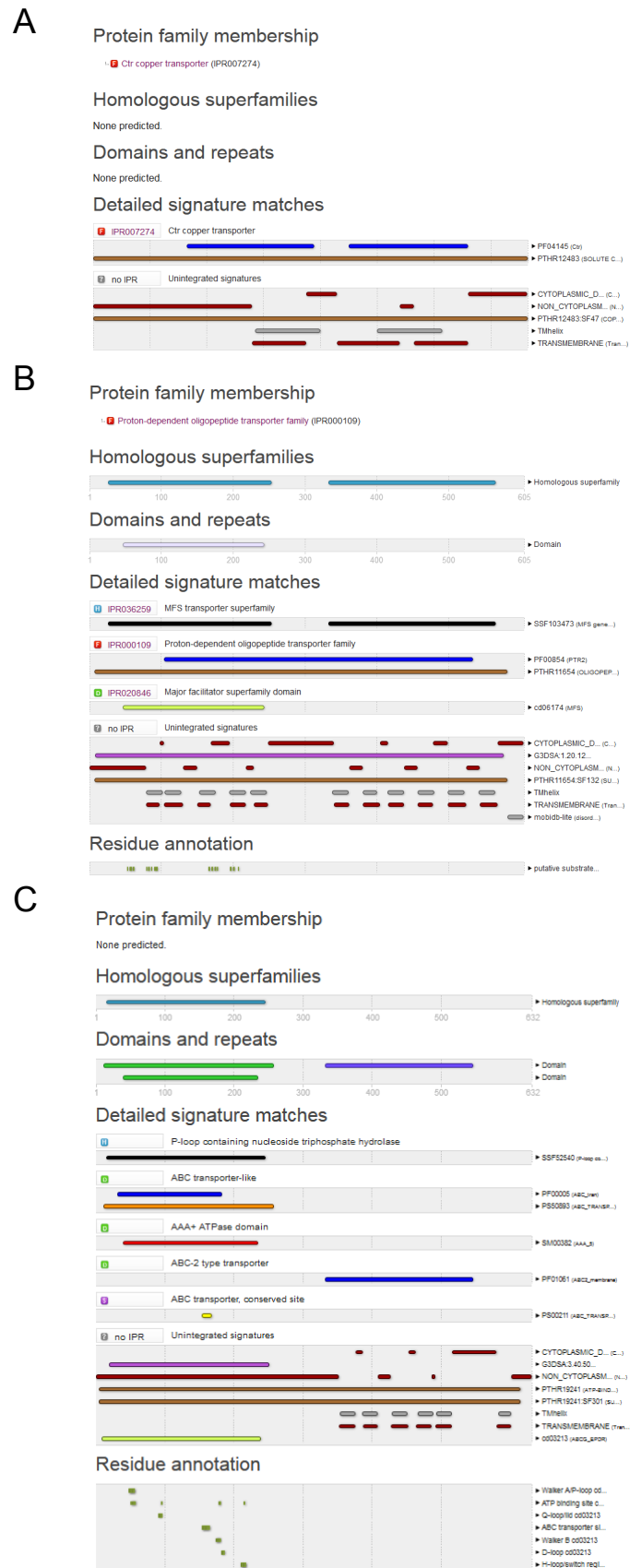


Fig 4: *In silico* analysis of MtCopMd1, MtOliMd1 and MtABCG3.

The deduced amino acid sequences of MtCopMd1 (A), MtOliMd1 (B), and MtABCG3 (C) was analyzed with *InterProScan* [24] using standard settings. Annotations were colored by source database.

Two to three transmembrane helices were detected in the amino acid sequence of *MtCopMd1* (Fig 4, A). A central region of the membrane transporter is potentially cytoplasmic, whereas the N terminus was predicted to be non-cytoplasmic (Fig 4, A). Concerning *MtOliMd1*, InterProScan predicted 11 transmembrane helices and a central, as well as a C terminal cytoplasmic domain of the protein (Fig 4, B). Furthermore, two domains also found in major facilitator superfamily (MFS) proteins were detected (Fig 4, B). Sequence analysis of *MtABCG3* indicated an ATPase region, a p-loop, containing a nucleoside triphosphate hydrolase, at the N terminus of the protein, being most likely not cytoplasmic (Fig 4, C). In addition, a cytoplasmic region close to the C terminus was predicted, whereas the actual C terminus was annotated as not cytoplasmic (Fig 4, C), eventually shedding light on the protein localization in membranes and its organizations as potential multimer.

In conclusion, the three AM-induced membrane transporter genes *MtCopMd1*, *MtOliMd1*, *MtABCG3*, and *MtAMT2;4* show, apart from expected features, such as transmembrane domains and features of associated superfamilies, such as ATPase- and MFS domains, similarities in C terminal located cytoplasmic regions. In contrast, a conserved AM-related signal peptide was not identified.

The AM-induced copper, oligopeptide, and ABC transporter genes *MtCopMd1*, *MtOliMd1*, and *MtABCG3* display a different spacio-temporal expression

To investigate the regulation of AM-related membrane transporter genes in a spacio-temporal manner, promoter *gusAint* fusions were used. Since a promoter *gusAint* fusion of the *MtAMT2;4* gene has already been generated and was shown to be expressed with the establishment of the first arbuscules [32], the *MtCopMd1*, *MtOliMd1*, and *MtABCG3*, were now in focus. Transgenic roots of *M. truncatula* A17 wild type plants expressing promoter *gusAint* fusions were mycorrhized for 42 dpi and analyzed via GUS- and Alexa-WGA Fluor⁴⁸⁸ staining (Fig 5).

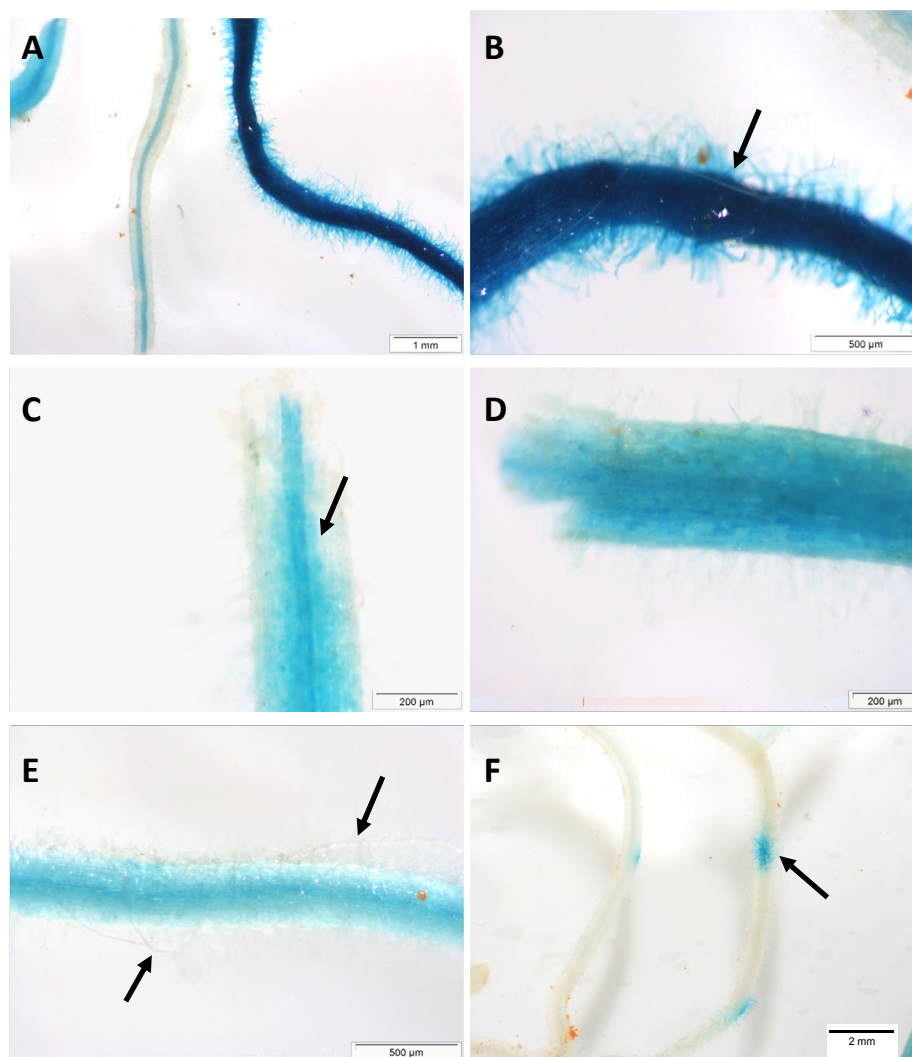


Fig 5: Mycorrhized *M. truncatula* roots expressing an *MtCopMd1-gusAint* fusion. Micrographs of GUS-stained roots are shown. Arrows indicate fungal hyphae (B and E), staining in the inner (C) or outer cortex of the root (F).

The expression of the *pMtCopMd1-gusAint* fusion led to a divergent expression pattern (Fig 5, A-F). After staining for eight hours, it was observed that roots with a homogenous dark GUS staining were colonized by fungal structures (Fig 5, E, black arrow). There were, however, prominent differences in the staining intensity (Fig 5, A, B). In several roots, dark blue spots were observed, which could either be the response of a local mechanical stress, or a local change in gene expression within the rhizodermal cell layer (Fig 5, F, black arrow). There was a slightly stronger staining in the inner cortex, the tissue with arbuscules (Fig 5, C).

It can be concluded that *MtCopMd1* expression is AM-induced but not strictly correlated to the presence of AM-fungal structures.

The promoter of the oligopeptide transporter gene *MtOliMd1* led to a different GUS-staining pattern (Fig 6).

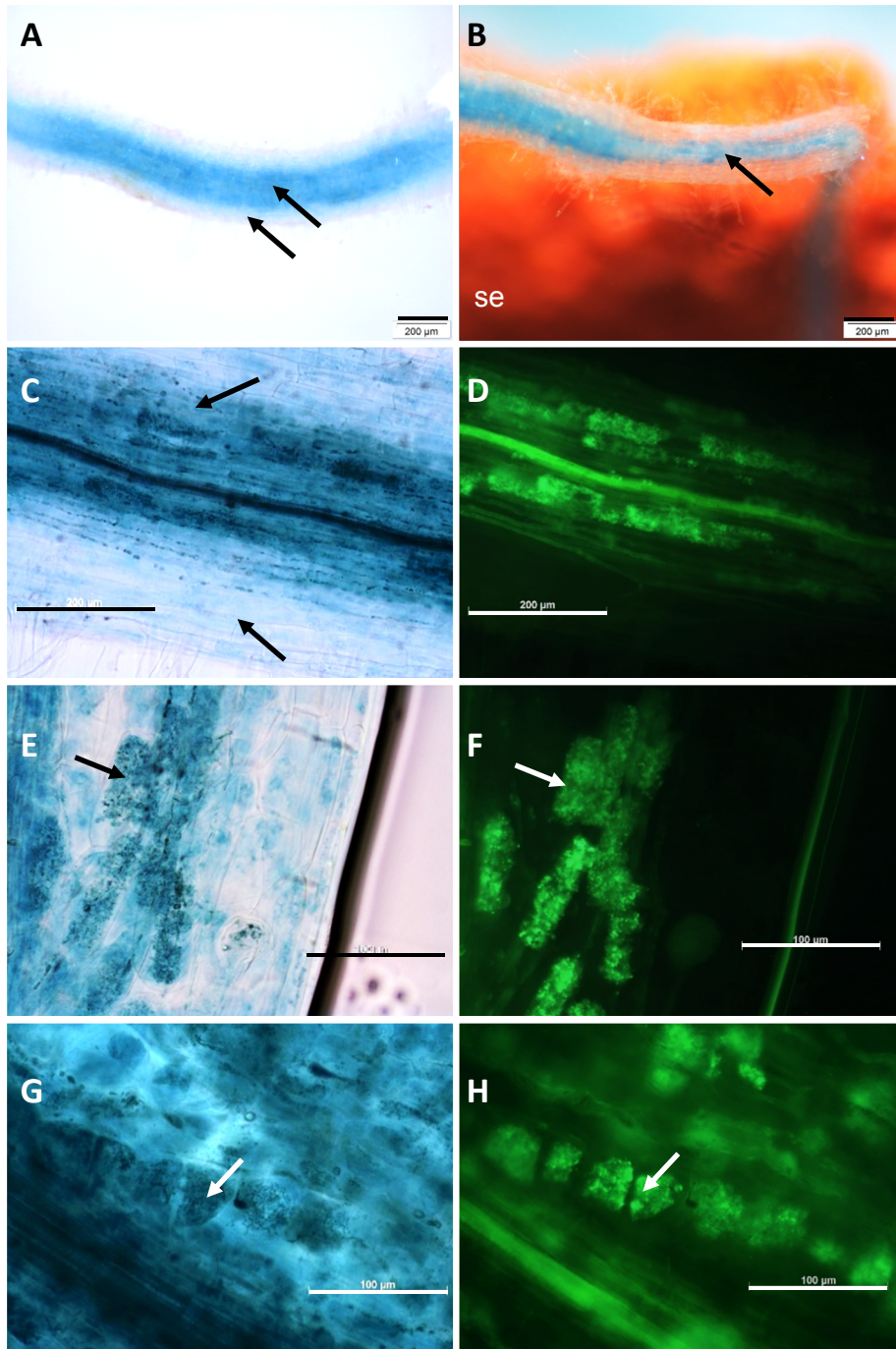


Fig 6: Mycorrhized *M. truncatula* roots expressing an *MtOliMd1-gusAint* fusion.

Micrographs of GUS-stained roots (A, B, C, E, and G) and corresponding WGA-Alexa 488 stainings (D, F, and H) are shown. Arrows indicate staining differences in the inner and outer cortex of the root (A, B and C), or staining in arbuscule-harboring cells (E-H). Abbreviations: se, Seramis particle

After over night staining, the blue coloration seemed most intense in cells of the inner cortex (Fig 6, A and B, black arrows), as it could be expected if the gene product was built in arbuscule-containing cells. Those showed an enhanced activity of the promoter, which apparently exceeded the staining intensity in comparison to neighboring cells (Fig 6, E-H, white arrows). In addition to those cells, also in the outer

cortex of the root, a slight GUS staining was detected (Fig 6; A, C). In conclusion, *MtOliMd1* expression is correlated to AM-fungal structures and is amplified in arbuscule-harboring cells.

The *MtABCG3*-promoter activity was different to the two genes studied before (Fig 7).

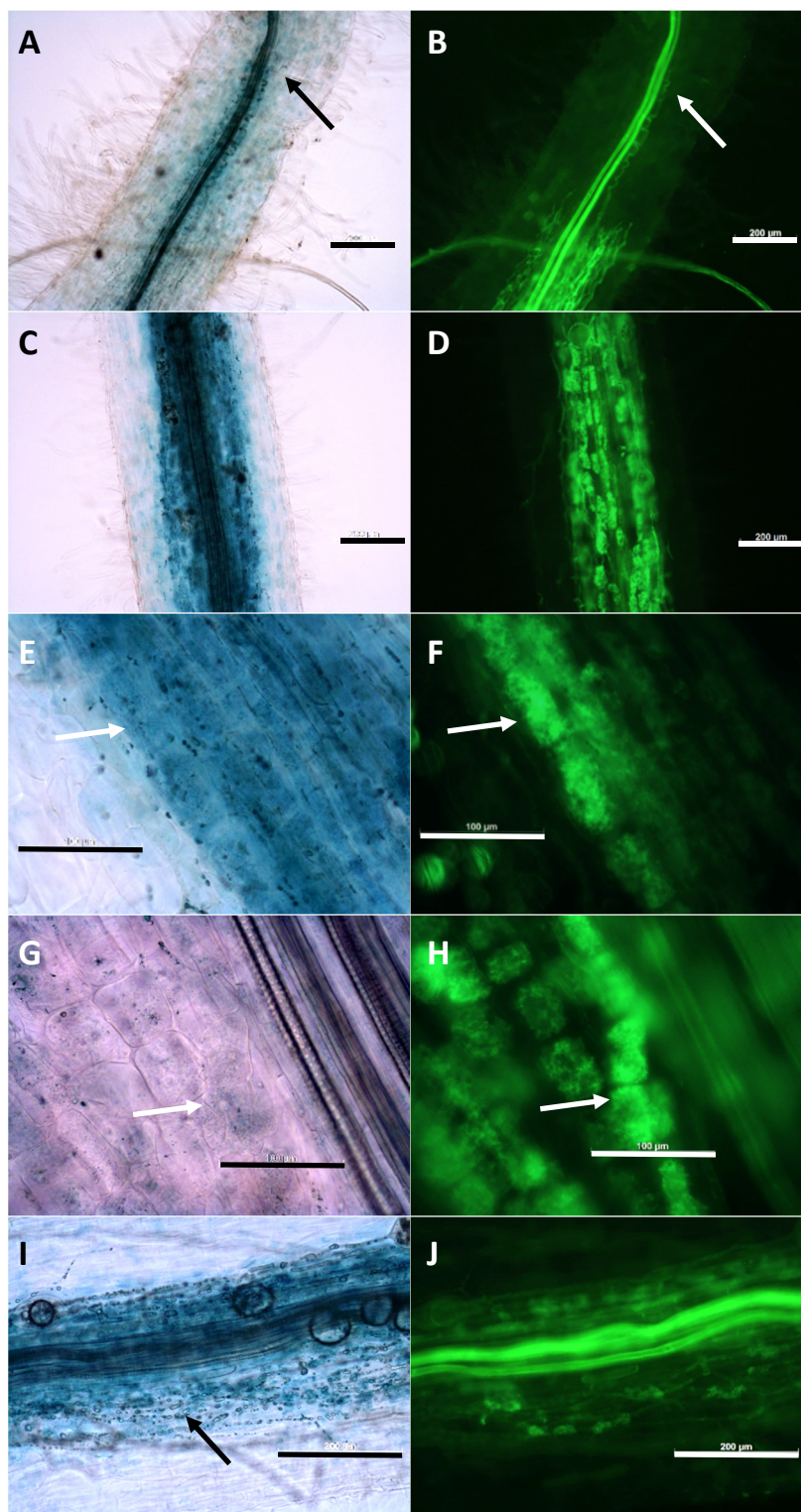


Fig 7: Mycorrhized *M. truncatula* roots expressing an *MtABCG3-gusAint* fusion. Micrographs of GUS stained roots (A, C, E, G, and I) and corresponding WGA-Alexa 488 stainings (B, D, F, H, and J) are shown. Arrows indicate staining differences in the inner cortex of the root (A, E, G, I), or staining in arbuscule-harboring cells (E-H).

Blue staining accompanied and slightly preceded the spreading of intraradical hyphae (Fig 7, A and B, arrows). This basal expression level, which was detectable after over night staining, then rose in arbuscule harbouring cells (Fig 7 C-F, white arrows). However, also surrounding cells of the inner roots cortex were slightly stained (Fig 7, C-F). In root sections that were colonized by older infection units, characterized by a high amount of lipid droplets in fungal hyphae and by the presence of vesicles, the staining intensity was reduced (Fig 7, I-J). Moreover, it was evident that the promoter activity in arbuscule harbouring cells varied to some extent (Fig 7, compare E-H, white arrows).

In conclusion, the expression of *MtABCG3* correlated with the establishment and development of fungal structures inside the root cortex.

Knockdown of the oligopeptide and ABC transporter genes *MtOliMd1* and *MtABCG3* affects AM marker gene expression

Artificial miRNAs are a tool that can be used to selectively knock down single (membrane transporter) genes [34]. Since *MtOliMd1* and *MtABCG3* expression was better correlated with fungal structures, this technique was applied to address the question, if *MtOliMd1* and *MtABCG3* are vital for the symbiosis. For the construction of vectors encoding an artificial micro RNA, gene-specific 21 bp oligonucleotides were cloned into a precursor, containing the sequence of a stem and loop enriched structural backbone of a native miRNA. One construct targeting *MtOliMd1* and a construct targeting *MtABCG3*, as well as a control construct were expressed in mycorrhized *M. truncatula* roots (Fig 8).

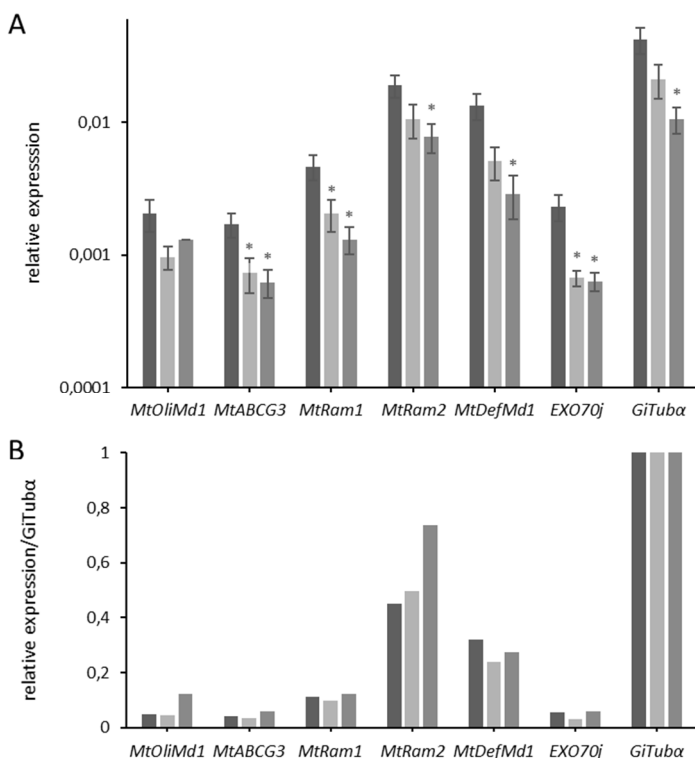


Fig 8: Relative expression of *MtOliMd1*, *MtABCG3*, and selected AM marker genes in mycorrhized amiRNA and control roots of *M. truncatula*.

Transcript amounts are shown relative to *MtTefα* (A) and were additionally normalized by building a ratio to *GiTubα*-expression (B). Measurements from amiRNA:*MtOliMd1* roots are colored in light grey, amiRNA:*MtABCG3* roots in medium grey, and corresponding amiRNA:*GUS* control measurements in dark grey. Roots were harvested at 28 days post inoculation with *R. irregularis*. n=12 biological replicates, depicted is the standard error of the mean. Statistical significances: * p<0.05, ** p<0.005

The transcript amounts of both genes were reduced in amiRNA roots in comparison to control roots (Fig 8, A, B). Whereas a reduction of ~50% of *MtOliMd1* expression in the corresponding amiRNA-roots was not significant, the reduction of ~30% *MtABCG3* in the corresponding amiRNA-roots expression was significant (Fig 8, A). The AM marker gene *MtRam1*, encoding a central GRAS TF controlling arbuscule development, was significantly downregulated in amiRNA:MtOliMd1- and amiRNA:MtABCG3 roots in comparison to control roots (Fig 8, A). *MtRAM2*, an *MtRAM1*-regulated lipid biosynthetic enzyme, which presumably assists in the production of β -monoacylglycerole (β -MAG) supplied to AMF [45], was significantly downregulated in amiRNA:MtABCG3 roots as well (Fig 8, A). This was also the case for the mycorrhiza-dependent defensin gene *MtDefMd1* and the EXOCYST gene *EXO70j* (Fig 8, A). Since *GiTub α* , a marker gene for fungal mass [46], was also differentially expressed in amiRNA roots (Fig 8, A), there is an indication of an altered root colonization by AMF, which could be either the cause or an effect of the measured differences.

It was thus attempted to normalize gene expression to the extent of root colonization by building a ratio with the *GiTub α* -expression (Fig 8, B). Doing so, *MtRAM2*-measurements in amiRNA:MtABCG3 roots peaked out, by being ~30% higher than in the control roots (Fig 8, B). In tendency, also *MtOliMd1* in relation to fungal *GiTub α* expression was enhanced (Fig 8, B). The enhanced *MtRAM2*-transcription could be a mechanism of compensation for a reduced level of MtABCG3 formation at the plant-fungal interface. Since a function of MtABCG3 in the delivery of fatty acids to the microsymbiont is proposed [43], this could imply the existence of an active amiRNA construct and a counteraction of the plant root by enhancing the relative activity of *MtRAM2*, encoding a key enzyme in the preface of fatty acid delivery towards the AM-fungi [45].

On the morphological level, a comparable mixture of root sections with small and scarce arbuscules (Fig 9; A, b; B, b and C, b) as well as areas with a high density of expanded, mature-appearing, arbuscules (Fig 9; A, d; B, d and C, d) was observed by a microscopic analysis of WGA-Alexa Fluor 488-stained amiRNA- and control roots (Fig 9). This indicates that none of the *MtOliMd1* and *MtABCG3* knockdowns resulted in a major AM-related phenotype.

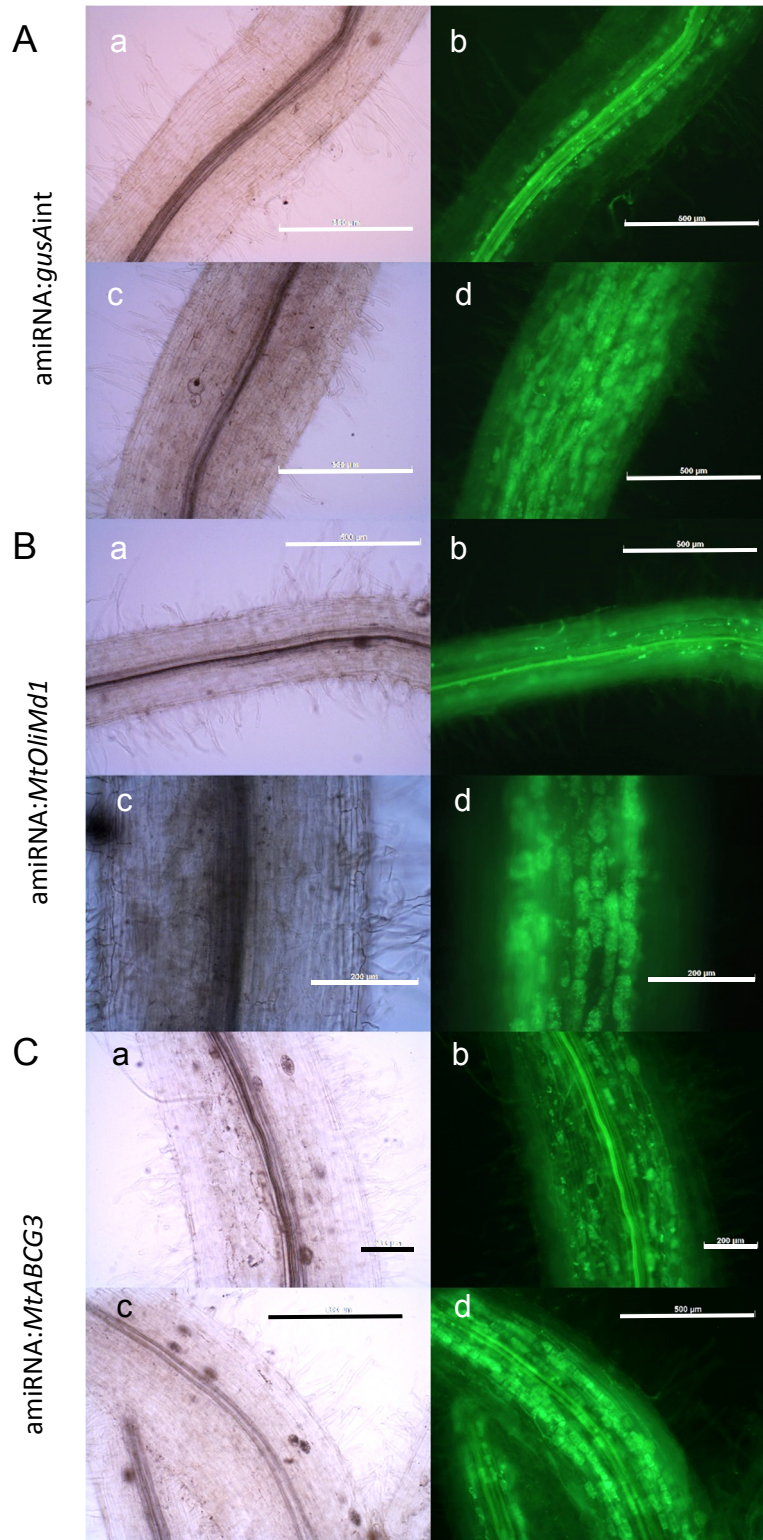


Fig 9: AM-phenotype of amiRNA:*MtOliMd1*, amiRNA:*MtABCG3*, and amiRNA:*gusAint* roots of *M. truncatula*.

The AM-phenotype in amiRNA:*gusAint* (A), amiRNA:*MtOliMd1* (B) and amiRNA:*MtABCG3* (C) transformed *M. truncatula* roots is shown. Bright field- (A, a and c; B, a and c; C, a and c) and WGA-Alexa Fluor 488 micrographs (A, b and d; B, b and d; C b and d) are shown. Plants were harvested after 42 dpi with *R. irregularis*.

Functional analysis of the ammonium transporter gene *MtAMT2;4* in arbuscular mycorrhiza

Knock-down of *MtAMT2;4* under nitrogen limitation does not affect AM marker gene expression

Since *MtAMT2;4* promoter activity coincided with the establishment of the first arbuscules at young AM-infection sites [32], it has been examined in a previous study, if a knock-down would affect the expression of AM marker genes. To reduce the transcription of *MtAMT2;4*, an RNAi construct, targeting a central region of the CDS, had been expressed in mycorrhized transgenic *M. truncatula* roots [32]. However, no significant knock-down of selected AM marker genes was found in mycorrhized RNAi-roots in comparison to wild type roots that were fertilized with half-strength Hoagland's solution [32]. To address the response of the *MtAMT2;4* promoter activity to nitrogen-limiting conditions, plants were supplied with a low amount of nitrogen. These tissues and samples from control roots transformed with an empty vector were studied for the expression of *MtAMT2;4* and selected AM marker genes (Fig 10).

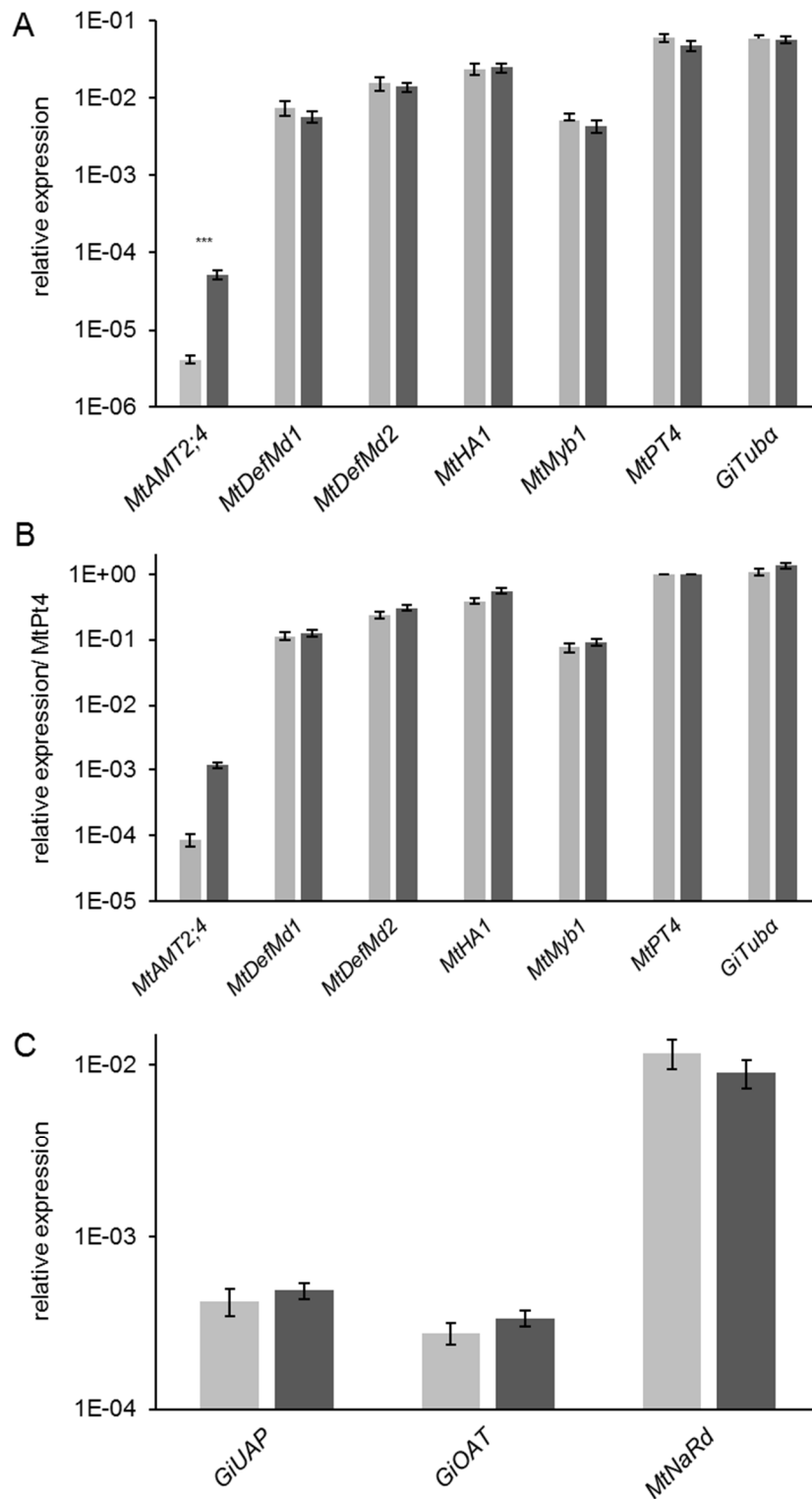


Fig 10: Relative expression of *MtAMT2;4* and selected AM marker genes in mycorrhizal RNAi:*MtAMT2;4* and RNAi:*gusAint* roots of *M. truncatula* under nitrogen limitation.

Transcript amounts are shown relative to *MtTefα* (A and C) and were additionally normalized by building a ratio to *MtPt4*-expression (B). Measurements from RNAi:*MtAMT2;4* roots are colored in light grey, corresponding RNAi:*gusAint* control measurements in dark grey. Roots were harvested at 28 days post inoculation with *R. irregularis*. n=12 biological replicates, depicted is the standard error of the mean. Statistical significances: * $p \leq 0.05$, ** $p \leq 0.005$

Since *MtAMT2;4* expression was knocked down to approximately 8%, only residual amounts of *MtAMT2;4* transcripts remained (Fig 10, A). The expression of the AM marker genes *MtDefMd1*, *MtDefMd2*, *MtHA1*, *MtMyb1*, *MtPt4*, and *GiTuba* did not differ significantly between RNAi and control roots (Fig 10, A and B). When normalized to the number of active arbuscules by building a ratio to *MtPt4*-expression (Fig 10, B), the reduction of *MtAMT2;4* transcript amounts remained significant. This was also observed, when transcript levels were normalized to fungal presence by building a ratio to *GiTuba* expression (not shown). Since the expression of *GiUAP* and *GiOAT*, fungal genes that relate to shuffling and storage of nitrogen compounds towards the symbiotic interface in fungal hyphae were not affected, there might exist other ammonium transporters, such as *MtAMT2;3* [47], that enable nitrogen exchange. In addition, the expression of the plant nitrate-reductase (*MtNaRd*) under investigation was not altered (Fig 10, C).

To study the activities of the AM-dependent membrane transporter genes described above, the expression of *MtOliMd1*, *MtCopMd1* and *MtABCG3* were measured in *MtAMT2;4*-RNAi roots (Fig 11). Their expression was not affected congruent to the measurements of AM marker genes (fig 11).

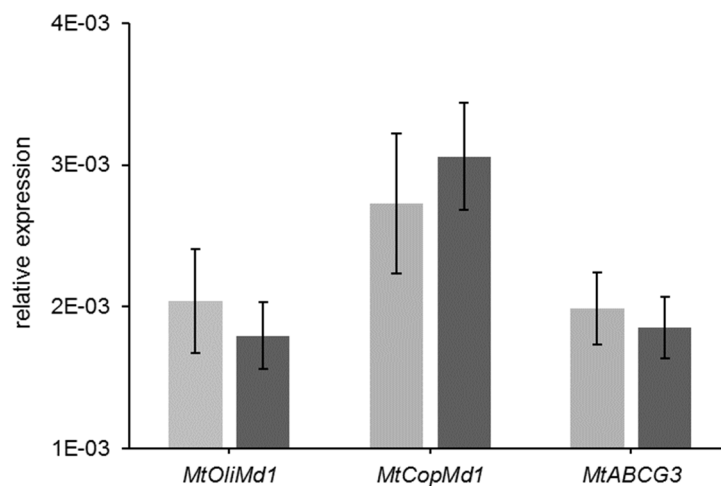


Fig 11: Relative expression of selected membrane transporter genes in mycorrhized RNAi:*MtAMT2;4* and RNAi:*gusAint* roots of *M. truncatula* under nitrogen limitation.

Transcript amounts are shown relative to *MtTefα*. Measurements from RNAi:*MtAMT2;4* roots are colored in light grey, corresponding RNAi:*gusAint* control measurements in dark grey. Roots were harvested at 28 days post inoculation with *R. irregularis*. n=12 biological replicates, depicted is the standard error of the mean.

Since the severe knock-down of *MtAMT2;4* did not lead to significant changes in AM-related gene expression, it was concluded that the ammonium transporter is not essential for the formation of active, nitrogen-transporting arbuscules. However, it was shown that the expression of *MtAMT2;4* is dependent on the N-supply during plant cultivation.

Heterologous translation of *MtAMT2;4* in oocytes of *X. laevis* indicates ammonia as potential substrate

The working mode of many AM-related membrane transporters is still in dispute. Therefore, a technique that allows to monitor ion transport across a membrane could provide new insights. As the AM-dependent transporter *MtAMT2;4* is an electrogenic transporter, its activity can be measured by injecting mRNA into *X. laevis* oocytes and applying the Two-electrode-voltage clamp technique. Thus, *MtAMT2;4*-mRNA was generated via *in vitro* transcription and subsequently checked in a non-denaturing agarose gel (Fig 12).

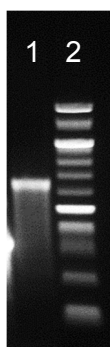


Fig 12: *In vitro* transcribed *MtAMT2;4*-mRNA.

Agarose gel-electrophoresis of the product of an *in vitro* transcription of *MtAMT2;4* is shown. Lane 1-2, from left to right: 1 μ l *MtAMT2;4*-transcript and 3 μ l 100 bp ladder.

The artificial mRNAs of *MtAMT2;4* had the expected length of 1.44 kb plus UTR sequences (Fig 12, lane 1). Consecutively, the heterologous expression experiment was set up with *MtAMT2;4*-mRNA transfected oocytes. The electric potential between in- and outside of the oocyte was measured in response to the supply of NH_4^+ (S1 Fig). Substrate amounts of 0 and 1.8 mM ammonium in a milieu of pH 5.5 and 7.2 were applied to the clamped oocytes and electrogenic fluxes between the two compartments were measured (Fig 13).

The control- and transfected oocyte's membranes responded with a similar inward current in response to alternating negative membrane potentials at pH 7.2 (Fig 13, A). The addition of NH_4^+ to the media did not significantly alter the currents. However, at pH 5.5 the currents induced by depolarizing voltages of control- and transfected oocyte's were higher (Fig 13, B). Apparently, the floating buffer led to slightly increased influx of ions in transfected oocytes at negative membrane potentials (Fig 13, B). The induction at acidic pH was ~ 5 fold for control- and ~ 7 fold for transfected oocytes, which is comparable to results obtained by S \ddot{o} gaard *et al.* [40].

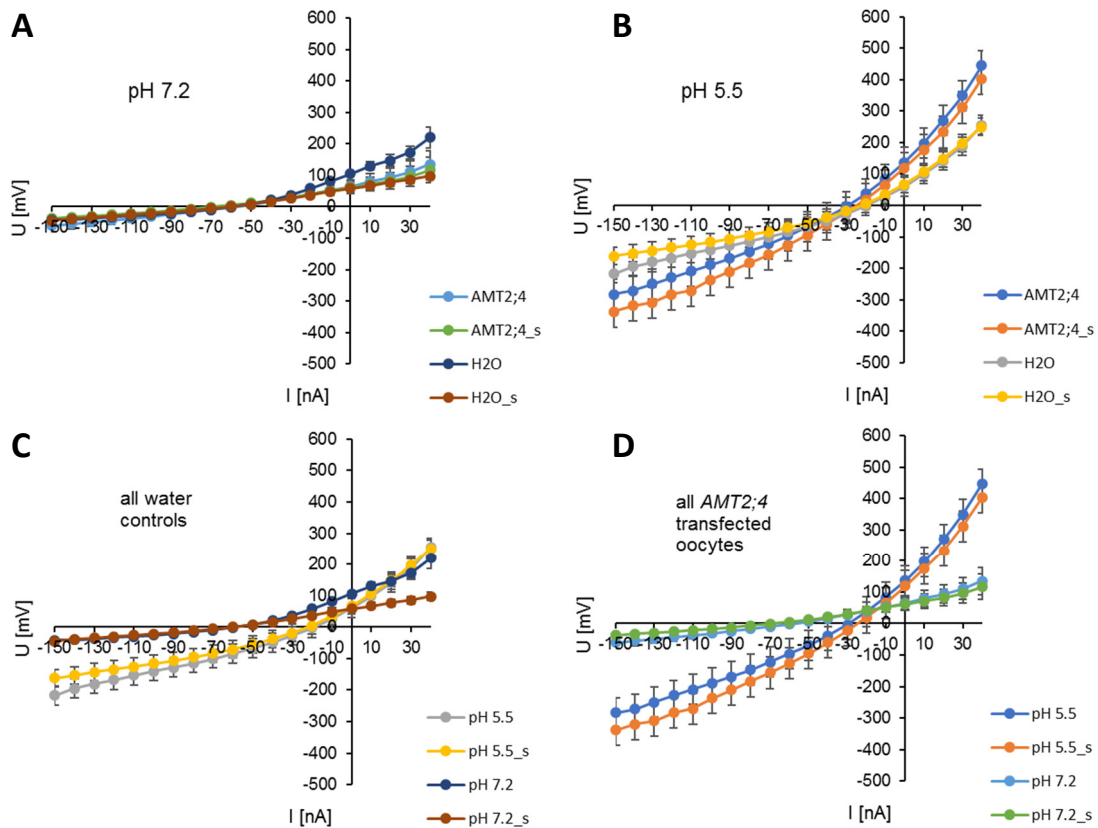


Fig 13: The pH-dependence of steady state currents in *MtAMT2;4* transfected and control *X. laevis* oocytes with and without NH_4^+ .

The mean of steady state currents of three consecutive measurements is shown. Measurements at pH 7.2 (A), pH 5.5 (B), of control (C) and *AMT2;4*-transfected oocytes (D) are depicted. Currents were recorded prior and during the addition of NH_4^+ , after floating the chamber for three minutes. Media with a pH of 7.2 and 5.5 were tested. Error bars represent the standard error of the mean. $n = 3-5$. Abbreviations: s, 1.8 mM NH_4^+ added

Nevertheless, currents induced in the control oocytes were comparable (Fig 13, B). The small differences between measurements with and without ammonia are possibly caused by only small currents being induced (Fig 13).

In conclusion, the question if *AMT2;4*-transfected oocytes translated *MtAMT2;4*-transcripts and were able to transport NH_4^+ requires more detailed investigations.

Localization of *MtAMT2;4*-GFP and subcellular markers in AM roots

It was described that *MtAMT2;4* is expressed in infection units as soon as the first arbuscule is established [32]. Semi-quantitative RT-PCR measurements further indicated that the gene activity rises, if plants were supplied with low amounts of N. Nevertheless, no hints for a disturbed PAM-biogenesis or -function, concluded from the knockdown of expression of selected AM marker genes, were detected in *RNAi:MtAMT2;4*-roots (Fig 10 and Fig 11). However, adaptations of transport processes in symbiotic plant cells remained unaddressed in those experiments. It was thus aimed to compare protein localization of *MtAMT2;4* with that of cell organelle markers in mycorrhizal roots.

To do so, reporter gene fusions consisting of a GFP-variant fused to the signal peptide of plasma membrane, endoplasmic reticulum or Golgi apparatus under the control of a double 35S-promoter were used. They were expressed in mycorrhizal transgenic roots and confocal microscopy was used to locate GFP fluorescence in the outer and inner root cortex (Fig 14).

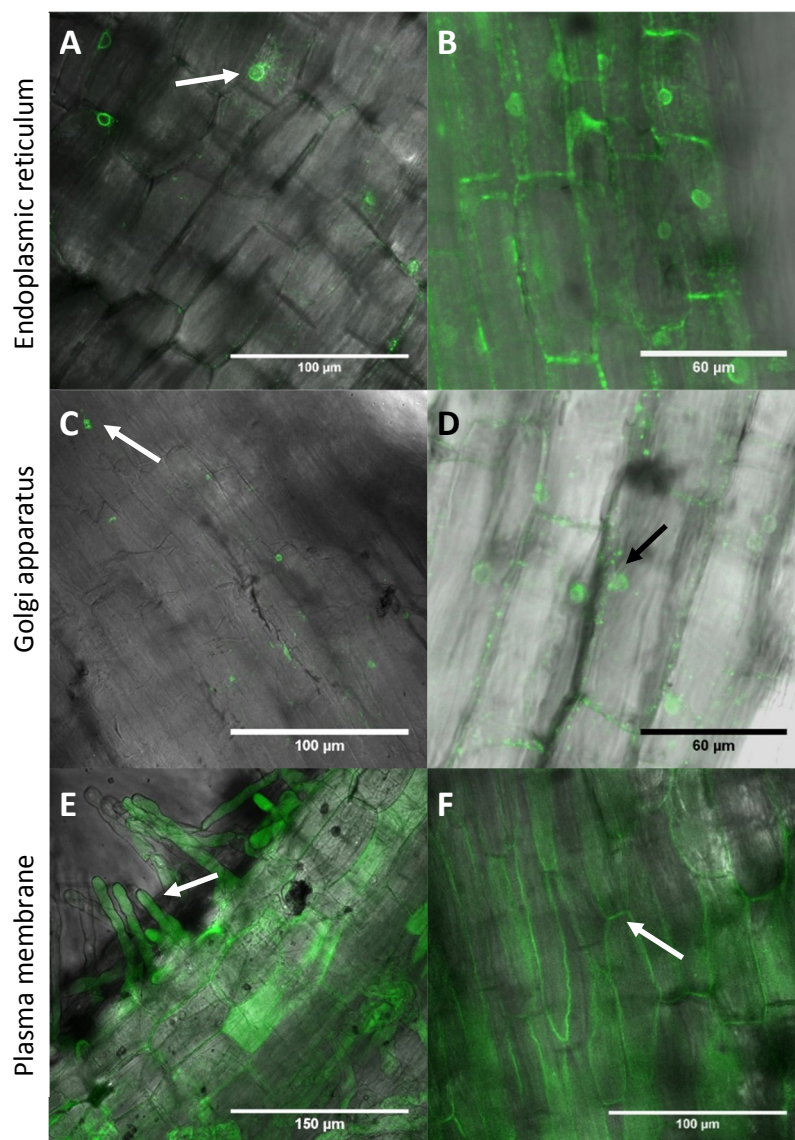


Fig 14: GFP localization of endoplasmic reticulum, Golgi apparatus, and plasma membrane in mycorrhizal *M. truncatula* roots.

Overlays of GFP-fusions and differential interference contrast micrographs of razor blade hand-cut sections of transgenic *M. truncatula* roots are shown. The roots expressing a marker for the endoplasmic reticulum (A and B), a marker for the Golgi apparatus (C and D), and a plasma membrane marker (E and F) were documented 30-47 days post inoculation with *R. irregularis*. Arrows indicate structures that were referred to in the text. n=15

Since these constructs were originally designed for the analysis of cell organelles in *Arabidopsis thaliana*, their functionality in *M. truncatula* had to be verified. For the ER-marker a spider-like web (Fig 14, A) around the nucleus as well as granular bodies at the edges of the cells (Fig 14, B) were expected [48]. The latter is also true for the Golgi-marker, with tinier, more loosely arranged spots

(Fig 14, C and D). In roots transformed with a plasma membrane marker, the shape of the cells should be stained (Fig 14, E and F) as the central vacuole occupies the biggest part of the cells volume. A high signal in root hairs was in addition monitored (Fig 14, E).

It can be concluded that the used *A. thaliana* cell organelle markers are also suitable for the analysis of cellular structures in *M. truncatula*. For a colocalization with AM-dependent membrane transporters, the ER-marker seemed to be most promising, since it could display a redirection of the secretion apparatus, which is characteristic for symbiotic cells [6], without being restricted to symbiotic cells. Since it was aimed to use mGFP6 [37] for translational fusions with AM-related membrane transporters, another fluorophore, RFP, fused to the ER-signal peptide was then tested. *M. truncatula* wild type plant were transformed with the RFP reporter construct to monitor the ER in arbuscule containing cells of mycorrhized roots, to prove if a redirection of the intracellular targeting would be apparent (Fig 15).

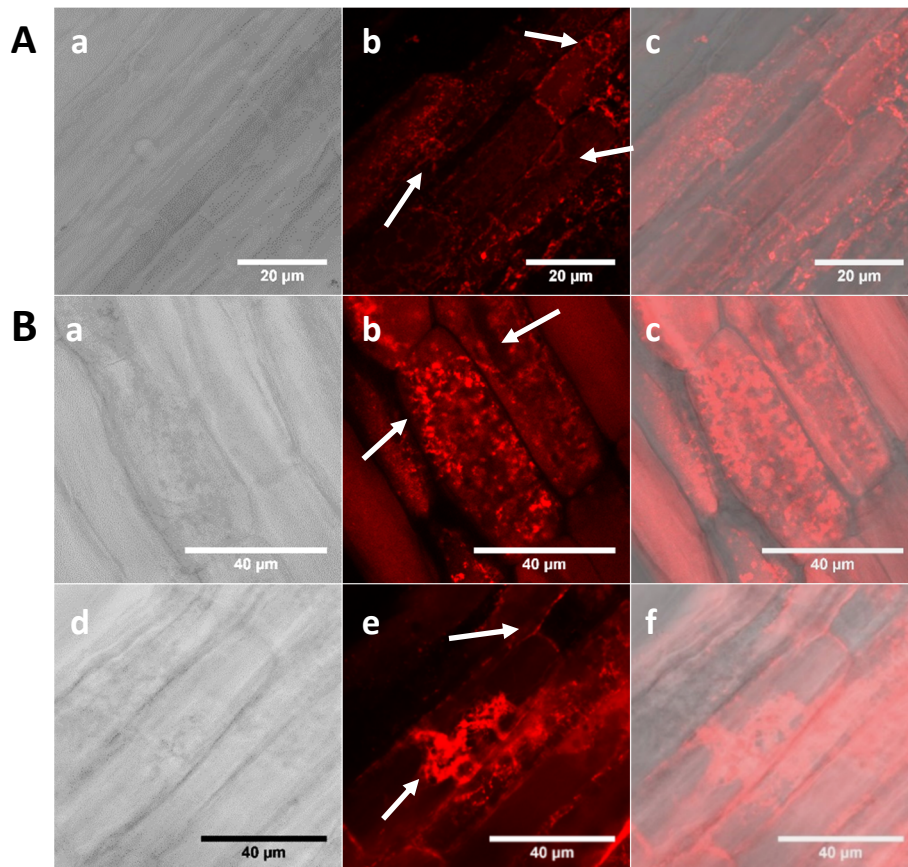


Fig 15: Localization of the endoplasmic reticulum in mycorrhized *M. truncatula* roots.

Non-symbiotic cells (A) and arbuscule-harboring cells (B) of the inner root cortex of *M. truncatula* are displayed. Differential interference contrast micrographs (A, a; B, a and d) and signals of RFP- (A, b; B, b and e), as well as overlays (A, c; B, c, f), generated by confocal microscopy of razor blade hand-cut sections of transgenic *M. truncatula* roots are shown. The roots were documented six weeks post inoculation with *R. irregularis*. Arrows indicate structures referred to in the text. n=15

As expected, a spider web structure surrounding the nucleus in addition to granular bodies at the edges of the cells was found (Fig 15, A, white arrows). In contrast, arbuscules were enclosed by a high density of ER-derived structures (Fig 15, B, white arrows). Thus, a shift in ER presence allowed a differentiation between arbuscule-harboring and uninfected cells.

In conclusion, the marker could -in combination with other translational fusions- be used as tool to monitor processes at the AM-interface.

To study the colocalization of *MtAMT2;4*, the coding region was fused in frame to *mGFP6* [37] (S3 Fig). Since previous studies indicated that the native *MtAMT2;4* promoter is probably too weak to support protein localizations in AM roots [32], *MtAMT2;4* was constitutively expressed in AM-roots, using the 35S promoter. Due to a signal peptide at the N-terminus and several membrane-spanning regions, *in silico* detected by *InterProScan* (S2 Fig), it was decided to fuse the mGFP6 at the C-terminus (S3 Fig). The translational fusion was transferred into the vectors pRedRoot and pBIN:ER-rk, the latter also encoding an endoplasmic reticulum (ER) RFP-marker [38]. Fluorescence- and confocal microscopy was then used for a measurement of dsRed or RFP and GFP fluorescence in the inner cortex of transgenic, mycorrhized *M. truncatula* roots (Fig 16).

Although ubiquitin- and 35S-promoter were not equally active in the inner root cortex, the emission of dsRed and GFP peaked in the arbuscule-containing cells, whereas the fluorescence levels from the outer root layers were lower in comparison (Fig 16, A). *MtAMT2;4*-mGFP6 co-located with fungal structures, while dsRed remained in the cytosol or the vacuolar space (Fig 16, A, c and d). Occasionally trunk regions were found mGFP6 positive, despite fluorescence levels being elevated in distal areas of the arbuscules, (Fig 16, B, a and b). These signals differed from the ER marker, which displayed spots in close proximity to the PAM of arbusculated cells (Fig 16, B, a). Via time-lapse imaging signals of *MtAMT2;4*-mGFP6 were found to last for more than 96 min. (Fig 16, C), indicating the possibility of a successive photo-documentation of AM-colonized root sections in *M. truncatula* could be performed. Taken together, the findings suggest that the ammonium transporter *AMT2;4* is located in the periarbuscular membrane.

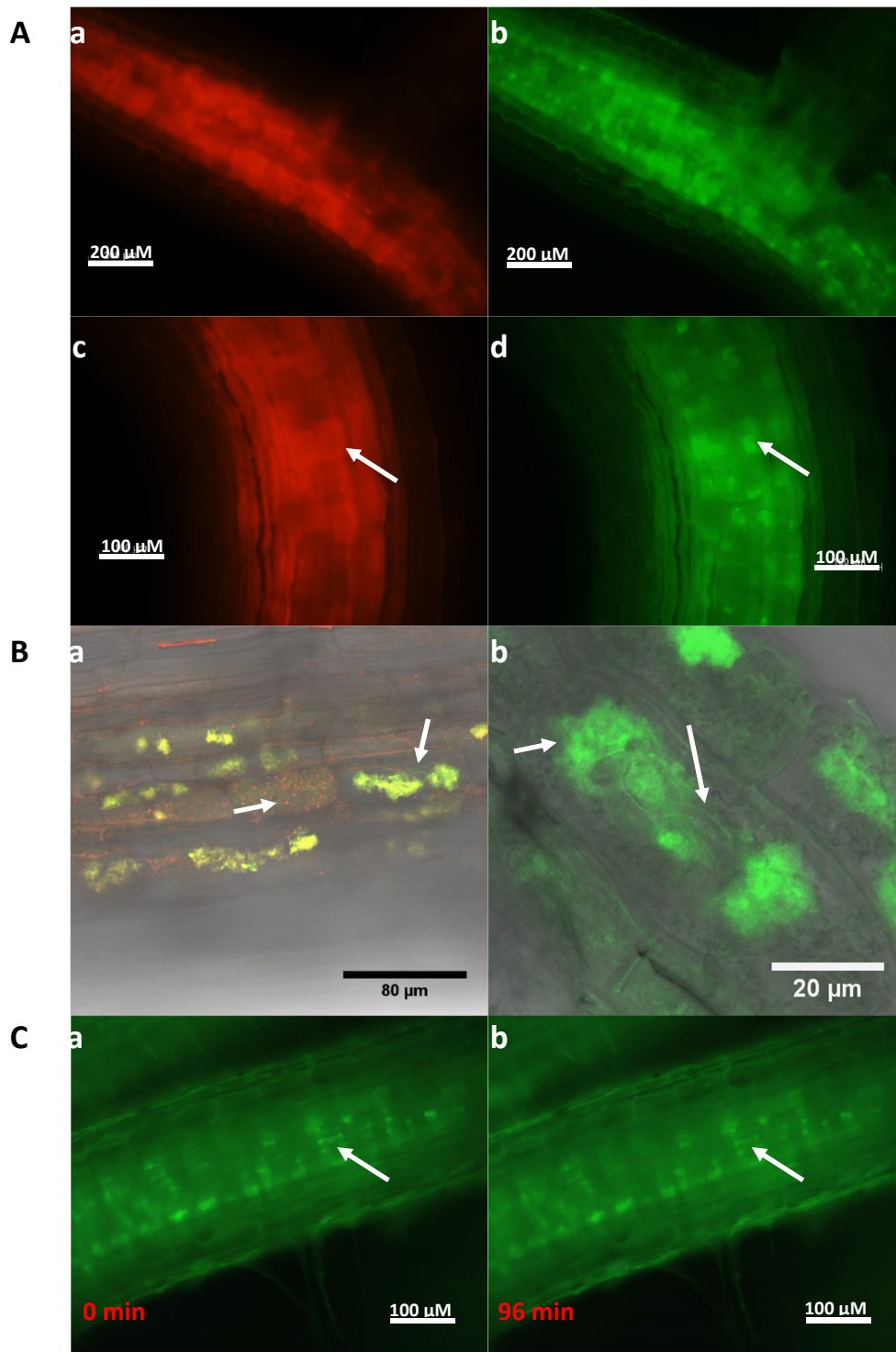


Fig 16: Localization of MTAMT2;4-mGFP6 and additional fluorescence marker proteins in mycorrhizal *M. truncatula* roots.

Fluorescence microscopy (A and C) as well as confocal microscopy (B) was used to localize MTAMT2;4-mGFP6 under the control of the 2x35S promoter (A, B and C) in roots transformed with a pRedRoot- (A and C) and pBIN:ER-rk-derivate, additionally encoding an ER-RFP fusion under the control of the 2x35S-promoter (B, a). Roots were mycorrhizal with *R. irregularis* for six weeks. Arrows in the micrographs indicate structures referred to in the text. $n \geq 10$ each, in three independent experiments

The expression of symbiosis-related membrane transporter genes is differentially affected in *ram1-1*- and *pt4-1* mutants, known for aberrant arbuscule morphology

Expression of AM-induced membrane transporter genes in *M. truncatula* roots was monitored via *Affymetrix GeneChip*-hybridizations. Based on these data, membrane transporter genes of interest were filtered for a ≥ 2 fold higher expression at $p \leq 0.05$ in mycorrhized control roots in comparison to mycorrhized *ram1-1* mutants (R. M. Hartmann, LUH, Hannover, unpublished), mycorrhized *pt4-1* mutants [38] as well as mycorrhized *MtMyb1*-RNAi roots (C. Hoge Kamp, LUH, Hannover, unpublished), all showing defects in AM-associated key regulator genes (Fig 17).

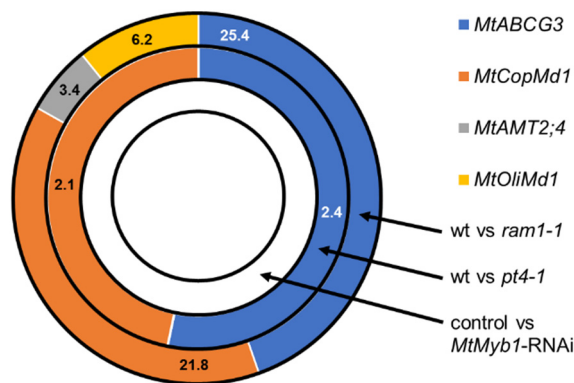


Fig 17: Induction of selected AM-induced membrane transporters genes in mycorrhized *M. truncatula* control roots vs. roots affected in the expression of key AM-related genes.

Data from *Affymetrix GeneChip* hybridizations are depicted. Fold changes of gene expression are shown in each section. Each ring represents results from one control vs. mutant/RNAi experiment. Only genes that were ≥ 2 fold induced at $p \leq 0.05$ in mycorrhized control roots in comparison to mycorrhized *ram1-1* mutant (R.M. Hartmann, LUH, unpublished), mycorrhized *pt4-1*-mutant [39] as well as mycorrhized *MtMyb1*-RNAi roots (C. Hoge Kamp, LUH, Hannover, unpublished) after inoculation of plants with *R. irregularis* were depicted. Biological replicates are three pools of 6 plant roots for each time point respectively. Abbreviations: wt, wild type; vs, versus

Whereas *ram1-1* mutants lack a key GRAS transcription factor (TF) that controls arbuscular branching, *pt4-1* mutants have a defect in the symbiotic phosphate transporter of the host, and *MtMyb1*-RNAi roots are affected in the expression of a TF that controls arbuscule degeneration. In *MtRam1*-expressing wild type roots, all four membrane transporter genes under investigation were induced ~ 3.4 to ~ 25.4 fold (Fig 17) in comparison to *ram1-1* mutants. In contrast, only *MtABCG3* and *MtCopMd1* expression was 2.1 to 2.4-fold induced in wild type roots compared to *pt4-1* mutants. Since there is evidence that the ABC-transporter is connected to the process of PAM biogenesis [43], which is disturbed in the *ram1-1* and *pt4-1* mutants [39], expression of these genes might be affected in the two mutants. Different from *MtOliMd1* and *MtABCG3*, the ammonium transporter gene *MtAMT2;4* as well as the oligopeptide transporter gene *MtOliMd1* were not repressed in *MtPt4*-defect mutants (Fig 17). In late wild type arbuscule-harboring cells, characterized by *MtMyb1* transcription, none of the

selected AM-induced membrane transporter genes was induced in comparison to the RNAi-roots (Fig 17).

It can be concluded that the selected membrane transporter genes are active independent of MtMyb1-transcription. This is conclusive, since their products are needed in the active phase of the AM symbiosis. Furthermore, expression of the investigated nitrogen or oligopeptide transporter genes is independent of fungal P-supply, evident by their unaffected expression in *MtPt4* mutants.

Discussion

During AM interactions, several factors, such as the extent of extraradical hyphae and quantity, as well as the morphology of arbuscules, are decisive for the nutrient flux between micro- and macrosymbiont. Apart from the adaptation of fungal structures towards environmental stress, soil and climate, a fine-tuned transcriptional reprogramming of the host plant alters the cost-benefit ratio of the symbiosis [49].

Here, promoter-GUS studies of membrane transporter genes belonging to several unrelated families of AM-induced genes were shown to display a variability in gene activities in different stages of fungal colonization. Therefore, they were monitored in mutant plants, displaying defects in genes required for the establishment of functional AM-symbioses.

The copper transporter gene *MtCopMd1* is primarily induced during the active stage of AM symbiosis

It was shown that AM symbioses can improve the supply of host plants with micronutrients [50, 51]. This was further supported by the identification of a copper transporter gene, which is specifically expressed in arbuscule containing cells [42, 52]. Copper (Cu^+) transporters of the Ctr family are sequence diverse eukaryotic proteins that function as pore. Bioinformatic analyses of sequenced Ctr proteins [53] revealed multiple paralogues in single organisms. Patterns of conserved hydrophobicity and amphipathicity in the second and third transmembrane spanners (TMs) could be vital for the mechanism of copper transport. The MX_3M motif in putative TMS2 may contain the transmembrane Cu^+ binding site in oligomeric channels that import Cu^+ by a passive, membrane potential-dependent mechanism [53]. The corresponding amino acid sequence of *MtCopMd1* is MLALM (Fig 3, B).

In the genome of the model legume *M. truncatula*, eight *COPT* genes were identified [44]. *MtCOPT1*, the only nodule-specific gene was found in the plasma membrane of differentiation, interzone and early fixation zones [4]. As its encoded protein enhanced the growth of yeast mutants on Cu-depleted media, the closely related AM-dependent *MtCopMd1* [44] could have a similar working mode. *In silico*, three transmembrane regions and a C-terminal as well as a central cytoplasmic region were detected (Fig 4). The expression of the gene *MtCopMd1* rose with the depletion of phosphate in mycorrhized plants. Mycorrhized *ram1-1* mutants displayed a lower expression level of the gene than control plants, and similarly *MtCopMd1* expression is hindered in mycorrhized *pt4-1* mutants in relation to controls. Together, this supports a function during the active phase of the arbuscule life cycle. In line with this, *MtCopMd1* transcript amounts did not differ between RNAi:Myb1 and control plants.

De Feo *et al.* [54] have proposed a model in which copper is transported along the center of a protein trimer. Furthermore, the human high affinity ($\sim 3 \mu\text{M}$) Ctr1, a homotrimer, imports copper by an energy-independent mechanism that is supported by extracellular acidic pH as well as high K^+

concentrations [55]. In this light, the preferential gene expression in arbuscule harboring cells is conclusive, as plant and fungal H⁺-ATPases were found to be situated in the PAM [22, 23]. GUS-staining indicated an enhanced activity of the AM-related copper transporter in arbuscule-containing cells. This could indicate a function in the molecule exchange at the active plant-fungal interface. However, GUS-staining revealed an expression within the rhizodermal cell layer as well, which could imply additional homeostatic functions, as was shown for the *Arabidopsis* CopT1 [56].

The proton-dependent oligopeptide transporter MtOliMd1 probably functions in the PAM

Proteins of the proton-dependent oligopeptide transporter (POT) family, also called the peptide transport (PTR) family are 400 to 600 amino acids in size and usually possess 12 membrane spanning α -helices [57, 58]. Using *InterProScan*, 11 helices and a central cytoplasmic-domain were predicted for the protein (Fig 4), indicating that it is likely situated in a membrane. Most members of the family are peptide transporters. However, in *Arabidopsis* a function as nitrate permease was found for such a transporter as well [59, 60]. Interestingly, members of the gene family, such as *MtOliMd1*, were highly induced in two different AM symbioses [42]. By a variation of phosphate and nitrogen supply of mycorrhized plants, it was shown that the expression of *MtOliMd1* rose with the depletion of phosphate, whereas it did not respond to severe nitrogen limitation. In this light, a function of *MtOliMd1* as nitrate permease was not supported. In contrast to the universal mechanisms of proton-symport, POT proteins were shown to differ in protein-stoichiometry and H⁺-import rates [61]. Since arbuscule-containing cells showed an enhanced activity of the *MtOliMd1* promoter, the proton-gradient might result in distinct H⁺-import rates.

Komarova *et al.* [62] reported that 7 amino acids within the hydrophilic N-terminal region of *Arabidopsis* PTR2, PTR4 and PTR6 are required for tonoplast (TP) localization. In the amino acid sequence of *MtOliMd1*, L(11) and I(12) of PTR2, which were found vital for TP targeting [62], are replaced by N (11) and G (12). Furthermore, *InterProScan* predicted a loop, required for the alternate targeting to the plasma membrane [62], in the amino acid sequence of *MtOliMd1*. In conclusion, a targeting to the plasma membrane (PM), which is locally altered in arbuscule-harboring cells [6], is likely. Since the deletion of either PM or TP targeting signals led to a retention in internal membranes, indicating that PTR trafficking to these destination membranes requires presumably distinct signals [62], additional signals for the guidance of the protein to the PAM might exist.

In *MtRam1*-expressing wild type roots, the gene was induced in comparison to the *ram1-1* mutants [63], defective in fine-branching of arbuscules. Furthermore, the gene was not repressed in RNAi:*MtMyb1* roots, giving an additional hint that *MtOliMd1* could function in the active stage of AM symbiosis. In mycorrhized roots transformed with an amiRNA-construct targeting *MtOliMd1*, the

transcript amount was reduced to 2-fold and the expression of AM marker genes, such as *MtABCG3* and *MtRam1*, was significantly reduced as well.

Taking together these data, the AM-related oligopeptide transporter MtOliMd1 functions during the active phase of AM, probably by contributing to the PAM composition

The ATP-binding cassette (ABC) transporter MtABCG3 could function during PAM biogenesis

The ABC superfamily contains uptake as well as efflux transport systems [64]. The structures of several ABC transporters, have been determined via high resolution X-ray crystallography-analyses, and transport mechanisms have been proposed [65, 66]. ABC transporters have two nucleotide binding domains (NBDs) that dimerize in a head-to-tail conformation and were categorized into three evolutionarily distinct families [67], named ABC1, ABC2 and ABC3. ATP hydrolysis without protein phosphorylation energizes transport.

Hogekamp *et al.* [42] and Luginbuehl *et al.* [43] have shown that the ABC transporter gene *MtABCG3* is specifically transcribed in arbuscule-containing cells, suggesting a function during the life cycle of arbuscules. Its activity rose with the depletion of phosphate, but it did not respond to severe nitrogen limitation (Fig 2). Zhang *et al.* [68] hypothesized that STR and STR2, two other ABC transporters from the subfamily G, could transport strigolactones. Subsequently, Kretschmar *et al.* [69] isolated ABC transporter genes, while searching potential efflux carriers of strigolactones in *Petunia* hybrids. They found that knockdown or knockout plants in the *PDR1* gene displayed a disturbed colonization of the roots by AM fungi. Less penetration events of hyphae as well as a slower spreading in the inner root cortex were hypothesized to be the reason for this phenomenon.

Since the lipid composition can be unique for each destination membrane, polar lipid trafficking is essential in eukaryotic cells. A striking example is the biogenesis of plastid membranes of plants. Some multidrug resistance (MDR) transporters catalyze lipid, lipopolysaccharide, or lipoprotein export, which takes place by a 'flip-flop' or a 'projection' mechanism [69]. The Tgd 1, 2, 3 system, composed of a permease and substrate binding component, a proposed lipid translocator and a small ABC-type ATPase, probably transfers ER-derived lipids to the thylakoid membrane [70].

Keymer *et al.* [71] showed that the promoters of *DIS* and *RAM2*, two AM-specific lipid biosynthesis genes, were active during arbuscule formation but not in cells harboring collapsing arbuscules. To that end, GUS staining indicated that the *MtABCG3* promoter activity was apparently bound to certain stages of the AM life cycle [Fig 7]. It accompanied and slightly preceded the spreading of intraradical hyphae. Although, it was evident that the promoter activity in arbuscule harboring cells varied, the activity of the gene was found to be arbuscule-enhanced. Contrasting this, a promoter gusAint fusion from Luginbuehl *et al.* [43] indicated an exclusive transcription in arbuscule containing cells. In mycorrhized *MtRam1* and *MtPt4*- expressing wild type roots, *MtABCG3* is induced in comparison to

knock down mutants. Both mutants are known for a massive reduction of the PAM biogenesis, suggesting a function of MtABCG3 in associated processes. Furthermore, a slightly enhanced *MtRAM2* expression in amiRNA roots targeting *MtABCG3*, was detected (Fig 8). This could further support a function during the active phase of AM, although no prominent aberrations in-between those arbuscules were detected (Fig 9).

EXO70i was shown to be required for the efficient incorporation of the two ABC transporter subfamily G (ABCG) proteins STR and STR2 into the periarbuscular membranes [72]. A similar addressing of vesicles containing MtABCG3 (Fig 18) to the PAM would thus be possible.

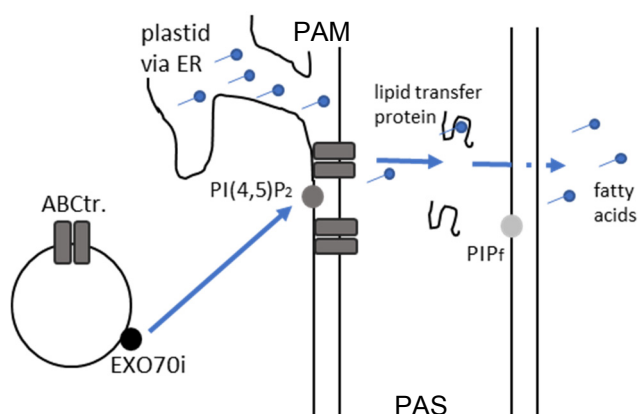


Fig 18: Hypothetical working mode of the ABC-transporter MtABCG3.

Targeting of MtABCG3 is depicted by a blue arrow. Fatty acids are shown in blue. Abbreviations: ABCtr., MtABCG3; PAM, periarbuscular membrane; PAS, periarbuscular space; PIP, phosphatidylinositol phosphate; PIP_f, fungal phosphatidylinositol phosphates

It is tempting to speculate that the MtABCG3 transporter functions in translocating plant-derived fatty acids, such as C16-bodies, across the PAM as illustrated in a hypothetical model (Fig 18).

The ammonium transporter MtAMT2;4 probably transports a non-electrogenic substrate across the PAM

Apart from phosphate, nitrogen is an essential nutrient for growth and productivity of plants [73]. Members of the ammonium transporter family (Amt) have a size of 391-622 amino acids and contain 11-12 transmembrane α -helices [74]. In *L. japonicus*, four high-affinity genes of the *AMT1* and *AMT2*-family were identified [75, 76]. Due to an AM-inducible ammonium transporter gene in *L. japonicus* and *Glycine max* [13, 14] Recorbet *et al.* [14] hypothesized that nitrogen in the form of ammonium could be a signal for arbuscule maintenance.

The promoter activity of *MtAMT2;4* has been correlated to the establishment of arbuscules [32]. In addition, it was shown here that the expression of *MtAMT2;4* rose with the depletion of phosphate and nitrogen (Fig 2). In *MtRam1* expressing wild type roots, *MtAMT2;4* was induced in comparison to

the knockout mutant [Fig 17]. Therefore, it can be concluded that *MtAMT2;4* expression is connected to the formation of fine branches in the PAM. Since *MtAMT2;4* is not repressed in RNAi:Myb1-plants, which are disturbed in late symbiotic processes, it is most likely expressed in an active, exchanging phase of the AM-symbiosis.

Via *InterProScan*, ten transmembrane helices and a c-terminal cytoplasmic region were predicted for *MtAMT2;4* (S2 Fig). Using an *MtAMT2;4*-mGFP6-fusion with additional cellular markers, an arbuscule correlated fluorescence was shown (Fig 16). Transporter proteins which are situated in the periarbuscular membrane, such as *MtPt4*, need to be incorporated in the *de novo* synthesized symbiotic membranes [5, 6, 7]. A marker for the endoplasmic reticulum has underlined the close connection of the secretory apparatus to the symbiotic membrane (Fig 15). Kobae *et al.* [13] identified two subdomains of the periarbuscular membrane, based on their differing localization and protein composition via live cell imaging. First, the trunk, which is the prolonged point of fungal entry into the cell and has a similar protein composition like the plasma membrane [13]. Second, the distal, highly branched, dendritic hyphae, where membrane transporters are situated [13]. In the latter, highest *MtAMT2;4*-mGFP6 levels were detected (Fig 16).

With respect to a possible *MtAMT2;4* structure, the related *E. coli* AmtB assembles as a trimer [77]. Apparently, it has two functions, on the one hand transporting NH_4^+ and on the other hand regulating nitrogen metabolism by interacting with regulatory proteins [78]. The latter could serve as a hypothetical model for N-dependent signaling in AM symbioses, especially since an ammonium transporter 2 family protein was shown to suppress arbuscule degeneration in *M. truncatula* [78].

Wang *et al.* [79] proposed an electrogenic transport mechanism for AmtB, where NH_4^+ is inert in the AmtB pore, getting into contact with a binding site from which it can transfer a proton to a histidine residue. Possibly, NH_3 subsequently traverses the pore, while the proton is co-transported via a conserved hydrogen-bonded His168-His318 pair. Since *MtAMT2;4* contains an endogenous His 183-His 320 pair, a congruent mode of transport is possible (Fig 19).

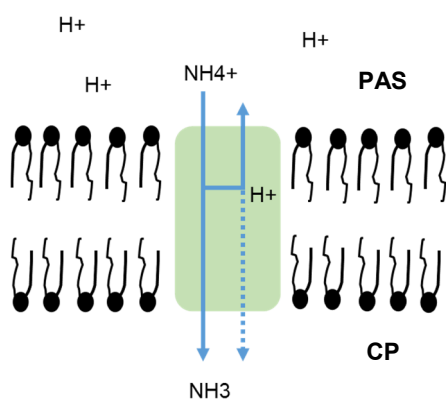


Fig 19: Hypothetical working mode of the putative ammonium transporter *MtAMT2;4*.

The traversal of ammonium is depicted by a blue arrow. A deprotonated proton could be relocated to the PAS, and in fewer cases alternatively to the CP. Abbreviations: PAS, periarbuscular membrane; CP, cytoplasm. (slightly modified, 40)

AMT2;3, a *M. truncatula* ammonium transporter 2 family protein, was shown to suppress premature arbuscule degeneration [78] in nitrogen-starved *MtPt4* mutant roots, although it did not complement an ammonium transport defect mutant in yeast [47]. In *Lotus japonicus*, Guether *et al.* [12] had found *LjAMT2;2* to be upregulated in arbuscules and to transport NH_3 instead of NH_4^+ . They suggested that the transporter binds charged ammonium in the apoplastic interface and releases the uncharged NH_3 into the plant cytoplasm [12]. Thus, protons derived from the deprotonation process of NH_4^+ remain in the PAS and maintain or even reinforce the gradient for H^+ -dependent transport processes and therefore reduce the required energy for transport [12].

In untransformed *X. laevis* oocytes, small currents were induced by the addition of NH_4^+ to the media. The oocytes were morphologically intact and kept their membrane potential, so this seems to be a response due to the presence of native transporters and channels. Although media had been optimized by a substitution of sodium chloride, which could generate a background flux of ions, with n-methyl-d-glucamine, which cannot travel across biomembranes, this current was not completely eliminated. *MtAMT2;4*-mRNA transfected oocytes displayed in general an enhanced electrogenic flux between the in and outside of frog oocytes under acidic conditions. This supports the intramolecular cotransport of protons and the work mode at the acidic PAM shown in Fig 19. Nevertheless, NH_3 is probably the transported substrate and small currents could be derived from small H^+ -fluxes, towards the cytoplasm.

Due to the fact that a knock-down of *MtAMT2;4* did not lead to significant changes in AM marker gene expression, the encoded ammonium transporter is probably not essential for the formation of active, nitrogen-transporting arbuscules under the conditions tested.

Acknowledgements

I am thankful to the Institute of Biophysics for the possibility to use instruments, and the provision of the vector pGEMHE. *GeneChip* hybridizations were carried out by João Sobral and Jörg D. Becker (Plant Genomics Lab and Gene Expression Unit, Instituto Gulbenkian de Ciência, Oeiras, Portugal).

References

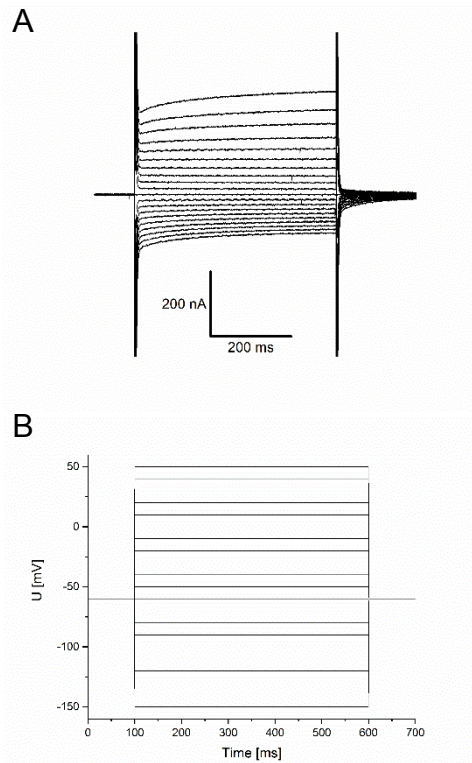
- [1] Fitter AH. What is the link between carbon and phosphorus fluxes in arbuscular mycorrhizas? A null hypothesis for symbiotic function. *New Phytol* 2006; 172(1): 3–6 [<https://doi.org/10.1111/j.1469-8137.2006.01861.x>][PMID: 16945083]
- [2] Simon L, Bousquet J, Lévesque RC, Lalonde M. Origin and diversification of endomycorrhizal fungi and coincidence with vascular land plants. *Nature* 1993; 363(6424): 67–9 [<https://doi.org/10.1038/363067a0>]
- [3] Heckman DS, Geiser DM, Eidell BR, Stauffer RL, Kardos NL, Hedges SB. Molecular evidence for the early colonization of land by fungi and plants. *Science* 2001; 293(5532): 1129–33 [<https://doi.org/10.1126/science.1061457>][PMID: 11498589]
- [4] Provorov NA, Borisov AY, Tikhonovich IA. Developmental Genetics and Evolution of Symbiotic Structures in Nitrogen-fixing Nodules and Arbuscular Mycorrhiza. *Journal of Theoretical Biology* 2002; 214(2): 215–32 [<https://doi.org/10.1006/jtbi.2001.2453>]
- [5] Cox G and Tinker PB (1976). Translocation and transfer of nutrients in vesicular-arbuscular mycorrhizas. I. The arbuscule and phosphorus transfer: a quantitative ultrastructural study. *New Phytologist* 77: 371.
- [6] Pumplun N, Zhang X, Noar RD, Harrison MJ. Polar localization of a symbiosis-specific phosphate transporter is mediated by a transient reorientation of secretion. *Proc Natl Acad Sci U S A* 2012; 109(11): E665–72 [<https://doi.org/10.1073/pnas.1110215109>][PMID: 22355114]
- [7] Harrison MJ, Dewbre GR, Liu J. A phosphate transporter from *Medicago truncatula* involved in the acquisition of phosphate released by arbuscular mycorrhizal fungi. *The Plant Cell* 2002; 14(10): 2413–29 [PMID: 12368495]
- [8] Karandashov V, Nagy R, Wegmüller S, Amrhein N, Bucher M (2004). Evolutionary conservation of phosphate transport in the arbuscular mycorrhizal symbiosis. *Proceedings of the National Academy of Sciences, USA* 101: 6285–6290.
- [9] Govindarajulu M, Pfeffer PE, Jin H, et al. Nitrogen transfer in the arbuscular mycorrhizal symbiosis. *Nature* 2005; 435: 819 EP -[<https://doi.org/10.1038/nature03610>]
- [10] Allen JW, Shachar-Hill Y. Sulfur Transfer through an Arbuscular Mycorrhiza. *Plant Physiology* 2009; 149(1): 549[<https://doi.org/10.1104/pp.108.129866>]
- [11] Johansen A, Jakobsen I and Jensen ES (1992). Hyphal transport of ¹⁵N-labelled nitrogen by a vesicular-arbuscular mycorrhizal fungus and its effect on depletion of inorganic soil N. *New Phytol.* 122, 281–288.; 1992.
- [12] Guether M, Neuhauser B, Balestrini R, Dynowski M, Ludewig U, Bonfante P. A Mycorrhizal-Specific Ammonium Transporter from *Lotus japonicus* Acquires Nitrogen Released by Arbuscular Mycorrhizal Fungi. *Plant Physiology* 2009; 150(1): 73–83 [<https://doi.org/10.1104/pp.109.136390>]
- [13] Kobae Y, Tamura Y, Takai S, Banba M, Hata S. Localized expression of arbuscular mycorrhiza-inducible ammonium transporters in soybean. *Plant Cell Physiol* 2010; 51(9): 1411–5 [<https://doi.org/10.1093/pcp/pcq099>][PMID: 20627949]
- [14] Recorbet G, Abdallah C, Renaut J, Wipf D, Dumas-Gaudot E. Protein actors sustaining arbuscular mycorrhizal symbiosis: Underground artists break the silence. *New Phytol* 2013; 199(1): 26–40 [<https://doi.org/10.1111/nph.12287>][PMID: 23638913]
- [15] Casieri L, Gallardo K, Wipf D. Transcriptional response of *Medicago truncatula* sulphate transporters to arbuscular mycorrhizal symbiosis with and without sulphur stress. *Planta* 2012; 235(6): 1431–47 [<https://doi.org/10.1007/s00425-012-1645-7>]
- [16] Sieh D, Watanabe M, Devers EA, Brueckner F, Hoefgen R, Krajinski F. The arbuscular mycorrhizal symbiosis influences sulfur starvation responses of *Medicago truncatula*. *New Phytol* 2013; 197(2): 606–16 [<https://doi.org/10.1111/nph.12034>]
- [17] Giovannetti M, Tolosano M, Volpe V, Kopriva S, Bonfante P. Identification and functional characterization of a sulfate transporter induced by both sulfur starvation and mycorrhiza formation in *Lotus japonicus*. *New Phytol* 2014; 204(3): 609–19 [<https://doi.org/10.1111/nph.12949>]

- [18] Wipf D, Mongelard G, van Tuinen D, Gutierrez L, Casieri L. Transcriptional responses of *Medicago truncatula* upon sulfur deficiency stress and arbuscular mycorrhizal symbiosis. *Front. Plant Sci.* 2014; 5: 1496 [https://doi.org/10.3389/fpls.2014.00680]
- [19] Farzaneh M, Vierheilig H, Lössl A, Kaul HP (2011) Arbuscular mycorrhiza enhances nutrient uptake in chickpea. *Plant Soil Environ* 57:465–470
- [20] Harrison MJ. The arbuscular mycorrhizal symbiosis: An underground association 1997; 2(2): 54–60 [https://doi.org/10.1016/S1360-1385(97)82563-0]
- [21] Maeda D, Ashida K, Iguchi K, *et al.* Knockdown of an arbuscular mycorrhiza-inducible phosphate transporter gene of *Lotus japonicus* suppresses mutualistic symbiosis. *Plant Cell Physiol* 2006; 47(7): 807–17 [https://doi.org/10.1093/pcp/pcj069][PMID: 16774930]
- [22] Gianinazzi-Pearson V, Smith SE, Gianinazzi S, Smith FA. Enzymatic studies on the metabolism of vesicular-arbuscular mycorrhizas. V. Is H⁺-ATPase a component of ATP-hydrolysing enzyme activities in plant-fungus interfaces? *New Phytol* 1991; 117(1): 61–74 [https://doi.org/10.1111/j.1469-8137.1991.tb00945.x]
- [23] Gianinazzi-Pearson V, Arnould C, Oufattole M, Arango M, Gianinazzi S. Differential activation of H⁺-ATPase genes by an arbuscular mycorrhizal fungus in root cells of transgenic tobacco. *Planta* 2000; 211(5): 609–13 [https://doi.org/10.1007/s004250000323][PMID: 11089672]
- [24] Philip Jones, David Binns, Hsin-Yu Chang, Matthew Fraser, Weizhong Li, Craig McAnulla, Hamish McWilliam, John Maslen, Alex Mitchell, Gift Nuka, Sebastien Pesseat, Antony F. Quinn, Amaia Sangrador-Vegas, Maxim Scheremetjew, Siew-Yit Yong, Rodrigo Lopez, and Sarah Hunter (2014). InterProScan 5: genome-scale protein function classification. *Bioinformatics*, Jan 2014; doi:10.1093/bioinformatics/btu031
- [25] Grant SG, Jessee J, Bloom FR, Hanahan D. Differential plasmid rescue from transgenic mouse DNAs into *Escherichia coli* methylation-restriction mutants. *Proc Natl Acad Sci U S A* 1990; 87(12): 4645–9 [https://doi.org/10.1073/pnas.87.12.4645][PMID: 2162051]
- [26] Quandt H-J. Transgenic Root Nodules of *Vicia hirsuta*: A Fast and Efficient System for the Study of Gene Expression in Indeterminate-Type Nodules. *MPMI* 1993; 6(6): 699 [https://doi.org/10.1094/MPMI-6-699]
- [27] Arnon, D.I., and Hoagland, D.R. (1940). Crop production in artificial culture solutions and in soils with special reference to factors influencing yields and absorption of inorganic nutrients. *Soil Sci.* 50, 463–483.; 1940.
- [28] Vieweg MF, Frühling M, Quandt H-J, *et al.* The promoter of the *Vicia faba* L. leghemoglobin gene Vflb29 is specifically activated in the infected cells of root nodules and in the arbuscule-containing cells of mycorrhizal roots from different legume and nonlegume plants. *Mol Plant Microbe Interact* 2004; 17(1): 62–9 [https://doi.org/10.1094/MPMI.2004.17.1.62][PMID: 14714869]
- [29] Pridmore RD. New and versatile cloning vectors with kanamycin-resistance marker. *Gene* 1987; 56(2-3): 309–12 [PMID: 3315864]
- [30] Küster H, Quandt HJ, Broer I, Perlick AM, Pühler A. The promoter of the *Vicia faba* L. VFENOD-GRP3 gene encoding a glycine-rich early nodulin mediates a predominant gene expression in the interzone II-III region of transgenic *Vicia hirsuta* root nodules. *Plant Mol Biol* 1995; 29(4): 759–72 [PMID: 8541502]
- [31] Limpens E, Ramos J, Franken C, *et al.* RNA interference in *Agrobacterium rhizogenes*-transformed roots of *Arabidopsis* and *Medicago truncatula*. *J Exp Bot* 2004; 55(399): 983–92 [https://doi.org/10.1093/jxb/erh122][PMID: 15073217]
- [32] Uhe M (2013). Funktionelle Analyse von Membrantransportergenen in der arbuskulären Mykorrhiza von *Medicago truncatula*. MSc-Arbeit, Leibniz Universität Hannover, Hannover
- [33] Schwab, R., Ossowski, S., Riestler, M., Warthmann, N., & Weigel, D. (2006). Highly specific gene silencing by artificial microRNAs in *Arabidopsis*. *The Plant Cell*, 18(5), 1121-1133.
- [34] Devers EA, Teply J, Reinert A, Gaude N, Krajinski F. An endogenous artificial microRNA system for unraveling the function of root endosymbioses related genes in *Medicago truncatula*. *BMC Plant Biol* 2013; 13: 82 [https://doi.org/10.1186/1471-2229-13-82][PMID: 23679580]
- [35] Branscheid A, Sieh D, Pant BD, May P, *et al.* (2010). Expression pattern suggests a role of MiR399 in the regulation of the cellular response to local Pi increase during arbuscular mycorrhizal symbiosis. *Molecular Plant-Microbe Interactions* 2010; 23(7), 915-926.
- [36] Govindarajulu M, Pfeffer PE, Jin H, Abubaker J, *et al.* Nitrogen transfer in the arbuscular mycorrhizal symbiosis. *Nature* 2005; 435(7043), 819.
- [37] Hohnjec N, Lenz F, Fehlberg V, *et al.* The signal peptide of the *Medicago truncatula* modular nodulin MtNOD25 operates as an address label for the specific targeting of proteins to nitrogen-fixing

- symbiosomes. *Mol Plant Microbe Interact* 2009; 22(1): 63–72 [<https://doi.org/10.1094/MPMI-22-1-0063>][PMID: 19061403]
- [38] Nelson BK, Cai X, Nebenführ A. A multicolored set of in vivo organelle markers for co-localization studies in Arabidopsis and other plants. *Plant J* 2007; 51(6): 1126–36 [<https://doi.org/10.1111/j.1365-313X.2007.03212.x>][PMID: 17666025]
- [39] Floss DS, Gomez SK, Park H-J, *et al.* A Transcriptional Program for Arbuscule Degeneration during AM Symbiosis Is Regulated by MYB1. *Current Biology* 2017; 27(8): 1206–12 [<https://doi.org/10.1016/j.cub.2017.03.003>]
- [40] Sjøgaard R, Alsterfjord M, MacAulay N, Zeuthen T. Ammonium ion transport by the AMT/Rh homolog TaAMT1;1 is stimulated by acidic pH. *Pflugers Arch - Eur J Physiol* 2009; 458(4): 733–43 [<https://doi.org/10.1007/s00424-009-0665-z>]
- [41] Benedito VA, Torres-Jerez I, Murray JD, *et al.* A gene expression atlas of the model legume *Medicago truncatula*. *Plant J* 2008; 55(3): 504–13 [<https://doi.org/10.1111/j.1365-313X.2008.03519.x>][PMID: 18410479]
- [42] Hogekamp C, Arndt D, Pereira PA, Becker JD, Hohnjec N, Küster H. Laser microdissection unravels cell-type-specific transcription in arbuscular mycorrhizal roots, including CAAT-box transcription factor gene expression correlating with fungal contact and spread. *Plant Physiology* 2011; 157(4): 2023–43 [<https://doi.org/10.1104/pp.111.186635>][PMID: 22034628]
- [43] Luginbuehl LH, Menard GN, Kurup S, *et al.* Fatty acids in arbuscular mycorrhizal fungi are synthesized by the host plant. *Science* 2017; 356(6343): 1175–8 [<https://doi.org/10.1126/science.aan0081>][PMID: 28596311]
- [44] Senovilla M, Castro-Rodríguez R, Abreu I, *et al.* *Medicago truncatula* copper transporter 1 (MtCOPT1) delivers copper for symbiotic nitrogen fixation. *New Phytol* 2018; 218(2): 696–709 [<https://doi.org/10.1111/nph.14992>]
- [45] Bravo A, Brands M, Wewer V, Dörmann P, Harrison MJ. Arbuscular mycorrhiza-specific enzymes FatM and RAM2 fine-tune lipid biosynthesis to promote development of arbuscular mycorrhiza. *New Phytol* 2017; 214(4): 1631–45 [<https://doi.org/10.1111/nph.14533>]
- [46] Gaudé N, Bortfeld S, Duensing N, Lohse M, Krajinski F. Arbuscule-containing and non-colonized cortical cells of mycorrhizal roots undergo extensive and specific reprogramming during arbuscular mycorrhizal development. *Plant J* 2012; 69(3): 510–28 [<https://doi.org/10.1111/j.1365-313X.2011.04810.x>][PMID: 21978245]
- [47] Straub D, Ludewig U, Neuhäuser B. A nitrogen-dependent switch in the high affinity ammonium transport in *Medicago truncatula*. *Plant Mol Biol* 2014; 86(4-5): 485–94 [<https://doi.org/10.1007/s11103-014-0243-4>]
- [48] Nelson BK, Cai X, and Nebenführ A. A multicolored set of in vivo organelle markers for co-localization studies in Arabidopsis and other plants. *Plant Journal* 2007; 51(6): 1126–1136 [<https://doi.org/10.1111/j.1365-313X.2007.03212.x>]
- [49] Smith SE and Read DJ (1997). *Mycorrhizal Symbiosis*. Academic Press, San Diego, CA.; 1997.
- [50] Clark RB, Zeto SK. Mineral acquisition by arbuscular mycorrhizal plants. *Journal of Plant Nutrition* 2000; 23(7): 867–902 [<https://doi.org/10.1080/01904160009382068>]
- [51] Parniske M. Arbuscular mycorrhiza: The mother of plant root endosymbioses. *Nat Rev Microbiol* 2008; 6(10): 763–75 [<https://doi.org/10.1038/nrmicro1987>][PMID: 18794914]
- [52] Gomez SK, Javot H, Deewatthanawong P, *et al.* *Medicago truncatula* and *Glomus intraradices* gene expression in cortical cells harboring arbuscules in the arbuscular mycorrhizal symbiosis. *BMC Plant Biol* 2009; 9: 10 [<https://doi.org/10.1186/1471-2229-9-10>][PMID: 19161626]
- [53] Dumay, Q.C., A.J. Debut, N.M. Mansour, and M.H. Saier, Jr. (2006). The copper transporter (Ctr) family of Cu⁺ uptake systems. *J. Mol. Microbiol. Biotechnol.* 11: 10-19. 16825786
- [54] Feo CJ de, Mootien S, Unger VM. Tryptophan scanning analysis of the membrane domain of CTR-copper transporters. *J Membr Biol* 2010; 234(2): 113–23 [<https://doi.org/10.1007/s00232-010-9239-4>][PMID: 20224886]
- [55] Lee J, Peña MMO, Nose Y, Thiele DJ. Biochemical characterization of the human copper transporter Ctr1. *J Biol Chem* 2002; 277(6): 4380–7 [<https://doi.org/10.1074/jbc.M104728200>][PMID: 11734551]
- [56] Sancenón V, Puig S, Mateu-Andrés I, Dorcey E, Thiele DJ, Peñarrubia L. The Arabidopsis copper transporter COPT1 functions in root elongation and pollen development. *J Biol Chem* 2004; 279(15): 15348–55 [<https://doi.org/10.1074/jbc.M313321200>][PMID: 14726516]
- [57] Paulsen IT, Skurray RA. The POT family of transport proteins. *Trends Biochem Sci* 1994; 19(10): 404 [PMID: 7817396]

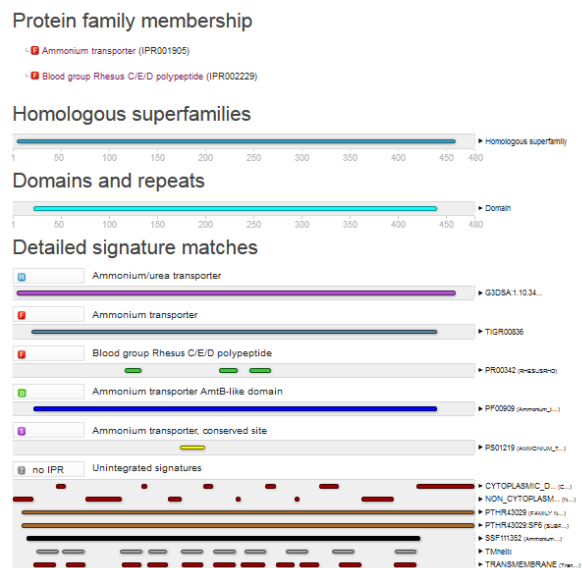
- [58] Cai H, Hauser M, Naider F, Becker JM. Differential Regulation and Substrate Preferences in Two Peptide Transporters of *Saccharomyces cerevisiae*. *Eukaryotic Cell* 2007; 6(10): 1805-13 [https://doi.org/10.1128/EC.00257-06]
- [59] Frommer, W. B., Hummel, S., & Rentsch, D. (1994). Cloning of an *Arabidopsis* histidine transporting protein related to nitrate and peptide transporters. *FEBS letters*, 347(2-3), 185-189.
- [60] Liu, K. H., & Tsay, Y. F. (2003). Switching between the two action modes of the dual-affinity nitrate transporter CHL1 by phosphorylation. *The EMBO journal*, 22(5), 1005-1013.
- [61] Chen H, Wong EA, Webb KE. Tissue distribution of a peptide transporter mRNA in sheep, dairy cows, pigs, and chickens. *Journal of Animal Science* 1999; 77(5): 1277 [https://doi.org/10.2527/1999.7751277x]
- [62] Komarova NY, Meier S, Meier A, Grotemeyer MS, Rentsch D. Determinants for *Arabidopsis* Peptide Transporter Targeting to the Tonoplast or Plasma Membrane. *Traffic* 2012; 13(8): 1090–105 [https://doi.org/10.1111/j.1600-0854.2012.01370.x]
- [63] Park 2015
- [64] Saurin W, Hofnung M and Dassa E (1999). Getting in or out: early segregation between importers and exporters in the evolution of ATP-binding cassette (ABC) transporters. *J. Mol. Evol.* 48: 22-41
- [65] Davidson, A. L., & Maloney, P. C. (2007). ABC transporters: how small machines do a big job. *Trends in microbiology*, 15(10), 448-455.
- [66] Lee S, Howell SB, Opella SJ. NMR and mutagenesis of human copper transporter 1 (hCtr1) show that Cys-189 is required for correct folding and dimerization. *Biochim Biophys Acta* 2007; 1768(12): 3127–34 [https://doi.org/10.1016/j.bbamem.2007.08.037][PMID: 17959139]
- [67] Shang Y, Xiao J, Ma L, *et al.* Characterization of a PDR type ABC transporter gene from wheat (*Triticum aestivum* L.). *Chin. Sci. Bull.* 2009; 54(18): 3249–57 [https://doi.org/10.1007/s11434-009-0553-0]
- [68] Zhang Q, Blaylock LA, Harrison MJ. Two *Medicago truncatula* half-ABC transporters are essential for arbuscule development in arbuscular mycorrhizal symbiosis. *The Plant Cell* 2010; 22(5): 1483–97 [https://doi.org/10.1105/tpc.110.074955][PMID: 20453115]
- [69] Kretzschmar T, Kohlen W, Sasse J, *et al.* A *petunia* ABC protein controls strigolactone-dependent symbiotic signaling and branching. *Nature* 2012; 483(7389): 341–4
- [69] Nagao K, Kimura Y, Mastuo M, Ueda K. Lipid outward translocation by ABC proteins. *FEBS Letters* 2010; 584(13): 2717–23 [https://doi.org/10.1016/j.febslet.2010.04.036][PMID: 20412807]
- [70] Lu J-F, Barron-Casella E, Deering R, *et al.* The role of peroxisomal ABC transporters in the mouse adrenal gland: The loss of *Abcd2* (ALDR), Not *Abcd1* (ALD), causes oxidative damage. *Lab Invest* 2007; 87(3): 261–72 [https://doi.org/10.1038/labinvest.3700512][PMID: 17260006]
- [71] Keymer DP, Lankau RA, Lau J. Disruption of plant-soil-microbial relationships influences plant growth. *J Ecol* 2017; 105(3): 816–27 [https://doi.org/10.1111/1365-2745.12716]
- [72] Zhang X, Pumplun N, Ivanov S, and Harrison MJ. EXO70I is required for development of a sub-domain of the periarbuscular membrane during arbuscular mycorrhizal symbiosis. *Current Biol* 2015; 25(16): 2189–2195 [https://doi.org/10.1016/j.cub.2015.06.075]
- [73] Gobert A, Plassard C. The Beneficial Effect of Mycorrhizae on N Utilization by the Host-Plant: Myth or Reality? In: Varma A, editor. *Mycorrhiza*. Berlin, Heidelberg: Springer Berlin Heidelberg 2008; 209–40.
- [74] Andrade, S.L. and O. Einsle. The Amt/Mep/Rh family of ammonium transport proteins. *Mol. Membr. Biol.* 24: 357-365. 17710640
- [75] Simon-Rosin U, Wood C, Udvardi MK. *Plant Mol Biol* 2003; 51(1): 99–108
- [76] D'Apuzzo, E., Rogato, A., Simon-Rosin, U., El Alaoui, H., Barbulova, A., Betti, M., ... & Udvardi, M. K. (2004). Characterization of three functional high-affinity ammonium transporters in *Lotus japonicus* with differential transcriptional regulation and spatial expression. *Plant Physiology*, 134(4), 1763-1774.
- [77] Blakey D, Leech A, Thomas GH, Coutts G, Findlay K, Merrick M. Purification of the *Escherichia coli* ammonium transporter AmtB reveals a trimeric stoichiometry. *Biochem J* 2002; 364(Pt 2): 527–35 [https://doi.org/10.1042/BJ20011761][PMID: 12023896]
- [78] Blauwkamp TA, Ninfa AJ. Antagonism of PII signaling by the AmtB protein of *Escherichia coli*. *Mol Microbiol* 2003; 48(4): 1017–28 [PMID: 12753193]
- [79] Wang S, Orabi EA, Baday S, Bernèche S, Lamoureux G. Ammonium transporters achieve charge transfer by fragmenting their substrate. *J Am Chem Soc* 2012; 134(25): 10419–27 [https://doi.org/10.1021/ja300129x][PMID: 22631217]
- [78] Breuillin-Sessoms, F., Floss, D. S., Gomez, S. K., Pumplun, N., Ding, Y., Levesque-Tremblay, V., ... Harrison, M. J. (2015). Suppression of Arbuscule Degeneration in *Medicago truncatula* phosphate transporter4 Mutants Is Dependent on the Ammonium Transporter 2 Family Protein AMT2;3. *The Plant Cell*, 27(4), 1352–1366. http://doi.org/10.1105/tpc.114.131144

Supporting information



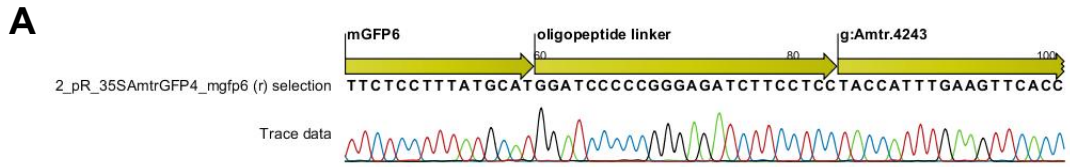
S1 Fig: Representative currents and voltage-pulse protocol of an *MtAMT2;4*-transfected *X. laevis* oocyte supplied with NH_4^+ .

The voltage-evoked currents of one representative *MtAMT2;4* transfected oocyte (A) as well as the program of applied voltage pulses (B) are shown. Currents were recorded during the addition of NH_4^+ . Media had a pH of 5.5. Abbreviations: nA, nanoamperes; ms, milliseconds; U, voltage; mV, millivolts



S2 Fig: *In silico* analyses of the putative ammonium transporter *MtAMT2;4*.

The annotated amino acid sequence of *MtAMT2;4* was analyzed with *InterProScan* using standard settings. Annotations were colored by source database.



B

2_pR_35SAmtrGFP4_mgfp6 (r) selection_rna rev translation frame +1 **GELQMVGGRRSPGGSMHKGE**

S3 Fig: Translational fusion of MtAMT2;4, an oligopeptide linker and mGFP6.

The translational fusion of MtAMT2;4 with an oligopeptide linker and mGFP6 on the nucleotide (A) and the amino acid level (B) is shown.

CHAPTER III

The mycorrhiza-dependent defensin *MtDefMd1* of *Medicago truncatula* acts during the late restructuring stages of arbuscule-containing cells

Scope:

In chapter III, the function of the mycorrhiza-dependent defensin gene *MtDefMd1* was investigated. The major part of this chapter was published in *PlosOne* (PLOS ONE 13(1): e0191841, 2018). Here, the study was completed with lipid staining assays as well as more detailed transcriptomic studies in AM-defective plant mutants. Furthermore, the transcription of genes from the *EXO70* family was related to *MtDefMd* gene expression.

Experimental contributions:

Marian Uhe: Conceived and designed the experiments, cultivated and mycorrhized plants, *in silico* analyses, gene expression, RNAi-, overexpression, and subcellular localization experiments, interpreted experimental data, and wrote the manuscript, where major parts of the chapter were published.

Rico M. Hartmann: Prepared RNA from mycorrhized roots of wild type plants and *ram1-1* mutants, set up a yeast two hybrid library, and provided unpublished MtGeneChip hybridization data.

Claudia Hogekamp: Analysis of *MtDefMd1* and *MtDefMd2* promoters, provided unpublished MtGeneChip hybridization data.

Natalija Hohnjec and Helge Küster: Participated in the interpretation of experimental data and edited the manuscript where major parts of the chapter were published.

Abstract

Different symbiotic and pathogenic plant-microbe interactions involve the production of cysteine-rich antimicrobial defensins. In *Medicago truncatula*, the expression of four *MtDefMd* genes, encoding arbuscular mycorrhiza-dependent defensins containing an N-terminal signal peptide and exhibiting some differences to non-symbiotic defensins, raised over the time of root colonization by *Rhizophagus irregularis*. Whereas the *MtDefMd1* and *MtDefMd2* promoters were inactive in cells containing young arbuscules, cells with fully developed arbuscules displayed different levels of promoter activities, indicating an up-regulation towards later stages of arbuscule formation. *MtDefMd1* and *MtDefMd2* expression was absent or strongly down-regulated in mycorrhized *ram1-1* and *pt4-2* mutants, known for defects in arbuscule branching or premature arbuscule degeneration, respectively. A ~97% knock-down of *MtDefMd1/MtDefMd2* expression did not significantly affect arbuscule size. Although overexpression of *MtDefMd1* in arbuscule-containing cells led to an up-regulation of *MtRam1* and *MtMyb1*, encoding key transcriptional regulators of arbuscule formation, or degradation, respectively, no morphological changes for most infection units were evident. However, the trunk region and first order branches were swollen and deformed in a small fraction of pPt4:*MtDefMd1*-overexpressing, arbuscule-containing cells. In roots with a reduced expression of *MtMyb1*, encoding a key transcription factor for arbuscule senescence and showing lower expression of *EXO70* gene family members, *MtDefMd*-transcription was also reduced. The *MtMyb1*-affected EXOCYST-member genes *EXO70j* and *EXO70k* were ~1.6- to 2-fold repressed in pUbi:*MtDefMd1* overexpressing roots, but only *EXO70j* was ~1.7-fold downregulated by an *MtPt4* promoter driven *MtDefMd1* overexpression in arbuscule-containing cells. This finding indicates that EXO70 proteins might assist in transporting cargos during processes, in which *MtDefMd1* takes part. In addition, these findings indicate differences in cellular targeting of arbuscule harboring cells during later symbiotic stages. Co-localization of an *MtDefMd1*-mGFP6 fusion with additional, subcellular markers revealed that this defensin is associated with arbuscules in later stages of their life-cycle. *MtDefMd1*-mGFP6 was detected in cells with older arbuscules about to collapse, and ultimately in vacuolar compartments. Comparisons with mycorrhized roots expressing a tonoplast marker indicated that *MtDefMd1* acts during late restructuring processes of arbuscule-containing cells, upon their transition into a post-symbiotic state. A yeast two-hybrid experiment identified several lipid-associated proteins as interactors of the hydrophobic *MtDefMd1*. This points to a detergent-like working mode of *MtDefMd1*, possibly by binding phosphatidylinositol phosphates in symbiotic membranes.

Introduction

The majority of terrestrial plants is able to form arbuscular mycorrhizal (AM) symbioses with a group of obligate biotrophic fungi designated *Glomeromycota* [1, 2]. In return for the supply with hexoses [3] and presumably lipids in the form of palmitic acid [4], AM-fungal mycelia recruit nutrients, especially phosphate, from soils and transport them to the host [5]. It is thought that 450 million years ago, AM fungi facilitated the colonization of land by early plant species [6, 7].

Prior to a colonization of plant roots with AM fungi, strigolactones from the host trigger germination of fungal spores and growth of extraradical hyphae [8, 9]. The hyphae penetrate root epidermal cells via hyphopodia and spread in the cortex from this initial infection site [10, 11]. Both in the epidermis and in the subsequently colonized cells of the root, a pre-penetration apparatus, derived from structures of the cytoskeleton, precedes fungal entry [12]. In cells of the inner cortex, the fungus establishes arbuscules, highly branched, dendritic hyphal ends, being of particular importance for the exchange of nutrients [13]. Nutrient transfer between both partners involves a tight control of the microsymbiont's life-cycle by the host. Fungal arbuscules are regularly degraded after several days, and previously infected cells are restructured for subsequent re-infections [10, 14, 15].

Two AM-specific transcription factors act as key control switches of arbuscule development. With respect to arbuscule build-up, RAM1, together with other GRAS-transcription factors, controls proper arbuscule branching [16]. During the late stages of arbuscule development, the Myb transcription factor MYB1 activates a transcriptional program associated with arbuscule degeneration, leading to the production of different hydrolases and other arbuscule-degrading enzymes [17].

During the formation of active arbuscules, a suite of mycorrhiza-specific phosphate transporter- and other nutrient transporter genes is activated [18, 19]. The transfer of nutrients between fungi and plants throughout the AM symbiosis is mediated by the periarbuscular membrane (PAM), which permanently separates micro- and macrosymbionts [20]. Although the picture of PAM biogenesis, including polarized secretion for spatial expansion of the plasma membrane, is up to now not complete, some key players such as vesicle-associated membrane proteins (VAMPs), syntaxins, vapyrin, and EXO70i were identified [21, 22, 23, 24].

On the other hand, the process of PAM degradation is less clear, and the switch to cell-autonomous arbuscule degeneration is not yet defined, although important components of the degradation program were identified [17]. In this context, Kobae *et al.* [14] raised the question, why infection units composed of arbuscules in different stages of their life-cycle disappear in a synchronized manner. Many eukaryotic cells express genes encoding bioactive, channel-forming amphipathic peptides, such as those belonging to the defensin superfamily [25]. Defensins are not legume-specific, and several members of the defensin family have long been known for their role as defense-related peptides in plants [26]. It was proven that some defensins are translated during the defense reaction towards

fungal pathogens [27], while filamentous fungi as well as yeast are considered to be targets as well. Characteristic for plant defensin proteins are an α -helix and a three-stranded, anti-parallel β -sheet, being interconnected by four disulfide bonds that create a cysteine-stabilized α - β motif [28]. In addition, these proteins lack a hydrophobic inner center, leading to a condensed knot-like structure. Some plant defensins have a fifth disulfide bond, which might be important for the stabilization of the protein core, and which allows variation in the surface loops [29]. Finally, the γ -core motif was proposed to be an essential region for the modes of action of the defensin MtDef4 of *Medicago truncatula* [30]. An insertion into target membranes has been proposed for some plant defensins, since high affinity binding sites exist [31], and since defensins can form weakly anion-selective channels [32].

Defensin genes of *Medicago truncatula* were found to be expressed in a variety of tissues and in response to different abiotic and biotic stimuli [33]. In the root nodule symbiosis, hundreds of root nodule-specific defensin-like proteins designated nodule cysteine-rich (NCR)-peptides act as effectors of bacteroid development [34, 35]. With respect to the AM symbiosis, Hanks *et al.* [33] were first to identify defensin genes induced in response to root colonization of *Medicago truncatula* by the AM fungus *Glomus versiforme*, using a combination of transcript sequencing and real-time RT-PCR. Subsequently, several genome-wide transcriptomic studies confirmed that a family of defensin genes is activated during the AM symbiosis of *Medicago truncatula* [19, 36, 37; 38, 18] and for some, an arbuscule-correlated expression was demonstrated [37, 18].

In congruence with the significant impact of NCR-peptides on terminal bacteroid differentiation in legume root nodules [34, 35], defensins could have important functions for the morphology and life-cycle of arbuscules as well. It is thus the aim of this study to contribute to the functional characterization of mycorrhiza-dependent defensins of *M. truncatula*, based on a set of four AM-induced *MtDefMd* genes identified in expression profiling experiments [37, 38, 18]. Focusing on the two *MtDefMd* genes most strongly activated in a time-course of mycorrhization, we are able to show that their general and cell-specific expression is dependent on key genes of arbuscule formation (*MtRam1*) and -function (*MtPt4*), respectively. Using translational fusions with subcellular fluorophore markers, we demonstrate that the *MtDefMd1* gene is not only specifically transcribed in arbuscule-containing cells, but that the encoded defensin is present during late restructuring processes of arbuscule-containing cells, providing novel insights into their transition into a post-symbiotic state.

Materials and Methods

Bioinformatic analyses

Amino acid sequences of mature defensins were aligned using the following settings: Gap open cost: 10.00; gap extension cost: 5; Kyte-Doolittle window length 5; polarity logo. *RaptorX* [39] was used to build a three-dimensional model of MtDefMds and AM-unrelated defensins. For this, the three-dimensional structures of HsAFP1 [40], RsAFP1 [41], major pollen allergen Art. v1 [42], and MtDef4 [30] were used as homology models. The coding sequences of *MtDefMd1* (Medtr.8g012805.1 in the *Medicago truncatula* genome [43, 44], Mtr.35854.1.S1_at in the *Medicago* Gene Expression Atlas (Benedito *et al.*, 2008), *MtDefMd2* (Medtr.8g012835.1, Mtr.7210.1.S1_at), *MtDefMd3* (Medtr.8g012875, Mtr.3215.1.S1_at), and *MtDefMd4* (Medtr.8g012885, Mtr.31214.1.S1_at) were analyzed with *SignalP* [45], *Plant-mPloc* [46], and *SherLoc2* [47]. Using *CLC Main Workbench 6.7.1* the protein charge of *M. truncatula* defensins was computed.

Plant cultivars, fungal, and bacterial strains

Medicago truncatula Gaertn. Jemalong A17 (Thierry Huguet, INRA Toulouse, France) was used for all plant experiments. Sterile *Rhizophagus irregularis* DAOM197198 spores (PremierTech, Rivière-du-Loup, Canada) were applied as fungal inoculum. *Escherichia coli* DH5 α mcr' [48] was used for cloning and the propagation of plasmids. Transgenic roots were induced by *Agrobacterium rhizogenes* Arqua1 [49].

Cloning of promoter-*gusAint* fusions

Using genomic DNA of *M. truncatula* leaves, the promoters of *MtDefMd1* and *MtDefMd2* (-1 to -1175 bp and -1 to -1457 bp relative to the translational start) were PCR-amplified using primers aaagaattcATTTGTCGTAAATAACCTTGC and aaaaagcttgCTTGCTTAATGTAAATGGAA (*MtDefMd1*) as well as aaaccgggCGCTTTTAGTTTTCGGTAGAT and aaaccgggGCTTGCTTAATGTAAATGGAA (*MtDefMd2*). Fragments were cleaved by *SmaI* and *EcoRI/HindIII*, respectively, and were cloned into pk18 [50]. The promoters were then subcloned into pGUS-INT [51], containing the *gusAint* reporter gene. Using *SpeI*, the transcriptional fusion was cleaved out, Klenow-blunted, and ligated into the *SmaI*-digested binary vector pRedRoot [52]. Promoter-*gusAint* fusions cloned in pRedRoot were transferred via electroporation into *A. rhizogenes* Arqua1.

Cloning of knock-down and overexpression constructs

To obtain an RNAi construct targeting the highly similar *MtDefMd1* and *MtDefMd2* genes, the coding sequence of *MtDefMd1* was PCR-amplified from position +2. *attB* sites were added for cloning into the entry vector pDONRTM221 (Gateway[®]-System, Invitrogen, Karlsruhe, Germany), using the BP clonase reaction. The LR clonase reaction was used for cloning into the destination vector pK7GWIWG2(II)-*Q10*:DsRED [53].

To obtain an overexpression construct, the coding sequence of *MtDefMd1* (656 bp, containing introns) was PCR-amplified, cleaved with *Bam*HI and *Spe*I and ligated into vector *p9RFP* [54, 55] containing the *MtPt4* or *ubiquitin* promoters, respectively. *Spe*I and *Bam*HI recognition sites as well as 5 additional adenosine bases were added to the primers aaaaactagtATGGCTTCCTCTGCTCTTAAAT and aaaaggatccTTAGCAGTTGAAGTAACAGAAGCAAG.

Cloning of constructs for subcellular localizations

A cassette of the native promoter and the coding sequence of *MtDefMd1* (-1 to -1175 bp; 656 bp coding region) was cloned into vector *p35S-OLI-mGFP6* [56]. This vector encodes an N-terminal GGRSPGGS oligopeptide (OLI) extension of mGFP6 that serves as a flexible linker to the protein of interest. The following cloning strategy were used: *Sph*I and *Kpn*I recognition sites were added to the primers for cloning the *MtDefMd1* promoter (aaagcatgcATTTGTCGTAAATAACCTTGCCT/aaaggtaccGCTTGCTTAATGTAAATGGAAATG), and *Kpn*I and *Bgl*II were used for the coding sequence (aaaggtacaaaaATGGCTTCCTCTGCTCTTA/aaaagatcttctccGCAGTTGAAGTAACAGAAG), allowing the translation of an MtDefMd1-OLI-mGFP6 fusion protein under the control of the native *MtDefMd1* promoter instead of p35S. All primers were extended by 3 additional adenosine bases. The *MtDefMd1-OLI-mGFP6* fusion was released using *Eco*RI and *Hind*III. The fragment was blunted using Klenow polymerase and ligated into the blunted *Sal*I site of binary vector *pBIN:ER-ck* [57] expressing an *ER-CFP* marker. Finally, the fusion of the *MtBcp1* promoter and signal peptide region to the coding sequence of mCherry (*MtBcp1_{SP}-mCherry*) was released from *pCMbB-TMEr* [58] using *Ecl*136II and *Sma*I. The insert was introduced into the *Sma*I site of the vector containing the *MtDefMd1-OLI-mGFP6* and *ER-CFP* fusions, resulting in a three-fluorophore vector designated *pBIN:ER-ck:MtDefMd1-OLI-mGFP6:MtBcp1_{SP}-mCherry*. Vector pBIN:tp-gk [57] was used for tonoplast localization.

Cultivation of *M. truncatula* plants

Plants were cultivated in a phytocabinet (Klimaschrank KPS 1700, Weisshaar, Bad Salzuflen, Germany) with 16 h/d light (Osram FLUORA L 18WI77 light tubes, 3100-3400 Lux) at 22°C with a relative humidity of 60%. Plants were fertilized with ½ strength Hoagland's solution [59] containing 20 µM phosphate. The solution was prepared with deionised water. For different phosphate (P) and nitrogen (N) supplies,

a PN-variation solution was set up as follows: 1 mM KHCO₃, 1.5 mM K₂SO₄, 1 mM MgSO₄, (0.32, 0.16, 0.081, or 0.02) mM NaH₂PO₄, equilibrated by Na₂SO₄, (1.43, 0.71, 0.36, 0.18) mM NH₄NO₃, (5.71, 2.9, 1.43, 0.71) mM Ca(NO₃)₂, equilibrated by CaCl₂, 0.6 mM NaFeEDTA, 0.2 μM Na₂MoO₄ × 2H₂O, 10 μM H₃BO₃, 0.2 μM NiCl₂ × 6 H₂O, 1 μM ZnSO₄ × 7 H₂O, 2 μM MnCl₂ × 2H₂O, 0.5 μM CuSO₄ × 5 H₂O, and 0.2 μM CoCl₂ × 6 H₂O. The solution was prepared with deionized water, the pH was adjusted to 6.3 with H₂SO₄. Plants were watered from the bottom.

Induction of transgenic *M. truncatula* roots and inoculation of *M. truncatula* with AM fungi or Rhizobia

Transgenic *M. truncatula* roots were generated as described previously [60]. In short, *Agrobacterium rhizogenes* Arqua1 strains were grown for two days at 30 °C on selective TY (0.5 g/l tryptone; 0.3 g/l yeast extract; 0.07 g/l CaCl₂×2H₂O) agar plates. Cells were resuspended in 4 ml PS buffer (40 mM Na₂HPO₄×2H₂O, 85 mM NaCl, 17 mM KH₂PO₄; pH 7 adjusted with HCl). *M. truncatula* seedlings were moisturized and cleared of their testa. The bacterial solution was injected in the hypocotyl of the seedlings with a sterile syringe. Subsequently, seedlings were planted in sterile seramis® (Seramis GmbH, Mogendorf, Germany) and incubated over night at 18 °C in the dark. Finally, they were transferred to the phytocabinet climate chamber. Transgenic hairy roots were screened and mycorrhized four to five weeks after germination. For most experiments, sterile *R. irregularis* spores were used for the inoculation of *M. truncatula* wild type and transgenic roots. 2000 spores were incubated with the shaded plant root for three hours in liquid. Subsequently, plants were potted in 9×9 cm pots with seramis (Seramis GmbH, Mogendorf, Germany) as a substrate. Remaining spores were pipetted on the roots. For RNAi experiments, *R. irregularis* inoculum from a leech preculture was used (Bettina Hause, IPB, Halle, Germany).

For the inoculation of root system with Rhizobia, *Sinorhizobium meliloti*-mRFP [61] was incubated on selective media for two days at 30°C. The bacteria were resuspended in 1x PBS (0.14 M NaCl, 2.7 mM KCl, 1 mM Na₂HPO₄×2H₂O, 1.8 mM KH₂PO₄; pH 7.3) and co-incubated with the shaded plant root for three hours. Subsequently, plants were potted in 9×9 cm pots with seramis (Seramis GmbH, Mogendorf, Germany) as a substrate. Remaining bacteria suspensions were pipetted on the roots.

Isolation of plant RNA from *M. truncatula* roots

RNA isolations were carried out using the RNeasy Plant Mini Kit (Qiagen, Hilden, Germany). β-mercaptoethanol was added to the RLT buffer and 600 μl of this mix were added to each sample. Tissues were disrupted using the FastPrep®-24 (MP Biomedicals, Santa Ana, USA) for 5 times 30 s (6.5 m/s). The RNA concentrations were measured using a Nanodrop (Thermo Fisher Scientific, Langenselbold, Germany) and checked on agarose gels.

Real-time RT-PCR

Real-time RT-PCR analyses were performed using the SensiFAST™ SYBR® No-ROX One-Step Kit (Qiagen, Hilden, Germany) with primers listed in the S1 Table. Primers were designed to match an annealing temperature of 55 °C and were tested for gene-specific amplifications. 5 ng of total RNA were used as a template in 20 µl for the mycorrhization time course, the *ram1-1* and the *MtDefMd1* overexpression experiment. Otherwise, 50 ng of total RNA were used. RT-PCR reactions followed a three-step cycling program: reverse transcription at 45 °C for 10 min; polymerase activation at 95 °C for 2 min; PCR amplification with 40 cycles at 95 °C for 5 sec, 55°C for 10 sec, and 72 °C for 8 sec.

Biological replicates were measured in three technical replicates. The housekeeping gene *MtTefα* was used for normalization. Average values were used to calculate gene expression levels via the $2^{-\Delta CT}$ method with $\Delta CT = CT_{\text{Gene}} - CT_{\text{MtTef}\alpha}$. To relate gene expression to the degree of fungal colonization or the presence of active arbuscules, a ratio with *GiTubα* or *MtPt4* expression was calculated, respectively. The degree of fungal colonization was estimated by measuring the expression of the *GiTubα* gene encoding an alpha-tubulin [37], whereas the *MtPt4* transcript amount served as an estimate for the presence of active, phosphate-transporting arbuscules [62]. The mean and standard error of the mean of all biological replicates was calculated after normalization and was visualized, if not stated differently. Using MS Excel 2016 (Microsoft Corp., Redmond, Washington, USA), two-tailed Student t-tests were performed to check differences in gene expression between mutant-, RNAi-, overexpression-, and wild type roots. To determine, if the expression of AM-related defensin- and AM marker genes is congruent during the course of mycorrhization, Pearson correlation was calculated by using the MS Excel 2016 (Microsoft Corp., Redmond, Washington, USA) KORREL function for comparing the average gene expression levels at each time point.

Affymetrix GeneChip hybridizations

Global gene expression data from *Affymetrix GeneChip* hybridizations studying a time course of root colonization by AM fungi from 0 to 42 dpi (Rico M. Hartmann, LUH, Hannover, personal communication), were filtered for ≥ 2 -fold at $p \leq 0.05$ induced gene expression between selected time points. In addition, gene expression in the mycorrhized *MtRam1* mutant *ram1-1* (Rico M. Hartmann, LUH, Hannover, personal communication), the mycorrhized *MtPt4* mutant *pt4-1* [62], and mycorrhized *MtMyb1*-RNAi roots (Claudia Hoge Kamp, LUH, Hannover, personal communication) was compared to the corresponding mycorrhized control roots, using the filter settings mentioned above.

Histological studies

To study the activity of promoter-*gusA* fusions, transgenic roots were incubated in GUS staining buffer described previously [51]. Cells with the strongest promoter activity were visible after 3 hours. After overnight staining, also cells with a weak promoter activity were stained. Finally, roots were rinsed with water.

To stain fungal structures for quantification of AM fungal matter via the gridline intersection method [63] and confocal microscopy, 1-2 cm root sections were incubated in 10 % (w/v) KOH at 95 °C for 7 minutes. Consecutively, the roots were washed three times with water and incubated in staining solution with 20 µg/ml WGA-Alexa Fluor 488 in 1x PBS (0.14 M NaCl, 2.7 mM KCl, 1 mM Na₂HPO₄·2H₂O, 1.8 mM KH₂PO₄; pH 7.3) for 12-24 hours. Samples were protected from light. Finally, excessive dye was washed out with water. Mycorrhized root samples were randomly collected and pooled from each plant. Three pools of 6 root sections were photo-documented by confocal microscopy.

For a staining of storage and membrane bound lipids, Neutral Red was diluted in 10 mM MOPS-buffer (pH 8) (1 µg ml⁻¹) and immediately applied to fresh root sections. The roots were incubated for 30 minutes in the staining solution and then transferred to 10 mM MOPS-buffer (pH 8).

For histological studies of nodules, a 1 mM LysoSensor™ Green DND-189-Solution (in DMSO) was diluted to 0.3 mM in 10 mM MOPS-buffer (pH 8). Samples were incubated for 3 h. Consecutively, the roots were photo-documented under the fluorescence binocular (Fig 19) using the bright field and the GFP-fluorescence channel. 1-2 cm sections of mycorrhized roots were pre-screened under the fluorescence binocular. Longitudinal thin sections were analyzed. They were generated by hand with a razor-blade and later stored in 10 mM MOPS-buffer (pH 8). Confocal microscopy was used to locate GFP and RFP in the inner root cortex.

Detection of reporter proteins via fluorescence microscopy

Transgenic *M. truncatula* roots were identified using a stereo microscope (Leica MZ10F, Sohns, Germany). 1-2 cm sections of mycorrhized roots were selected. For the localization of fluorescent reporter proteins, longitudinal root sections were cut by hand with a razor blade. These sections were transferred into a physiological buffer (39 mM Na₂HPO₄·2H₂O, 86 mM NaCl, 22 mM KH₂PO₄; pH 7). GFP (500-520 nm), CFP (460-490 nm) and mCherry (599-621 nm) were detected in the inner root cortex using a hybrid detector and confocal microscopy (Leica TCS SP8 MP, Sohns, Germany). To evaluate, if the detected signals originate from the correct fluorophore, lambda-scans were performed in the range of 498-553 nm (mGFP6), 458-513 nm (CFP), and 575-635 nm (mCherry). Each lambda-scan contained eleven detection steps with 5 (mGFP6 and CFP), and 11 (mCherry) nm bandwidth, respectively. For promoter-GUS studies, an Eclipse TE2000-E inverse confocal laser scanning microscope (Nikon GmbH, Düsseldorf, Germany) and software EZ-C1 (Nikon GmbH, Düsseldorf,

Germany) were used. In nodules LysoSensor™ Green DND-189 (598-618), mRFP (790-795) and WGA-Alexa Fluor 488 (510-531 nm) were detected in the inner root cortex using a hybrid detector and confocal microscopy (Leica TCS SP8 MP, Soehnle, Germany). With the same hardware Neutral Red-stained lipids were detected in the yellow (540-560 nm) and red range of the light spectrum (590-609 nm).

Heterologous expression of *MtDefMd1* in *S. cerevisiae*

The yeast two-hybrid screens were performed with the Matchmaker® Gold system from Clontech (Canada) following the manual's instructions. The complete CDS of *MtDefMd1* was PCR amplified and integrated via *SmaI* restriction sites into the bait-vector *pGBKT7*. As recommended, the bait was tested for toxicity and the library was tested for viability according to the manufacturer's protocol. The yeast transformation was performed according to (Daniela Floss, Cornell University, NY, USA, personal communication):

Yeast strains were incubated onto SD plates Trp- (*Y2HGold*) or Leu- (*Y187*), grown at 30°C for 2-3 days. Pre-streak yeast strains were pre-streaked onto YPDA plates, or on SD –Leu or –Trp, in case of carrying a plasmid, respectively. They were incubated overnight. Then liquid cultures (5-15 ml) of yeast strains were started, incubated at 30°C shaking at 150 rpm. The culture was centrifuged at 1000 x g for 5 min. It was washed in sterilized H₂O (same volume as overnight culture) and vortexed to get a suspension. The washing step was repeated. Afterwards 1ml aliquots of the cell suspension were made. Those can be stored at -70°C. For the transformation, the supernatant was removed by a centrifugation of 1000 xg for 5 min. 100 µl 1-step buffer (freshly prepared; 0.2 N Lithium Acetate, 40% PEG 3350, 100mM β-mercaptoethanol), were used for the resuspension of cells. 6 µl carrier DNA mix (primarily heat the carrier DNA at 99°C for 5 min, then chill on ice) were added. The vector DNA (~100 ng) was added to the cells and mixed by tapping. Consecutively the cells were incubated at 45°C for 30 min, they were vortexed every 10 min. Then 40 µl suspensions were spread on selection plates. Plates were incubated at 28°C for 3 days.

Results

Arbuscular mycorrhiza-related defensins differ from defense-related defensins

The four AM-related defensin genes *MtDefMd1*, *MtDefMd2*, *MtDefMd3*, and *MtDefMd4* (identifiers Mtr.35854.1.S1_at, Mtr.7210.1.S1_at, Mtr.3215.1.S1_at, and Mtr.31214.1.S1_at in the *Medicago* Gene Expression Atlas [64], respectively) were primarily identified based on their strong up-regulation in mycorrhizal roots [37].

In the deduced amino acid sequences of MtDefMd1-4, signal peptides were located up to the 29th amino acid (Fig 1, S2 Table), suggesting that the defensins MtDefMd1-4 are secreted. Since it is known that the ER-Golgi network is redirected during the establishment of arbuscules [65], a targeting of MtDefMd1-4 to the periarbuscular space (PAS) in symbiotic cells is thus possible.

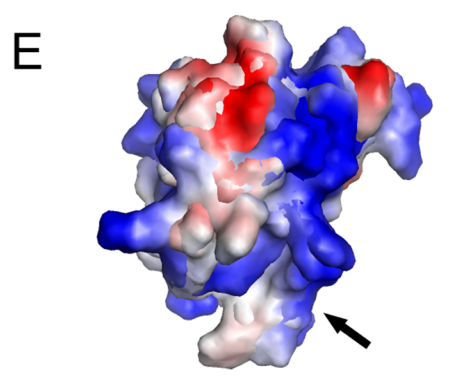
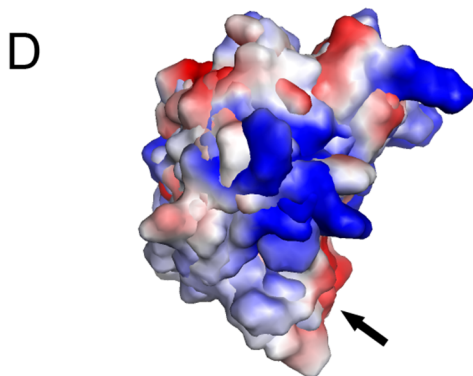
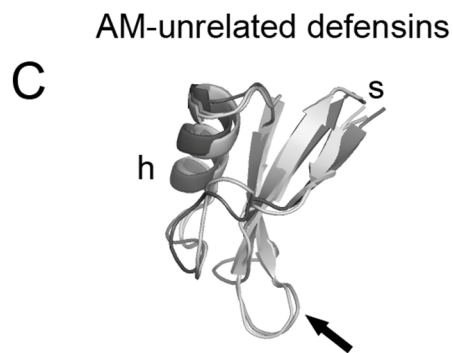
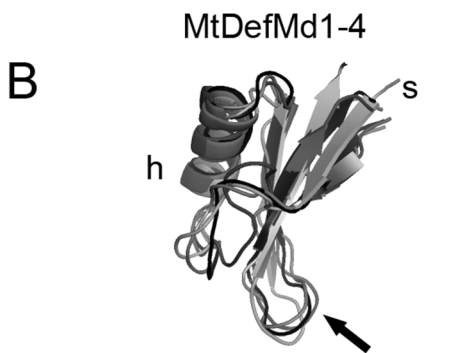
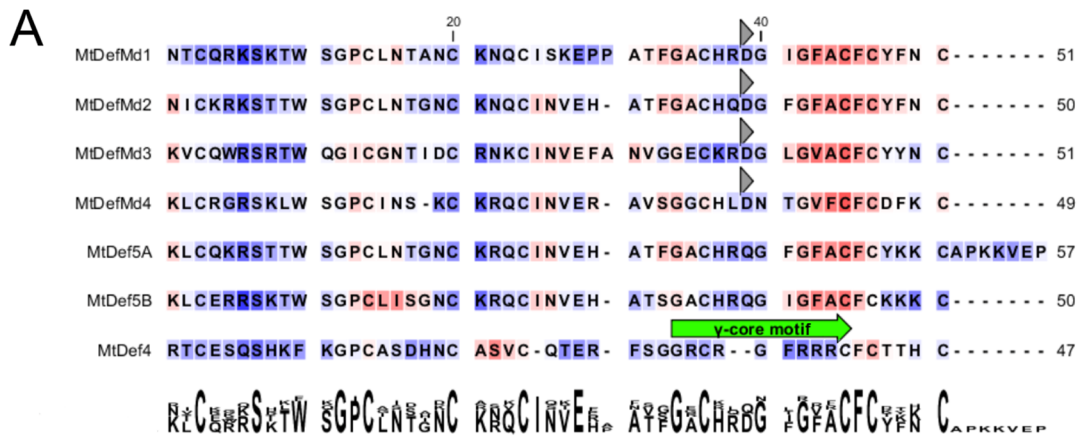


Fig 1. Sequence analyses of AM-dependent defensins MtDefMd1-4 and AM-unrelated defensins.

Secondary structures of MtDefMd1-4 and AM-unrelated defensin-like proteins of *M. truncatula* (A), a representation of their three-dimensional structures (B and C), as well as surface electrostatics (D and E) are shown. Predicted signal peptides were removed from the mature amino acid sequences. Consecutively, the defensins were aligned based on their secondary structures. Background colorization of the amino acids (in A) indicate hydrophobicity in a scale from red to blue (red: high hydrophobicity). A conserved aspartic acid in the C-terminal region of MtDefMds is marked with a grey triangle. For the bi-domain defensin MtDef5, the domains MtDef5A (including a 7 amino acid linker towards the MtDef5B domain) and MtDef5B are shown. After modelling the three-dimensional structures of the MtDefMd1-4, MtDef4 and MtDef5A/B defensins, they were visualized (B and C) and their surface electrostatics were calculated (D and E). The region congruent to the γ -core motif is indicated with arrows. The following proteins were used for comparisons in addition to MtDefMd1-4: MtDef5 A [66], MtDef5 B [66] and MtDef4 [30].

To investigate the secondary structures of the AM-dependent defensins MtDefMd1-4 in comparison to the AM-unrelated defensins MtDef4 [30] and MtDef5A/B [66], the amino acid sequences of the mature proteins were compared (Fig 1, A). Subsequently, the three-dimensional structures of MtDefMd1-4 [based on HsAFP1, 40; RsAFP1, 41; HsAFP1, 40; and major pollen allergen Art. v1, 42], MtDef5A [based on HsAFP1, 40], MtDef5B [based on HsAFP1, 40], and MtDef4 [MtDef4, 30] were modeled and visualized (Fig 1, B and C).

AM-dependent MtDefMds as well as AM-unrelated defensins are structurally conserved, being composed of one α -helix, three β -strands and the γ -core motif (Fig 1, B and C). The four AM-related defensins are characterized by a hydrophobic C-terminus and an acidic amino acid (aspartic acid) at position 42 (Fig 1, A). Although this discriminates them from the AM-unrelated defensin MtDef4 [30], both domains of the AM-unrelated defensin MtDef5A/B, which was shown to confer a broad antifungal activity [66], also display hydrophobic amino acids at the C-terminus (Fig 1, A). Interestingly, some areas of the MtDefMd1-4 and AM-unrelated defensins exhibit a different distribution of cationic amino acids (Fig 1, D and E) and the region corresponding to the γ -core motif, a variable loop essential for entry of MtDef4 in fungal cells [30], displays a differing pattern of surface electrostatics in AM-dependent and -unrelated defensins (Fig 1, D and E). To study this further, the protein charge of AM-dependent, AM-unrelated defensins were computed in a range of pH milieus (Fig 2).

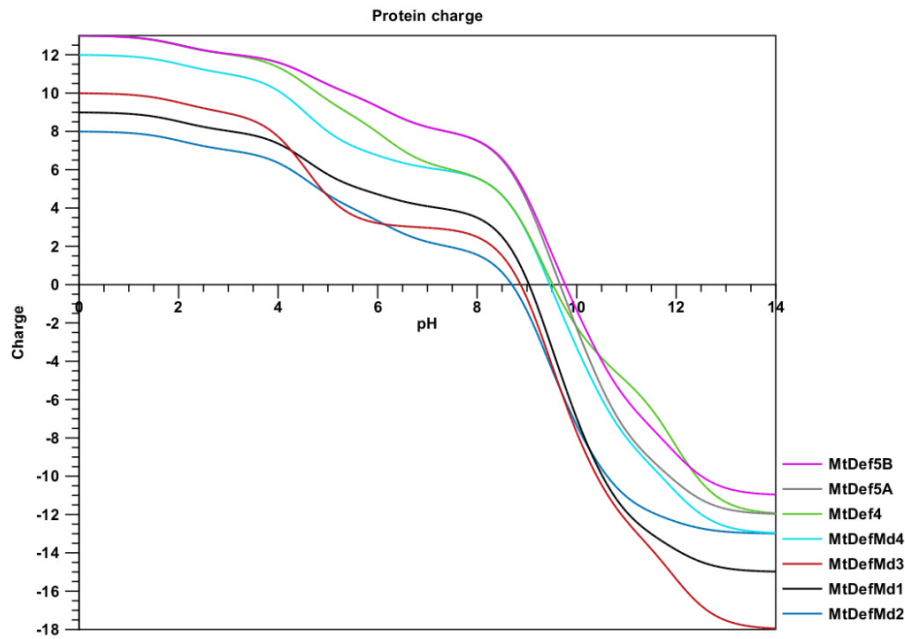


Fig 2: Protein charge of AM-dependent and AM-unrelated defensins in the pH range of 0 to 14. Charges were computed based on the amino acid sequence.

Globally, the defensins and the NCR-peptide 247 show a similar charge in the pH range of 7 to 14 (Fig 2), but in an acidic milieu, the symbiosis related antimicrobial peptides/proteins have a slightly lower charge than the AM-unrelated defensins (Fig 2). Due to an acidic pH in symbiotic compartments, this could be of relevance for their function.

In conclusion, MtDefMd proteins exhibit some differences to non-symbiotic defensins and are predicted to be secreted, suggesting a function at the interface between plants and AM fungi.

Heterologous translation in *S. cerevisiae* underlines the impact of hydrophobic amino acids for the AM-related defensin MtDefMd1

To further investigate the properties of AM-dependent defensins, it was attempted to overexpress one member of the *MtDefMd* gene family (*MtDefMd1*) in yeast. The full-length CDS of the defensin gene was transferred into the bait vector *pGBKT7* and a library screening was performed. Since the library was composed of mycorrhized, uninfected, nodulated and Nod-factor treated *M. truncatula* roots, it is suitable to detect symbiosis-related targets (Rico M. Hartmann, LUH, unpublished).

No candidate, identified during the initial library screening, did interact strongly enough with MtDefMd1 to grow on high-stringency medium, containing Aureobasidin and X- α Gal, but lacking four essential amino acids (data not shown). However, candidates that could grow and turned slightly blue on medium-stringency medium were picked and checked via colony PCR and DNA-sequencing (Table 1).

Table 1: Candidates for MtDefMd1 interactors from yeast two-hybrid library screening.

GeneChip identifier	Genome ID	Annotation*
Mtr.16164.1.S1_at	Medtr4g079680.1	putative transmembrane protein
Mtr.8617.1.S1_at	Medtr8g005420.1	plant acid phosphatase
Mtr.13497.1.S1_at	Medtr4g020040.1	plant inositol phosphorylceramide synthase
Mtr.18649.1.S1_s_at	Medtr2g034470.2	glucan endo-1,3-beta-glucosidase
Mtr.3115.1.S1_at	Medtr3g053650.1	cytochrome C oxidase assembly protein CtaG/COX11
Mtr.31199.1.S1_s_at	Medtr8g100135.1	cytochrome P450 family protein
Mtr.5779.1.S1_at	Medtr7g063470.2	bHLH transcription factor-like protein
Mtr.40313.1.S1_at	Medtr6g013210.1	40S ribosomal protein S28-1
Mtr.8497.1.S1_at	Medtr3g435460.1	light-harvesting complex I chlorophyll A/B-binding
no hit	Medtr1g112190.1	no homology
no hit	chr1:50731847-50744037	no homology

*Candidate interactors associated with lipid breakdown or processes at biomembranes are shaded in grey

Apart from sequences that could not be annotated, transcripts of high abundance such as ribosomal and photosynthesis related proteins, and redox-related proteins, the candidate interactors were associated with lipid breakdown or processes at biomembranes (Table 1, shaded in grey). In general, this supports the hydrophobic nature of the MtDefMd1 amino acid composition. Furthermore, since plant acid phosphatases, inositol phosphorylceramide synthases, and beta-glucosidases are often found in acidic membrane enclosed compartments, such as late endosome-derived structures, conclusions on the native milieu of MtDefMd1 may be drawn. However, since the short traversal of the nuclear envelope towards the nucleus in yeast cells differs from the stepwise passing and subsequent modification in the ER *cisternae* of plant cells expressing *MtDefMd1*, these conclusions have to be treated with caution.

Together, the potential candidate interactors belonging to membrane-related processes indicate that the mature MtDefMd1 protein could be associated with membrane lipids and could function in membranes of the plant-fungus interface.

***MtDefMd* transcription is upregulated in the course of mycorrhization and depends on phosphate and nitrogen supply**

A mycorrhization time course was set to define the temporal regulation of *MtDefMd1-4* expression. *M. truncatula* plants were inoculated with *R. irregularis* spores using ½ strength Hoagland's solution containing 20 µM phosphate for fertilization, and the root system was harvested weekly from 7 to 42 days post inoculation (dpi). The expression of *MtDefMd1-4*, a fungal α -tubulin (*GiTub α*) gene [36], and two *M. truncatula* AM marker genes (*MtPt4* [67], *MtMyb1* [17]) was measured via real-time RT-PCR (Fig 2), using the *MtTefa* gene encoding a translation elongation factor for normalization.

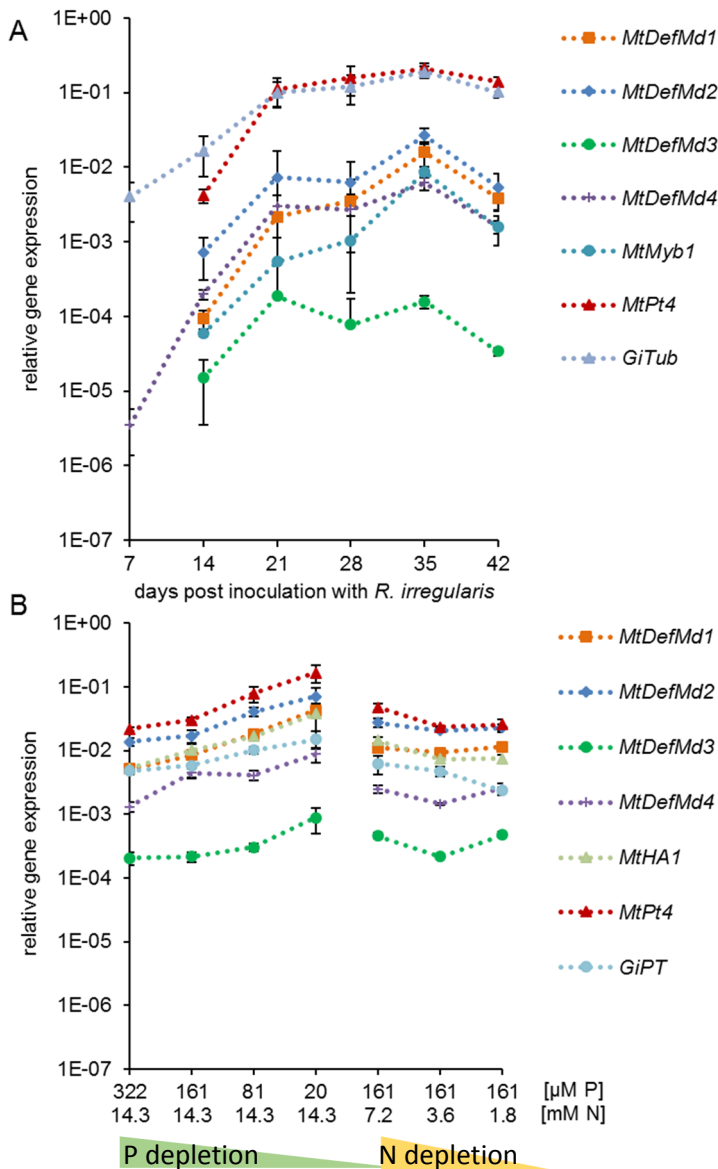


Fig 3: Relative expression of *MtDefMd1-4* and selected AM marker genes in *M. truncatula* roots in a time course of mycorrhization and under different phosphate and nitrogen regimes.

Gene expression is given in relation to the expression of *MtTefa*. Plant roots were harvested from 7 to 42 days post inoculation weekly (A) and at 28 days (B) post inoculation with *R. irregularis*. Biological replicates are three pools of four (A) or one pool of six (B) plant roots per treatment, respectively. Pi depletion is indicated with a green triangle and N depletion with a yellow triangle. The standard deviation of three pools of biological replicates (A) and the standard error of the mean of three technical replicates (B) is given. Abbreviations: P, phosphate; N, nitrogen

Expression of *MtDefMd1-4*, the fungal α -tubulin gene *GiTub α* [36] as well as the *M. truncatula* AM marker genes *MtPt4* [67] and *MtMyb1* [17] *MtDefMd1*, *MtDefMd2*, and *MtDefMd4* expression strongly correlated ($r \geq 0.8$) to that of all AM marker genes, while the correlation *MtDefMd3* transcription was lower but still positive ($r \geq 0.51$, S3 Table). Transcription of the *MtDefMd* genes thus followed the colonization of plant roots with *R. irregularis*, estimated by the expression of the fungal and plant AM marker genes *GiTub α* , *MtPt4*, and *MtMyb1* (Fig 2). Whereas transcription of the fungal α -tubulin gene and *MtDefMd4* already rose from 7 dpi in a constant manner (Fig 3, A), expression of the other three *MtDefMd* genes as well as the AM markers genes *MtPt4* [67] and *MtMyb1* [17] strongly enhanced from 14 dpi on. Apparently, fungal mass enhanced from the start of inoculation, while arbuscules were effectively built from 14 dpi on. Interestingly, at 42 dpi, the expression of all genes measured decreased, possibly due to a control of the degree of mycorrhization by the plant. The delivery of phosphate and nitrogen compounds to the plant is essential for regular arbuscule

development [67, 68, 69]. To investigate whether availability of either nutrient influences *MtDefMd* expression, variable amounts of 20-322 μM phosphate and 1.5-14.3 μM nitrogen (delivered as ammonia and nitrate) were used to fertilize *M. truncatula* (Fig 3, B) during 28 days of mycorrhization. These experiments indicated that *MtDefMd* expression is congruent to the arbuscule-specific phosphate transporter gene *MtPt4* and the H^+ -ATPase gene *MtHA1*, showing increase at lowered phosphate and decrease at low nitrogen concentrations (Fig 3, B).

It can be summarized that on a whole-root level, the expression of the four AM-activated *MtDefMd* genes correlates with the expression of marker genes for root colonization and AM formation.

***MtDefMd1* and *MtDefMd2* promoters are active in cells with fully developed arbuscules**

Since *MtDefMd1* and *MtDefMd2* are the defensin genes activated most strongly during the later colonization stages of *M. truncatula* roots with *R. irregularis* (Fig 3), we focused on these genes for further studies. Transcriptional fusions of the promoters of *MtDefMd1* and *MtDefMd2* with the *gusAint* reporter gene were expressed in transgenic roots of *M. truncatula* A17 wild type to investigate their spacio-temporal expression during AM. Roots were mycorrhized for 18 dpi and analyzed via GUS and WGA-Alexa Fluor 488 staining (Fig 4).

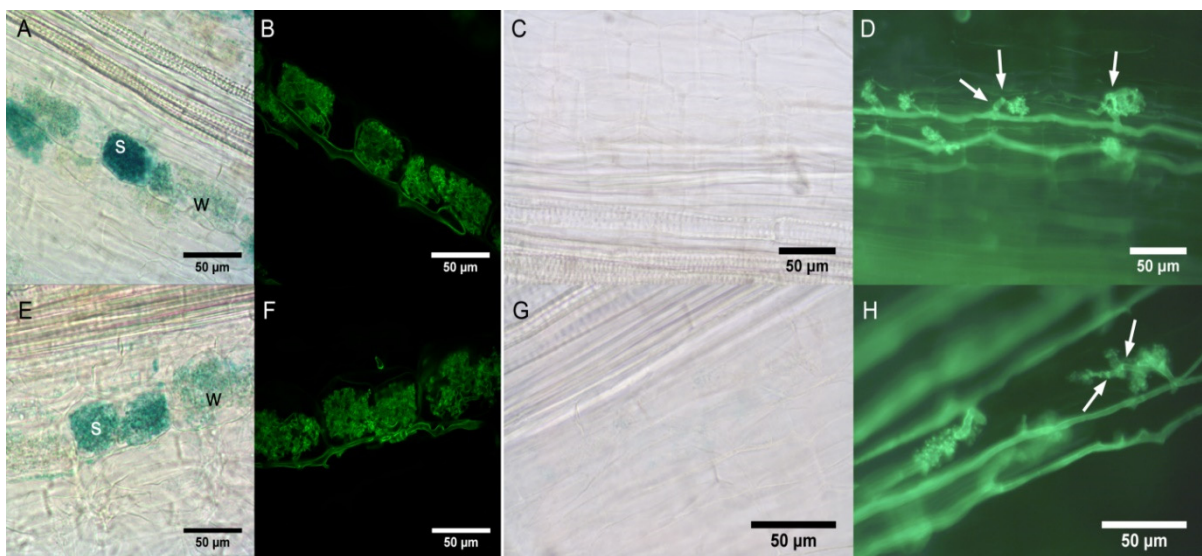


Fig 4: Histochemical localization of *MtDefMd1* and *MtDefMd2* promoter activities.

Activities of *MtDefMd1* (A-D) and *MtDefMd2* (E-H) promoters were studied in transgenic, mycorrhized roots of *M. truncatula* A17 wild type (A, B, E, and F) and *pt4-2* roots (C, D, G, and H). Representative images of roots after 18 (A, B, E, and F) or 56 (C, D, G, and H) days post inoculation with *R. irregularis*. The GUS-staining (A, C, E, and G) as well as the WGA-Alexa Fluor 488 staining (B, D, F, and H) were performed over night. Septa are denoted by arrows. Abbreviations: w, cells with weak promoter activity; s, cells with strong promoter activity

Activities of the *MtDefMd1* and *MtDefMd2* promoters were investigated from 7 to 56 dpi. In wild type roots, their activities varied from cell to cell, as shown for 18 dpi in Fig 4 (A and E). While in pre-arbuscular stages and in cells with arbuscules appearing very young, no promoter activities were

detected, GUS staining was present in cells with fully developed and apparently active arbuscules. While arbuscule-containing cells with the highest promoter activities were already visible after 3 hours (data not shown), others were only visible after overnight staining (Fig 4, A and E). This indicates that the *MtDefMd1* and *MtDefMd2* promoters are activated in cells containing mature, fully developed arbuscules. To correlate *MtDefMd1* and *MtDefMd2* promoter activities with arbuscule development, the corresponding *gusAint* fusions were expressed in *pt4-2* mutants displaying premature arbuscule degeneration (PAD) [68]. Interestingly, there was no activity of the *MtDefMd1* and *MtDefMd2* promoters detectable even after 56 dpi (Fig 4, C, D, G, and H) and overnight staining. This observation corresponds to a downregulation of these genes in *pt4-2* mutant in comparison to wild type roots [17]. In conclusion *MtDefMd1* and *MtDefMd2* promoter activities are correlated with the presence of fully developed, active arbuscules, while pre-mature arbuscule degradation does not involve transcription of these defensin genes. This suggests that MtDefMd defensins are not part of the PAD program activated in *pt4-2* mutants.

***MtDefMd1* and *MtDefMd2* expression is impaired in *ram1-1* mutants forming birdfoot arbuscules**

To pinpoint the stage of arbuscule development, which coincides with *MtDefMd1* and *MtDefMd2* transcription, *ram1-1* mutants [69] were used. These mutants lack the transcription factor MtRam1, an important regulator that coordinates the further development of arbuscules post the birdfoot stage by activating the transcription of a suite of AM-associated genes. To study *MtDefMd1* and *MtDefMd2* expression in relation to arbuscule maturation, mycorrhized *ram1-1* and wild type RNA samples were analyzed via real-time RT-PCR (Fig 5).

Whereas no *MtDefMd1* and *MtPt4* transcripts were detectable in mycorrhized *ram1-1* mutants, the expression of *MtDefMd2*, *MtDefMd3*, *MtDefMd4* and *GiTubα* appeared strongly reduced. Only a fungal phosphate transporter gene (*GiPt*) was not affected in expression. When normalizing gene expression to the level of root colonization by building a ratio with *GiTubα* expression, only the expression of *MtDefMd1*, *MtDefMd2*, and *MtPt4* appeared absent or strongly downregulated in *ram1-1* mutants (fig 5, B).

Based on these studies, the time point of MtDefMd1 and MtDefMd2 action can be placed in the arbuscule-containing cells, post the birdfoot stage. This corresponds to the observation that the promoters of AM-related defensin genes are active in cells containing fully developed arbuscules.

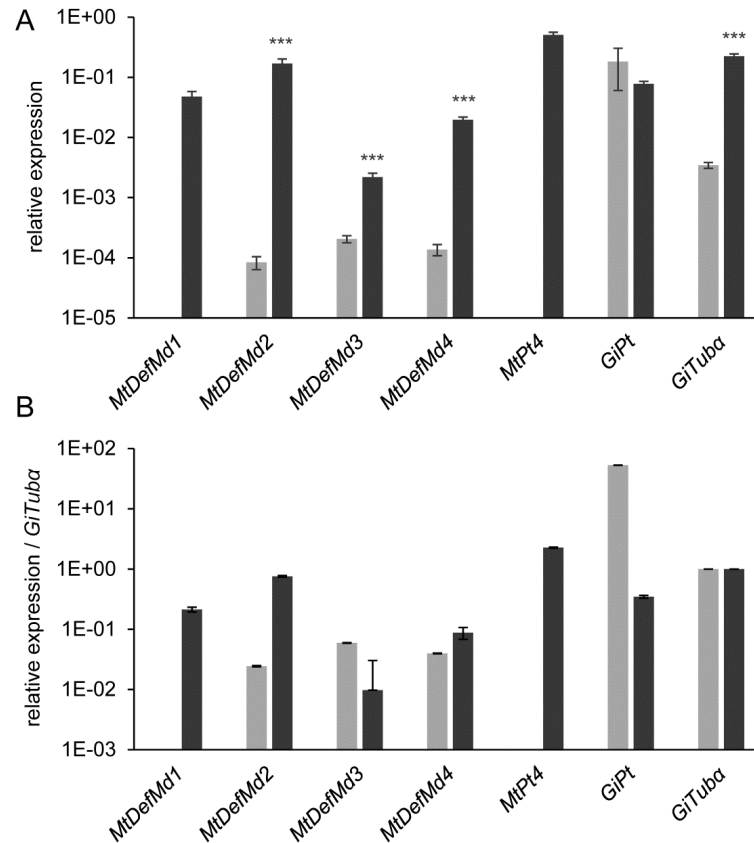


Fig 5: Relative expression of *MtDefMd* and selected AM marker genes in mycorrhizal *M. truncatula* A17 wild type and *ram1-1* roots.

Transcript amounts are shown relative to *MtTefa* (A) and were additionally normalized by building a ratio with *GiTuba*-expression (B). *ram1-1* measurements are colored in light grey, the corresponding wild type measurements in dark grey. Roots were harvested at 36 days post inoculation with *R. irregularis*. n=12 biological replicates, depicted is the standard error of the mean. Statistical significance: *** $p \leq 0.0005$

Five AM-related *MtDefMd* and three EXOCYST genes change their expression in dependence of the formation of a functional symbiotic interaction

To complete the picture of *MtDefMd*-expression, genome-wide *Affymetrix GeneChip* hybridizations from a time course of mycorrhization, presented in Chapter II (Fig 17) were evaluated (R.M. Hartmann, LUH, unpublished). In addition to defensin genes, *EXOCYST* gene expression over time was studied. Subsequently, defensin and *EXOCYST* genes that were ≥ 2 fold induced at $p \leq 0.05$ in mycorrhized control roots in comparison to mycorrhized *ram1-1* and *pt4-1* mutant lines (R.M. Hartmann, LUH, unpublished and 41) as well as mycorrhized *MtMyb1*-RNAi-roots (Claudia Hoge Kamp, LUH, unpublished), showing defects in AM-associated key regulator genes, were identified (Fig 6).

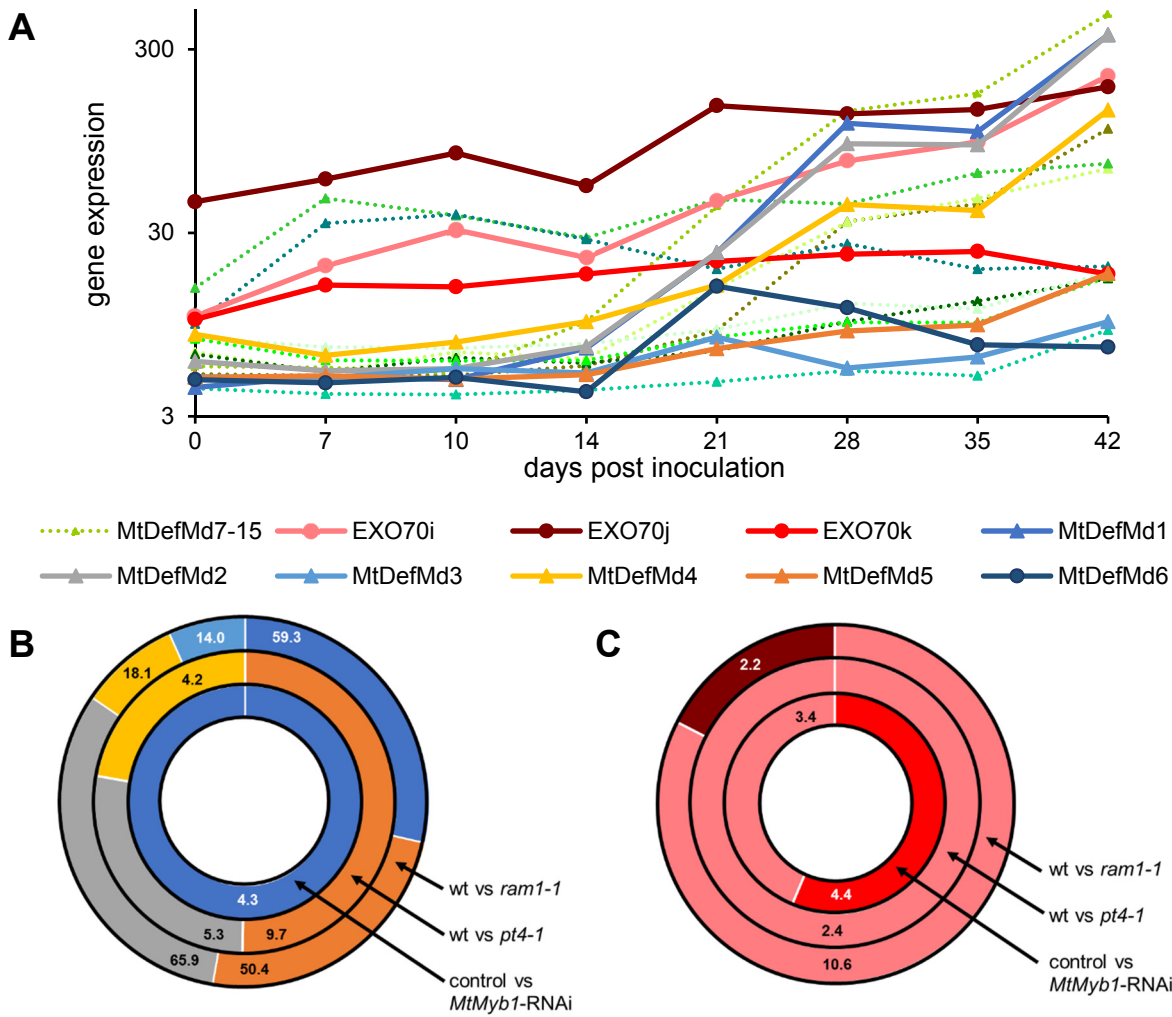


Fig 6: Expression of *MtDefMd*- and AM-induced *EXOCYST* genes in mycorrhized *M. truncatula* control and mutant roots.

Data from *Affymetrix GeneChip* hybridizations are depicted in A to C. *Defensin* and *EXOCYST* gene expression over a time course of root colonization by AMF (A) (Rico M. Hartmann, LUH, unpublished) as well as *defensin* and *EXOCYST* gene induction in mycorrhized *M. truncatula* control roots vs. roots defective in symbiotic functions (B and C) are shown. In A, on the y-axis, the expression levels of *defensin* and *EXOCYST* genes, depicted as Bi-weight average signals from *GeneChip* hybridization, are shown. Only genes that were ≥ 2 fold at $p \leq 0.05$ induced at least in one time point in comparison to 0 dpi were depicted at 0, 7, 10, 14, 21, 28, 35 and 42 days after inoculation of plants with *R. irregularis*. Genes were sorted in two gene families, the *defensin* genes being depicted in various colors and the *EXOCYST* genes being depicted in red. Non AM-related *MtDefMd* genes that were not studied in B are represented by dotted lines. B to C sections show fold changes of gene expression. Each segment represents a *defensin* (B) or *EXOCYST* gene (C). Each ring represents a Gene Chip hybridization. Only genes that were ≥ 2 fold induced at $p \leq 0.05$ in mycorrhized control roots in comparison to mycorrhized *ram1-1* mutants (R.M. Hartmann, LUH, unpublished), mycorrhized *pt4-1* mutants [41] as well as mycorrhized *MtMyb1*-RNAi-roots (C. Hoge Kamp, LUH, Hannover, unpublished) after inoculation of plants with *R. irregularis* (*ram1-1* and *MtMyb1*-RNAi) or *Gigaspora gigantea* (*pt4-1*), respectively, were shown. Biological replicates are three pools of 6 plant roots per time point, each, respectively. The *defensin* and *EXO70* genes and their genome identifiers are as follows: *EXO70i* (*Medtr1g017910.1*); *EXO70j* (*Medtr2g096230.1*); *EXO70k* (*Medtr5g073460.1*); *MtDefMd1* (*Medtr8g012805.1*); *MtDefMd2* (*Medtr8g012835.1*); *MtDefMd3* (*Medtr8g012875.1*); *MtDefMd4* (*Medtr8g012885.1*); *MtDefMd5* (*Medtr8g012845.1*); *MtDefMd6* (*Medtr8g070770.1*); *MtDefMd7* (*Medtr8g012820.1*); *MtDefMd8* (*Medtr8g012835.1*); *MtDefMd9* (*Medtr8g012860.1*); *MtDefMd10* (*Medtr8g012885.1*); *MtDefMd11* (*Medtr8g012865.1*); *MtDefMd12* (*Medtr8g012885.1*); *MtDefMd13* (*Medtr8g012815.1*); *MtDefMd14* (*Medtr8g012845.1*); *MtDefMd15* (*Medtr3g097420*). Abbreviations: wt, wild type; vs, versus

In general, AM-induced defensin genes displayed an expression that mostly increased strongly, for example ~83- (MtDefMd1), ~60- (MtDefMd2), ~2- (MtDefMd3), ~16.7 (MtDefMd4), and ~3.7 (MtDefMd5) from 0 to 42 dpi (Fig 6, A; see data CD). Although some of the defensin genes may be induced due to processes of root growth and aging, *MtDefMd1*, *MtDefMd2*, *MtDefMd3*, *MtDefMd4*, and *MtDefMd5* are dependent on MtRam1 (Fig 6, B). Here, those five defensin genes were induced in wild type roots from ~14- to ~69-fold (Fig 6, B), indicating MtRam1-dependency, whereas only three of these *MtDefMd* genes were ≥ 2 fold induced in control roots in comparison to *pt4-2*-mutant plants (Fig 6, B), which indicated that they depend on active arbuscules. Only *MtDefMd1* was induced in control roots vs. *MtMyb1*-RNAi roots, displaying that the defensin gene could be MtMyb1-induced and thus be connected to a later stage in the symbiosis (Fig 6, B).

Apparently, a differing composition of MtDefMds is accompanying the arbuscule life cycle and corresponds to the activity of key regulator genes of the AM symbiosis, such as *MtRam1*, *MtPt4*, and *MtMyb1*.

Recently, the existence of specialized cargos during the AM symbiosis was suggested, as there is usually a large variety of AM-related EXO70 proteins [23]. If the corresponding genes were visualized as has been described afore for *MtDefMd* genes, each key regulator step in arbuscular life again includes the presence of a defined set of family members. Interestingly, several members require MtMyb1-transcription, as they are suppressed in RNAi:Myb1-roots (Fig 6, A). These findings imply that during the turnover of former arbusculated into regenerated post-symbiotic cells, the intracellular targeting could be remodeled.

Knockdown of *MtDefMd1* and *MtDefMd2* does not affect expression of AM marker genes

Since *MtDefMd1* and *MtDefMd2* promoter activities were connected to fully developed arbuscules, it was investigated, if their knock-down would affect arbuscule development. To reduce transcription of *MtDefMd1* and *MtDefMd2* simultaneously, an RNA interference (RNAi) construct targeting both genes was expressed in mycorrhized transgenic *M. truncatula* roots.

Due to high similarities between the short *MtDefMd1* and *MtDefMd2* sequences, it was not possible to design gene-specific primers outside the region affected by the RNAi construct. Therefore, both genes were measured simultaneously in mycorrhized transgenic RNAi- and control roots (Fig 7). Since *MtDefMd2* expression alone was knocked down to 5.9 %, the concomitant *MtDefMd1* and *MtDefMd2* reduction to appr. 3 % indicated that similar to *MtDefMd2*-, only residual amounts of *MtDefMd1* transcripts remained, confirming an efficient knock-down of both *MtDefMd1* and *MtDefMd2* expression (Fig 7, A). In contrast, transcript amounts of *MtDefMd3*, *MtDefMd4*, *MtPt4*, and *GiTub α* did not differ significantly between RNAi- and control roots (Fig 7, A and B). When normalized to the number of active arbuscules by building a ratio to *MtPt4*-expression (Fig 7, B), the reduction of

MtDefMd1 and *MtDefMd2* transcript amounts remained very strong. This was also observed, when transcript levels were normalized to fungal presence by building a ratio to *GiTuba* expression (not shown).

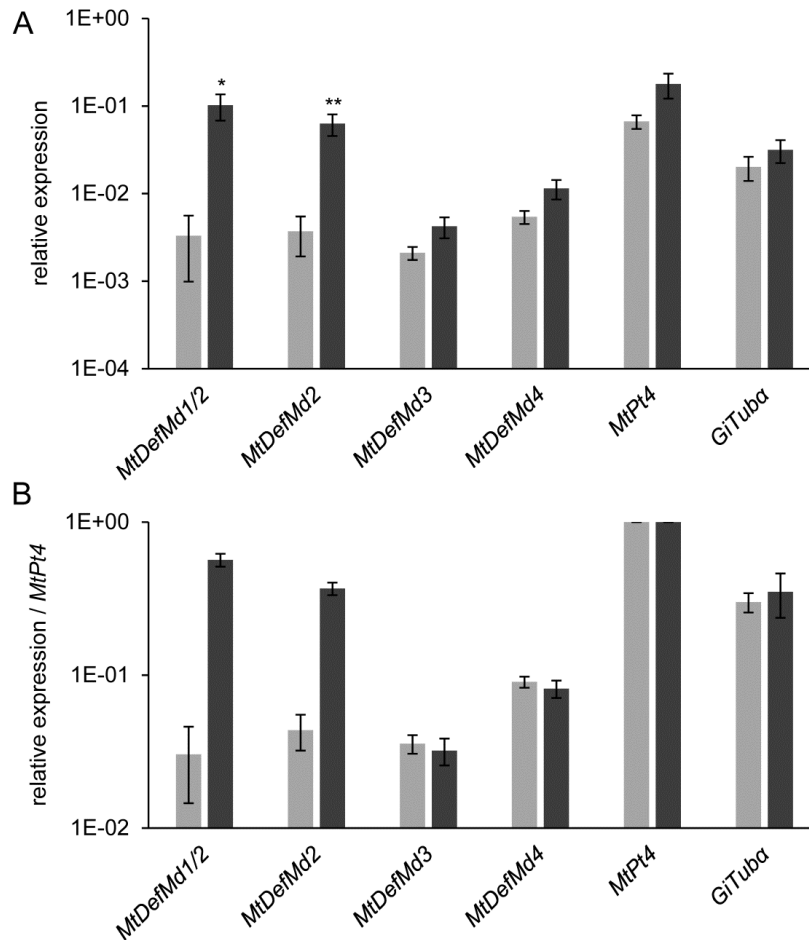


Fig 7: Relative expression of *MtDefMd* and selected AM marker genes in mycorrhizal RNAi:*MtDefMd1/2* and RNAi:*gusAint* roots of *M. truncatula*.

Transcript amounts are shown relative to *MtTefα* (A) and were additionally normalized by building a ratio to *MtPt4*-expression (B). Measurements from RNAi:*MtDefMd1/2* roots are colored in light grey, corresponding RNAi:*gusAint* control measurements in dark grey. Roots were harvested at 28 days post inoculation with *R. irregularis*. n=12 biological replicates, depicted is the standard error of the mean. Statistical significances: * $p \leq 0.05$, ** $p \leq 0.005$

Since the severe knock-down of *MtDefMd1* and *MtDefMd2* did not lead to significant changes in *MtPt4* and *GiTuba* expression, we conclude that these *MtDefMd* genes are not essential predecessors for a successful fungal colonization and for the formation of active, phosphate-transporting arbuscules.

Overexpression of *MtDefMd1* activates *MtDefMd3* and *MtRam1*

Due to the possibility that the four AM-related *MtDefMds* studied here and other yet undiscovered AM-related defensins act in parallel, it is difficult to elucidate their function by knocking down just two

of them. Therefore, it was attempted to get insights into the role of defensins during AM by overexpressing the *MtDefMd1* gene in mycorrhized transgenic roots under the control of the *Ubiquitin*- and the *MtPt4*-promoter, mediating a general or a specific expression in arbuscule-containing cells, respectively (Fig 8).

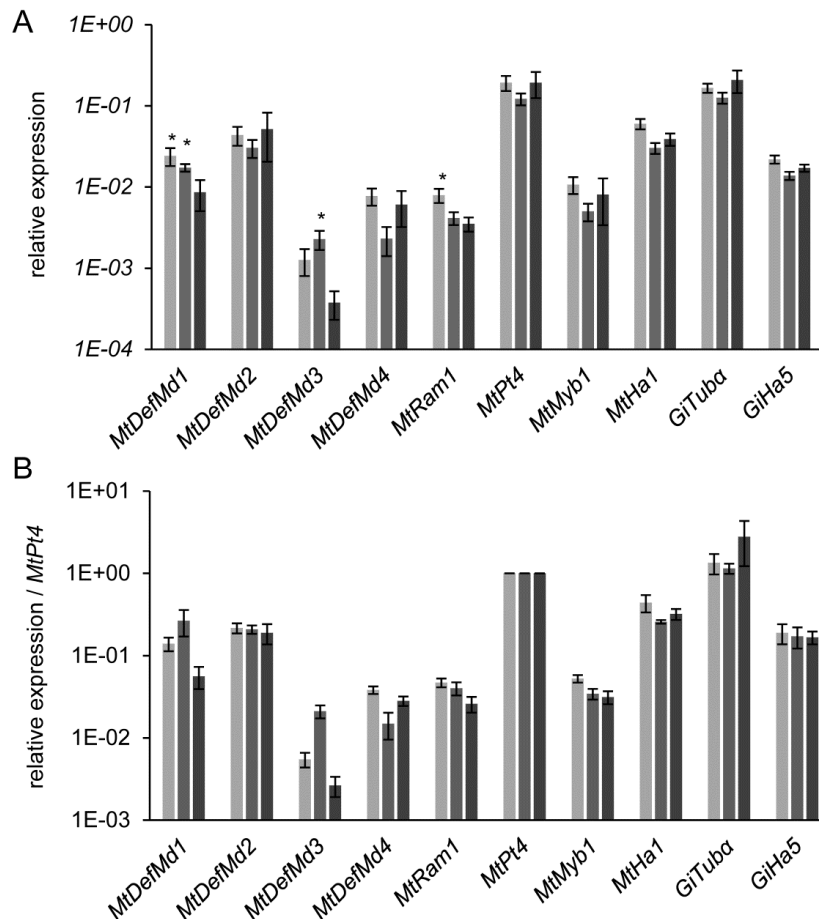


Fig 8: Relative expression of *MtDefMd1* and selected AM marker genes in mycorrhized *MtDefMd1*-overexpression and pPt4:*gusAint*-expressing control roots of *M. truncatula*.

Transcript amounts are shown relative to *MtTefa* (A) and were additionally normalized by building a ratio to *MtPt4*-expression (B). Measurements of pPt4:*MtDefMd1* overexpression roots are colored in light grey, measurements of pUbi:*MtDefMd1* overexpression roots in medium grey, and measurements of pPT4:*gusAint* control roots in dark grey. Roots were harvested at 28 days post inoculation with *R. irregularis*. n=12 biological replicates, depicted is the standard error of the mean. Statistical significance: * $p \leq 0.05$

Overexpression of *MtDefMd1* under control of the *MtPt4*- and the *Ubiquitin*-promoter led to a significant 2.8-fold and 2-fold overexpression of this defensin, respectively (Fig 8, A). Whereas *MtDefMd3* was co-activated by *MtDefMd1* overexpression controlled by the *Ubiquitin*-promoter, expression of *MtDefMd2* and *MtDefMd4* was not affected (Fig 8, A and B). Interestingly, the transcription of *MtRam1* was 2.3-fold upregulated in case of an *MtDefMd1* overexpression driven by the *MtPt4* promoter. To further assess co-activation of *MtRam1* and *MtDefMd3*, transcript levels were normalized by building a ratio to *MtPt4* expression (Fig 8, B), since the *MtDefMd1* and *MtDefMd2*

promoters are specifically activated in the arbuscule-containing cells. Thereby, the overexpression of *MtDefMd1*, *MtRam1* and *MtDefMd3* was verified in relation to the formation of active arbuscules (Fig 8, A and B).

Overexpression of *MtDefMd1* in tendency activates *MtABCG3* and suppresses *EXO70k* and *EXO70j* transcription

Since the enhanced *MtRam1*-expression could be interpreted as a marker for a faster arbuscule-establishment, the AM-dependent ABC-transporter gene *MtABCG3* (Chapter II: Fig 4, A; Fig 7; Fig 9; Fig 18; Fig 19) was measured via RT-PCR as a marker gene for arbuscule biogenesis (Fig 9).

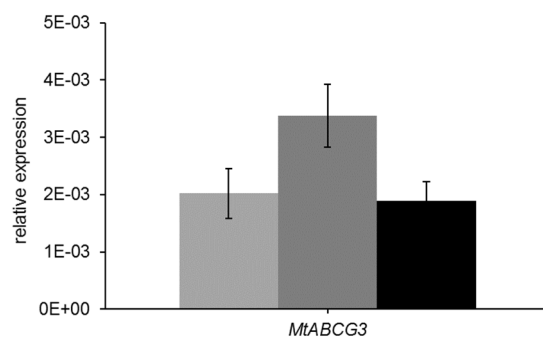


Fig 9: Relative expression of *MtABCG3* in mycorrhized *MtDefMd1*-overexpression and *pPt4:gusAint*-expressing control roots of *M. truncatula*.

Transcript amounts are shown relative to *MtTefa*. Measurements of *pPt4:gusAint* control roots are colored in light grey, measurements of *pPt4:MtDefMd1* overexpression roots in medium grey, and measurements of *pUbi:MtDefMd1* overexpression roots in dark grey. Roots were harvested at 28 days post inoculation with *R. irregularis*. n=12 biological replicates, depicted is the standard error of the mean.

MtDefMd1 overexpressing and control roots displayed no significant difference in *MtABCG3* transcription (Fig9). However, in tendency *MtABCG3* was stronger expressed in *p:Pt4:MtDefMd1* roots than in *p:Pt4gusAint*- and *p:Ubi:MtDefMd1* roots.

Subsequently, the transcript amounts of *MtMyb1*-induced *EXO70* genes (Fig 6), were measured in plant roots overexpressing *MtDefMd1*, to investigate if the defensin interferes with the transport machinery in late symbiotic stages (Fig 10).

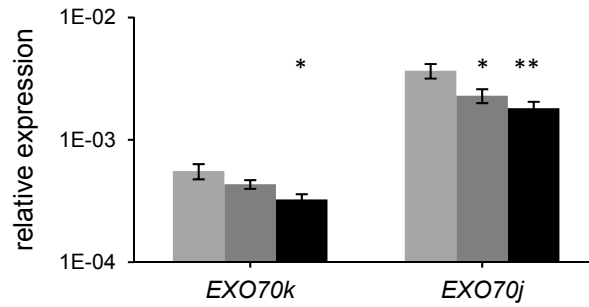


Fig 10: Relative expression of selected *EXOCYST* genes in mycorrhized *MtDefMd1*-overexpression and pPt4:*gusAint*-expressing control roots of *M. truncatula*.

Transcript amounts are shown relative to *MtTefα*. Measurements of pPt4:*gusAint* control roots are colored in light grey, measurements of pPt4:*MtDefMd1* overexpression roots in medium grey, and measurements of pUbi:*MtDefMd1* overexpression roots in dark grey. Roots were harvested at 28 days post inoculation with *R. irregularis*. n=12 biological replicates, depicted is the standard error of the mean. Statistical significance: * p≤0.05; ** p≤0.005

In constructs overexpressing *MtDefMd1* under control of the ubiquitin promoter, *EXO70k* and *EXO70j* expression was decreased between ~1.6 and ~2 fold (Fig 10). Whereas the latter gene was also ~1.7 fold repressed by a pPt4 driven overexpression of *MtDefMd1*, the transcript amounts of *EXO70k* were not significantly affected (Fig 10).

Overexpression of *MtDefMd1* did not alter the global lipid content in AM roots

Since there were indications that the associated transport processes in transgenic, *MtDefMd1*-overexpressing *M. truncatula* roots could be altered, the question rose, whether the fungal life cycle would be affected.

An enhanced neutral lipid-body formation was described for the late stages of AM symbiosis [15]. Thus, histological staining of lipids from mycorrhized pUbi:*MtDefMd1* and pUbi:*gusAint* plant roots were performed to monitor arbuscule morphology (Fig 11).

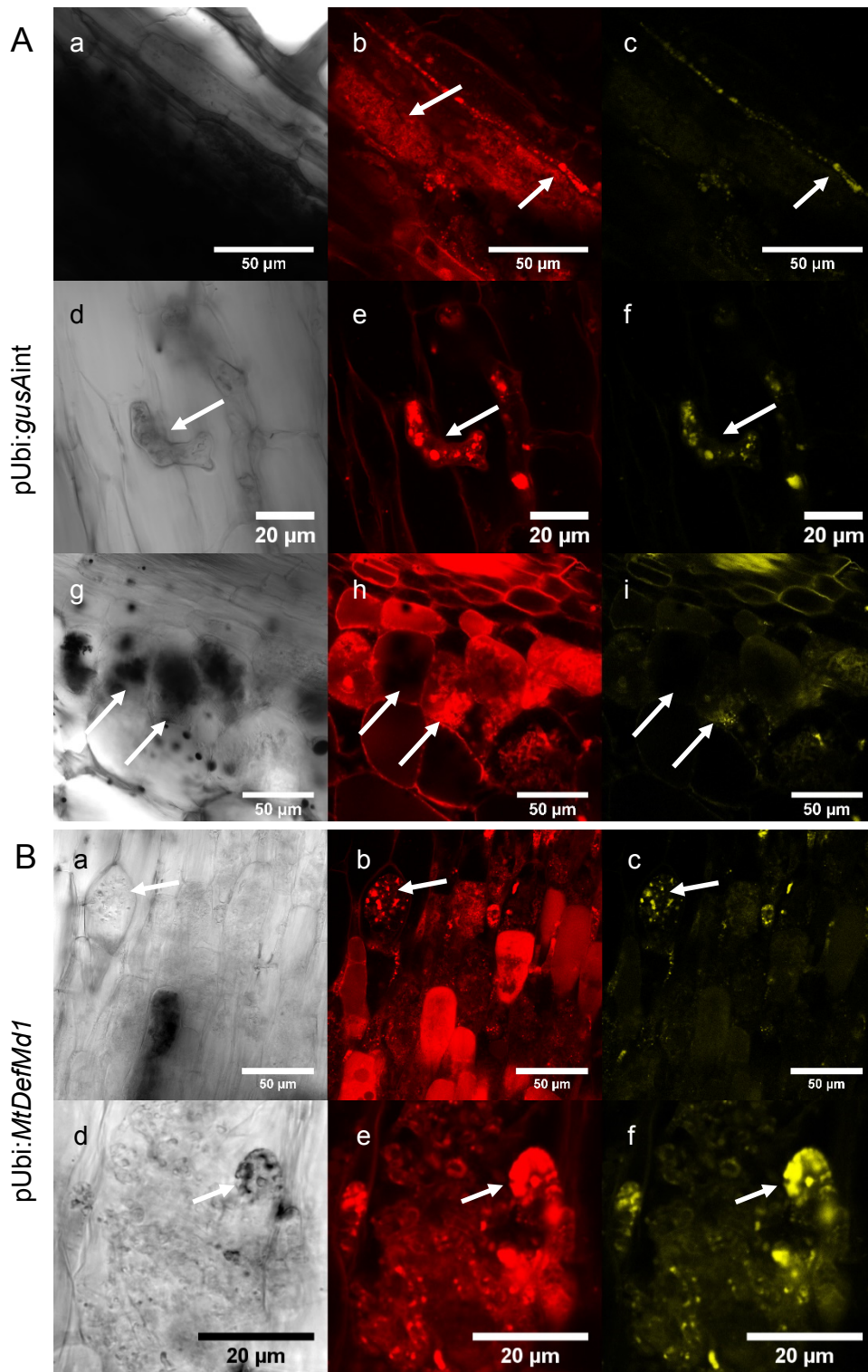


Fig 11: Lipid staining of mycorrhized *M. truncatula* pUbi:MtDefMd1-overexpression and pUbi:gusAint control roots.

Micrographs of Neutral Red-staining from pPt4:gusAint control roots (A) and pUbi:MtDefMd1-overexpression (B) are shown. Differential interference contrast (DIC) (A, a, d, g; B, a, d,), Fluorescence_{540-560nm} (A, b, e, h; B, b, e) and Fluorescence_{590-609nm} (A, c, f, i; B, c, f) are displayed. Roots were harvested at 42 days post inoculation with *R. irregularis*. n=12

As was reported by Kobae *et al.* [15], neutral red stained mycorrhized roots were investigated via fluorescence microscopy by detecting signals from the “golden” (540-560 nm) to the “red” (590-609 nm) part of the light spectrum (Fig 11). However, the intensity of staining varies in dependency of the spectral window for signal detection after excitation at 488 nm (Fig 11, A and B second vs third column). Apparently, a shift in the band maxima of the emission spectra of Neutral Red, is caused by the different composition of bound lipids. As was suggested by Kobae *et al.* [15], neutral lipids are found in vesicles (Fig 11, B, a-c, white arrows). Lipid bodies of intraradical hyphae and trunk regions of arbuscules were predominantly documented at 540-560 nm (Fig 11; A, d-f, white arrows; B, d-f, white arrows). At 590-609 nm, the named structures and membranes were detected globally (Fig 11, A, b and h, white arrows; B, b and e). Furthermore, some arbuscules, were emitting less-, or even absorbing light, visible as black structures in the differential interference contrast (DIC) micrographs (Fig 11; A, g-l, white arrows; B, a-c). Apparently, their morphology did not differ from other arbuscules in the fluorophore channel (Fig 11; A, g-l, white arrows; B, a-c).

In conclusion, no differences between mycorrhized *MtDefMd1* overexpressing and control roots from *Medicago truncatula* were detected.

Knockdown of *MtDefMd1/2* transcription and overexpression of *MtDefMd1* has no significant impact on the arbuscule size distribution

To visualize possible phenotypic effects in mycorrhized RNAi:*MtDefMd1/2* and *MtDefMd1*-overexpression in relation to pPT4:*gusAint* control roots, arbuscule size distributions were measured via confocal microscopy of WGA-Alexa Fluor 488-stained root sections (Fig 12).

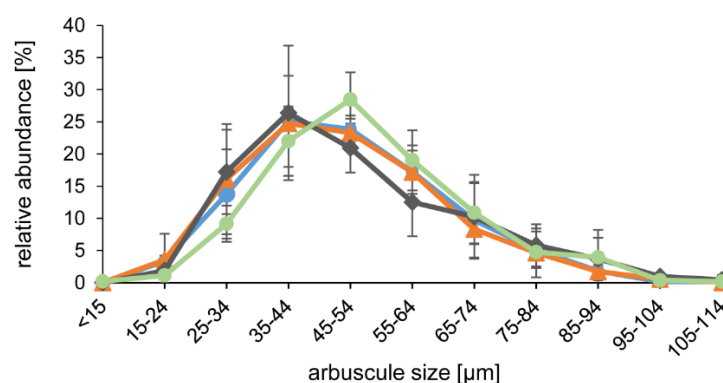


Fig 12: Size distribution of arbuscules in mycorrhized *M. truncatula* *MtDefMd1*-overexpression, *MtDefMd1/2*-knockdown, and pPt4:*gusAint* control roots.

Arbuscules were sorted into one of eleven size categories. In total, the size distribution of arbuscules in pUbi:*MtDefMd1*-overexpression (647 arbuscules), pPt4:*MtDefMd1*-overexpression (509 arbuscules), RNAi:*MtDefMd1/2*-knockdown (625 arbuscules), and pPt4:*gusAint* control roots (529 arbuscules) is depicted in orange, blue, green, and grey, respectively. Roots were harvested at 28 days post inoculation with *R. irregularis*. For each construct, three pools of root fragments, each pool being derived from four plants, were analyzed. Depicted is the standard error of the mean.

Although the transcription factor gene *MtRam1* was upregulated by *MtDefMd1* overexpression (Fig 8), the sorting of arbuscules in different size categories indicated no significant difference between overexpression and control roots (Fig 12). Apparently, the global distribution of arbuscule sizes was congruent. Although a slight shift towards larger sizes was evident (Fig 12), no significant alteration of arbuscule size was recorded for the RNAi:*MtDefMd1/2* knock-down roots, although a slight shift towards larger sizes was evident (Fig 12).

It can be concluded that neither an appr. 97% reduction of *MtDefMd1/2* transcription nor an up to 2.8-fold overexpression of *MtDefMd1* has a detectable effect on the steady-state distribution of arbuscule sizes. Similarly, no significant alteration of arbuscule size was recorded for the RNAi:*MtDefMd1/2* knock-down roots, although a slight shift towards larger sizes was evident (Fig 12). As the changes could be more subtle alterations in the fine structure of arbuscules, fungal structures in mycorrhized RNAi:*MtDefMd1*-, *MtDefMd1*-overexpression- and control roots were monitored after Alexa-WGA Fluor⁴⁸⁸-staining via confocal microscopy (Fig 13).

Considering the range of arbuscule size (Fig 12) and the naturally occurring variations in shape, most arbuscules of pPt4 (Fig 13, A, a-c) or pUbi (Fig 13, C, a-c) driven overexpression of *MtDefMd1* were comparable to the arbuscule phenotype in control roots (Fig 13, B, d-f). However, in a small fraction of pPt4:*MtDefMd1*-overexpressing roots, the trunk region and first order branches of arbuscules were swollen and deformed (fig 13, A, a-c). Although in some transgenic control roots, arbuscules with thickened, bubble-like trunk regions were monitored (fig 13, B, a-c) as well, their proportion was even more rare and discovered alteration not as severe as in case of defensin overexpression.

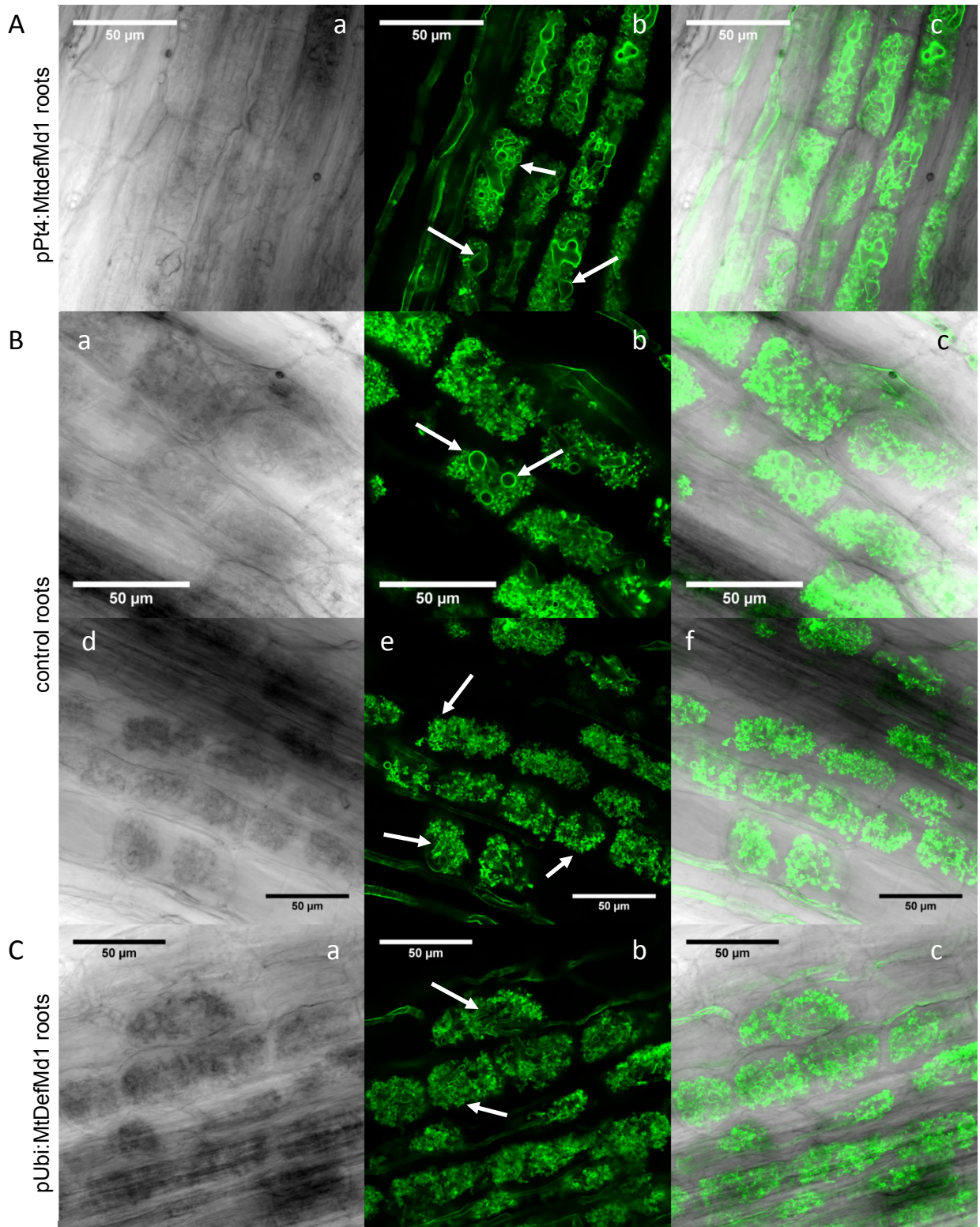


Fig 13: WGA-Alexa Fluor 488-stainings of arbuscules in mycorrhizized *M. truncatula* pUbi:MtDefMd1-, pPt4:MtDefMd1- and pPt4:*gusAint* control roots.

Differential interference contrast (DIC) (A, a and d; B, a; C, a), Alexa-WGA 488-staining (A, b and e; B, b; C, b), and merge (A, c and f; B, c; C, c) micrographs from pPt4:MtDefMd1-overexpression (A, a-c), pUbi:*gusAint* control roots (B, a-f), and pUbi:MtDefMd1-overexpression (C, a-c), are shown. Roots were harvested at days post inoculation with *R. irregularis*. n=12

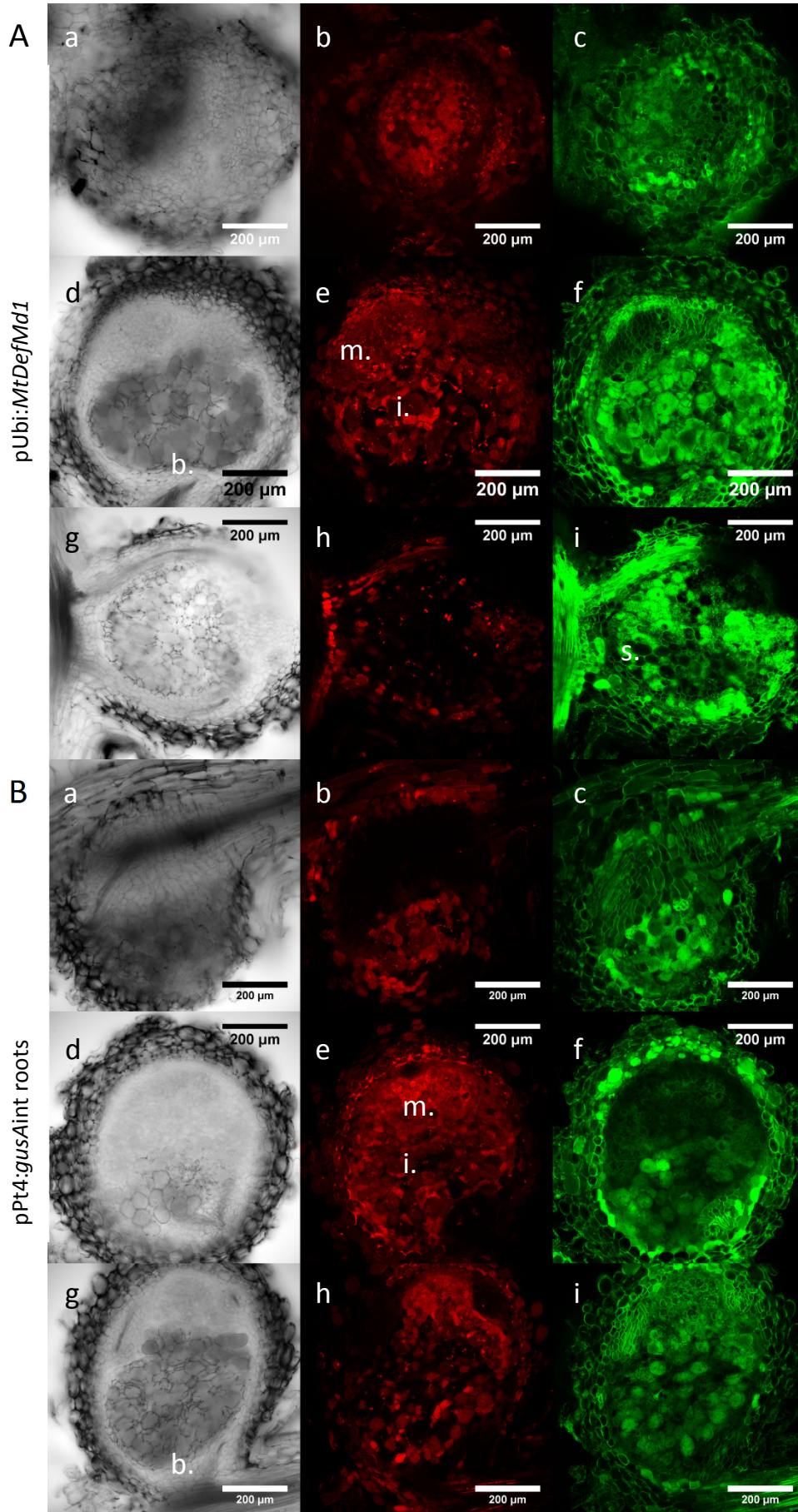
Overexpression of *MtDefMd1* in root nodules did not significantly alter the fine-structures of bacteroid-harboring cells

As initially stated, defensins are, apart from the AM symbiosis, also transcribed during the root nodule symbiosis. Therefore, morphological studies of bacteroids in pUbi:*MtDefMd1* transformed nodules, could indicate whether or not the defensin modulates the morphology of microsymbionts. To check this hypothesis, transgenic pUbi:*MtDefMd1*-expressing plants were nodulated. Using an *mRFP*-containing *Sinorhizobium* strain, the pH-dependent dye *DND189-LysoSensor* and WGA-Alexa Fluor 488-stainings the nodules were investigated with confocal microscopy (Fig 14).

On a whole-nodule level, all stages of the symbiosis were abundant in both groups of the experiment: In longitudinal sections of young and medium aged nodules, the meristem (Fig 14), the infection zone (Fig 14) and the active zone (Fig 14) in terms of bacteroid-harboring cells were detected. The fraction of senescent cells was, probably due to the age of the interaction, low (Fig 14).

Fig 14: Nodules of *M. truncatula MtDefMd1*-overexpression and pPt4:*gusAint* control roots.

Shown are Differential interference contrast (DIC) (A, a, d and g; B, a, d, and g), *mRFP* (A, b, e, and h; B, b, e, and h) and *DND189LysoSensor* (A, c, f, and i; B, c, f, and i) micrographs of WGA-Alexa Fluor 488-stainings from pUbi:*MtDefMd1*-overexpression (A) and pPt4:*gusAint* control roots (B). Roots were harvested at 35 days post inoculation with *S. meliloti*. n=12



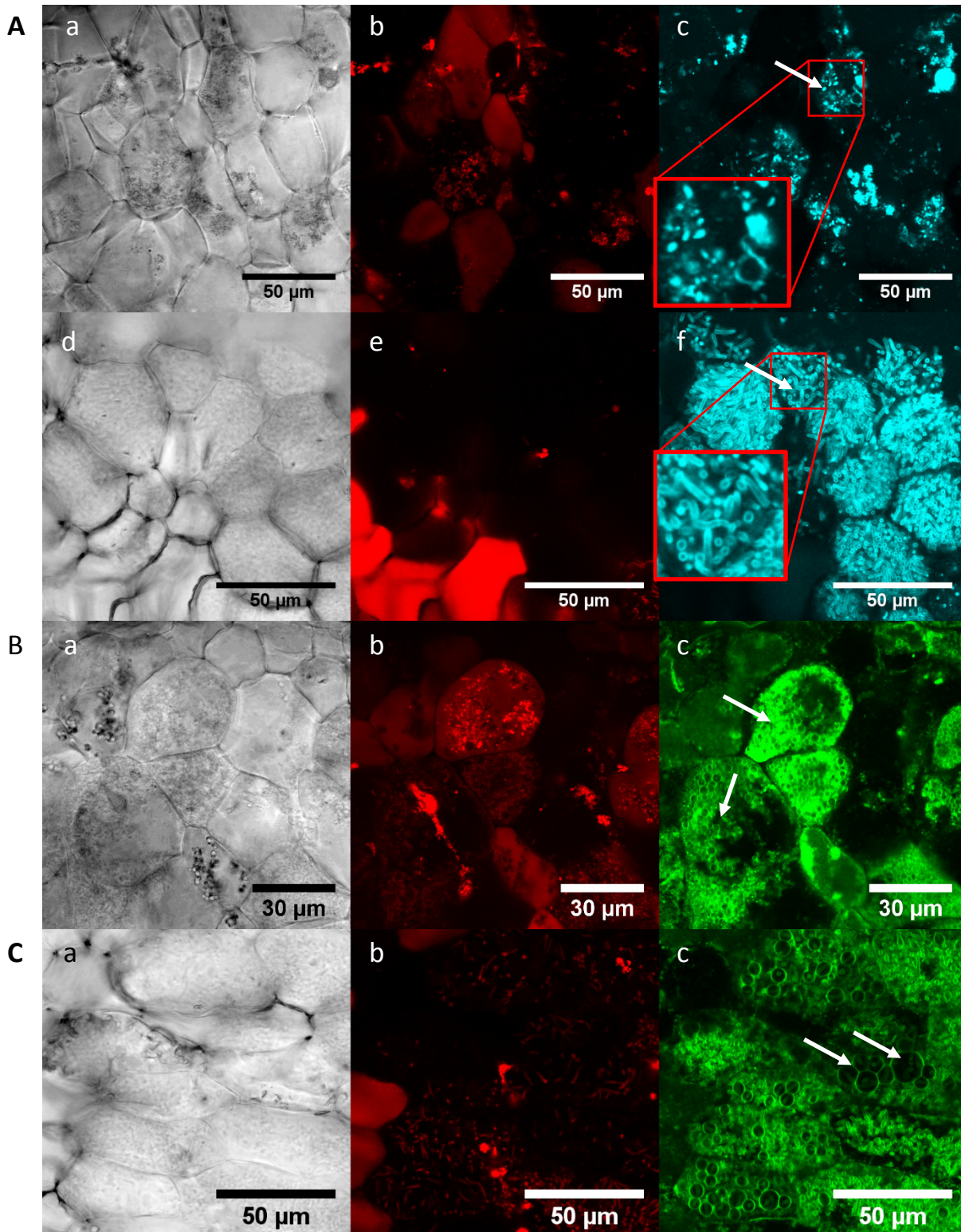


Fig 15: Morphology of bacteroids in nodules of *M. truncatula* *MtDefMd1*-overexpression and *pPt4:gusAint* control roots.

DIC (A, a and d; B, a; C, a), mRFP (A, b and e; B, b; C, b), WGA-Alexa Fluor 488 (A, c and f) and DND189Lysosensor (B, c; C, c) micrographs of -staining from *pPt4:gusAint* control roots (A) and *pUbi:MtDefMd1*-overexpression (B and C) are shown. Roots were harvested at 42 days post inoculation with *R. irregularis*. n=12

To monitor bacterial and bacteroid development, mRFP-, Lysosensor DND189, and WGA-Alexa Fluor 488-signals were compared (Fig 15). WGA-Alexa Fluor 488-stainings of longitudinal hand-cuttings of

nodules apparently only stained a portion of bacterial cells (Fig 15; A, c). This could imply that differences, such as in vitality, influence the amount of fluorophore in bacterial cells. Nevertheless, no difference in between defensin-overexpressing and control nodules was detected.

The peribacteroid space of differentiated bacteroids, characterized by a longitudinal enlargement, was stained by WGA-Alexa Fluor 488 (Fig 15, A, f). This raises the question, if the bacteroids secreted molecules that were stained, such as lipo-chitooligosaccharides (LCOs). LCOs consist of an acylated chitin backbone with various functional group substitutions and therefore share a similarity to fungal cell walls, which could be targeted by WGA-Alexa Fluor 488. In contrast, the lumen of undifferentiated bacterial cells was stained in some cases, whereas the lumen of others remained unstained (Fig 15; A, c). In general, there was no significant quantitative or qualitative difference between control- and pUbi:MtDefMd1-nodules detected.

Using a pH dependent dye, the incorporation of bacteria that were released from the infection thread into round spheres in infected cells (Fig 15, B, C) was monitored for both control and pUbi:MtDefMd1-nodules. Those spheres filled most of the plant's cells volume (Fig 15, B) and seemed to become elliptic and then stretch longitudinally during the differentiation of bacteria into bacteroids. In some infected cells of the pUbi:MtDefMd1-nodules bigger round spheres, containing one or several differentiated bacteroids were monitored (Fig 15; C, c). To a lower extent, this was also observed in control nodules. This phenomenon resembles the swollen and deformed arbuscule trunks and branches in some infection units of pPt4:MtDefMd1-roots.

In conclusion, in the majority of bacteroid-harboring cells, the symbiotic fine-structures were not altered.

MtDefMd1 acts during late restructuring stages of arbuscule-containing cells

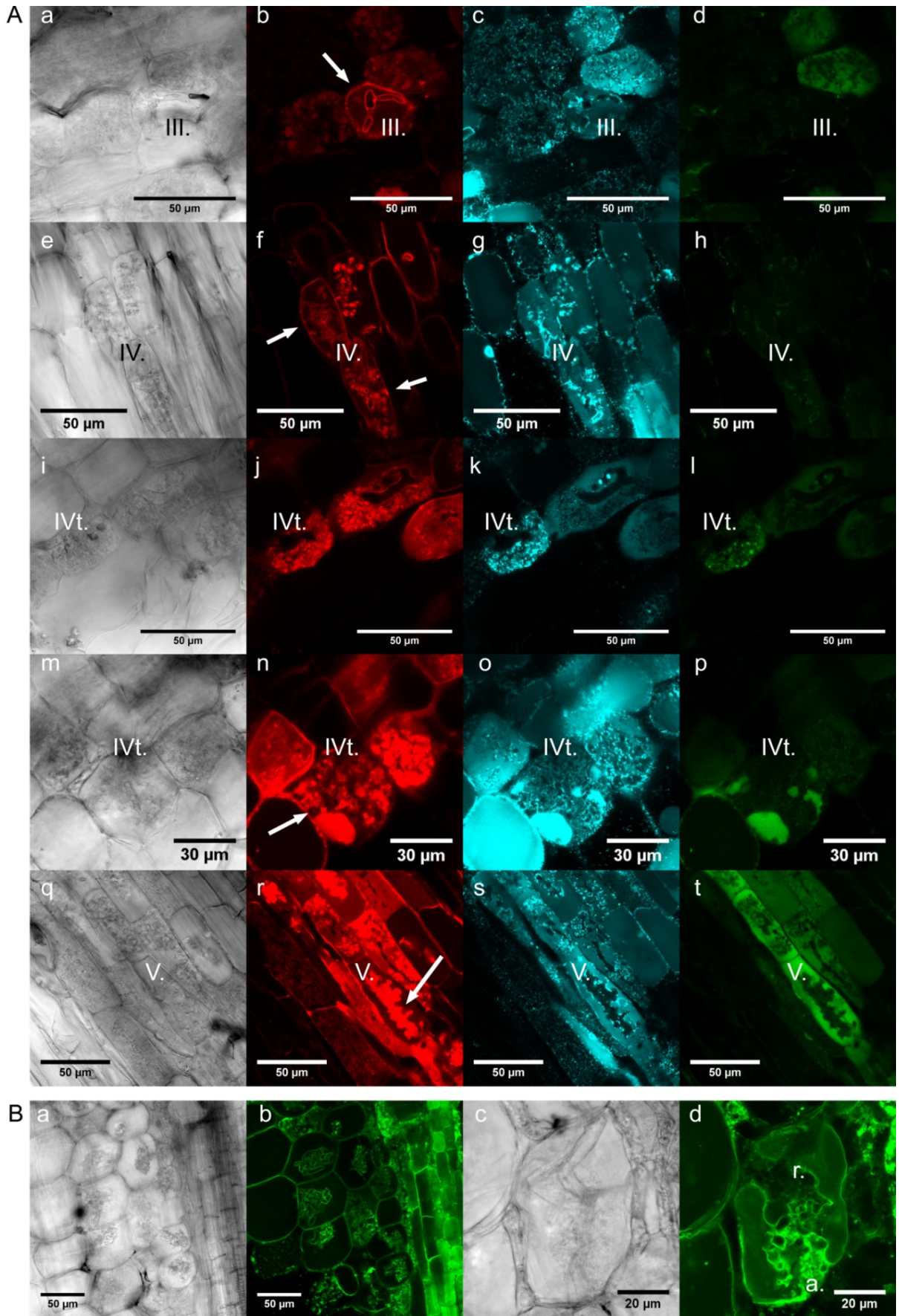
From promoter studies, it was concluded that the two highly similar *MtDefMd1* and *MtDefMd2* genes are expressed in cells containing fully developed arbuscules. To monitor MtDefMd1 protein distribution and accumulation during the life-cycle of an arbuscule-containing cell, a triple fluorophore reporter construct was designed. First, the *MtDefMd1* coding region was fused to *mGFP6*. In the resulting MtDefMd1-mGFP6 fusion, both regions are separated by a flexible linker. This modification enables free rotation between the two regions and was previously used to localize symbiosome-targeted proteins in the infected cells of root nodules [56]. To achieve a correctly regulated expression in the arbuscule-containing cells, the MtDefMd1-mGFP6 fusion was expressed under the control of the *MtDefMd1* promoter. To visualize protein secretion that is known to be transiently redirected towards the arbuscules [65] a constitutive endoplasmic reticulum (ER) CFP-marker [57] was introduced. The signal peptide of *MtBcp1* fused to *mCherry* [58] and expressed under the control of the *MtBcp1* [19] promoter, was used to define consecutive stages of the arbuscule life-cycle. MtBcp1 is present in the

stem region of young and is more evenly distributed in the PAM of mature, fully developed arbuscules, thus allowing to define arbuscule stages [58]. All reporter fusions were concomitantly expressed in mycorrhized transgenic roots, and confocal microscopy was used to locate mCherry, CFP, and GFP fluorescence in the inner cortex (Fig 16).

In congruence to the MtBcp1-localisation reported by Ivanov and Harrison [58], the trunks of arbuscules in the birdfoot stage (stage III.) were positive for MtBcp1_{SP}-mCherry (Fig 16; A, b). In addition, also the symplast membrane of cells in the symbiotic root tissues exhibited a certain level of mCherry fluorescence (Fig 16; A, f). In mature, fully developed arbuscules, presumably active in metabolite exchange (stage IV.), MtBcp1_{SP}-mCherry signals expanded to the whole PAM (Fig 16; A, f and j). Since the ER-marker was originally designed for the analysis of cell organelles in *Arabidopsis thaliana* [57], its functionality in *M. truncatula* had to be verified. It was expected that a spider web structure surrounding the nucleus, granular bodies at the edges of the cells as well as components of the cytoskeleton used to direct transport vesicles were stained. However, this was only the case for cells not containing arbuscules (Panel A in S1 Fig; A, c). In arbuscule-containing cells of the inner cortex, a close connection of ER-structures to the PAM (Fig 16; A, c, g, k, o, and s) and a CFP signal in the vacuole of GFP-positive cells (Fig 16, A, o) was detected, indicating a massive reorganization of vesicle traffic to or from the PAM. MtDefMd1-GFP signals were only observed in a fraction of the arbuscule-containing cells (Fig 16; A, l, p, and t) and were not detected in cells prior to arbuscule branching (Fig 16; A, d). In cases of low GFP signals, small dots and spheres in close proximity to the PAM of fully developed arbuscules were apparent (Fig 16; A, l). These signals match the patterns of CFP-labeled ER-structures (Fig 16; A, k, o and s) and while they are too large for being vesicles, they might be conglomerates of such. This points towards MtDefMd1 being part of the transportome redirected to the PAM. The MtDefMd1-mGFP6 signal increased strongly in cells with older, collapsing arbuscules (Fig 16; A, p and t). These were characterized by structures appearing condensed and clumpy. In those cells, the mGFP6 signal gets very intensive and seems to be more and more present in the vacuole (Fig 16; A, p and t).

Fig 16: Localization of MtDefMd1-mGFP6 and additional fluorescence marker proteins in mycorrhized *M. truncatula* roots.

Differential interference contrast micrographs of razor blade hand-cut sections of transgenic *M. truncatula* roots are shown (A; a, e, i, m, and q; B; a and c). Confocal microscopy was used to localize a fusion of the signal peptide of MtBcp1 with mCherry under the control of the *MtBcp1* promoter (A; b, f, j, n, and r), an ER-CFP fusion under the control of the 2x35S-promoter (A; c, g, k, o, and s), and an MtDefMd1-mGFP6 fusion under the control of the *MtDefMd1* promoter (A; d, h, i, p, and t). Additionally, a tonoplast membrane-directed GFP fusion under the control of a 2x35S-promoter was studied (B; b and d). Roots were mycorrhized with *R. irregularis* for six weeks. Arrows in the MtBcp1_{SP}-mCherry micrographs indicate structures referred to in the text. Abbreviations: a., arbuscule branches; r., restructuring; III, birdfoot arbuscule; IV, active arbuscule; IVt, fully developed arbuscule prior to collapsing; V, collapsed arbuscule



To further investigate if the GFP pattern of intensively colored cells matches restructuring processes of the vacuole during the AM symbiosis, transgenic roots expressing a tonoplast membrane GFP-marker [56], were mycorrhized and GFP-fluorescence was analyzed (Fig 16; B, b and d). Whereas in non-mycorrhized roots, the space occupied by the cytoplasm, i.e. the volume close to the cell wall and cytoplasmic transvacuolar strains, are indirectly visualized (Panel B in S1 Fig; B, b), the space taken by the arbuscule is clearly defined by the surrounding GFP-labeled tonoplast (Fig 16; B, b and d). The remaining space comprises the cytoplasm, the PAS and the symbiotic membranes from both organisms. Tonoplast membranes switch from a very close contact with arbuscule branches to a looser one (Fig 16; B, d, areas a. and r.). The morphology of cells exhibiting this phenomenon fits to those containing arbuscules in late stages of their life-cycle, characterized by a high level of MtDefMd1-mGFP6 (Fig 16; A, p). The MtBcp1_{SP}-mCherry, ER-CFP, and MtDefMd1-mGFP6 colocalization indicates that arbuscule structures undergo a transitional change between stages IV. (fully developed) and V. (degrading), which will be termed IVt. from now on. Once the distinct MtBcp1-mCherry signal in the arbuscule trunk (stage III.) extends towards the tips of the arbuscule branches (Fig 8, A, j), the MtDefMd-mGFP6 signal starts to co-localize to these structures (Fig 16, A, l; stage IV.t). Now, the distal tips of the arbuscule branches tend to get crescent-shaped or swollen, collapse (Fig 16; A, j and n), and the space occupied by the arbuscule looks increasingly clumpy. Occasionally, the cell lumen contains non-fluorescent spheres of differing sizes, possibly representing partially degraded arbuscules (Panel A in S1 Fig, A, g). Strongly mGFP6-positive, most likely vacuolar compartments are increasingly created during stage IVt. and are abundant in stage V. (Fig 16, A, p, and t). The creation of fluorophore-positive vacuoles indicates a recycling of PAM-targeted vesicles and proteins, which were previously located in the perisymbiotic membrane. Since the increase of MtDefMd1-mGFP6 levels is strongest during this rather short and late stage of the arbuscule life-cycle (Fig 16, A, l), it marks the beginning of the turnover from a symbiotic into a post-symbiotic cell.

Discussion

AM-related defensins of the MtDefMd family can be distinguished from other antimicrobial peptides. First, the γ -core motif, which was vital for MtDef4 entry into *Fusarium graminearum* [30], is strikingly different in AM-related defensins. Second, a calculation of surface hydrophobicity identified a distinct pattern of hydrophobic amino acids and an aspartic acid residue close to the C-terminal region only for AM-related defensins, suggesting specific symbiotic targets for their function.

Genes of the *MtDefMd*-family were activated during distinct stages of the AM interaction. This was visualized by monitoring the transcript fold changes of their members in different AM mutants in comparison to wild type plants. These changes were ordered from mutants where the symbiosis is disturbed in early stages (*ram1-1*), followed by those having an impact on the active phase (*pt4-1*) and finally by RNAi roots, affected in processes occurring in the later stages of interaction (*MtMyb1*-RNAi). Apparently, each of those steps requires a unique set AM-dependent defensins. This could imply a multitude of functions in the life cycle of arbuscules, co-occurring with several vital steps of arbuscule biogenesis. The shift of MtBcp1-mCherry from arbuscule trunks to the PAM allowed not only to differentiate between pre-mature, fully developed, and collapsing arbuscules, but also to relate MtDefMd1-mGFP6 signals to these stages of arbuscule formation and degradation (Fig 16; A, h to t). In contrast to MtBcp1-mCherry, MtDefMd1-mGFP6 signals were not detected prior to arbuscule branching (Fig 16; A, d). Together with the observation that strongest MtDefMd1-mGFP6 signals were found in cells with collapsing arbuscules and increasingly in vacuoles (Fig 16; A, p and t), this indicates that MtDefMd1 functions during later stages of the arbuscule life-cycle, and here during the initiation of a regular turnover of symbiotic structures that involves massive restructuring of the PAM (Fig 16; A, transition from h to l, l to p, and p to t). This is in line with the observation that *MtDefMd1* and *MtDefMd2* promoters are activated in fully developed arbuscules and that the premature arbuscule degradation observed in *pt4-2* mutants does not involve *MtDefMd* genes.

Using *in planta* time-lapse imaging, it was shown that in contrast to their formation, arbuscule collapse is a rapid event [14]. Recent evidence indicates that the arbuscule degeneration program activated by MtMyb1 [17] plays an important role to initiate this step. In this light, it is conclusive that MtDefMd1 accumulation happens in a short period of time, defined by the IVt. stage (Fig 16; A, i to p). The strong RNAi-mediated knock-down of *MtDefMd1* and *MtDefMd2* had no detectable impact on the function of arbuscules. Since the symbiotic nutrient exchange largely occurs before the onset of stage IVt, this could be expected. On the other hand, an *MtPt4*-promoter controlled overexpression of *MtDefMd1* led to higher *MtRam1* transcription, indicating that an enhanced level of *MtDefMd* transcripts can lead to differential expression of a key transcription factor that invokes a faster development of the arbuscule interface (MtRam1) [16]. In this context the existence of an MtRAM1 regulated lipid export

pathway [70] is of great interest. Via the arbuscules, the AMF are supplied with C16 fatty acids, most likely 2-monopalmitin [71], indicating an enhanced lipid supply in *MtDefMd1* overexpressing roots. Interestingly, nodule-specific defensins were found in *Alnus glutinosa* root nodules [72]. AG5, one of these, caused physiological changes of *Frankia* vesicles and increased their permeability [72], whereas four additional defensins displayed partly overlapping functions [71]. Apart from classical non-symbiotic and symbiotic defensins, more than 700 defensin-like peptides containing N-terminal signal peptides and conserved cysteine residues were identified in legume plants [26]. These nodule-specific cysteine rich (NCR) peptides either contain 4 or 6 cysteines, and some of them display remarkable similarities with AM-related defensins. NCR-peptides are targeted to symbiosomes via the secretory pathway [35, 72]. Inside the lumen of nitrogen-fixing bacteroids, multiple targets of NCR-peptides were observed, e.g. ribosomal proteins, cell cycle regulators, ATP synthases, nitrogenase, and components of the TCA cycle [73, 74]. In concert, the effects of hundreds of cell-specific NCR-peptides lead to terminal bacteroid differentiation in the indeterminate-type legume root nodules [75]. Vacuolar V-SNARE receptors are recruited in early steps of bacteroid senescence [76, 77]. Cargo vesicles originally addressed to the vacuole are now delivered to degrading symbiosome membranes, transforming the enclosed perisymbiotic space to an acidic lytic compartment [78, 79]. Fragmented vacuoles are adaptations of mature arbuscule-containing cells [80], so these processes are of interest for AM as well. In addition, it was reported that similar to the peribacteroid space, the periarbuscular space is acidic [81]. This environment might be decisive for a protonation of the aspartic acid residue in the characteristic C-terminal region of mycorrhiza-related defensins, and this might be important for their function.

Interestingly, two members of the *EXOCYST* gene family and *MtDefMd1* were reduced in expression in *MtMyb1*-RNAi in comparison to control roots. The co-regulation of *EXOCYST* and defensin genes could shed light on the conflict of cell-autonomous arbuscule breakdown on one hand and a synchronous vanishing of arbuscular infection units on the other hand, as documented by Kobae *et al.* [14]. One of the genes, *EXO70j*, is also present during the interaction of *M. truncatula* with nitrogen-fixing bacteria [23]. Possibly, in both symbioses exocytotic transport processes also share features of late targeting. In this light it is suggestive that in later stage of both symbioses, membranes that envelope the microsymbiont must be reshaped. Thus, the massive formation of fluorophore-positive vacuoles at a specific point of the arbuscule life-cycle (Fig 16; A, p and t) probably reflects the recycling of PAM-derived fatty acids and proteins by the host. This is a clue for a hypothetical model of functions in later arbuscule maturation and degradation processes for *MtDefMd1/2*, which are summarized in Fig 17. The presence of large amounts of *MtDefMd1*-mGFP6 was not only confined to a rather short, but also to a very late moment in the arbuscule life-cycle (stage IVt.; Fig 16; l, p, and t), a time point matched by the accumulation of oil droplets [15].

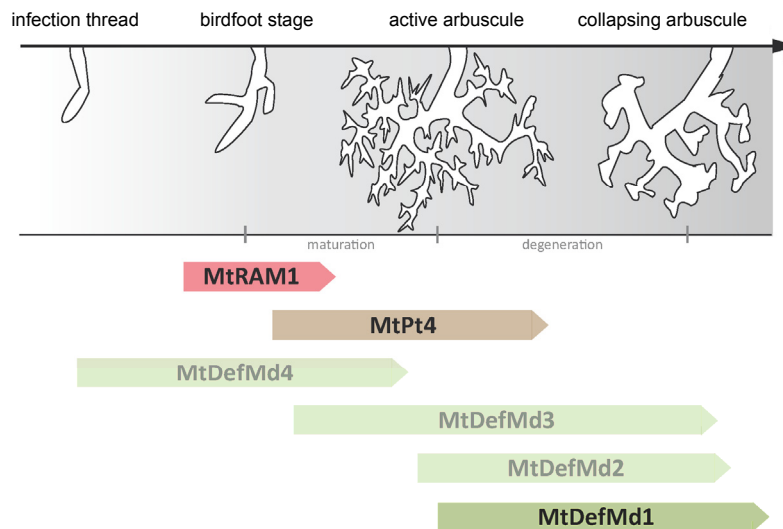


Fig 17: Proposed time course of MtDefMd protein presence in relation to AM markers in *M. truncatula* roots after inoculation with *R. irregularis*.

The depicted genes are as follows: *MtRam1* (Medtr7g027190.1), *MtPt4* (Medtr1g028600.1), *MtDefMd1* (Medtr.8g012805.1), *MtDefMd2* (Medtr.8g012835.1), *MtDefMd3* (Medtr.8g012875), and *MtDefMd4* (Medtr.8g012885). For shaded MtDefMd proteins no fluorophore protein markers are available at present, so the positioning relies on gene expression in symbiotic mutants.

Since AM fungi are oleogenic, the discovery that lipid droplets coincide with collapsed arbuscular branches [15] opens new perspectives for MtDefMd function.

Studies on *MtRam1* and *MtRam2* mutants demonstrated that in addition to sugars, fatty acids from the host are supplied to intraradical fungal structures [70, 83], thus compensating the lack of fungal multidomain fatty acid synthases [15, 84]. This direct supply of monoacylglycerol is probably an important source for the synthesis of triacylglycerol stored in lipid bodies of the intraradical mycelium [85, 15]. The transfer of fatty acids probably occurs during the active, nutrient-exchanging phase of the arbuscule. Later, the arbuscules are regularly degraded, and this process generates another source of lipids. Although it is currently unknown, what mechanisms are used for the attachment of defensins to fungal membranes [30], it is intriguing that the *Raphanus sativus* AFP2 and the *Dahlia merckii* AMP1 defensins are known to bind sphingolipids [31, 86, 30]. Although MtDefMd defensins exhibit some differences to non-symbiotic defensins, they are likely to have direct antifungal activity like other cationic, AM-unrelated defensins. AM-dependent defensins including their γ -core motifs share significant homologies with the recently published bi-domain MtDef5A/B, which exhibits potent antifungal activity *in vitro* [65]. Interestingly, MtDef5A/B has been shown to bind several phospholipids *in vitro*, including phosphatidylinositol monophosphates (PIP) and PIP₂ [66]. It is thus likely that MtDefMd1 and MtDefMd2 also bind to phospholipids and this binding might be important for their biological function during later stage of the AM symbiosis. Taking the peak of MtDefMd1-mGFP6 synthesis in a short and late period of the arbuscule life-cycle into consideration, it is tempting to

hypothesize that MtDefMd defensins bind specific lipid compounds during the massive digestion of degrading arbuscules, containing a significant amount of membrane lipids. During this process, these lipids might act as carriers for an endocytic incorporation of MtDefMd proteins, thereby limiting excessive fungal access to host lipids due to a potential toxicity of the defensins at high concentrations. This toxicity can e.g. be mediated via Ca^{2+} -influx, K^+ -efflux, and a loss of membrane potential [87, 88, 89]. Since phytopathogenic fungi are supplied with host fatty acids as well and reduced fatty acid synthesis impairs infections [83], mechanisms hindering the loss of plant fatty acids are an important mode of control.

The quick and strong accumulation of MtDefMd1 marks the initiation of a turnover in arbuscule-containing cells, ultimately leading to the post-symbiotic formation of cortical cells ready to be re-colonized. This transition requires not only transcriptional changes and cellular restructuring, but also antimicrobial treatments. Specifically, fungal structures collapse during the arbuscule degeneration initiated by MtMyb1 [17], while the now abandoned symbiotic market place is enriched with proteins and lipids of symbiotic membranes [14]. It might thus be beneficial for the plant to recycle such molecules by redirecting them to the vacuole that grows due to the fusion of initially fragmented areas. Absence of *MtDefMd1* and *MtDefMd2* transcription in *pt4-2* and *ram1-1* mutants has thus to be expected, since in defect or prematurely degraded arbuscules, no expanded symbiotic interface exists, where lipids need to be reconquered. However, the multitude of AM-related defensin genes suggests that there are possibly alternative defensins present during the post symbiotic cellular restructuring. Here, as consequence of a lesser acidified symbiotic space, alternative biochemical properties of MtDefMds could be needed.

In Fig 18, a hypothetical model for the mode of MtDefMd1 action is presented. After secretion and stepwise modification in the cisternae of the endoplasmic reticulum, vesicles with the mature defensin could be targeted to the fungal membrane or alternatively directly to lytic compartments (Fig 18). The MtDefMd1 released into the PAS can interact with other proteins and compounds of the symbiotic membranes. Then, homo- or hetero-multimers of defensins, which might interact with other molecules as well, could form membrane channels. This could lead to a loss of small charged molecules into the PAS. Also, an uptake into lytic- or vacuolar compartments seems plausible, which are, apart from the association with lipids, possible targets of MtDefMd1 (Fig 18, green arrows). The stepwise degradation of sphingolipids and glycosphingolipids takes place in acidic subcellular compartments, such as endosomes and lysosomes, resulting in sphingosine via ceramide as intermediate. Thus, it was hypothesized that most of these lipid breakdown products were released and reintroduced into sphingolipid biosynthesis [90]. Due to the multiply of their modes of action (Fig 18), functional assessments of defensin-like proteins are challenging.

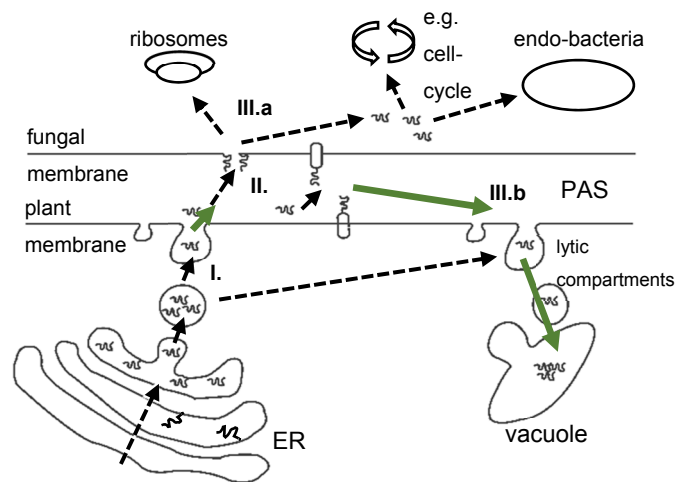


Fig 18: Hypothetical modes of action of MtDefMd1.

The traversal of MtDefMd1 from cellular structures of the plant host towards potential targets of the microsymbiont are shown as arrows. Green arrows represent MtDefMd1 localization monitored by confocal microscopy. Abbreviations: PAS, periarbuscular space; I, first phase; II, second phase; IIIa/b, third phase

In the fungal cytoplasm, ribosomes, components of the cell-cycle as well as endobacteria are, in congruence to the action of NCR-peptides, plausible targets of AM-related defensins. Apart from the mentioned plethora of possible targets and effects, all defensin-like proteins have a detergent-like working mode in common, which could be most important for processes during AM symbiosis. *MtDefMd1*, a member of the newly described *MtDefMd* family of mycorrhiza-activated defensins, is not only specifically transcribed during AM interactions, but is translated during the restructuring processes of arbuscule-containing cells. The MtdefMd1 presence at this defined, late stage of the arbuscule life-cycle might be a hallmark of the regular transition from symbiotic to post-symbiotic cells. Since the timing of defensin presence described here coincides with the reported accumulation of AM-fungal lipids [15], an association of AM-related defensins with these molecules is a starting point for further studies of MtDefMd function in the AM symbiosis.

Acknowledgements

I am thankful to Manfred K. Schenk (Institute of Plant Nutrition, Leibniz Universität Hannover, Hannover, Germany) for helpful advice on the setup of plant nutrition solutions and Natascha Köppens (Institute of Plant Genetics, Leibniz Universität Hannover, Hannover, Germany) for excellent technical assistance. *Medicago truncatula pt4-2* and *ram1-1* seeds were kindly provided by Maria Harrison (Boyce Thompson Institute, Ithaca, NY, USA) and Giles Oldroyd (John Innes Centre, Norwich, UK), respectively. I am grateful to Bettina Hause (IPB, Halle, Germany) for supplying AM fungal inoculum, to Miriam Laxa (Institute für Botanik, Leibniz Universität Hannover, Hannover, Germany) for the cell organelle localization vectors pBIN:tp-gk and pBIN:er-ck, to Franziska Krajinski-Barth (Institute für Biologie, Universität Leipzig, Leipzig, Germany) for the overexpression vectors 315p9RFP-Pt4-Expr and 917p9RFP-ubi3-Expr, to Erik Limpens (Department of Plant Sciences, Wageningen University, Wageningen, The Netherlands) for the RNAi vector pK7GWIWG2(II)-Q10:DsRED, and to Maria Harrison (Boyce Thompson Institute, Ithaca, NY, USA) for the MtBcp1 localization vector *pCMbB-TMEr*. GeneChip hybridisations were carried out by João Sobral and Jörg D. Becker (Plant Genomics Lab and Gene Expression Unit, Instituto Gulbenkian de Ciência, Oeiras, Portugal).

References

- [1] Charpentier M, Bredemeier R, Wanner G, Takeda N, Schleiff E, and Parniske M. *Lotus japonicus* CASTOR and POLLUX are ion channels essential for perinuclear calcium spiking in legume root endosymbiosis. *Plant Cell* 2008; 20(12): 3467–3479 [<https://doi.org/10.1105/tpc.108.063255>]
- [2] Schüssler A, Schwarzott D, and Walker C. A new fungal phylum, the Glomeromycota: phylogeny and evolution. *Mycol Res* 2001; 105(12):1413-1421
- [3] Bago B. Carbon export from arbuscular mycorrhizal roots involves the translocation of carbohydrate as well as lipid. *Plant Physiol* 2003; 131(3): 1496–1507 [<https://doi.org/10.1104/pp.102.007765>]
- [4] Wewer V, Brands M, and Dörmann P. Fatty acid synthesis and lipid metabolism in the obligate biotrophic fungus *Rhizophagus irregularis* during mycorrhization of *Lotus japonicus*. *Plant Journal* 2014; 79(3): 398–412 [<https://doi.org/10.1111/tpj.12566>][PMID: 24888347]
- [5] Smith SE and Smith FA. Roles of arbuscular mycorrhizas in plant nutrition and growth: New paradigms from cellular to ecosystem scales. *Annu Rev Plant Biol* 2011; 62(1): 227–250 [<https://doi.org/10.1146/annurev-arplant-042110-103846>][PMID: 21391813]
- [6] Simon L, Bousquet J, Lévesque RC, and Lalonde M. Origin and diversification of endomycorrhizal fungi and coincidence with vascular land plants. *Nature* 1993; 363(6424): 67–69 [<https://doi.org/10.1038/363067a0>]
- [7] Heckman DS, Geiser DM, Eidell BR, Stauffer RL, Kardos NL, and Hedges SB. Molecular evidence for the early colonization of land by fungi and plants. *Science* 2001; 293(5532): 1129–1133 [<https://doi.org/10.1126/science.1061457>][PMID: 11498589]
- [8] Akiyama K, Matsuzaki Ki, and Hayashi H. Plant sesquiterpenes induce hyphal branching in arbuscular mycorrhizal fungi. *Nature* 2005; 435(7043): 824–827 [<https://doi.org/10.1038/nature03608>]
- [9] Besserer A, Puech-Pagès V, Kiefer P, Gomez-Roldan V, Jauneau A, Roy S, *et al.* Strigolactones stimulate arbuscular mycorrhizal fungi by activating mitochondria. *PLoS Biol* 2006; 4(7): e226 [<https://doi.org/10.1371/journal.pbio.0040226>][PMID: 16787107]
- [10] Harrison MJ. The arbuscular mycorrhizal symbiosis: An underground association. *Trends Plant Sci* 1997; 2(2): 54–60 [[https://doi.org/10.1016/S1360-1385\(97\)82563-0](https://doi.org/10.1016/S1360-1385(97)82563-0)]
- [11] Strack D, Fester T, Hause B, Schliemann W, and Walter MH. Arbuscular mycorrhiza: Biological, chemical, and molecular aspects. *J Chem Ecol* 2003; 29(9): 1955–1979 [PMID: 14584670]

- [12] Genre A, Chabaud M, Timmers T, Bonfante P, and Barker DG. Arbuscular mycorrhizal fungi elicit a novel intracellular apparatus in *Medicago truncatula* root epidermal cells before infection. *Plant Cell* 2005; 17(12): 3489–3499 [https://doi.org/10.1105/tpc.105.035410][PMID: 16284314]
- [13] Cox G and Tinker PB. Translocation and transfer of nutrients in vesicular-arbuscular mycorrhizas. I. The arbuscule and phosphorus transfer: A quantitative ultrastructural study. *New Phytol* 1976; 77(2): 371–378 [https://doi.org/10.1111/j.1469-8137.1976.tb01526.x]
- [14] Kobae Y and Hata S. Dynamics of periarbuscular membranes visualized with a fluorescent phosphate transporter in arbuscular mycorrhizal roots of rice. *Plant Cell Phys* 2010; 51(3): 341–353 [https://doi.org/10.1093/pcp/pcq013][PMID: 20097910]
- [15] Kobae Y, Gutjahr C, Paszkowski U, Kojima T, Fujiwara T, and Hata S. Lipid droplets of arbuscular mycorrhizal fungi emerge in concert with arbuscule collapse. *Plant Cell Phys* 2014; 55(11): 1945–1953 [https://doi.org/10.1093/pcp/pcu123][PMID: 25231957]
- [16] Park HJ, Floss DS, Levesque-Tremblay V, Bravo A, and Harrison MJ. Hyphal branching during arbuscule development requires reduced arbuscular mycorrhiza 1. *Plant Physiol* 2015; 169(4):2774-2788 [http://doi.org/10.1104/pp.15.01155]
- [17] Floss DS, Gomez SK, Park HJ, MacLean AM, Müller LM, Bhattarai KK, *et al.* A transcriptional program for arbuscule degeneration during AM symbiosis is regulated by MYB1. *Current Biol* 2017; 27(8): 1206–1212 [https://doi.org/10.1016/j.cub.2017.03.003]
- [18] Hogekamp C and Küster H. A roadmap of cell-type specific gene expression during sequential stages of the arbuscular mycorrhiza symbiosis. *BMC Gen* 2013; 14(1): 306 [https://doi.org/10.1186/1471-2164-14-306]
- [19] Hohnjec N, Vieweg MF, Pühler A, Becker A, and Küster H. Overlaps in the transcriptional profiles of *Medicago truncatula* roots inoculated with two different *Glomus* fungi provide insights into the genetic program activated during arbuscular mycorrhiza. *Plant Physiol* 2005; 137(4): 1283–1301 [https://doi.org/10.1104/pp.104.056572] [PMID: 15778460]
- [20] Provorov NA, Borisov AY, and Tikhonovich IA. Developmental genetics and evolution of symbiotic structures in nitrogen-fixing nodules and arbuscular mycorrhiza. *J of Theoretical Biol* 2002; 214(2): 215–232 [https://doi.org/10.1006/jtbi.2001.2453]
- [21] Ivanov S, Fedorova EE, Limpens E, De Mita S, Genre A, Bonfante P, *et al.* Rhizobium-legume symbiosis shares an exocytotic pathway required for arbuscule formation. *Proc Natl Acad Sci U S A* 2012; 109(21): 8316–8321 [https://doi.org/10.1073/pnas.1200407109]
- [22] Zhang X, Pumplun N, Ivanov S, and Harrison MJ. EXO70I is required for development of a sub-domain of the periarbuscular membrane during arbuscular mycorrhizal symbiosis. *Current Biol* 2015; 25(16): 2189–2195 [https://doi.org/10.1016/j.cub.2015.06.075]
- [23] Harrison, MJ and Ivanov, S. Exocytosis for endosymbiosis: membrane trafficking pathways for development of symbiotic membrane compartments. *Current Op Plant Biol* 2017; 38:101-108 [https://doi.org/10.1016/j.pbi.2017.04.019]
- [24] Huisman R, Hontelez J, Mysore KS, Wen J, Bisseling T, and Limpens E. A symbiosis-dedicated syntaxin of plants 13II isoform controls the formation of a stable host-microbe interface in symbiosis. *New Phytol* 2016; 211(4): 1338–1351 [https://doi.org/10.1111/nph.13973]
- [25] Chen JS, V. Reddy, JH Chen, Shlykov MA, Zheng WH, Cho J, *et al.* Phylogenetic characterization of transport protein superfamilies: superiority of SuperfamilyTree programs over those based on multiple alignments. *J. Mol Microbiol. Biotechnol* (2011). 21(3-4): 83-96. 22286036
- [26] Maróti G, Downie JA, and Kondorosi É. Plant cysteine-rich peptides that inhibit pathogen growth and control rhizobial differentiation in legume nodules. *Current Op Plant Biol* 2015; 26: 57–63 [https://doi.org/10.1016/j.pbi.2015.05.031]
- [27] Thomma BPHJ, Cammue BPA, and Thevissen K. Plant defensins. *Planta* 2002; 216(2): 193–202 [https://doi.org/10.1007/s00425-002-0902-6][PMID: 12447532]
- [28] García-Olmedo F, Molina A, Alamillo JM, and Rodríguez-Palenzuela P. Plant defense peptides. *Biopolymers* 1998; 47(6): 479–491 [https://doi.org/10.1002/(SICI)1097-0282(1998)47:6<479::AID-BIP6>3.0.CO;2-K]
- [29] Van der Weerden NL and Anderson MA. Plant defensins: common fold, multiple functions. *Fungal Biol Rev* 2013; 26(4):121-131 [http://doi.org/10.1128/AAC.00365-13]
- [30] Sagaram US, El-Mounadi K, Buchko GW, Berg HR, Jagdeep Kaur J, Pandurangi RS, *et al.* Structural and functional studies of a phosphatidic acid-binding antifungal plant defensin MtDef4: Identification of an RGFRRR motif governing fungal cell entry. *PLoS ONE* 2013; 8(12): e82485 [https://doi.org/10.1371/journal.pone.0082485]

- [31] Thevissen K, Osborn RW, Acland DP, and Broekaert WF. Specific binding sites for an antifungal plant defensin from Dahlia (*Dahlia merckii*) on fungal cells are required for antifungal activity. *Mol Plant Microbe Interact* 2000; 13(1): 54–61 [https://doi.org/10.1094/MPMI.2000.13.1.54][PMID: 10656585]
- [32] Kagan BL, Selsted ME, Ganz T, and Lehrer RI. Antimicrobial defensin peptides form voltage-dependent ion-permeable channels in planar lipid bilayer membranes. *Proc Natl Acad Sci U S A* 1990; 87(1): 210–214 [https://doi.org/10.1073/pnas.87.1.210]
- [33] Hanks JN, Snyder AK, Graham MA, Shah RK, Blaylock LA, Harrison MJ, et al. Defensin gene family in *Medicago truncatula*: Structure, expression and induction by signal molecules. *Plant Mol Biol* 2005; 58(3): 385–399 [https://doi.org/10.1007/s11103-005-5567-7]
- [34] Alunni B and Gourion B. Terminal bacteroid differentiation in the legume–Rhizobium symbiosis: nodule-specific cysteine-rich peptides and beyond. *New Phytol* 2016; 211(2):411-417 [http://dx.doi.org/10.1111/nph.14025]
- [35] van de Velde W, Zehirov G, Szatmari A, Debreczeny M, Ishihara H, Kevei Z, et al. Plant peptides govern terminal differentiation of bacteria in symbiosis. *Science* 2010; 327(5969): 1122–1126 [https://doi.org/10.1126/science.1184057][PMID: 20185722]
- [36] Gomez SK, Javot H, Deewatthanawong P, Ivone Torres-Jerez I, Tang Y, Blancaflor EB, et al. *Medicago truncatula* and *Glomus intraradices* gene expression in cortical cells harboring arbuscules in the arbuscular mycorrhizal symbiosis. *BMC Plant Biol* 2009; 9(1): 10 [https://doi.org/10.1186/1471-2229-9-10]
- [37] Hoge Kamp C, Arndt D, Pereira PA, Becker JD, Hohnjec N, and Küster H. Laser microdissection unravels cell-type-specific transcription in arbuscular mycorrhizal roots, including CAAT-Box transcription factor gene expression correlating with fungal contact and spread. *Plant Physiol* 2011; 157(4): 2023–2043 [https://doi.org/10.1104/pp.111.186635]
- [38] Gaude, N, Bortfeld, S, Duensing, N, Lohse M, and Krajinski F. Arbuscule-containing and non-colonized cortical cells of mycorrhizal roots undergo extensive and specific reprogramming during arbuscular mycorrhizal development. *Plant Journal* 2012; 69(3): 510-528 [http://dx.doi.org/10.1111/j.1365-313X.2011.04810.x]
- [39] Källberg M, Wang H, Wang S, Peng J, Wang Z, Lu H, et al. Template-based protein structure modeling using the RaptorX web server. *Nat Protoc* 2012; 7(8): 1511–1522 [https://doi.org/10.1038/nprot.2012.085]
- [40] Vriens K, Cools TL, Harvey PJ, Craik DJ, Spincemaille P, Cassiman D, et al. Synergistic activity of the plant defensin HsAFP1 and caspofungin against *Candida albicans* biofilms and planktonic cultures. *PLoS ONE* 2015; 10(8): e0132701 [https://doi.org/10.1371/journal.pone.0132701][PMID: 26248029]
- [41] Fant F, Vranken W, Broekaert W, and Borremans F. Determination of the three-dimensional solution structure of *Raphanus sativus* Antifungal Protein 1 by 1H NMR11. *J of Mol Biol* 1998, 279 (1): 257-270 [https://doi.org/10.1006/jmbi.1998.1767.]
- [42] Razzera G, Gadermaier G, de Paula V, Almeida MS, Egger M, Jahn-Schmid B, et al. Mapping the interactions between a major pollen allergen and human IgE antibodies. *Structure* 2010; 18(8): 1011–1021 [https://doi.org/10.1016/j.str.2010.05.012]
- [43] Krishnakumar V, Kim M, Rosen BD, Karamycheva S, Bidwell SL, Tang H, et al. MTGD: The *Medicago truncatula* genome database. *Plant Cell Physiol* 2015; 56(1):e1 [https://doi.org/10.1093/pcp/pcu179]
- [44] Tang H, Krishnakumar V, Bidwell S, Rosen B, Chan A, Zhou S, et al. An improved genome release (version Mt4.0) for the model legume *Medicago truncatula*. *BMC Gen* 2014; 15: 312 [https://doi.org/10.1186/1471-2164-15-312][PMID: 24767513]
- [45] Petersen, T, Brunak, S, von Heijne G, and Nielsen H. SignalP 4.0: discriminating signal peptides from transmembrane regions. *Nature Methods* 2011; 8(10):785-786 [http://dx.doi.org/10.1038/nmeth.1701]
- [46] Chou KC and Shen HB. Plant-mPLOC: A top-down strategy to augment the power for predicting plant protein subcellular localization. *PLoS ONE* 2010; 5(6): e11335 [https://doi.org/10.1371/journal.pone.0011335][PMID: 20596258]
- [47] Briesemeister S, Blum T, Brady S, Lam Y, Kohlbacher O, and Shatkay H. SherLoc2: A high-accuracy hybrid method for predicting subcellular localization of proteins. *J Proteome Res* 2009; 8(11): 5363–5366 [https://doi.org/10.1021/pr900665y]
- [48] Grant SG, Jessee J, Bloom FR, and Hanahan D. Differential plasmid rescue from transgenic mouse DNAs into *Escherichia coli* methylation-restriction mutants. *Proc Natl Acad Sci U S A* 1990; 87(12): 4645–4649 [https://doi.org/10.1073/pnas.87.12.4645]

- [49] Quandt HJ. Transgenic root nodules of *Vicia hirsuta*: A fast and efficient system for the study of gene expression in indeterminate-type nodules. *Mol Plant Microbe Interact* 1993; 6(6): 699 [https://doi.org/10.1094/MPMI-6-699]
- [50] Pridmore RD. New and versatile cloning vectors with kanamycin-resistance marker. *Gene* 1987; 56(2-3): 309–312 [https://doi.org/10.1016/0378-1119(87)90149-1]
- [51] Küster H, Quandt HJ, Broer I, Perlick AM, and Pühler A. The promoter of the *Vicia faba* L. VfENOD-GRP3 gene encoding a glycine-rich early nodulin mediates a predominant gene expression in the interzone II-III region of transgenic *Vicia hirsuta* root nodules. *Plant Mol Biol* 1995; 29(4): 759–772 [https://doi.org/10.1007/BF00041166]
- [52] Limpens, E, Ramos, J, Franken, C, Raz V, Compaan B, Franssen H, *et al.* RNA interference in *Agrobacterium rhizogenes*-transformed roots of *Arabidopsis* and *Medicago truncatula*. *J Exp Bot* 2004; 55(399): 983-992
- [53] Limpens E, Mirabella R, Fedorova E, Franken C, Franssen H, Bisseling T, *et al.* Formation of organelle-like N₂-fixing symbiosomes in legume root nodules is controlled by DMI2. *Proc Natl Acad Sci U S A* 2005; 102(29): 10375–10380 [https://doi.org/10.1073/pnas.0504284102]
- [54] Devers EA, Teply J, Reinert A, Gaude N, and Krajinski F. An endogenous artificial microRNA system for unraveling the function of root endosymbioses related genes in *Medicago truncatula*. *BMC Plant Biol* 2013; 13: 82 [https://doi.org/10.1186/1471-2229-13-82][PMID: 23679580]
- [55] Harrison MJ, Dewbre GR, and Liu J. A phosphate transporter from *Medicago truncatula* involved in the acquisition of phosphate released by arbuscular mycorrhizal fungi. *Plant Cell* 2002; 14(10): 2413–2429 [PMID: 12368495]
- [56] Baier M, Hohnjec N, Lenz F, Fehlberg V, Vieweg MF, Hause B, *et al.* The signal peptide of the *Medicago truncatula* modular nodulin MtNOD25 operates as an address label for the specific targeting of proteins to nitrogen-fixing symbiosomes. *Mol Plant Microbe Interact* 2009; 22(1): 63–72 [https://doi.org/10.1094/MPMI-22-1-0063][PMID: 19061403]
- [57] Nelson BK, Cai X, and Nebenführ A. A multicolored set of in vivo organelle markers for co-localization studies in *Arabidopsis* and other plants. *Plant Journal* 2007; 51(6): 1126–1136 [https://doi.org/10.1111/j.1365-313X.2007.03212.x]
- [58] Ivanov S and Harrison MJ. A set of fluorescent protein-based markers expressed from constitutive and arbuscular mycorrhiza-inducible promoters to label organelles, membranes and cytoskeletal elements in *Medicago truncatula*. *Plant Journal* 2014; 80(6): 1151–1163 [https://doi.org/10.1111/tpj.12706]
- [59] Arnon, DI and Hoagland, DR. Crop production in artificial culture solutions and in soils with special reference to factors influencing yields and absorption of inorganic nutrients. *Soil Sci.* 1940; 50: 463-483.
- [60] Vieweg MF, Frühling M, Quandt H-J, Heim U, Bäumlein H, Pühler A, *et al.* The promoter of the *Vicia faba* L. leghemoglobin gene VfLb29 is specifically activated in the infected cells of root nodules and in the arbuscule-containing cells of mycorrhizal roots from different legume and nonlegume plants. *Mol Plant Microbe Interact* 2004; 17(1): 62–69 [https://doi.org/10.1094/MPMI.2004.17.1.62]
- [61] Smit P, Raedts J, Portyanko V, Debelle F, *et al.* NSP1 of the GRAS protein family is essential for rhizobial Nod factor-induced transcription. *Science* 2005; 308(5729), 1789-1791.
- [62] Javot H, Penmetsa RV, Breuillin F, Bhattarai KK, Noar RD, Gomez SK, *et al.* *Medicago truncatula* MtPt4 mutants reveal a role for nitrogen in the regulation of arbuscule degeneration in arbuscular mycorrhizal symbiosis. *Plant Journal* 2011; 68(6): 954–965 [https://doi.org/10.1111/j.1365-313X.2011.04746.x][PMID: 21848683]
- [63] Brundrett M, Bougher N, Dell B, Grove T, and Malajczuk N. Working with mycorrhizas in forestry and agriculture. ACIAR monograph 1996; ACIAR: Canberra [Publication Code: MN032][ISBN: 1 86320 181 5]
- [64] Benedito VA, Torres-Jerez I, Murray JD, *et al.* A gene expression atlas of the model legume *Medicago truncatula*. *Plant Journal* 2008; 55(3): 504–513 [https://doi.org/10.1111/j.1365-313X.2008.03519.x][PMID: 18410479]
- [65] Pumplun N, Zhang X, Noar RD, and Harrison MJ. Polar localization of a symbiosis-specific phosphate transporter is mediated by a transient reorientation of secretion. *Proc Natl Acad Sci U S A* 2012; 109(11): E665-672 [https://doi.org/10.1073/pnas.1110215109][PMID: 22355114]
- [66] Islam KT, Velivelli SLS, Berg RH, Oakley B, and Shah DM. A novel bi-domain plant defensin MtDef5 with potent broad-spectrum antifungal activity binds to multiple phospholipids and forms oligomers. *Sci Rep* 2017; 7(1): 135 [https://doi.org/10.1038/s41598-017-16508-w]
- [67] Javot H, Penmetsa RV, Terzaghi N, Cook DR, and Harrison MJ. A *Medicago truncatula* phosphate transporter indispensable for the arbuscular mycorrhizal symbiosis. *Proc Natl Acad Sci U S A* 2007; 104(5): 1720–1725 [https://doi.org/10.1073/pnas.0608136104][PMID: 17242358]

- [68] Bonneau L, Huguet S, Wipf D, Pauly N, and Truong HN. Combined phosphate and nitrogen limitation generates a nutrient stress transcriptome favorable for arbuscular mycorrhizal symbiosis in *Medicago truncatula*. *New Phytol* 2013; 199(1): 188–202 [<https://doi.org/10.1111/nph.12234>][PMID: 23506613]
- [69] Gobbato E, Marsh JF, Vernié T, Wang E, Mailliet F, Kim J, *et al.* A GRAS-type transcription factor with a specific function in mycorrhizal signaling. *Current Biol* 2012; 22(23): 2236–2241 [<https://doi.org/10.1016/j.cub.2012.09.044>][PMID: 23122845]
- [70] Luginbuehl LH, Menard GN, Kurup S, Van Erp H, Radhakrishnan GV, Breakspear A, *et al.* Fatty acids in arbuscular mycorrhizal fungi are synthesized by the host plant. *Science* 2017; 356(6343): 1175–1178 [<https://doi.org/10.1126/science.aan0081>][PMID: 28596311]
- [71] Bravo A, Brands M, Wewer V, Dörmann P, Harrison MJ. Arbuscular mycorrhiza-specific enzymes FatM and RAM2 fine-tune lipid biosynthesis to promote development of arbuscular mycorrhiza. *New Phytol* 2017; 214(4): 1631–45 [<https://doi.org/10.1111/nph.14533>][PMID: 28380681]
- [72] Carro L, Pujic P, Alloisio N, Fournier P, Boubakri H, Hay AE, *et al.* *Alnus* peptides modify membrane porosity and induce the release of nitrogen-rich metabolites from nitrogen-fixing *Frankia*. *ISME J* 2015; 9(8): 1723–1733 [<https://doi.org/10.1038/ismej.2014.257>]
- [71] Carro L, Pujic P, Alloisio N, Fournier P, Boubakri H, Poly F, *et al.* Physiological effects of major up-regulated *Alnus glutinosa* peptides on *Frankia* sp. ACN14a. *Microbiology* 2016; 162(7): 1173–1184 [<https://doi.org/10.1099/mic.0.000291>]
- [72] Mergaert P. A novel family in *Medicago truncatula* consisting of more than 300 nodule-specific genes coding for small, secreted polypeptides with conserved cysteine motifs. *Plant Physiol* 2003; 132(1): 161–173 [<https://doi.org/10.1104/pp.102.018192>]
- [73] Penterman J, Abo RP, De Nisco NJ, Arnold MFF, Longhi R, Zanda M, *et al.* Host plant peptides elicit a transcriptional response to control the *Sinorhizobium meliloti* cell cycle during symbiosis. *Proc Natl Acad Sci U S A* 2014; 111(9): 3561–3566 [<https://doi.org/10.1073/pnas.1400450111>][PMID: 24501120]
- [74] Farkas A, Maróti G, Durgó H, Györgypál Z, Lima RM, Medzihradzsky KF, *et al.* *Medicago truncatula* symbiotic peptide NCR247 contributes to bacteroid differentiation through multiple mechanisms. *Proc Natl Acad Sci U S A* 2014; 111(14): 5183–5188 [<https://doi.org/10.1073/pnas.1404169111>][PMID: 24706863]
- [75] Maróti, G. and Kondorosi, É. Nitrogen-fixing Rhizobium-legume symbiosis: Are polyploidy and host peptide-governed symbiont differentiation general principles of endosymbiosis? *Front Microbiol.* 2014; 5(359): 636 [<https://doi.org/10.3389/fmicb.2014.00326>]
- [76] Limpens E, Ivanov S, van Esse W, Voets G, Fedorova E, and Bisseling T. *Medicago* N₂-fixing symbiosomes acquire the endocytic identity marker Rab7 but delay the acquisition of vacuolar identity. *Plant Cell* 2009; 21(9): 2811–2828 [<https://doi.org/10.1105/tpc.108.064410>]
- [77] Pierre O, Engler G, Hopkins J, Brau F, Boncompagni E, and Hérouart D. Peribacteroid space acidification: A marker of mature bacteroid functioning in *Medicago truncatula* nodules. *Plant Cell Environ* 2013; 36(11): 2059–2070 [<https://doi.org/10.1111/pce.12116>]
- [78] Pladys D and Vance CP. Proteolysis during development and senescence of effective and plant gene-controlled ineffective alfalfa nodules. *Plant Physiol* 1993; 103(2): 379–384 [<https://doi.org/10.1104/pp.103.2.379>]
- [79] van de Velde W, Guerra JCP, De Keyser A, De Rycke R, Rombauts S, Maunoury N, *et al.* Aging in legume symbiosis. A molecular view on nodule senescence in *Medicago truncatula*. *Plant Physiol* 2006; 141(2): 711–720 [<https://doi.org/10.1104/pp.106.078691>][PMID: 16648219]
- [80] Hause B and Fester T. Molecular and cell biology of arbuscular mycorrhizal symbiosis. *Planta* 2005; 221(2): 184–196 [<https://doi.org/10.1007/s00425-004-1436-x>][PMID: 15871030]
- [81] Krajinski F, Courty PE, Sieh D, Franken P, Zhang H, Bucher M, *et al.* The H⁺-ATPase HA1 of *Medicago truncatula* is essential for phosphate transport and plant growth during arbuscular mycorrhizal symbiosis. *Plant Cell* 2014; 26(4): 1808–1817 [<https://doi.org/10.1105/tpc.113.120436>]
- [83] Jiang Y, Wang W, Xie Q, Liu N, Liu L, Wang D, *et al.* Plants transfer lipids to sustain colonization by mutualistic mycorrhizal and parasitic fungi. *Science* 2017; 356(6343): 1172–1175 [<https://doi.org/10.1126/science.aam9970>][PMID: 28596307]
- [84] Tisserant E, Malbreil M, Kuo A, Annegret Kohler A, Symeonidi A, Balestrini R, *et al.* Genome of an arbuscular mycorrhizal fungus provides insight into the oldest plant symbiosis. *Proc Natl Acad Sci U S A* 2013; 110(50): 20117–20122 [<https://doi.org/10.1073/pnas.1313452110>] [PMID: 24277808]
- [85] Bago B. Translocation and utilization of fungal storage lipid in the arbuscular mycorrhizal symbiosis. *Plant Physiol* 2002; 128(1): 108–124 [<https://doi.org/10.1104/pp.128.1.108>]
- [86] Thevissen K, De Mello Tavares P, Xu D, Blankenship J, Vandenbosch D, Idkowiak-Baldys J, *et al.* The plant defensin RsAFP2 induces cell wall stress, septin mislocalization and accumulation of ceramides in

- Candida albicans*. *Mol Microbiol* 2012; 84(1): 166–180 [<https://doi.org/10.1111/j.1365-2958.2012.08017.x>][PMID: 22384976]
- [87] Hayes BME, Bleackley MR, Wiltshire JL, Anderson MA, Traven A, and van der Weerden NL. Identification and mechanism of action of the plant defensin NaD1 as a new member of the antifungal drug arsenal against *Candida albicans*. *Antimicrob Agents Chemother* 2013; 57(8): 3667–3675 [<https://doi.org/10.1128/AAC.00365-13>][PMID: 23689717]
- [88] Lobo DS, Pereira IB, Fragel-Madeira L, Medeiros LN, Cabral LM, Faria J, *et al.* Antifungal *Pisum sativum* defensin 1 interacts with *Neurospora crassa* cyclin F related to the cell cycle. *Biochemistry* 2007; 46(4): 987–996 [<https://doi.org/10.1021/bi061441j>][PMID: 17240982]
- [89] van der Weerden NL, Lay FT, and Anderson MA. The plant defensin, NaD1, enters the cytoplasm of *Fusarium oxysporum* hyphae. *J Biol Chem* 2008; 283(21): 14445–14452 [<https://doi.org/10.1074/jbc.M709867200>][PMID: 18339623]
- [90] Kitatani K, Idkowiak-Baldys J, and Hannun YA. The sphingolipid salvage pathway in ceramide metabolism and signaling. *Cell Signaling*. 2008; 20 (6): 1010–1018. [<https://doi:10.1016/j.cellsig.2007.12.006>. PMC 2422835][PMID 18191382]

Supporting information

S1 Table: Primers used in real-time RT-PCR experiments.

Gene	Identifier*	Primers
<i>MtDefMd1</i>	Medtr8g012805.1	GCTTCCTCTGCTCTTAAATA/TGTTGCCGGTGGTTCCTTAC
<i>MtDefMd2</i>	Medtr8g012835.1	AAAGGAAAAGCACAACATGG/CAGAAGCAAGCAAATCCAAA
<i>MtDefMd1/2</i>	Medtr8g012805.1/Medtr8g012835.1	GGGACATTAAGCAAGCATG/TCACATTGCTTGAGCAGAAA
<i>MtDefMd3</i>	Medtr8g012875.1	TGCTCGTAAATTCCTCACAA/CTTCGCCATTGACAACTTT
<i>MtDefMd4</i>	Medtr8g012885.1	TTGTAGAGGGAGAAGCAAAC/CCAGTGTTATCAAGGTGACA
<i>MtTefa</i>	Medtr6g021805.1	AAGCTAGGAGGTATTGACAAG/ACTGTGCAGTAGTACTTGTTG
<i>MtPt4</i>	Medtr1g028600.1	TCGCGCGCCATGTTTGTGT/GCGAAGAAGAATGTTAGCCC
<i>MtMyb1</i>	Medtr7g068600.1	TACTGCCAAATTTCTGTTCTA/GGATTGTGTTTTAAAGGATTC
<i>MtRam1</i>	Medtr7g027190.1	CATTACTACTCCGCAATTTTC/CAACAAACAACCTTTATCCTC
<i>MtHa1</i>	Medtr8g006790.1	AGGTTCTAACATCTATTGGGA/GACAACCTTATGTGAACCAATG
<i>GiHa5</i>	GQ205019.1	AAATTACGGTTTCTTCTGCAC/TGGAACATCTTCCTTCATTTCA
<i>GiPt</i>	AY037894.1	AACACGATGTCAACAAAGCAAC/AAGACCGATTCCATAAAAAAGCA
<i>GiTuba</i>	GW088233.1	TGTCCAACCGTTTTAAAGT/AAAGCACGTTTGGCGTACAT

* From the *Medicago truncatula* genome 4.0 or GenBank accession numbers, respectively.

S2 Table: Properties and cleavage sites of the *MtDefMd* signal peptides predicted by *SignalP*.

Defensin	Cleavage site*	D	D-cutoff	Transmembrane region
<i>MtDefMd1</i>	VQG-NT	0.853	0.450	No
<i>MtDefMd2</i>	VQG-NI	0.892	0.450	No
<i>MtDefMd3</i>	VEA-KV	0.877	0.450	No
<i>MtDefMd4</i>	VQA-KL	0.919	0.450	No

* Cleavage is between positions 29 and 30 in each case.

S3 Table: Correlation of *MtDefMd* and AM marker gene expression in the course of mycorrhization.

	<i>MtDefMd1</i>	<i>MtDefMd2</i>	<i>MtDefMd3</i>	<i>MtDefMd4</i>
<i>MtDefMd1</i>	1.00	0.99	0.57	0.92
<i>MtDefMd2</i>	0.99	1.00	0.68	0.96
<i>MtDefMd3</i>	0.57	0.68	1.00	0.82
<i>MtDefMd4</i>	0.92	0.96	0.82	1.00
<i>MtMyb1</i>	0.99	0.98	0.51	0.88
<i>MtPt4</i>	0.80	0.81	0.67	0.89
<i>GiTuba</i>	0.87	0.89	0.74	0.95

S4 Table: Percentage of colonized and arbuscule-containing areas in mycorrhized *Medicago truncatula* *MtDefMd1*-overexpression (pPt4:*MtDefMd1*, pUbi:*MtDefMd1*) and pPt4:*gusAint* roots.

Construct	Plants [n]	Grid line intersections	Intersections with fungal structures [%]	Intersections with arbuscules [%]
pPt4: <i>MtDefMd1</i>	6	300	60*	46*
pUbi: <i>MtDefMd1</i>	12	300	71*	59*
pPt4: <i>gusAint</i>	9	300	64	54

* No significant difference to pPt4:*gusAint* control roots

S5 Table: Percentage of colonized and arbuscule-containing areas in mycorrhized *Medicago truncatula* MtDefMd1/2-knock-down (RNAi:MtDefMd1/2) and RNAi:gusAint roots.

Construct	Plants [n]	Grid line intersections	Intersections with fungal structures [%]	Intersections with arbuscules [%]
RNAi:MtDefMd1/2	5	301	52*	41*
RNAi:gusAint	8	308	59	57

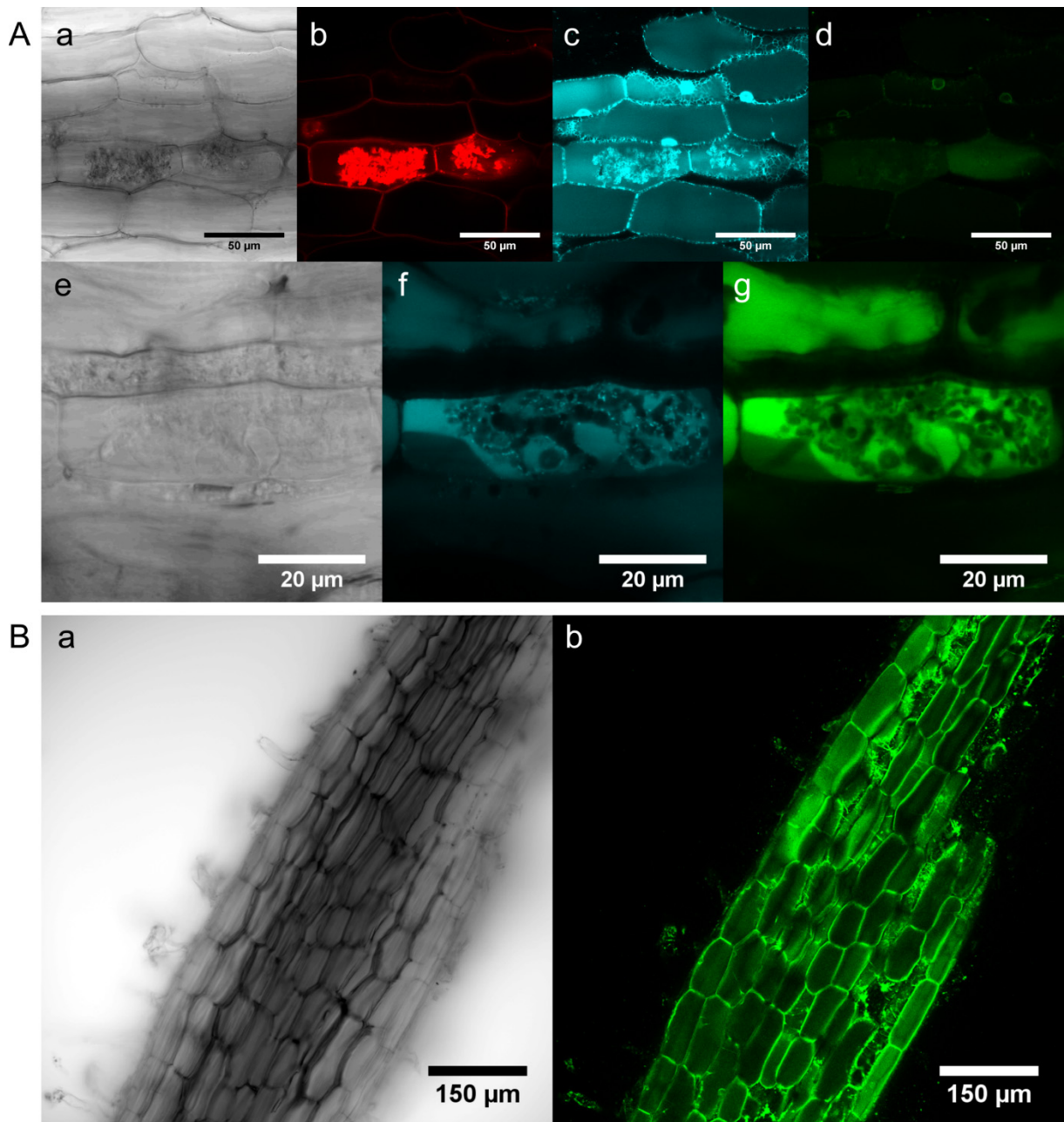
* No significant difference to RNAi:gusAint control roots

S6 Table: Underlying data points for the size distribution of arbuscules in mycorrhized *Medicago truncatula* MtDefMd1-overexpression (pPt4:MtDefMd1, pUbi:MtDefMd1), MtDefMd1/2-knockdown (RNAi:MtDefMd1/2), and pPT4:gusAint roots.

Construct expressed in transgenic roots	Arbuscule size category	Arbuscules per category			Relative amount of arbuscules per category			Mean of relative amounts	Standard deviation	t-test* vs pt4:GusAint
		I	II	III	I	II	III			
pPt4:MtDefMd1	<15	0	0	0	0	0	0	0.00	0.00	-
pPt4:MtDefMd1	15-24	5	6	11	2.49	3.21	4.25	3.31	0.88	0.070
pPt4:MtDefMd1	25-34	17	21	56	8.46	11.23	21.62	13.77	6.94	0.566
pPt4:MtDefMd1	35-44	38	44	85	18.91	23.53	32.82	25.08	7.09	0.866
pPt4:MtDefMd1	45-54	52	45	56	25.87	24.06	21.62	23.85	2.13	0.311
pPt4:MtDefMd1	55-64	43	32	34	21.39	17.11	13.13	17.21	4.13	0.292
pPt4:MtDefMd1	65-74	30	20	9	14.93	10.70	3.47	9.70	5.79	0.921
pPt4:MtDefMd1	75-84	10	15	6	4.98	8.02	2.32	5.10	2.85	0.796
pPt4:MtDefMd1	85-94	5	4	2	2.49	2.14	0.77	1.80	0.91	0.397
pPt4:MtDefMd1	95-104	1	0	0	0.50	0	0	0.17	0.29	0.042
pPt4:MtDefMd1	105-114	0	0	0	0	0	0	0.00	0.00	0.374
pUbi:MtDefMd1	<15	0	0	0	0	0	0	0.00	0.00	-
pUbi:MtDefMd1	15-24	15	5	0	7.98	2.59	0	3.52	4.07	0.522
pUbi:MtDefMd1	25-34	41	39	8	21.81	20.21	6.25	16.09	8.56	0.865
pUbi:MtDefMd1	35-44	42	52	32	22.34	26.94	25.00	24.76	2.31	0.805
pUbi:MtDefMd1	45-54	39	48	31	20.74	24.87	24.22	23.28	2.22	0.408
pUbi:MtDefMd1	55-64	25	36	25	13.30	18.65	19.53	17.16	3.37	0.269
pUbi:MtDefMd1	65-74	17	11	13	9.04	5.70	10.16	8.30	2.32	0.654
pUbi:MtDefMd1	75-84	8	2	11	4.26	1.04	8.59	4.63	3.79	0.707
pUbi:MtDefMd1	85-94	1	0	6	0.53	0	4.69	1.74	2.57	0.468
pUbi:MtDefMd1	95-104	0	0	2	0	0	1.56	0.52	0.90	0.480
pUbi:MtDefMd1	105-114	0	0	0	0	0	0	0.00	0.00	0.374
RNAi:MtDefMd1/2	<15	1	0	0	0.55	0.00	0.00	0.18	0.32	0.374
RNAi:MtDefMd1/2	15-24	2	6	0	1.09	2.24	0.00	1.11	1.12	0.349
RNAi:MtDefMd1/2	25-34	15	33	12	8.20	12.31	6.94	9.15	2.81	0.122
RNAi:MtDefMd1/2	35-44	42	72	28	22.95	26.87	16.18	22.00	5.40	0.554
RNAi:MtDefMd1/2	45-54	44	87	50	24.04	32.46	28.90	28.47	4.23	0.083
RNAi:MtDefMd1/2	55-64	32	41	42	17.49	15.30	24.28	19.02	4.68	0.186
RNAi:MtDefMd1/2	65-74	29	17	18	15.85	6.34	10.40	10.86	4.77	0.899
RNAi:MtDefMd1/2	75-84	10	11	8	5.46	4.10	4.62	4.73	0.69	0.611

RNAi:MtDefMd1/2	85-94	5	1	15	2.73	0.37	8.67	3.93	4.28	0.940
RNAi:MtDefMd1/2	95-104	2	0	0	1.09	0.00	0.00	0.36	0.63	0.231
RNAi:MtDefMd1/2	105-114	1	0	0	0.55	0.00	0.00	0.18	0.32	0.626
pPt4:gusAint	<15	0	0	0	0	0	0	0.00	0.00	-
pPt4:gusAint	15-24	2	4	4	1.28	2.05	2.26	1.86	0.52	-
pPt4:gusAint	25-34	31	19	39	19.87	9.74	22.03	17.22	6.56	-
pPt4:gusAint	35-44	30	42	68	19.23	21.54	38.42	26.40	10.48	-
pPt4:gusAint	45-54	39	34	36	25.00	17.44	20.34	20.92	3.82	-
pPt4:gusAint	55-64	13	36	19	8.33	18.46	10.73	12.51	5.29	-
pPt4:gusAint	65-74	17	32	6	10.90	16.41	3.39	10.23	6.54	-
pPt4:gusAint	75-84	10	17	4	6.41	8.72	2.26	5.80	3.27	-
pPt4:gusAint	85-94	10	9	0	6.41	4.62	0	3.68	3.31	-
pPt4:gusAint	95-104	2	2	1	1.28	1.03	0.56	0.96	0.36	-
pPt4:gusAint	105-114	2	0	0	1.28	0	0	0.43	0.74	-

* Two-tailed Student's t-test



S1 Fig: Localization of MtDefMd1-mGFP6 in mycorrhizal *M. truncatula* roots expressing a multi-fluorophore reporter construct and a tonoplast marker.

Confocal micrographs of razor blade hand-cuttings of transgenic *M. truncatula* roots. The roots express an MtDefMd1-mGFP6 fusion under the control of the native promoter (A; d and g), an ER-CFP fusion under the control of the 2x35S-promoter (A; c and f), and a fusion of the signal peptide of MtBcp1 with mCherry under the control of the native promoter (A; b). Additionally, a tonoplast membrane directed GFP fusion under the control of a 2x35S-promoter (B, b) is shown. Differential interference contrast (DIC) micrographs are shown for each root section (A; a and e; B, a). Roots were mycorrhizal with *R. irregularis* for six weeks.

GENERAL DISCUSSION

During the past decade, the understanding of transport in AM symbioses, including the uptake of molecules from the soil solution [1, 2], traversal across two symbiotic membranes [3], as well as intracellular targeting processes of the host cells [4], has constantly been refined. From the beginning, the improved biomass of plants in association with AM fungi was noticed [5]. Subsequently, phosphate, which is a major plant growth-limiting factor, moved into focus [1] and additional nutrients, which were affected in uptake in AM plants, were identified [6, 7, 8, 9, 10]. In Chapter I, it was shown that the expression of marker genes for mycorrhization such as *GiTub α* , *GiPT*, and *MtPt4* enhanced during the colonization of *Medicago truncatula* roots by *Rhizophagus irregularis*, in dependence of phosphate and nitrogen supply. The latter two marker genes are indicators for the establishment of arbuscules, the major interface for nutrient exchange [11, 12, 13, 14, 15]. This was mirrored by the amount of intraradical fungal structures, such as arbuscules and vesicles (Chapter I, Fig 7). Root colonization by AMF, as well as the arbuscule-rate were enhanced by P depletion (Chapter I, Fig 7), suggesting that nutrient supply from the microsymbiont is important under this nutrient regime. Interestingly, more than 100 membrane transporter genes, were already induced in the early stages of the AM interaction of *M. truncatula* and *R. irregularis* (Chapter I, Fig 8, A). After one week, their cumulated gene expression level was four-fold higher (Chapter I, Fig 8, B). Candidate genes from five highly induced gene families, encoding copper (MtCopMd1), oligopeptide (MtOliMd1), ABC (MtABCG3), and nitrogen transporters (MtAMT2;4), as well as a defensin (MtDefMd1), were selected here in order to unravel processes at the plant-fungal interface.

Arbuscular mycorrhiza-related *M. truncatula* membrane transporter genes associated with the active stage of the symbiosis

The arbuscular mycorrhiza symbiosis between plants and beneficial fungi is influenced by a multitude of factors. In some cases, phenotypic data, such as the growth improvement of AM plants and fungal structures, have been related to each other. This was first achieved, when the PAM was identified as a main interface for the exchange of minerals, in exchange for sugar and fatty acids [16, 17, 18, 19, 20, 21, 22, 23].

Here, single nutrient transporters were found to be closely connected to PAM biogenesis [24, 25, 26, 27, 28, 29, 30, 31, 32]. In addition, several cell organelles adapt to the symbiotic stage of cells. In parallel to the formation of arbuscules, the central vacuoles traverse into connected tubular structures [33, 34, 35, 36]. Furthermore, plastids and mitochondria proliferate and move towards the arbuscule [37, 38, 39]. A high surface to volume ratio, a sufficient proton-motive force, a correct composition of transporters, and metabolic fine-tuning are additional traits of functional arbuscule-containing cells.

Pumplin *et al.* [4] described that a unique set of proteins is generated to provide a specific protein presence of the plant-fungus interface, including many membrane transporters. The creation, sustaining, and degeneration of the symbiotic interface requires complex mechanisms of regulation. Nutrient stresses were shown to influence the arbuscular life-cycle in addition to and possibly interfering with the common SYM-pathway that regulates pre-contact signaling and early infection of the AM interaction [40].

In this thesis, the activation of membrane transporter genes was monitored in different symbiotic scenarios. In Chapter II, the expression of *MtCopMd1*, *MtOliMd1*, *MtABCG3*, and *MtAMT2;4*, encoding arbuscular mycorrhiza-dependent membrane transporters, varied in different phosphate and nitrogen regimes during AM-fungal colonization (Chapter II, Fig 4). Whereas *MtOliMd1* and *MtABCG3* were solely expressed in a phosphate dependent manner, the promoters of *MtCopMd1* and *MtAMT2;4* were also induced by strong nitrogen depletion.

During root colonization by AMF, the expression of *MtCopMd1*, *MtOliMd1*, *MtABCG3*, and *MtAMT2;4* was shown to correlate with the expression of the AM marker genes *MtHa1* and *MtPt4* (chapter II, Fig 3), being connected to the establishment of functional P-transporting arbuscules. This tight connection to the PAM-interface was also monitored for all genes under varying P- and N-supplies during plant cultivation (Chapter II, Fig 2). Furthermore, transcriptional analyses of mutants in the key AM regulator genes *MtRam1* and *MtPt4* as well as *MtMyb1*-RNAi roots displayed a divergent pattern of the membrane transporter genes investigated. Nevertheless, none of the membrane transporter genes was downregulated in *MtMyb1*-RNAi roots, suggesting a function in the active stage of AM for all of them (Chapter II, Fig 17). Wild type arbuscule-harboring cells of *M. truncatula* displayed different spacio-temporal levels of promoter activities (Chapter II, Fig 5-7), indicating different signal cascades for fine-tuning the regulation of the AM-dependent membrane transporter genes selected.

In mycorrhized *M. truncatula* roots expressing artificial microRNAs directed against *MtABCG3*, a reduced *MtRam1* expression was observed (Chapter II, Fig 8). Since it was hypothesized that the ABC transporter supports the AMF with β -MAG [23] to support fungal lipid synthesis, this connection to arbuscule biogenesis on the fungal side could further underline the importance of the gene product for the active stage of interaction and the establishment of symbiotic organs.

Finally, the AM-dependent ammonium transporter *MtAMT2;4* was shown to be inducible under certain conditions, such as nitrogen deprivation. Recorbet *et al.* [32] suggested that ammonium acts as a signal to the arbuscule and it was demonstrated that AMT2;3 has a function in restoring the regular arbuscule phenotype under suitable N-regimes [41]. Thus, it was attempted to knockdown *MtAMT2;4*. In nitrogen-starved mycorrhizal RNAi-roots, a ~92% knock-down of *MtAMT2;4* expression was achieved (Chapter II, Fig 10). This was not the case in transgenic roots supplied with higher amounts of nitrogen, indicating that especially the impact of less prominent membrane transporters

can only be studied with an adjusted experimental set up. However, despite the arbuscule-dependent expression of the *MtAMT2;4* gene, an essential function was not shown, since RNAi-roots, grown under nitrogen depletion, were not affected in the expression of selected AM marker genes. Furthermore, no flux of ammonium was shown in transfected *Xenopus laevis* oocytes (Chapter II, Fig 13), indicating that ammonium (NH_4^+) is not the preferred substrate (Chapter II, Fig 15) and that NH_3 could be transported instead (Chapter II, Fig 17). Nevertheless, an MtAMT2;4-mGFP6 fusion displayed highest fluorescence intensities close to the PAM of arbuscule harboring cells (Chapter II, Fig 16), indicating the presence of the transporter in the symbiotic membrane (Fig 4).

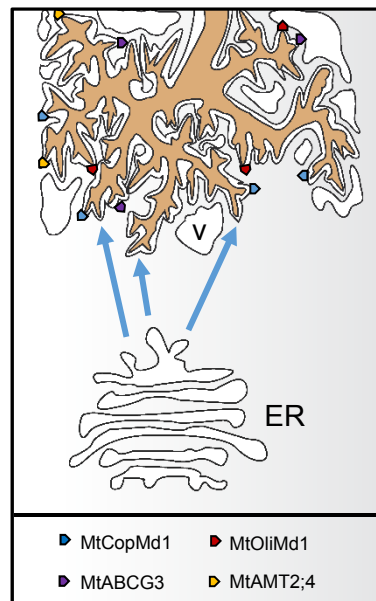


Fig 4: Proposed localization of AM-related membrane transporters during PAM biogenesis in the AM symbiosis of *M. truncatula* and *R. irregularis*.

ER-related targeting processes from the plant host towards symbiotic membranes are shown as arrows. Membrane transporter localizations are proposed based on the studies presented in Chapter II. The fungal cytoplasm is depicted in brown, the periarbuscular space, v, and ER in white and plant cytoplasm in a white to grey scale. Abbreviations: ER, endoplasmic reticulum; v, vacuole

In *ram1-1* mutants, lacking a functional TF that regulates arbuscular fine-branching, *MtCopMd1*, *MtOliMd1*, *MtABCG3*, and *MtAMT2;4* were not activated (Chapter II, Fig 17), indicating that morphologically mature arbuscules coincide with the expression of membrane transporter genes. Taken together, it is likely that the gene products of these membrane transporter genes are localized in the PAM, as shown in Fig 4.

Arbuscular mycorrhiza-related *M. truncatula* defensin genes are associated with the late stage of the symbiosis

During arbuscule development, the PAM is addressed by vesicles with defined protein compositions for incorporation into the plant-fungus interface. This was supported by the visualization of MtBCP1, which is found in the trunk of young and globally in the PAM of mature arbuscules (Chapter III, Fig 15). Transporter proteins, which are situated in the periarbuscular membrane, such as MtPt4, need to be secreted and incorporated in the *de-novo* synthesized symbiotic membranes [41, 42, 43]. ER-rich cytoplasm accumulates at certain sites of the arbuscule, which led to the hypothesis that this process precedes the formation of new branches [18]. To that end, EXO70i was shown to be required for the efficient incorporation of the two ABC transporter subfamily G (ABCG) proteins STR and STR2 into the periarbuscular membranes [44, 45]. Congruent mechanisms are likely to occur for other AM-dependent transporters. While endosymbioses were initially thought to rely on endocytotic processes for the intracellular uptake of microsymbionts, the insight that exocytosis is essential for endosymbioses [48] allowed a deeper understanding of cellular targeting in the root nodule and the AM symbiosis. Transgenic roots, expressing subcellular fluorescence markers that were designed to monitor cell structures and organelles, such as an ER and a tonoplast marker, as well as AM markers, such as MtBsp1, MtAMT2;4 and MtDefMd1 (chapter II, Fig 14, 15, and 17; chapter III, Fig 16) allowed to differentiate the five phases described for AMF-colonized root cortical cells [46], out of which the transition from stage IV. to V. is schematically shown in Fig 5.

The controlled delivery of vesicles, containing either components needed for PAM biogenesis or degradation can be distinguished in different stages of the AM symbiosis (Fig 5). Whereas cells harboring younger and presumably active arbuscules were surrounded by a spider-web like structure of the ER and characterized by MtBcp1-marker presence, older and condensed arbuscules had different characteristics (Chapter III, Fig 17 and S1 Fig). Here, the ER marker displayed prominent spots on the surface of the space, occupied by the arbuscule (Chapter III, Fig 17, A and S1 Fig, A). Furthermore, the tonoplast membrane switched from fine structures that were occupying the free space in cells filled with the dendritic hyphae of mature arbuscules, to a more condensed localization in cells containing degrading arbuscules, characterized by their shrinking volume (Chapter III, Fig 17, B; S1 Fig, B).

Taken together, cellular targeting in arbuscule containing cells from stage I to IV (General Introduction, Fig 3) differs dramatically from the processes initiated in stage IVt. (Fig 5, left to right).

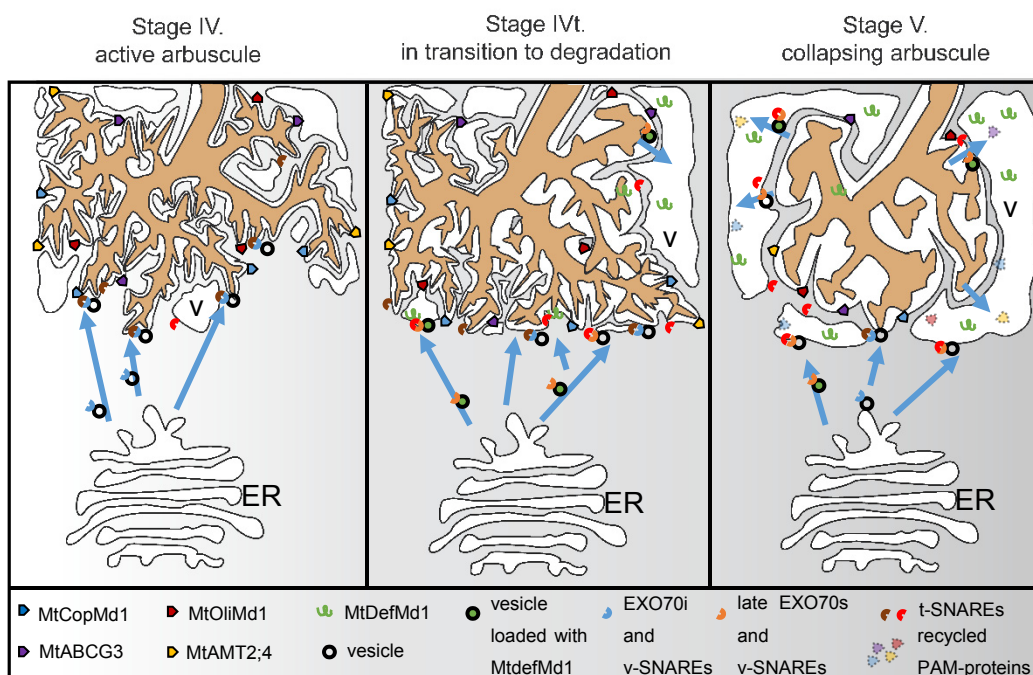


Fig 5: Proposed localization of AM-related membrane proteins during PAM biogenesis and degradation in the AM symbiosis of *M. truncatula* and *R. irregularis*.

ER-related targeting processes from the plant host towards symbiotic membranes are shown as arrows. The fungal cytoplasm is depicted in brown, the periarbuscular space, v and ER in white and plant cytoplasm in a white to grey scale. SNARE and EXO70 proteins are depicted according to the literature [47, 48, 49, 50], membrane transporter localizations are proposed based on the studies presented in Chapter II, whereas the MtDefMd1 localization was studied in Chapter III. Abbreviations: ER, endoplasmic reticulum; v, vacuole

Until Floss *et al.* [47] identified MYB1 as key TF for arbuscule turnover, no molecular switch, associated with the controlled degeneration of arbuscules, was described. Although MYB1 was found to regulate a range of hydrolase genes, such as protease, lipase and chitinase encoding genes [51], *MtMyb1* mutants surprisingly displayed no prolonged life span of arbuscules [51, 52]. It was proposed that this is due to control mechanisms from the host plant that could trigger a rapid turnover of arbuscules, being not effective in terms of nutrient exchange, to counteract poorly performing microsymbionts [52, 55].

Hanks *et al.* [53] were first to identify defensin genes induced in response to root colonization of *M. truncatula* by the AM-fungus *Glomus versiforme*, using transcript sequencing and real-time RT-PCR. Subsequently, several genome-wide transcriptomic studies confirmed that a family of defensin genes is activated during the AM symbiosis of *M. truncatula* [54, 14; 43, 56] and for some, an arbuscule-correlated expression was demonstrated [14, 18]. In Chapter III, a core set of the AM-related defensin genes was described and their expression was placed relative to key AM regulator genes (Chapter III, Fig 4-6). In *M. truncatula*, the expression of four *MtDefMd* genes, encoding defensins with specific structural properties (Chapter III, Fig 1), raised over the time of fungal colonization. Whereas the *MtDefMd1* and *MtDefMd2* promoters were inactive in cells containing young arbuscules, cells with

fully developed arbuscules displayed different levels of promoter activities, indicating an up-regulation towards later stages of arbuscule formation. *MtDefMd1*-mGFP6 was detected in cells with old arbuscules prior to collapse, and finally in vacuolar compartments (Fig 5; Chapter III, Fig 16). Apparently, the transcriptional program and effectors needed for pre-mature arbuscule control and degeneration differs from that of highly adapted symbiotic cells. Here, the vacuole as well as the space taken by the fungus need to be rearranged in terms of a volume transition (Fig 5). Furthermore, the milieu (pH and solvent proteins) of these structures has to be reconstituted to the non-symbiotic status of the cell.

At this point, the conflict between cell-autonomous arbuscule breakdown processes vs. the systemic degradation of infection units, as raised by Kobae *et al.* [31], moves into focus. This could be correlated here with generally expressed defensin genes and in particular to the expression of *MtDefMd1* in response to *MtMyb1* transcription (Chapter II, Fig 6, B). Briefly, there is apparently a program for the degradation of old arbuscules that differs from the control program for the digestion of non-functional arbuscules. Although it was already described in the literature that cells, hosting root nodule bacteria, alter ER targeting during the life-span of bacteroids [50], this feature is not completely understood in AM-symbioses. A ~97% knock-down of *MtDefMd1/MtDefMd2* expression did not significantly affect arbuscule size distribution. Although overexpression of *MtDefMd1* in arbuscule-containing cells led to an up-regulation of *MtRam1* and in tendency of *MtMyb1*, encoding key transcriptional regulators of arbuscule formation, or degradation, respectively, no morphological changes for most of the infection units were evident. One possible effect could nevertheless be the slightly faster turnover of the regular life cycle of arbuscules. This would be masked in roots containing mixed AM stages, unless time lapse imaging experiments of *MtDefMd1* overexpressing and control roots is performed.

The expression of genes connected to AM-related vesicle trafficking, such as *VAPYRIN*, *EXO70i* and *EXO70j*, was shown to respond to *MtRam1* transcription [57, 58, 48, Chapter III; Fig 6, C]. Genes from the EXOCYST family are active in root nodule-, as well as in AM-symbioses [52]. Furthermore, some *EXO70* gene family members were repressed by *MtDefMd1*-overexpression (Chapter III, Fig 10).

During the establishment of fungal structures in the inner root cortex, cell entry, and the creation of an AM exchange interface, cellular targeting differs in comparison to the processes of arbuscule degeneration, digestion and ultimately restructuring of the cells for a post-symbiotic status (Fig 5, Stage IVt. and V.). Under the assumption that cargo-specific EXOCYST members exist [49], the altered expression of *EXO70k* and *EXO70j* (Fig 10) could be an additional mode of compensation for *MtDefMd1* overexpression (Chapter III, Fig 6 and Fig 10), since the biogenesis of active defensins relies on the stepwise modification and maturation in the Golgi network. Thus, the amount of mature *MtDefMd*-loaded granules could be lower than the expression levels of *MtDefMd1*-overexpressing roots indicated. Here, the gene product of *EXO70k* could fulfill a role in the transport of *MtDefMd1/2* and

EXO70j could assist in the delivery of further, pre-arbuscule MtDefMds from the basic set of AM-related defensins.

In this context, it is remarkable that proteins from both families, the EXO70 and defensin family, are known to interact with phospholipids such as phosphatidylinositol 4,5-bisphosphates (PIP₂) [59, 60]. These are also known to have a regulatory impact in the interaction with fungal pathogens [61]. In 1990, Emberhard *et al.* [62] showed that the application of phosphoinositid (PIs)-specific phospholipase C into digitonin-permeabilized chromaffin cells decreased PI levels, and inhibited calcium-triggered exocytosis. Since the inhibition was preferential for an ATP-dependent stage, this indicated that PI function is required for secretion. In consecutive studies, PIP₂ specific antibodies strongly inhibited exocytoses, providing evidence that PIP₂ have a pivotal role during the processes of LDCV (Large dense core vesicle) exocytosis [63, 64]. In conclusion, MtDefMds could, by binding PIPs, alter the targeting during later stages in AM symbiosis and thereby be drivers for the life cycle of symbiotic structures.

By monitoring different membrane transporter genes of the plant-fungus-interface during the AM symbiosis of *M. truncatula* and *R. irregularis*, this thesis provides novel insights on processes that occur in active and degrading arbuscules. To that end, the induction of transcriptional changes to provoke morphological effects and the use of translational fusion with fluorophores to localize membrane transporters *in planta* specifically shed light on transport processes at the plant fungal interface during the late AM symbiosis. Based on fluorophore localizations (Chapter II, Fig 17), the IVt. stage, a transition stage of the late AM interaction, has been described in terms of the impact of *MtDefMd*-genes and new hypotheses and questions concerning cellular targeting processes, especially involving genes of the *EXO70* family, have been stated. These are starting points for further studies of cellular targeting towards symbiotic membranes during the biogenesis- and especially during degradation-related processes at the plant-fungal-interface.

Perspectives

It was shown that regular half strength's Hoagland solution [65] is an appropriate fertilizer for plant cultivation to achieve maximal transcript amounts of the membrane transporter studied here. However, a nitrogen depletion can be vital to induce high gene expression levels of *MtAMT2;4*. Possibly, the *MtAMT2;4*-mGFP6 fusion can be reassessed with the native promotor in regimes of N depletion. New time-lapse imaging studies could be performed to investigate the life span of arbuscules as well as of *R. irregularis* infection units in *M. truncatula* roots. To that end, the nutrient variation RNA-libraries of mycorrhized roots can be used to detect suitable settings for investigations of further candidate membrane transporter genes.

General Discussion

Furthermore, some constructs were cloned, which are up to know not fully analyzed (S1 Fig, S2 Fig, S1 Table). Those can be used to investigate several aspects of membrane transport during mycorrhiza. For example, the AM-related copper transporter gene *MtCopMd1* can, when expressed in *X. laevis* oocytes, be used to obtain data for a functional analysis of MtCopMd1.

With respect to the time-lapse imaging in rice [66] and first experiments as detailed in chapter II, mycorrhized *in vitro* root cultures that express the generated ER-colocalization markers could be useful to further investigate processes of cellular restructuring in AM symbiosis of *M. truncatula*.

Studies of AM-dependent defensins, presented in chapter III, have revealed a core set of defensins that up to now lacks a full characterization. Members of arbuscule-specific or -unspecific, of early or late activated, defensin genes could be manipulated in *ram1-1* and *pt4-1* mutants to obtain information about their functions. Since MtDefMd1 was shown to regulate the presence of certain members of *EXO70* genes, the role of MtDefMds as cargos or competitive binding partners of specifically addressed vesicles is intriguing. Here, overexpression and co-localization are suitable tools that could be tested with additional MtDefMds. A knockdown of the invested *EXO70* genes could hinder the maturation and transport of MtDefMds and therefore result in a “no MtDefMd phenotype”. Furthermore, co-overexpression of *MtDefMd1* and *EXOCYST* genes, such as *EXO70k* or *EXO70j*, could enhance the impact of the defensin. In this context, an overexpression of *MtDefMd* genes in plants inoculated with a range of haustoria-forming and none haustoria-forming fungal pathogens could further define the biological, possibly antifungal, impact of AM-dependent defensins.

In addition, a transfer to another symbiotic interaction, such as root nodules, could be repeated to provide novel insights, since phenotypes that can easier be interpreted might be achieved. Here, the maturation of bacteria to bacteroids has been well described and several mutants with altered defensin-like NCR-expression were monitored [67]. Compared to arbuscules, the sizes are more homogeneous and fine-structures seem less complex.

Also, an *MtMyb1* overexpression might lead to *MtDefMd1/2* upregulation, as this TF gene is an important switch during the late stages of the symbiosis [51]. A construct leading to *MtMyb1* overexpression could then be combined with the MtDefMd1-GFP fusion. In case the defensin gene is regulated by MtMyb1, on the one hand an induced GFP-overexpression should be detected, and on the other hand, in dependence of the chosen promoter for *MtMyb1* overexpression, the targeting of the translational fusion protein could be matched to that of proteins expressed during infection of root cortical cells, PAM-biogenesis or even to that of non-mycorrhized cells.

GENERAL MATERIALS AND METHODS

Standard Protocols

Isolation of genomic DNA from *M. truncatula*

As a template genomic DNA from *M. truncatula* was isolated with the *DNeasy Plant Kit* for PCR. 200 mg fresh leaf material were used for isolation, following the instructions of the manufacturer. The homogenization was performed with a *FastPrep®-24* for 4 x 30 s with 6.5 m/s.

Preparation of plasmid DNA

Confluent colonized selective agar-plates were used for the isolation of bacterial clones. The preparation was performed with *QIAPrep Spin mini Kit*, following the manufacturer's instructions.

A fast and efficient protocol for low cost isolations of plasmids are HB-lyses, performed by a modified protocol of Becker *et al.* [68]:

1. A bacterial colony (1 cm²) was transferred with a glass pipetting tip into 200 µl HB1-buffer and resuspended via inverting and vortexing.
2. 200 µl HB2-buffer were added and the mixture was inverted four times.
3. 200 µl HB3-buffer were added and the mixture was inverted four times.
4. This was followed by 10 min centrifugation at 14500 rpm.
5. The supernatant was added to 500 µl isopropanol and inverted four times.
6. Consecutively the samples were centrifuged for 20 min at 13000 rpm.
7. The supernatant was removed via pipetting and the pellet washed with 500 µl 70 % (v/v) EtOH.
8. 2 minutes centrifugation at 13000 rpm.
9. The supernatant was removed with a pipette and the pellet was dried at room temperature until the remaining ethanol was vaporized.
10. Finally, the pellet was resuspended in 35 µl Millipore® water.

For the isolation of plasmid DNA from agrobacteria or low copy plasmids, the protocol was altered:

1. 100 ml overnight liquid culture in selective media was centrifuged 5 minutes at 12000 rpm.
2. Consecutively the supernatant was removed, and it was proceeded as indicated before in a 20x upscale reaction volume

3. Finally, the plasmid purification *QIAPrep Spin mini* Kit from *Qiagen* was used according to the manufacturer's instruction. For the elution 50 µl H₂O were used.

Quantification of nucleic acids

The purity and quantity of nucleic acids was monitored via *Nanodrop* measurements. The absorbance at 260 nm, 230 nm and 280 nm were monitored. Nucleic acids have their maximum of absorbance at 260 nm. Therefore, measurements of this part of the spectrum can be used to estimate their concentration. Ratios of 260/280 nm and 260/230 nm indicate whether or not the samples contain proteins or phenolic compounds. For each measurement, a volume of 1 µl was used. Blank measurements were performed with elution buffer.

Agarose gel-electrophoresis

Genomic DNA, plasmid DNA, PCR-fragments and restriction reactions were controlled via agarose gel-electrophoresis:

1. 1 or 1.5 % agarose was poured in the electrophoresis chamber and a ridge was added.
2. TA-buffer was added after the solidification of the gel and the ridge was removed.
3. A droplet of brom-phenolic-blue was added to the samples.
4. The voltage was set to 100 V.
5. Electrophoresis took place for ~25 min.
6. The gel was stained for ~2.5 min with ethidium-bromide in a staining solution (0.04 µL/mL in water) and afterwards destained for ~2 min.
7. A Transilluminator with UV-light was used for documentation.
8. DNA-ladders were added to the gel.

Polymerase Chain Reaction (PCR)

Standard PCRs

Phusion HOT START II® *High-Fidelity* DNA polymerase was used for regular PCRs. The reaction and program for PCR are listed in Table 1 and Table 2, respectively.

Table 1: Standard PCR reaction.

compound	volume [µl]	final concentration
Polymerase-Puffer hf (5 x)	10 µl	1 x
dNTP-Mix (10 mM)	1 µl	0.2 mM
Primer (h) (100 mM) ²	0.25 µl	0.5 mM
Primer (r) (100 mM) ²	0.25 µl	0.5 mM
Template DNA ¹ (~145 ng/µl)	1 µl	145 ng
Phusion Hot Start II-Polymerase (5 u/µl)	0.5 µl	2.5 u

¹ *M. truncatula* cv. Jemalong A17

²siehe Table 2

The volume of the reaction was filled to 20 µl with H₂O.

Table 2: Standard PCR program.

step	temperature [°C]	time	cycles
initial denaturation	98	2min	1
denaturation	98	20 s	30
Primer-annealing	65	30 s	
elongation	72	1 min	
final elongation	72	10 min	1
cooling down	4	∞	1

The samples were stored at -20 °C.

Extraction of DNA-fragments from agarose gels

The *Nucleospin II-Kit* of Macherey-Nagel was used for the extraction of DNA. Therefore, they were purified from agarose gels.

Sequencing and sequence analysis

For sequencing, 14 µl reactions with a DNA amounts of 1000 ng were prepared. The missing volume was substituted by Millipore-*Water*[®]. To each reaction 1 µl sequencing primer (20 µM) was added. Sequencing reactions were performed by *Seqlab*. The software *CLC DNA Workbench* was used for the evaluation.

Cloning

Cloning techniques, as detailed in the following sections, based on the protocols of Sambrook *et al.* [67].

Restriction digestions

The final volume was 20 µl, containing 2 µl 10 x restriction buffer and 1 µl restriction enzyme. The DNA amount was estimated after gel-electrophoresis. The reaction was performed for 2.5 h or overnight at 37°C.

Filling of 5'-overhangs with the Klenow-polymerase

The *Klenow*-Polymerase, a Fragment of a DNA-Polymerase, was used to fill up 5'-overhangs after restriction reactions.

1. In a 20 µl reaction were pipetted:
 - 15 µl cleaved DNA
 - 2 µl 10 x Klenow- buffer

- 2 µl dNTP-Mix (10 mM/nucleotide)
 - 1 µl Klenow-Polymerase (1 U/µl)
2. The samples were incubated for 15 min at 37°C.
 3. 1 µl 200 mM EDTA with pH 8.0 were added.
 4. The Klenow-fragment was deactivated via an incubation for 10 min at 75°.
 5. Finally, the *Nucleospin II PCR/gel clean* Kit was used for purification.

Purification of DNA-fragments

The purification of DNA-fragments was done with the *Nucleospin II PCR/ gel purification Kit* according to manufacturer's instructions.

Dephosphorylation

To hinder the religation of empty vectors, 5'- phosphate residue was removed. In 20 µL reaction volume 2 µl 10x SAP-Puffer, 1 µL SAP-Phosphatase and 1-17 µL cleaved plasmid were incubated for 15 min at 37 °C. Finally, the phosphatase was deactivated at 70 °C for 15 min.

Ligation of DNA-fragments

1. Cleaved vector-DNA and insert were mixed in a≈1:3-ratio (in a 1.5 ml reaction vessel).
2. 1-3 µl T4-DNA-Ligase were added (for *sticky ends* 1 µl; for *blunt ends* 3 µl).
3. Consecutively 2 µl ligase buffer were added.
The volume was filled up to 20 µl with sterile Millipore® water. The sample was inverted, shortly centrifuged and incubated in a ligation vessel overnight at 8°C.

Transformation and cultivation of bacteria

Generation of heat-shock competent *E. coli*-cells

E. coli cells can be enabled with a rubidium-chloride treatment to incorporate DNA during a heat shock. To create these competent cells, 10 µl of *E. coli* DH5 α mcr' glycerol-culture were used to start a 10 ml LB liquid culture, rotating at 37°C over night. Five 200 ml liquid LB-medium were inoculated with 2 ml of the starter culture. As soon as an OD₆₀₀ of 0.6-0.8 was reached, the medium was aliquoted in 50 ml Falcon tubes and centrifuged 15 min with 4000 rpm at 4°C. The pellet of bacterial cells was resuspended in 30 ml Tbf1 buffer. Consecutively the centrifugation was repeated. The pellet was then resuspended in 2ml Tbf2 buffer. 100 µl aliquots were frozen immediately in liquid nitrogen and later stored at -80°C.

Transformation of *E. coli* via heat-shock

To transform *E. coli* cells via heat shock the following protocol was used:

General Material and Methods

1. An aliquot of competent cells thaw on ice water.
2. 100 µl competent cells, 50 µl TCM buffer and 10 µl recombinant DNA were pipetted together and incubated on ice for 30 min.
3. This was followed by a heat shock of 1:15 min at 42 °C.
4. The cells were incubated for 5 min on ice.
5. Finally, the transformed cells were incubated for 1 h at 37°C and streaked out on selective agar plates (100 µl, 200 µl and the bacterial pellet) for incubation at 37 °C over night.

Transformation of *A. rhizogenes* via electroporation

To transform *A. rhizogenes* cells the following protocol was used:

1. One aliquot of competent cells thaw on ice water, meanwhile the cuvette for electroporation was cooled on ice.
2. 3 µl DNA were pipetted to 100 µl competent cells.
3. The assay was transferred into the cooled cuvette.
4. Remaining water on the surface of the cuvette was removed with tissue, the cuvette was transferred into the electroporator and an electric impulse of 1200 V was induced.
5. The cells were immediately resuspended with 1 ml TY medium in the cuvette. Consecutively they were transferred in a new 1.5 ml reaction vessel.
6. Finally, the transformed cells were incubated for 2 h at 30°C and streaked out on selective agar plates (100 µl, 200 µl and the bacterial pellet) for incubation at 30 °C over night.

Oligonucleotides

Oligonucleotides for PCR-, RT-PCR and sequencing reactions were synthesized by *Sigma Aldrich* (Munich, Germany).

Media for the cultivation of microbes, antibiotics and additives

Culture media

All cultivation media were dissolved in *Millipore*[®] water and autoclaved. Antibiotic were added via sterile filtration as soon as the media cooled down to approximately 50°C. Recipes are detailed in the following:

LB-Medium [67]

- 1 % (w/v) tryptone
- 0.5 % (w/v) yeast extract
- 0.5 % (w/v) NaCl

The buffer was adjusted to pH 7.4

TY-Medium [70]

- 0.5 % (w/v) tryptone
- 0.3 % (w/v) yeast extract
- 0.07 % (w/v) CaCl₂ x 2H₂O

The buffer was adjusted to pH 7.4

PA-Medium

- 1.75 % (w/v) Antibiotic Medium No. 3/ Penassay Broth (PA)

15 g/l agar agar were added in addition to the components listed below to brew solid media.

Antibiotics and additives

Antibiotics were dissolved in ultrapure Millipore®-water (Table 3) and sterilized via microfiltration. Stock solutions were stored at -20°C until being added to autoclaved media.

Table 3: Antibiotics for the selective cultivation of bacteria strains.

antibiotic	stock solution	final concentration in medium
Ampicillin (Ap)	100 mg/mL	100 µg/mL
Kanamycin (Km)	50 mg/mL	50 µg/mL
Spectomycin (Spec)	100 mg/mL	100 µg/mL
Streptomycin (Sm)	300 µg/mL	600 mg/ml

For the cultivation of agrobacteria, the concentration of kanamycin was raised to 100 mg/ml.

For blue-white-screening were added:

- X-Gal: resolve 20 mg in 1 mL N,N-Dimethylformamide, protected from light
- IPTG: sterile filtration of 25 mg resolved in 1 mL Aqua ultra-filtrated

Per plate IPTG and X-Gal were mixed and plated.

Buffers and solutions

Buffer and solutions for gel-electrophoresis

1 x TA-buffer

- 40 mM Tris-HCl
- 10 mM sodium-acetate
- 1 mM EDTA

Adjust pH with acetic acid to 7.8

Bromide-phenolic-blue/ glycerol-solution

- 80 mL glycerol 87 %
- 10 mL 1x TA-buffer
- 2.5 g bromide-phenolic-blue

1/1.5/2 % Agarose

- 1/1.5/2 % (w/v) agarose was added to TA-buffer, cooked, resolved and stored at 60°C.

Ethidium-bromide-solution for staining

- 0.04 µL/mL Ethidium-bromide-solution in water (neutral pH)

Buffers for the cultivation of competent bacteria

Tbf1-buffer

- 100 mM RbCl
- 10 mM MES
- 10 mM CaCl₂ x 2 H₂O
- 50 mM MnCl x 3 H₂O

The MnCl₂ -solution was composed separately, autoclaved and added as final step.
The pH was adjusted to 6.

Tbf2-buffer 10 mM MOPS

- 75 mM CaCl₂ x 2 H₂O
- 10 mM RbCl
- 50 mM glycerol (87 %)

pH was adjusted to 6.5

Buffer for bacterial suspensions

The PS-buffer is a buffer with physiological concentrations of ions that can be used to resuspended bacterial cells.

PS-buffer

- 0.7 % (w/v) Na₂ HPO₄ x 2H₂O
- 0.5 % (w/v) NaCl
- 0.3 % (w/v) KH₂ PO₄

Adjust pH to 7, using HCl

Buffers for HB-Lyses

The buffers for HB-lysis were modified from Becker *et al.* [68].

HB1-buffer

- 50 mM Tris-HCl
- 10 mM EDTA

Adjust pH to 8, using HCl

HB2-buffer

- 200 mM NaOH
- 1 % (w/v) SDS

HB3-buffer

- 2.55 M potassium--acetate

Adjust pH to 4.8, using acetic acid

Buffers for enzymatic reactions

10 x TA-buffer

- 660 mM potassium-acetate
- 330 mM Tris HCl
- 100 mM MgCl₂
- 5 mM DTT
- 1 mg/mL BSA

Adjust pH to 7.5 with acetic acid

RNaseA-Solution

- 10 mg/mL RNaseA
- 10 mM Tris-HCl
- 15 mM NaCl

TCM-buffer

- 10 mM CaCl₂
- 10 mM MgCl₂
- 10 mM Tris HCl

Adjust pH to 7.5

Buffer and solutions for histochemical analyses

Buffer and Solutions for GUS-staining

Tris-HCl/NaCl-buffer

- 100 mM Tris HCl
- 50 mM NaCl

Adjust pH to 7.0, using HCl

K-Ferri-/Ferrocyanide-storage solution

- 100 mM K-Ferricyanid
- 100 mM K-Ferrocyanid

Storage at -20 °C.

X-Gluc-storage solution

- 25 mg X-Gluc (5-Brom-4-Chloro-3-Indolyl/beta-D-Glucoside) was resolved in 500 µL N,N-Dimethyl-formamide.

GUS-staining buffer

The GUS-buffer was composed in accordance to the protocol of Beckmann and Engler [71]:

- 960 µL Tris-HCl/NaCl
- 20 µL K-Ferri-/Ferrocyanid storage solution
- 20 µL X-Gluc storage solution

Buffer and Solutions for WGA-Alexa Fluor 488-stainings

10x PBS-buffer

- 1,4 M NaCl
- 27mM KCl
- 10mM Na₂HPO 4 x 2 H 2 O
- 18 mM KH₂PO 4

Adjust pH to 7.3

WGA-Alexa Fluor 488 stock solution: 1 mg/mL *WGA-Alexa Fluor 488* was resolved in Millipore-water®.

For staining the solution was diluted to 20 µg/ml *WGA-Alexa Fluor 488* in 1x PBS-buffer.

Buffer and Solutions for Ink staining

Ink staining buffer

- 10 % (v/v) KOH
- Staining solution: 5 % (v/v) black ink
- 8 % (v/v) acetic acid
- Destaining solution: 0,8 % (v/v) acetic acid

Enzymes and Buffers

Table 4: Enzymes and buffers for cloning and PCR used in this thesis.

enzyme/buffer	company
10x <i>Klenow</i> fragment buffer	Fermentas, St. Leon-Rot, Germany
10x shrimp alkaline phosphatase buffer	Fermentas, St. Leon-Rot, Germany
10x T4-DNA ligase buffer	Fermentas, St. Leon-Rot, Germany
5x first strand buffer	Invitrogen, Karlsruhe, Germany
5x Phusion DNA polymerase buffer hf	Finnzymes, Vantaa, France
<i>Klenow</i> fragment (10 U/μL)	Fermentas, St. Leon-Rot, Germany
<i>Klenow</i> -Fragment (10 U/μl)	Thermo Fisher Scientific, Waltham, Massachusetts, USA
Phire Hot-Start Polymerase	Thermo Fisher Scientific, Waltham, Massachusetts, USA
Phusion HF Polymerase	Thermo Fisher Scientific, Waltham, Massachusetts, USA
Phusion HOTstart DNA Polymerase II (0.5 U/ μL)	Finnzymes, Vantaa, France
restriction enzymes	Thermo Fisher Scientific, Waltham, Massachusetts, USA
RNAse A	Serva, Heidelberg, Germany
RNAse A	SERVA Electrophoresis, Heidelberg, Germany
Sall	Thermo Fisher Scientific, Waltham, Massachusetts, USA
shrimp alkaline phosphatase (1 U/μL)	Fermentas, St. Leon-Rot, Germany
Shrimp Alkaline Phosphatase (1 U/μl)	Invitrogen, Carlsbad, California, USA (Thermo Fisher Scientific, Waltham, Massachusetts, USA)
SuperScript RT III	Invitrogen, Karlsruhe, Germany
T4-DNA ligase (1 U/μL)	Fermentas, St. Leon-Rot, Germany
T4-Ligase (1 U/μl)	Thermo Fisher Scientific, Waltham, Massachusetts, USA

Kits

Table 5: Commercial kits used in this thesis.

kit	company
NucleoSpin® Extract II Kit	Macherey-Nagel, Düren, Germany
QIAprep® Spin Miniprep Kit	Qiagen, Hilden, Germany
RNeasy® Plant Mini Kit	Qiagen, Hilden, Germany
SensiFAST™ SYBR No-ROX One-Step Kit	Bioline, Luckenwalde, Germany
RNAse free DNase Set	Qiagen, Hilden, Germany
RNAse free DNase Set	Thermo Fisher Scientific, Waltham, Massachusetts, USA
Superscript RT III Kit	Invitrogen, Karlsruhe, Germany
DNaseI	Fermentas, St. Leon-Rot, Germany
DNaseI	Qiagen, Hilden, Germany
DNeasy Plant Mini Kit	Qiagen, Hilden, Germany
Nucleospin II	Qiagen, Hilden, Germany
Matchmaker® Gold yeast Two-Hybrid System	Clontech Laboratories, Inc. A Takara Bio Company, Mountain View, USA

Chemicals

Table 6: Chemicals used in this thesis.

Chemical substance	company
2-(N-Morpholino)ethansulfonsäure (MES)	SERVA Electrophoresis, Heidelberg, Germany
3-Morpholinopropane-1-sulfonic acid (MOPS)	AppliChem, Darmstadt, Germany
acetic acid	Roth, Karlsruhe, Germany
agar-agar	Invitrogen, Karlsruhe, Germany
Agarose PeqGold	Peqlab, Erlangen, Germany
Antibiotic Medium No. 3	Oxoid, Wesel, Germany
brome-phenolic-blue	Merck, Darmstadt, Germany
BSA (bovine serumalbumin)	Serva, Heidelberg, Germany
Ca(NO ₃) ₂ x4H ₂ O	Roth, Karlsruhe, Germany
CaCl ₂ x2H ₂ O	Merck, Darmstadt, Germany
CoCl ₂ x6H ₂ O	Sigma Aldrich, München, Germany
CuSO ₄ x5H ₂ O	Sigma Aldrich, München, Germany
DEPC-treated H ₂ O	Roth, Karlsruhe, Germany
dNTP's	Fermentas, St. Leon-Rot, Germany
DTT	Sigma Aldrich, München, Germany
EDTA (Titriplex)	Merck, Darmstadt, Germany
ethanole	Merck, Darmstadt, Germany
ethidium-bromide	Roth, Karlsruhe, Germany
GeneRuler/Marker (50 bp, 100 bp and 1 kb)	Thermo Fisher Scientific, Waltham, Massachusetts, USA
glycerine	AppliChem, Darmstadt, Germany
H ₂ SO ₄	Roth, Karlsruhe, Germany
H ₃ BO ₃	Sigma Aldrich, München, Germany
HCl	Roth, Karlsruhe, Germany
ink	Sheaffer, Shelton, Connecticut, USA
IPTG	Roth, Karlsruhe, Germany
isopropanole	Roth, Karlsruhe, Germany
K ₂ HPO ₄	Merck, Darmstadt, Germany
KCl	Merck, Darmstadt, Germany
K-Ferricyanide	Sigma Aldrich, München, Germany
K-Ferrocyanide	Sigma Aldrich, München, Germany
KH ₂ PO ₄	Merck, Darmstadt, Germany
KNO ₃	Sigma Aldrich, München, Germany
KOH	Roth, Karlsruhe, Germany
MgCl ₂ x6H ₂ O	Merck, Darmstadt, Germany
MgSO ₄ x7H ₂ O	Merck, Darmstadt, Germany
MnCl ₂ x2H ₂ O	Merck, Darmstadt, Germany
MnSO ₄ x1H ₂ O	Sigma, Taufkirchen, Germany
MOPS	AppliChem, Darmstadt, Germany
N,N-Dimethylformamide	Merck, Darmstadt, Germany
N ₂ (liquid nitrogen)	Linde, Pullach, Germany
Na ₂ HPO ₄ x2H ₂ O	Merck, Darmstadt, Germany
Na ₂ MoO ₄ x2H ₂ O	Sigma Aldrich, München, Germany
NaCl	Sigma Aldrich, München, Germany
NaClO	Carl Roth, Karlsruhe, Germany
NaFe EDTA	Sigma Aldrich, München, Germany
NaO-Ac (Natriumacetat)	Merck, Darmstadt, Germany
NaOCl	Roth, Karlsruhe, Germany
NaOH	Merck, Darmstadt, Germany
NiCl ₂ x6H ₂ O	Roth, Karlsruhe, Germany

General Material and Methods

Phytoagar	Duchefa, Haarlem, NL
Chemical substance	company
Polyethyleneglycole (PEG)	SERVA Electrophoresis, Heidelberg, Germany
potassium-acetate	Merck, Darmstadt, Germany
RbCl	Merck, Darmstadt, Germany
SDS	Serva, Heidelberg, Germany
β-mercaptoethanole	Sigma Aldrich, München, D
Tris	MP Biomedicals, Santa Ana, USA
tryptone	Oxoid, Wesel, Germany
Tween20	Merck, Darmstadt, Germany
WGA-Alexa Fluor 488	Invitrogen, Carlsbad, Kalifornien, USA
X-Gal	Roth, Karlsruhe, Germany
X-Gluc	Duchefa, Haarlem, Netherlands
yeast extract	Oxoid, Wesel, Germany
ZnSO ₄ ·7H ₂ O	Merck, Darmstadt, Germany

Desposables

Table 7: Desposables used in this thesis.

desposables	company
1.5 ml reaction vessels	Sarstedt, Nümbrecht, Germany
1.5 mL reaction vessels (RNase-free)	Carl Roth, Karlsruhe, Germany
1.5/2 ml-Reaktionsgefäß (safe lock)	Eppendorf, Hamburg, Germany
13 mL-Reaktionsgefäß	Greiner, Kremsmünster, Austria
96 plates for real-time PCR	Biozym, Hess. Oldendorf, Germany
centrifuge vessels (15/50 ml)	Greiner, Kremsmünster, Austria
cover lids	Roth, Karlsruhe, Germany
cuvettes	Sarstedt, Nümbrecht, Germany
cuvettes for electroporation	Peqlab, Erlangen, Germany
FastPrep-Tubes	MP Biomedicals, Santa Ana, Canada
filter	Sarstedt, Nümbrecht, Germany
filter paper	Whatman, Dassel, Germany
glas pipettes	Brand, Wertheim/Main, Germany
glas vessels	Schott, Mainz, Germany
gloves	Ansell, München, Germany
Lysing Matrix D	MP Biomedicals, USA
nitril gloves	Ansell, Richmond, Australia
nitril gloves	StarLab, Hamburg, Germany
object slides	Roth, Karlsruhe, Germany
optical cover folia for Real-time PCR	Biozym, Hess. Oldendorf, Germany
Parafilm	Bemis NA, Neenah, Wisconsin, USA
<i>Pasteur</i> pipettes	Brand, Wertheim/Main, Germany
PCR-tubes	Sarstedt, Nümbrecht, Germany
petri-dish (12 x 12 cm)	Novodirekt, Kehl, Germany
petri-dish (9 cm)	Greiner, Kremsmünster, Austria
pipetting tips (10, 100, 1000 µl)	Eppendorf, Sarstedt, Germany
pipetting tips with filter (10, 100, 1250 µl)	Biozym, Hess. Oldendorf, Germany
pipetting tips with filter (10, 100, 1250 µl)	StarLab, Hamburg, Germany
PP-tubes (13,15, 50 ml)	Greiner bio-one, Frickenhausen, Germany
Razor blades	ScienceServices, München, Germany
RNAse-free reaction vesselss (1.5 ml)	Roth, Karlsruhe, Germany
scalpel	B. Braun, Melsungen, Germany
Seramis	Seramis, Mogendorf, Germany
serologic single use pipetting tips (10 ml)	Roth, Karlsruhe, Germany

General Material and Methods

single use syringe(5 ml)	Sigma Aldrich, München, Germany
desposables	company
syringe	BD Medical, Franklin Lakes, New Jersey, USA
wipes	Kimberley-Clark, Koblenz, Germany

Technical devices

Table 8: Technical devices used in this thesis.

device	company
Autoclave <i>WX150</i>	Systec, Wetztenberg, Germany
Cleanbench <i>HERASafe K518</i>	Thermo, Langenselbold, Germany
climate cupboard <i>KPS 1700</i>	Weisshaar, Bad Salzuflen, Germany
Confocal laser microscope <i>TCS SP8 MP</i>	Leica, Sohns, Germany
Cooling centrifuge <i>5810 R with the rotors H1030 and A-4-62</i>	Eppendorf, Hamburg, Germany
Device for homogenizing tissues <i>FastPrep®-24</i>	MP Biomedicals, Santa Ana, Canada
Digital camera <i>XC50</i>	Olympus, Tokyo, Japan
electroporator <i>Cellject Uno</i>	Thermo, Langenselbold, Germany
fluorescence-binocular <i>EL6000</i>	Leica, Sohns, Germany
fluorescence-mikroskope <i>Axio observer.Z1</i>	Carl Zeiss, Oberkochen/Jena, Germany
gel documentation station <i>UV Solo</i>	Biometra, Göttingen, Germany
Heating block <i>Thriller</i>	Peqlab, Erlangen, Germany
Hitzeschrank/Sterilisator <i>T 6420</i>	Thermo, Langenselbold, Germany
incubation cupboard <i>B6</i>	Thermo, Langenselbold, Germany
millipore-pump <i>Arium®611 UV</i>	Sartorius, Göttingen, Germany
<i>Nanodrop 2000</i>	Thermo, Langenselbold, Germany
on table centrifuge <i>5424</i>	Eppendorf, Sarstedt, Germany
PCRmaschine <i>Mastercycler pro S</i>	Eppendorf, Hamburg, Germany
pH-meter <i>Basic Meter PB-11</i>	Sartorius, Göttingen, Germany
pH-meter <i>pH 7110</i>	Inolab, Mexico City, Mexico
Photometer <i>BioPhotometer plus</i>	Eppendorf, Hamburg, Germany
Plant cultivation chamber <i>JC-ESC 300</i>	Johnson Controls, Milwaukee, Wisconsin, USA
Real-time PCR-machine <i>Mastercycler realplex²</i>	Eppendorf, Hamburg, Germany
Shaker device <i>Certomat® IS</i>	Sartorius, Göttingen, Germany
Shaker device <i>Gyrotory G2</i>	New Brunswick Scientific, Edison, New Jersey, USA
Transilluminator	Biometra, Göttingen, Germany
Vibratome <i>VT1000S</i>	Leica, Sohns, Germany
Vortex <i>M53 basic</i>	IKA, Staufen, Germany
water bath <i>1002, 1003</i>	GFL, Burgwedel, Germany
Weightingmaschine <i>Extend</i>	Sartorius, Göttingen, Germany
Nanoliter Injector	World precision Instruments, Berlin, Germany
voltage-clamp amplifier <i>Turbo TEC-10 CD</i>	npi electronic, Tamm, Germany
ICP-OES Spektro <i>Flame Modula</i> with axial plasma window	SPECTRO Analytical Instruments GmbH, Kleve, Germany
CNS-analyzer <i>Vario EL III</i>	Elementar Analysensysteme GmbH, Langenselbold, Germany

Software and internet tools

Table 9: Software used in this thesis.

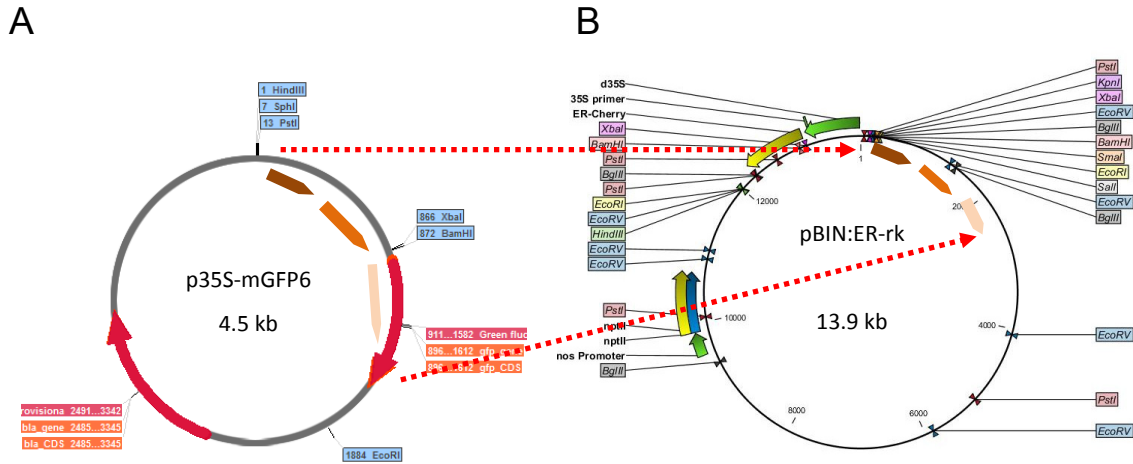
Name	Provider
Citavi 5.4.0.2	Swiss Academic Software, 2001-2016
CLC Main Workbench 7.0.3	CLC bio (QIAGEN), 2008-2013
Fiji (ImageJ 1.51r)	Wayne Rasband, National Institutes of Health, USA
Microsoft Office 2010/2016	Microsoft, 2016
Nanodrop 2000	Thermo Fisher Scientific, 2009-2014
Realplex 2.2	Eppendorf, 2005-2008, Sarstedt, Germany
PerlPrimer v1.1.20 Copyright © 2003-2011	Owen Marshall
SerialCloner (Version 2.5)	Frank Perez SerialBasics
Pulse/PulseFit	HEKA, Lambrecht/Pfalz, Germany

Table 10: Internet tools used in this thesis.

tool	website
InterProScan Signature Recognition Search Against the Integrated Resource of Protein Domains and Functional Sites EBI	http://www.ebi.ac.uk/Tools/pfa/iprscan/
Medicago truncatula Hapmap Projekt	http://www.medicagohapmap.org/tools/blastform
National Center for Biotechnology Information	http://www.ncbi.nlm.nih.gov/
Medicago truncatula Gene Expression Atlas V3	https://mtgea.noble.org/v3/
Medicago truncatula Genome Database v4.0	http://www.medicagogenome.org/

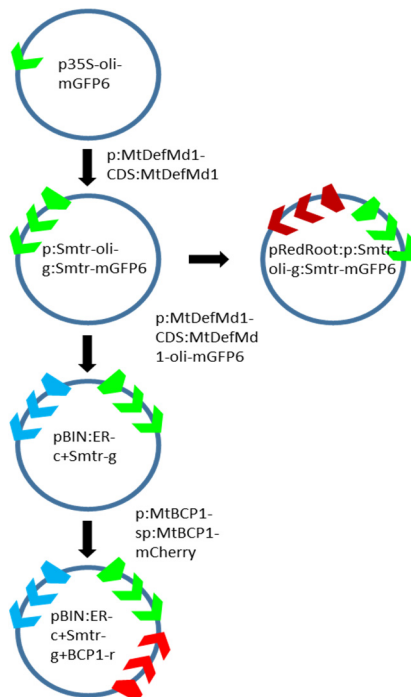
APPENDIX

Plasmid maps



S1 Fig: The vectors p35S-mGFP6neu and pBIN:ER-rk.

The vector *p35S-mGFP6neu* (A) encodes mGFP6 preceded by an oligopeptide-linker integrated in between the *Xba*I and *Bam*HI restriction sites [72]. This linker contains *Kpn*I and *Bgl*III restriction sites. Variants of the vector were used to purify promoter (native or 35S, brown coloured arrow) and CDS of a transporter fused to mGFP (light brown and beige colored arrows). The fusion was then transferred into a vector that contains a cell organelle marker (red dotted arrows). The plasmid pBIN:ER-rk (B) [73] can be used for the DNA transfer via agrobacteria into the plant. It contains typical LB and RB border sequences. The sequence in between the borders will be cleaved out and transferred to the nucleus of the plant to be permanently integrated into the genome. In addition to the insert, the vector has a constitutively expressed ER-targeted mCherry [73].



S2 Fig: Cloning strategy of vectors for the localization and co localization of MtDefMd1.

The green GFP cassette, blue CFP cassette, red mCherry cassette, and far red dsRed cassette are shown. Abbreviations: p, promoter; sp, signal peptide; CDS, codon determining sequence.

Supplemental Tables

S1 Table: Bacterial and yeast clones.

ID	Organism	resistance	Size [kb]	Description
pk18	<i>E. coli</i> DH10B	Kan50	2.6	Cloning vector, contains a <i>lacZ</i> gene [74]
pGUS-INT	<i>E. coli</i> DH5 α mcr'	Amp100	5.4	Cloning vector, contains a <i>gusAint</i> gene [75]
pRedRoot	<i>E. coli</i> DH5 α mcr'	Kan50	13.5	Cloning vector, binary plasmid, contains a dsRed cassette controlled by the ubiquitin promoter [76]
pk7GWIWG2-dsRed	<i>A. rhizogenes</i> ARqua1	Strep600/Spec100	15.3	RNAi cloning vector, contains a dsRed cassette and 2 x attR sites under control of the ubiquitin promoter [77]
pk18:p:Oligptr.4863#2	<i>E. coli</i> DH5 α mcr'	Kan50	4.5	pk18-derivate, promoter (-1 to -1939) of <i>MtOliMd1</i> cloned via <i>SphI</i> and <i>XmaI</i>
pk18:p:Coptr.37110#7	<i>E. coli</i> DH5 α mcr'	Kan50	3.9	pk18-derivate, promoter (-2 to -1276) of <i>MtCopMd1</i> cloned via <i>EcoRI</i> and <i>HindIII</i>
pk18:p:ABCtr.52071#3	<i>E. coli</i> DH5 α mcr'	Kan50	4.1	pk18-derivate, promoter (-1 to -1510) of <i>MtABCG3</i> cloned via <i>EcoRI</i> and <i>HindIII</i>
pGUS-INT:p:Oligptr.4863#7	<i>E. coli</i> DH5 α mcr'	Amp100	4.5	pGUSINT-derivate, promoter (-1 to -1939) of <i>MtOliMd1</i> cloned via <i>SphI</i> and <i>XmaI</i>
pGUS-INT:p:Coptr.37110#1	<i>E. coli</i> DH5 α mcr'	Amp100	3.9	pGUSINT-derivate, promoter (-2 to -1276) of <i>MtCopMd1</i> cloned via <i>EcoRI</i> and <i>HindIII</i>
pGUS-INT:p:ABCtr.52071#5	<i>E. coli</i> DH5 α mcr'	Amp100	4.1	pGUSINT-derivate, promoter (-1 to -1510) of <i>MtABCG3</i> cloned via <i>EcoRI</i> and <i>HindIII</i>
pRedRoot:p:Oligptr.4863#2	<i>E. coli</i> DH5 α mcr	Kan50	15.5	pRedRoot-derivate, cloned via <i>SpeI</i> and <i>Klenow</i> blunting into <i>SmaI</i> -site, promoter (-1 to -1939) of <i>MtOliMd1</i> upstream of the <i>gusAint</i> -gene
pRedRoot:p:Coptr.37110#7	<i>E. coli</i> DH5 α mcr	Kan50	14.9	pRedRoot-derivate, cloned via <i>SpeI</i> and <i>Klenow</i> blunting into <i>SmaI</i> -site, promoter (-2 to -1276) of <i>MtCopMd1</i> upstream of the <i>gusAint</i> -gene
pRedRoot:p:ABCtr.52071#3	<i>E. coli</i> DH5 α mcr	Kan50	15	pRedRoot-derivate, cloned via <i>SpeI</i> and <i>Klenow</i> blunting into <i>SmaI</i> -site, promoter (-1 to -1510) of <i>MtABCG3</i> upstream of the <i>gusAint</i> -gene
pRedRoot:p:Oligptr.4863#2	<i>A. rhizogenes</i> Arqua1	Strep600/Kan100	15.5	pRedRoot-derivate, cloned via <i>SpeI</i> and <i>Klenow</i> blunting into <i>SmaI</i> -site, promoter (-1 to -1939) of <i>MtOliMd1</i> upstream of the <i>gusAint</i> -gene
pRedRoot:p:Coptr.37110#7	<i>A. rhizogenes</i> Arqua1	Strep600/Kan 100	14.9	pRedRoot-derivate, cloned via <i>SpeI</i> and <i>Klenow</i> blunting into <i>SmaI</i> -site, promoter (-2 to -1276) of <i>MtCopMd1</i> upstream of the <i>gusAint</i> -gene
pRedRoot:p:ABCtr.52071#3	<i>A. rhizogenes</i> Arqua1	Strep600/Kan 100	15	pRedRoot-derivate, cloned via <i>SpeI</i> and <i>Klenow</i> blunting into <i>SmaI</i> -site, promoter (-1 to -1510) of <i>MtABCG3</i> upstream of the <i>gusAint</i> -gene
pk7GWIWG2:gus	<i>A. rhizogenes</i> ARqua1	Spec100/Strep600	13.1	pk7GWIWG2-derivate, contains two attB-site flanked 263 bp exon sequences of the <i>gusAint</i> gene (+920 to +1188) as RNAi-cassette
pk7GW:RNAi 35854	<i>A. rhizogenes</i> Arqua1	Spec100/Strep600	14	pk7GWIWG2-derivate, contains two attB-site flanked 357 bp exon sequences of <i>MtDefMd1</i> (+2 to +359) as RNAi-cassette
pk7GW:RNAi 4243	<i>E. coli</i> DH10B	Spec100/Kan50	13.8	pk7GWIWG2-derivate, contains two attB-site flanked 276 bp exon sequences of <i>MtAMT2;4</i> (+599 to +876) as RNAi-cassette
pGolm813 leer	<i>A. rhizogenes</i> ARqua1	Strep600/Spec50	12.61	=813p9RFP-D35s-Expr, plasmid containing 2x35S promoter and a dsRed-cassette [76]
pGolm:2x35S:amiRNA:Oligptr.4863	<i>E. coli</i> DH5 α mcr'	Kan50	12.8	813p9RFP-D35S-Expr-derivate, amiRNA-construct, targeting <i>MtOliMd1</i> , 2x35S-promoter, cloned via <i>SpeI</i> + <i>MluI</i> , contains 2 mismatches in the strand that is less often incorporated into the RISC-complex

ID	Organism	resistance	Size [kb]	Description
pGolm:2x35S:amiRNA:ABC tr.52071	<i>E. coli</i> DH5α mcr'	Kan50	12.8	813p9RFP-D35S-Expr-derivate, amiRNA-construct, targeting <i>MtABCG3</i> , 2x35S-promoter, cloned via <i>SpeI</i> + <i>MluI</i> , contains 2 mismatches in the strand that is less often incorporated into the RISC-complex
pGolm:2x35S:amiRNA:Olig ptr.4863	<i>A. rhizogenes</i> Arqua1	Strep600/Kan100	12.8	813p9RFP-D35S-Expr-derivate, amiRNA-construct, targeting <i>MtOliMd1</i> , 2x35S-promoter, cloned via <i>SpeI</i> + <i>MluI</i> , contains 2 mismatches in the strand that is less often incorporated into the RISC-complex
pGolm:2x35S:amiRNA:ABC tr.52071	<i>A. rhizogenes</i> Arqua1	Strep 600/Kan100	12.8	813p9RFP-D35S-Expr-derivate, amiRNA-construct, targeting <i>MtABCG3</i> , 2x35S-promoter, cloned via <i>SpeI</i> + <i>MluI</i> , contains 2 mismatches in the strand that is less often incorporated into the RISC-complex
pGolmUbi:G US	<i>A. rhizogenes</i> ARqua1	Strep600/S pec100	14.7	917p9RFP-ubi3-Expr-derivate, control plasmid for overexpression, contains ~2.1 kb <i>gusAint</i> , cleaved out of the vector pGUSINT via <i>SacI</i> and <i>SmaI</i> , blunted with Klenow and inserted at <i>SmaI</i> site
pGolmPT4	<i>A. rhizogenes</i> ARqua1	Strep600/S pec100	12.7	= 315p9RFP-Pt4-Expr, plasmid used for gene overexpression
pGolm:pt4:S mtr.35854#3	<i>E. coli</i> DH5 alpha mcr'	Strep 150/Spec 50	12.6	315p9RFP-D35s-Expr-derivate, contains CDS of <i>MtDefMd1</i> (656 bp) fused to dsRed controlled by MtPt4 promoter, dsRed-cassette
pGolm:ubi:S mtr.35854#4	<i>E. coli</i> DH5 alpha mcr'	Strep 150/Spec 50	12.6	315p9RFP-D35s-Expr-derivate, contains CDS of <i>MtDefMd1</i> (656 bp) fused to dsRed controlled by ubiquitin promoter, dsRed-cassette
pGolm:pt4:S mtr.35854#1	<i>A. rhizogenes</i> Arqua1	Strep600/Spec 100	12.6	315p9RFP-D35s-Expr-derivate, contains CDS of <i>MtDefMd1</i> (656 bp) fused to dsRed controlled by MtPt4 promoter, dsRed-cassette
pGolm:ubi:S mtr.35854#1	<i>A. rhizogenes</i> Arqua1	Strep600/Spec 100	12.6	315p9RFP-D35s-Expr-derivate, contains CDS of <i>MtDefMd1</i> (656 bp) fused to dsRed controlled by ubiquitin promoter, dsRed-cassette
pGEM-HE#1	<i>E. coli</i> DH5α mcr'	Amp100	3	cloning vector for the heterologous expression in <i>X. laevis</i> oocytes, contains 3' and 5' UTRs for artificial mRNAs, coding for ampicillin resistance, T7-promoter and m13 primer binding sites
pGEM-HE:Copr.371 10#12	<i>E. coli</i> DH5α mcr	Amp100	4.4	pGEM-HE#1-derivate, for the heterologous expression of MtCopMd1, CDS without introns, 474 bp, cloned via <i>SmaI</i> and <i>HindIII</i> , contains <i>X. laevis</i> UTRs, ampicillin resistance gene, T7 promoter and m13-primer binding sites
pGEM-HE:Amtr.424 3#5	<i>E. coli</i> DH5α mcr	Amp100	3.4	pGEM-HE#1-derivate, for the heterologous expression of <i>MtAMT2;4</i> , CDS without introns, 1443 bp, cloned via <i>BamHI</i> and <i>HindIII</i> , contains <i>X. laevis</i> UTRs, ampicillin resistance gene, T7 promoter and m13-primer binding sites
pBIN:G-gk#1	<i>E. coli</i> DH5α mcr	Kan50	13.9	pBIN-derivate, binary vector, cell organelle marker for Golgi apparatus controlled by 2x35S promoter, signal peptide PIP2A-sGFP fusion [73]
pBIN:ER-gk#1	<i>E. coli</i> DH5α mcr	Kan50	13.9	pBIN-derivate, binary vector, cell organelle marker for the endoplasmic reticulum via WAK2A-mGFP5 fusion controlled by 2x35S promoter [73]
pBIN:ER-rk#1	<i>E. coli</i> TOP10	Kan50	13.9	pBIN-derivate, binary vector, cell organelle marker for the endoplasmic reticulum via WAK2A-mCherry fusion controlled by 2x35S promoter [73]
pBIN:ER-ck#1	<i>E. coli</i> TOP10	Kan50	13.9	pBIN-derivate, binary vector, cell organelle marker for the endoplasmic reticulum via WAK2A-CFP fusion controlled by 2x35S promoter, contains two not annotated residues of the MCS [73]
pBIN:pm-gk#1	<i>E. coli</i> DH5α mcr	Kan50	12.3	pBIN-derivate, binary vector, cell organelle marker for plasma membrane, cytoplasmic tail and TM-region fused with sGFP controlled by 2x35S promoter [73]
pBIN:tp-gk#1	<i>E. coli</i> TOP10	Kan50	14.2	pBIN-derivate, binary vector, cell organelle marker for tonoplast membrane via Arabidopsis gamma TIP ORF (At2g36830) signal peptide GFP fusion controlled by 2x35S promoter [73]

ID	Organism	resistance	Size [kb]	Description
pCM-TMEg#1	<i>E. coli</i> DH5α mcr	Strep150/Spec50	11.5	pBm43GW-derivate, promoter and signal peptide of <i>MtBCP1</i> as well as eGFP inserted [78]
pCM-TMEr#1	<i>E. coli</i> DH5α mcr	Strep150/Spec50	11.5	pBm43GW-derivate, promoter and signal peptide of <i>MtBCP1</i> as well as mRFP inserted [78]
pBIN:G-gk#1	<i>A. rhizogenes</i> Arqua 1	Strep600/Kan100	13.9	pBIN-derivate, binary vector, cell organelle marker for the Golgi apparatus via PIP2A-sGFP fusion controlled by 2x35S promoter [78]
pBIN:ER-gk#1	<i>A. rhizogenes</i> Arqua 1	Strep600/Kan100	13.9	pBIN-derivate, binary vector, cell organelle marker for the endoplasmatic reticulum, via signal peptide WAK2A-mGFP5 fusion controlled by 2x35S promoter hinter d35S-Promotor [73]
pBIN:ER-rk#1	<i>A. rhizogenes</i> Arqua 1	Strep600/Kan100	13.9	pBIN-derivate, binary vector, cell organelle marker for the endoplasmatic reticulum, via signal peptide WAK2A-mCherry fusion controlled by 2x35S promoter hinter d35S-Promotor [73]
pBIN:ER-ck#1	<i>A. rhizogenes</i> Arqua 1	Strep600/Kan100	13.9	pBIN-derivate, binary vector, cell organelle marker for the endoplasmatic reticulum via WAK2A-CFP fusion, controlled by 2x35S promoter, contains two not annotated residues of the MCS [73]
pBIN:pm-gk#1	<i>A. rhizogenes</i> Arqua 1	Strep600/Kan100	12.3	pBIN-derivate, binary vector, cell organelle marker for plasma membrane, cytoplasmatic tail and TM-region fused with sGFP controlled by 2x35S promoter [73]
pBIN:tp-gk#1	<i>A. rhizogenes</i> Arqua 1	Strep600/Kan100	14.2	pBIN-derivate, binary vector, cell organelle marker for tonoplast membrane via Arabidopsis gamma TIP ORF (At2g36830) signal peptide GFP fusion controlled by 2x35S promoter [73]
pCM-TMEg#1	<i>A. rhizogenes</i> Arqua 1	Strep600/Spec100	11.5	pBm43GW-derivate, promoter and signal peptide of <i>MtBCP1</i> as well as eGFP inserted via recombination [78]
pCM-TMEr#1	<i>A. rhizogenes</i> Arqua 1	Strep600/Spec100	~ 11.5 kb	pBm43GW-derivate, promoter and signal peptide of <i>MtBCP1</i> as well as mRFP inserted via recombination [78]
p:35S-Olig:Amtr.4243-mGFP6#17	<i>E. coli</i> DH5α mcr'	Kan50	6	p:35S-derivate, contains CDS of <i>AMT2;4</i> mGFP6-Fusion with oligopeptide linker, fused via <i>KpnI</i> and <i>BglII</i> in frame under control of the 35S-promoter (~2.3 kb and 0.8 kb)
pRedRoot:p:35S-Olig:Amtr.4243-mGFP6#4	<i>E. coli</i> DH5α mcr	Strep600/Kan100	16.3	pRedRoot-derivate, mGFP6 fusion, containing the 35S promoter and CDS of <i>MtAMT2;4</i> (~0.8 kb and ~2.3 kb), with oligopeptide linker, cloned via <i>EcoRI</i> und <i>HindIII</i> after Klenow blunting into <i>SmaI</i> -site
pRedRoot:p:35S-Olig:Amtr.4243-mGFP6#4	<i>A. rhizogenes</i> Arqua 1	Strep600/Kan100	16.3	pRedRoot-derivate, mGFP6 fusion, containing the 35S promoter and CDS of <i>MtAMT2;4</i> (~0.8 kb and ~2.3 kb), with an oligopeptide linker, cloned via <i>EcoRI</i> und <i>HindIII</i> after Klenow blunting into <i>SmaI</i> -site
p:Smtr.-Olig:Smtr.35854-mGFP6#6	<i>E. coli</i> DH5α mcr'	Amp100	5.5	p:35S-derivate, contains promoter and CDS of <i>MtDefMd1</i> (-1 to -1175 promoter, 645 bp CDS), with oligopeptide linker, cloned via <i>SphI</i> , <i>KpnI</i> und <i>BglII</i> in frame with mGFP6
pRedRoot:p:Smtr.-Olig:Smtr.35854-mGFP6#13	<i>E. coli</i> DH5α mcr'	Kan50	15	pRedRoot-derivate, ~2830 bp fragment of a mGFP6 fusion, containing promoter and CDS of <i>MtDefMd1</i> (-1 to -1175 promoter, 645 bp CDS, ~1 kb mGFP6), cloned via <i>EcoRI</i> und <i>HindIII</i>
pRedRoot:p:Smtr.-Olig:Smtr.35854-mGFP6#1	<i>A. rhizogenes</i> Arqua 1	Strep600/Kan100	15	pRedRoot-derivate, ~2830 bp fragment of a mGFP6 fusion, containing promoter and CDS of <i>MtDefMd1</i> (-1 to -1175 promoter, 645 bp CDS, ~1 kb mGFP6), cloned via <i>EcoRI</i> und <i>HindIII</i>
pBIN:ER-r-p:35S-oli-g:Amtr.4243-mGFP6#4	<i>E. coli</i> DH5α mcr'	Kan50	16.8	pBIN-derivate, binary vector, contains cell organelle marker for the endoplasmatic reticulum in form of a WAK2A signal peptide fused to CFP controlled by 2x35S promoter, integrated via <i>HindIII</i> und <i>SpeI</i> in front of <i>KpnI</i> site, in addition mGFP6 fusion, containing the 35S promoter and CDS of <i>MtAMT2;4</i> (~0.8 kb and ~2.3 kb), with an oligopeptide linker, cloned via <i>EcoRI</i> und <i>HindIII</i> after Klenow blunting into <i>SmaI</i> -site

ID	Organism	resistance	Size [kb]	Description
pBIN:ER-r-p:35S-olig:Amtr.4243-mGFP6#1	<i>A. rhizogenes</i> Arqua 1	Strep600/ Kan100	16.8	pBIN-derivate, binary vector, contains cell organelle marker for the endoplasmatic reticulum in form of a WAK2A signal peptide fused to CFP controlled by 2x35S promoter, integrated via <i>HindIII</i> and <i>SpeI</i> in front of <i>KpnI</i> site, in addition mGFP6 fusion, containing the 35S promoter and CDS of <i>MtAMT2;4</i> (~0.8 kb and ~2.3 kb), with an oligopeptide linker, cloned via <i>EcoRI</i> und <i>HindIII</i> after Klenow blunting into <i>SmaI</i> -site
pBIN:ER-c+Smtr-g#4	<i>E. coli</i> DH5α mcr'	Kan50	16.8	pBIN-derivate, binary vector, contains cell organelle marker for the endoplasmatic reticulum in form of a WAK2A signal peptide fused to CFP controlled by 2x35S promoter, integrated via <i>HindIII</i> and <i>SpeI</i> in front of <i>KpnI</i> site, in addition an mGFP6-Fusion with promoter and CDS of <i>MtDefMd1</i> (~1.2 kb and ~0.7 kb) via an oligopeptide linker, integrated via <i>SmaI</i> and <i>EcoRI</i> into <i>SmaI</i> site
pBIN:ER-c+Smtr-g#4	<i>A. rhizogenes</i> Arqua 1	Strep600/ Kan100	16.8	pBIN-derivate, binary vector, contains cell organelle marker for the endoplasmatic reticulum in form of a WAK2A signal peptide fused to CFP controlled by 2x35S promoter, integrated via <i>HindIII</i> and <i>SpeI</i> in front of <i>KpnI</i> site, in addition an mGFP6-Fusion with promoter and CDS of <i>MtDefMd1</i> (~1.2 kb and ~0.7 kb) via an oligopeptide linker, integrated via <i>SmaI</i> and <i>EcoRI</i> into <i>SmaI</i> site
pBIN:ER-c+Smtr-g+BCP-r#4	<i>E. coli</i> DH5α mcr'	Kan50	19.8	pBIN-derivate, binary vector, contains cell organelle marker for the endoplasmatic reticulum in form of a WAK2A signal peptide fused to CFP controlled by 2x35S promoter, integrated via <i>HindIII</i> and <i>SpeI</i> in front of <i>KpnI</i> site, in addition an mGFP6-Fusion with promoter and CDS of <i>MtDefMd1</i> (~1.2 kb and ~0.7 kb) via an oligopeptide linker, as well as <i>MtBCP1</i> -promoter, signal peptide and mRFP via <i>Ecl163II</i> und <i>SmaI</i> into <i>SmaI</i> site
pBIN:ER-c+Smtr-g+BCP-r#1	<i>A. rhizogenes</i> Arqua 1	Strep600/ Kan100	19.8	pBIN-derivate, binary vector, contains cell organelle marker for the endoplasmatic reticulum in form of a WAK2A signal peptide fused to CFP controlled by 2x35S promoter, integrated via <i>HindIII</i> and <i>SpeI</i> in front of <i>KpnI</i> site, in addition an mGFP6-Fusion with promoter and CDS of <i>MtDefMd1</i> (~1.2 kb and ~0.7 kb) via an oligopeptide linker, as well as <i>MtBCP1</i> -promoter, signal peptide and mRFP via <i>Ecl163II</i> und <i>SmaI</i> into <i>SmaI</i> site
pGBKT7:MtDefMd1#2	<i>E. coli</i> DH5α mcr'	Kan50	7.5	bait construct for Y2H screening, CDS of <i>MtDefMd1</i> in frame without the DNA-binding domain under control of the T7-promoter
<i>S. cerevisiae</i> Y2H Gold	<i>S. cerevisiae</i> Y2H Gold	-	-	Bait strain for Clontech Matchmaker Gold yeast two-hybrid System. Y2HGold includes the sensitive Aureobasidin A antibiotic resistance gene as one of four reporters—providing exceptionally stringent yeast two-hybrid (Y2H) screening. This strain contains distinct ADE2, HIS3, MEL1, and AUR1-C reporter constructs that are only expressed in the presence of GAL4-based protein interactions.
<i>S. cerevisiae</i> Y187	<i>S. cerevisiae</i> Y187	-	-	Prey/Library strain for Clontech's Matchmaker Gold yeast two-hybrid System as a mating partner for the Y2HGold reporter strain. Clontech's Mate & Plate™ Libraries are constructed in Y187.
PGADT7 AD	<i>S. cerevisiae</i> Y187	Leu	8	Y2H library vector that is designed to express a protein of interest fused to a GAL4 activation domain (AD; amino acids 768–881). Transcription of the GAL4 AD fusion is driven by the constitutively active ADH1 promoter (PADH1). The GAL4 AD fusion contains an N-terminal SV40 nuclear localization signal (SV40 NLS; 1) that targets the protein to the yeast nucleus, and a hemagglutinin epitope tag (HA Tag), located between the GAL4 AD and the protein of interest. The T7 promoter (PT7), located just upstream of the HA tag sequence, allows in vitro transcription and translation of the HA-tagged protein of interest (without the GAL4 AD and the SV40 NLS). pGADT7 AD replicates autonomously in both <i>E. coli</i> and <i>S. cerevisiae</i> from the pUC and 2 μ ori, respectively. The vector also contains an ampicillin resistance gene (Ampr) for selection in <i>E. coli</i> and a LEU2 nutritional marker for selection in yeast.

ID	Organism	resistance	Size [kb]	Description
pGADT7-T	<i>S. cerevisiae</i> Y187	Leu	10	Y2H positive control plasmid encoding a fusion of the SV40 large T antigen (a.a. 87–708) and the GAL4 AD (a.a. 768–881). The SV40 large T antigen cDNA (GenBank Locus SV4CG), which was derived from the plasmid referenced in [79], was cloned into pGADT7; plasmid modification was performed at Clontech
pGBKT7:MtDefMd1#2	<i>S. cerevisiae</i> Y2H Gold	Trp	7.5	bait construct for Y2H screening, CDS of <i>MtDefMd1</i> in frame without the DNA-binding domain under control of the T7-promoter

References

- [1] Sanders FE, Tinker PB, Black RLB, Palmerley SM. The development of endomycorrhizal root systems: i. Spread of Infection and Growth-Promoting Effects with four species of Vesicular-Arbuscular Endophyte. *New Phytol* 1977; 78(2): 257–68 [https://doi.org/10.1111/j.1469-8137.1977.tb04829.x]
- [2] Fitter AH. What is the link between carbon and phosphorus fluxes in arbuscular mycorrhizas? A null hypothesis for symbiotic function. *New Phytol* 2006; 172(1): 3–6 [https://doi.org/10.1111/j.1469-8137.2006.01861.x][PMID: 16945083]
- [3] Provorov NA, Borisov AY, Tikhonovich IA. Developmental Genetics and Evolution of Symbiotic Structures in Nitrogen-fixing Nodules and Arbuscular Mycorrhiza. *Journal of Theoretical Biology* 2002; 214(2): 215–32 [https://doi.org/10.1006/jtbi.2001.2453]
- [4] Pumpin N, Zhang X, Noar RD, Harrison MJ. Polar localization of a symbiosis-specific phosphate transporter is mediated by a transient reorientation of secretion. *Proc Natl Acad Sci U S A* 2012; 109(11): E665–72 [https://doi.org/10.1073/pnas.1110215109][PMID: 22355114]
- [5] Bielecki RL. Phosphate Pools, Phosphate Transport, and Phosphate Availability. *Annu. Rev. Plant. Physiol.* 1973; 24(1): 225–52 [https://doi.org/10.1146/annurev.pp.24.060173.001301]
- [6] Jakobsen I (1986). Vesicular-Arbuscular Mycorrhiza in Field-Grown Crops. III. Mycorrhizal Infection and Rates of Phosphorus Inflow in Pea Plants. *New Phytologist* Vol. 104, No. 4 (pp. 573–581); 1986.
- [7] Dunne MJ and Fitter AH (1989). The phosphorus budget of a fieldgrown strawberry (*Fragaria x ananassa* cv. Hapil) crop: Evidence for a mycorrhizal contribution. *Ann Appl Biol* 114:185–193; 1989.
- [8] Merryweather J and Fitter A (1995). Arbuscular mycorrhiza and phosphorus as controlling factors in the life history of the obligately mycorrhizal *Hyacinthoides non-scripta* (L.) Chouard ex Rothm. *New Phytol.* 129: 629–636; 1995.
- [9] Cely MVT, Oliveira AG de, Freitas VF de, *et al.* Inoculant of Arbuscular Mycorrhizal Fungi (*Rhizophagus clarus*) Increase Yield of Soybean and Cotton under Field Conditions. *Front. Microbiol.* 2016; 7(e70633): 271 [https://doi.org/10.3389/fmicb.2016.00720]
- [10] Faber BA, Zasoski RJ, Bureau RG, Uriu K. Zinc uptake by corn as affected by vesicular-arbuscular mycorrhizae. *Plant Soil* 1990; 129(2): 121–30 [https://doi.org/10.1007/BF00032404]
- [11] Cox G and Tinker PB. Translocation and transfer of nutrients in vesicular-arbuscular mycorrhizas. I. The arbuscule and phosphorus transfer: A quantitative ultrastructural study. *New Phytol* 1976; 77(2): 371–378 [https://doi.org/10.1111/j.1469-8137.1976.tb01526.x]
- [12] Bonfante P, Perotto S. Tansley Review No. 82. Strategies of arbuscular mycorrhizal fungi when infecting host plants. *New Phytol* 1995; 130(1): 3–21 [https://doi.org/10.1111/j.1469-8137.1995.tb01810.x]
- [13] Holley JD, Peterson RL. Development of a vesicular-arbuscular mycorrhiza in bean roots. *Can. J. Bot.* 1979; 57(19): 1960–78 [https://doi.org/10.1139/b79-246]
- [14] Hogekamp C, Küster H. A roadmap of cell-type specific gene expression during sequential stages of the arbuscular mycorrhiza symbiosis. *BMC Genomics* 2013; 14: 306 [https://doi.org/10.1186/1471-2164-14-306][PMID: 23647797]
- [15] Hohnjec N, Vieweg MF, Pühler A, Becker A, Küster H. Overlaps in the transcriptional profiles of *Medicago truncatula* roots inoculated with two different *Glomus* fungi provide insights into the genetic program activated during arbuscular mycorrhiza. *Plant Physiol* 2005; 137(4): 1283–301 [https://doi.org/10.1104/pp.104.056572][PMID: 15778460]
- [16] Shachar-Hill Y, Pfeffer PE, Douds D, Osman SF, Doner LW, Ratcliffe RG. Partitioning of Intermediary Carbon Metabolism in Vesicular-Arbuscular Mycorrhizal Leek. *Plant Physiol* 1995; 108(1): 7–15 [PMID: 12228450]
- [17] Pfeffer, Douds DD, JR, Becard, Shachar-Hill. Carbon uptake and the metabolism and transport of lipids in an arbuscular mycorrhiza. *Plant Physiol* 1999; 120(2): 587–98 [PMID: 10364411]
- [18] Bago B, Pfeffer PE, Shachar-Hill Y. Carbon metabolism and transport in arbuscular mycorrhizas. *Plant Physiol* 2000; 124(3): 949–58 [PMID: 11080273]
- [19] Helber N, Wippel K, Sauer N, Schaarschmidt S, Hause B, Requena N. A versatile monosaccharide transporter that operates in the arbuscular mycorrhizal fungus *Glomus* sp is crucial for the symbiotic relationship with plants. *Plant Cell* 2011; 23(10): 3812–23 [https://doi.org/10.1105/tpc.111.089813][PMID: 21972259]
- [20] Bravo A, Brands M, Wewer V, Dörmann P, Harrison MJ. Arbuscular mycorrhiza-specific enzymes FatM and RAM2 fine-tune lipid biosynthesis to promote development of arbuscular mycorrhiza. *New Phytol* 2017; 214(4): 1631–45 [https://doi.org/10.1111/nph.14533][PMID: 28380681]

- [21] Jiang Y, Wang W, Xie Q, *et al.* Plants transfer lipids to sustain colonization by mutualistic mycorrhizal and parasitic fungi. *Science* 2017; 356(6343): 1172–5 [https://doi.org/10.1126/science.aam9970][PMID: 28596307]
- [22] Keymer, A., Pimprikar, P., Wewer, V., Huber, C., Brands, M., Bucerius, S. L., ... & Eisenreich, W. (2017). Lipid transfer from plants to arbuscular mycorrhiza fungi. *Elife*, 6.
- [23] Luginbuehl LH, Menard GN, Kurup S, *et al.* Fatty acids in arbuscular mycorrhizal fungi are synthesized by the host plant. *Science* 2017; 356(6343): 1175–8 [https://doi.org/10.1126/science.aan0081][PMID: 28596311]
- [24] Harrison MJ, Dewbre GR, Liu J. A phosphate transporter from *Medicago truncatula* involved in the acquisition of phosphate released by arbuscular mycorrhizal fungi. *The Plant Cell* 2002; 14(10): 2413–29 [PMID: 12368495]
- [25] Karandashov V, Nagy R, Wegmüller S, Amrhein N, Bucher M (2004). Evolutionary conservation of phosphate transport in the arbuscular mycorrhizal symbiosis. *Proceedings of the National Academy of Sciences, USA* 101: 6285–6290.
- [26] Govindarajulu M, Pfeffer PE, Jin H, *et al.* Nitrogen transfer in the arbuscular mycorrhizal symbiosis. *Nature* 2005; 435: 819 EP -[https://doi.org/10.1038/nature03610]
- [27] Allen JW, Shachar-Hill Y. Sulfur Transfer through an Arbuscular Mycorrhiza. *Plant Physiology* 2009; 149(1): 549[https://doi.org/10.1104/pp.108.129866]
- [28] Johansen A, Jakobsen I and Jensen ES (1992). Hyphal transport of ¹⁵N-labelled nitrogen by a vesicular-arbuscular mycorrhizal fungus and its effect on depletion of inorganic soil N. *New Phytol.* 122, 281–288.; 1992.
- [29] Tinker PB, Nye PH (2000). *Solute Movement in the Rhizosphere*. Oxford University Press, New York; 2000.
- [30] Guether M, Neuhauser B, Balestrini R, Dynowski M, Ludewig U, Bonfante P. A Mycorrhizal-Specific Ammonium Transporter from *Lotus japonicus* Acquires Nitrogen Released by Arbuscular Mycorrhizal Fungi. *Plant Physiology* 2009; 150(1): 73–83 [https://doi.org/10.1104/pp.109.136390]
- [31] Kobae Y, Tamura Y, Takai S, Banba M, Hata S. Localized expression of arbuscular mycorrhiza-inducible ammonium transporters in soybean. *Plant Cell Physiol* 2010; 51(9): 1411–5 [https://doi.org/10.1093/pcp/pcq099][PMID: 20627949]
- [32] Recorbet G, Abdallah C, Renaut J, Wipf D, Dumas-Gaudot E. Protein actors sustaining arbuscular mycorrhizal symbiosis: Underground artists break the silence. *New Phytol* 2013; 199(1): 26–40 [https://doi.org/10.1111/nph.12287][PMID: 23638913]
- [33] Cox, G, & Sanders, F. (1974). Ultrastructure of the host-fungus interface in a vesicular-arbuscular mycorrhiza, *Nevj Phytologist*, 73, 901-912,
- [34] Scannerini, S., & Bonfante-Fasolo, P. (1983). Comparative ultrastructural analysis of mycorrhizal associations. *Canadian Journal of Botany*, 61(3), 917-943.
- [35] Krajinski, F., Hause, B., Gianinazzi-Pearson, V., & Franken, P. (2002). *Mtha1*, a plasma membrane H⁺-ATPase gene from *Medicago truncatula*, shows arbuscule-specific induced expression in mycorrhizal tissue. *Plant Biology*, 4(6), 754-761.
- [36] Pumplin, N., & Harrison, M. J. (2009). Live-cell imaging reveals periarbuscular membrane domains and organelle location in *Medicago truncatula* roots during arbuscular mycorrhizal symbiosis. *Plant physiology*, 151(2), 809-819.
- [37] Fester, T., Strack, D., & Hause, B. (2001). Reorganization of tobacco root plastids during arbuscule development. *Planta*, 213(6), 864-868.
- [38] Hans, J., Hause, B., Strack, D., & Walter, M. H. (2004). Cloning, characterization, and immunolocalization of a mycorrhiza-inducible 1-deoxy-d-xylulose 5-phosphate reductoisomerase in arbuscule-containing cells of maize. *Plant physiology*, 134(2), 614-624.
- [39] Lohse, S., Schliemann, W., Ammer, C., Kopka, J., Strack, D., & Fester, T. (2005). Organization and metabolism of plastids and mitochondria in arbuscular mycorrhizal roots of *Medicago truncatula*. *Plant Physiology*, 139(1), 329-340.
- [40] Oldroyd, G.E. and Downie, J.A. (2006) Nuclear calcium changes at the core of symbiosis signaling. *Curr. Opin. Plant Biol.* 9: 351–357.
- [41] Breuillin-Sessoms, F., Floss, D. S., Gomez, S. K., Pumplin, N., Ding, Y., Levesque-Tremblay, V., ... Harrison, M. J. (2015). Suppression of Arbuscule Degeneration in *Medicago truncatula* phosphate transporter4 Mutants Is Dependent on the Ammonium Transporter 2 Family Protein AMT2;3. *The Plant Cell*, 27(4), 1352–1366. <http://doi.org/10.1105/tpc.114.131144>
- [43] Gomez SK, Javot H, Deewatthanawong P, Ivone Torres-Jerez I, Tang Y, Blancaflor EB, *et al.* *Medicago truncatula* and *Glomus intraradices* gene expression in cortical cells harboring arbuscules in the

- arbuscular mycorrhizal symbiosis. *BMC Plant Biol* 2009; 9(1): 10 [<https://doi.org/10.1186/1471-2229-9-10>]
- [44] Zhang, X., Pumplin, N., Ivanov, S., & Harrison, M. J. (2015). EXO70I is required for development of a sub-domain of the periarbuscular membrane during arbuscular mycorrhizal symbiosis. *Current Biology*, 25(16), 2189-2195.
- [45] Bravo A, Brands M, Wewer V, Dörmann P, Harrison MJ. Arbuscular mycorrhiza-specific enzymes FatM and RAM2 fine-tune lipid biosynthesis to promote development of arbuscular mycorrhiza. *New Phytol* 2017; 214(4): 1631–45 [<https://doi.org/10.1111/nph.14533>]
- [46] Gutjahr, C. and Parniske, M. (2013) Cell and developmental biology of the arbuscular mycorrhiza symbiosis. *Annu. Rev. Cell Dev. Biol.* 29: 593–617
- [47] Ivanov S, Fedorova EE, Limpens E, De Mita S, Genre A, Bonfante P, *et al.* Rhizobium-legume symbiosis shares an exocytotic pathway required for arbuscule formation. *Proc Natl Acad Sci U S A* 2012; 109(21): 8316–8321 [<https://doi.org/10.1073/pnas.1200407109>]
- [48] Zhang X, Pumplin N, Ivanov S, and Harrison MJ. EXO70I is required for development of a sub-domain of the periarbuscular membrane during arbuscular mycorrhizal symbiosis. *Current Biol* 2015; 25(16): 2189–2195 [<https://doi.org/10.1016/j.cub.2015.06.075>]
- [49] Harrison, MJ and Ivanov, S. Exocytosis for endosymbiosis: membrane trafficking pathways for development of symbiotic membrane compartments. *Current Op Plant Biol* 2017; 38:101-108 [<https://doi.org/10.1016/j.pbi.2017.04.019>]
- [50] Huisman R, Hontelez J, Mysore KS, Wen J, Bisseling T, and Limpens E. A symbiosis-dedicated syntaxin of plants 13II isoform controls the formation of a stable host-microbe interface in symbiosis. *New Phytol* 2016; 211(4): 1338–1351 [<https://doi.org/10.1111/nph.13973>]
- [51] Floss DS, Gomez SK, Park HJ, MacLean AM, Müller LM, Bhattarai KK, *et al.* A transcriptional program for arbuscule degeneration during AM symbiosis is regulated by MYB1. *Current Biol* 2017; 27(8): 1206–1212 [<https://doi.org/10.1016/j.cub.2017.03.003>]
- [52] Keymer, A., Pimprikar, P., Wewer, V., Huber, C., Brands, M., Bucerius, S. L., ... & Eisenreich, W. (2017). Lipid transfer from plants to arbuscular mycorrhiza fungi. *Elife*, 6.
- [53] Hanks JN, Snyder AK, Graham MA, Shah RK, Blaylock LA, Harrison MJ, *et al.* Defensin gene family in *Medicago truncatula*: Structure, expression and induction by signal molecules. *Plant Mol Biol* 2005; 58(3): 385–399 [<https://doi.org/10.1007/s11103-005-5567-7>]
- [54] Hohnjec N, Vieweg MF, Pühler A, Becker A, and Küster H. Overlaps in the transcriptional profiles of *Medicago truncatula* roots inoculated with two different *Glomus* fungi provide insights into the genetic program activated during arbuscular mycorrhiza. *Plant Physiol* 2005; 137(4): 1283–1301 [<https://doi.org/10.1104/pp.104.056572>] [PMID: 15778460]
- [55] Pimprikar, P., Carbonnel, S., Paries, M., Katzer, K., Klingl, V., Bohmer, M. J., ... & Gutjahr, C. (2016). A CCaMK-CYCLOPS-DELLA complex activates transcription of RAM1 to regulate arbuscule branching. *Current Biology*, 26(8), 987-998.
- [56] Hogekamp C and Küster H. A roadmap of cell-type specific gene expression during sequential stages of the arbuscular mycorrhiza symbiosis. *BMC Gen* 2013; 14(1): 306 [<https://doi.org/10.1186/1471-2164-14-306>]
- [57] Pumplin N, Zhang X, Noar RD, and Harrison MJ. Polar localization of a symbiosis-specific phosphate transporter is mediated by a transient reorientation of secretion. *Proc Natl Acad Sci U S A* 2012; 109(11): E665-672 [<https://doi.org/10.1073/pnas.1110215109>][PMID: 22355114]
- [58] Rich, M. K., Schorderet, M., Bapaume, L., Falquet, L., Morel, P., Vandebussche, M., & Reinhardt, D. (2015). The petunia GRAS transcription factor ATA/RAM1 regulates symbiotic gene expression and fungal morphogenesis in arbuscular mycorrhiza. *Plant physiology*, 168(3), 788-797.
- [59] Islam KT, Velivelli SLS, Berg RH, Oakley B, and Shah DM. A novel bi-domain plant defensin MtDef5 with potent broad-spectrum antifungal activity binds to multiple phospholipids and forms oligomers. *Sci Rep* 2017; 7(1): 135 [<https://doi.org/10.1038/s41598-017-16508-w>]
- [60] He, B., Xi, F., Zhang, X., Zhang, J., & Guo, W. (2007). Exo70 interacts with phospholipids and mediates the targeting of the exocyst to the plasma membrane. *The EMBO journal*, 26(18), 4053-4065.
- [61] Ghugtyal, V., Garcia-Rodas, R., Seminara, A., Schaub, S., Bassilana, M., & Arkowitz, R. A. (2015). Phosphatidylinositol-4-phosphate-dependent membrane traffic is critical for fungal filamentous growth. *Proceedings of the National Academy of Sciences*, 112(28), 8644-8649.
- [62] Eberhard, David A, *et al.* (1990). "Evidence that the inositol phospholipids are necessary for exocytosis. Loss of inositol phospholipids and inhibition of secretion in permeabilized cells caused by a bacterial phospholipase C and removal of ATP". *Biochemical Journal*. 268: 15–25. doi:10.1042/bj2680015.

- [63] Hay, Jesse C, Thomas M (1993). "Phosphatidylinositol transfer protein required for ATP-dependent priming of Ca²⁺-activated secretion". *Nature*. 366: 572–575. doi:10.1038/366572a0.
- [64] Hay, Jesse C, *et al.* (1995). "ATP-dependent inositide phosphorylation required for Ca²⁺ positive-activated secretion". *Nature*. 374: 173–177. doi:10.1038/374173a0.
- [65] Arnon, DI and Hoagland, DR. Crop production in artificial culture solutions and in soils with special reference to factors influencing yields and absorption of inorganic nutrients. *Soil Sci.* 1940; 50: 463-483.
- [66] Kobae Y and Hata S. Dynamics of periarbuscular membranes visualized with a fluorescent phosphate transporter in arbuscular mycorrhizal roots of rice. *Plant Cell Phys* 2010; 51(3): 341–353[<https://doi.org/10.1093/pcp/pcq013>][PMID: 20097910]
- [67] Alunni, B., & Gourion, B. (2016). Terminal bacteroid differentiation in the legume– rhizobium symbiosis: nodule-specific cysteine-rich peptides and beyond. *New Phytologist*, 211(2), 411-417.
- [68] Becker A, Kleickmann A, Arnold W and Pühler A (1993). Analysis of the *Rhizobium meliloti* *exoH/exoK/exoL* fragment: ExoK shows homology to excreted β -1,3-1,4-glucanases and ExoH resembles membrane proteins. *Mol Gen Genet* 238:145–154
- [69] Sambrook J., Fritsch EF and MANIATIS T (1989). *Molecular Cloning: a laboratory manual*. 2nd ed. N.Y., Cold Spring Harbor Laboratory, Cold Spring Harbor Laboratory Press. 1659 p. ISBN 0-87969-309-6.
- [70] Beringer, J. E. (1974). R factor transfer in *Rhizobium leguminosarum*. *Microbiology*, 84(1), 188-198.
- [71] Beeckman, T., & Engler, G. (1994). An easy technique for the clearing of histochemically stained plant tissue. *Plant Molecular Biology Reporter*, 12(1), 37-42.
- [72] Baier M, Hohnjec N, Lenz F, Fehlberg V, Vieweg MF, Hause B, *et al.* The signal peptide of the *Medicago truncatula* modular nodulin MtNOD25 operates as an address label for the specific targeting of proteins to nitrogen-fixing symbiosomes. *Mol Plant Microbe Interact* 2009; 22(1): 63–72 [<https://doi.org/10.1094/MPMI-22-1-0063>][PMID: 19061403]
- [73] Nelson BK, Cai X, and Nebenführ A. A multicolored set of in vivo organelle markers for co-localization studies in *Arabidopsis* and other plants. *Plant Journal* 2007; 51(6): 1126–1136 [<https://doi.org/10.1111/j.1365-313X.2007.03212.x>]
- [74] Pridmore RD (1987). New and versatile cloning vectors with kanamycin-resistance marker. *Gene*, 56 (2-3): 309-312
- [75] Küster H, Quandt HJ, Broer I, Perlick AM, and Pühler A. The promoter of the *Vicia faba* L. *VfENOD-GRP3* gene encoding a glycine-rich early nodulin mediates a predominant gene expression in the interzone II-III region of transgenic *Vicia hirsuta* root nodules. *Plant Mol Biol* 1995; 29(4): 759–772 [<https://doi.org/10.1007/BF00041166>]
- [76] Limpens, E, Ramos, J, Franken, C, Raz V, Compaan B, Franssen H, *et al.* RNA interference in *Agrobacterium rhizogenes*-transformed roots of *Arabidopsis* and *Medicago truncatula*. *J Exp Bot* 2004; 55(399): 983-992
- [77] Limpens E, Mirabella R, Fedorova E, Franken C, Franssen H, Bisseling T, *et al.* Formation of organelle-like N₂-fixing symbiosomes in legume root nodules is controlled by DMI2. *Proc Natl Acad Sci U S A* 2005; 102(29): 10375–10380 [<https://doi.org/10.1073/pnas.0504284102>][76] Devers EA, Teply J, Reinert A, Gaude N, and Krajinski F. An endogenous artificial microRNA system for unraveling the function of root endosymbioses related genes in *Medicago truncatula*. *BMC Plant Biol* 2013; 13: 82 [<https://doi.org/10.1186/1471-2229-13-82>][PMID: 23679580]
- [78] Ivanov S and Harrison MJ. A set of fluorescent protein-based markers expressed from constitutive and arbuscular mycorrhiza-inducible promoters to label organelles, membranes and cytoskeletal elements in *Medicago truncatula*. *Plant Journal* 2014; 80(6): 1151–1163 [<https://doi.org/10.1111/tpj.12706>]
- [79] Li B, and Fields S. Identification of mutations in p53 that affect its binding to SV40 large T antigen by using the yeast two-hybrid system. *The FASEB Journal* 1993, 7(10), 957-963.

Supporting information on the Data CD

The Data CD provided contains...

...for each Chapter a folder containing:

Chapter I: an *Excel* file named “global AM transport”. It contains global gene expression data from Affymetrix GeneChip hybridizations studying a time course of root colonization by AM fungi from 0 to 42 dpi (Rico M. Hartmann, LUH, Hannover, personal communication), filtered for ≥ 2 -fold at $p \leq 0.05$ induced gene expression between selected time points.

Chapter II: data from the heterologous expression of *AMT2;4* in *X. laevis* and an *Excel* file named “MtCOPs_time course”. The latter contains global gene expression data from Affymetrix GeneChip hybridizations studying a time course of root colonization by AM fungi from 0 to 42 dpi (Rico M. Hartmann, LUH, Hannover, personal communication), filtered for ≥ 2 -fold at $p \leq 0.05$ induced gene expression between selected time points.

Chapter III: *Excel* files named “global MtDefMds and EXO70s time course”, as well as “MtDefMds and EXO70s”. The first file contains global gene expression data from Affymetrix GeneChip hybridizations studying a time course of root colonization by AM fungi from 0 to 42 dpi (Rico M. Hartmann, LUH, Hannover, personal communication), filtered for ≥ 2 -fold at $p \leq 0.05$ induced gene expression between selected time points. The latter contains, gene expression in the mycorrhized MtRam1 mutant *ram1-1* (Rico M. Hartmann, LUH, Hannover, personal communication), the mycorrhized MtPt4 mutant *pt4-1* [Floss *et al.*, 2017, see reference in Chapter III], and mycorrhized MtMyb1-RNAi roots (Claudia Hoge Kamp, LUH, Hannover, personal communication) compared to the corresponding mycorrhized control roots, using the filter settings mentioned above.

...a .pdf-file of this document named “Dissertation_Uhe_2018”.

...a pdf-file named “abstract_Dissertation_Uhe_2018”.

List of Figures

GENERAL INTRODUCTION

- Fig 1:** Symbiotic signaling and root colonization in arbuscular mycorrhiza symbioses. 2
Fig 2: Nutrient exchange during AM symbioses. 4
Fig 3: Arbuscule development from trunk to degenerating arbuscules during AM symbioses. 5

CHAPTER I

- Fig 1:** Dry weights of shoots from mycorrhized *M. truncatula* fertilized with different phosphate and nitrogen amounts. 23
Fig 2: Nitrogen and phosphate concentration in the substrate of mycorrhized *M. truncatula* plants fertilized with different phosphate and nitrogen amounts. 24
Fig 3: Relative nitrogen, carbon, phosphorus, zinc and copper contents in shoot dry matter of mycorrhized *M. truncatula* plants fertilized with different phosphate or nitrogen amounts. 25
Fig 4: Monitoring of fungal structures in mycorrhized *M. truncatula* wild type and *pt4-2* mutant roots. 27
Fig 5: Relative expression of selected AM marker genes in mycorrhized *M. truncatula* roots at 7 and 42 days post inoculation with *R. irregularis*. 28
Fig 6: Growth response of mycorrhized *M. truncatula* plants and habitus under different nutrient regimes. 29
Fig 7: Relative abundance of fungal structures, arbuscules, and vesicles in *M. truncatula* roots supplied with different phosphate and nitrogen amounts. 30
Fig 8: Activation of membrane transporter genes during root colonization of *M. truncatula* by *R. irregularis*. 31
Fig 9: AM-dependant transcription of selected membrane transporter and defensin genes in *M. truncatula*. 32
S1 Fig: Statistical parameters of dry mass distribution of mycorrhized *M. truncatula* plants supplied with different phosphate and nitrogen amounts. 36

CHAPTER II

- Fig 1:** Native, *MtOliMd1*, and *MtABCG3* amiRNA precursors. 46
Fig 2: Relative expression of selected AM-related membrane transporter and marker genes in mycorrhized *M. truncatula* roots supplied with different phosphate and nitrogen amounts. 54
Fig 3: Expression and sequence analyses of *MtCopMd1* and AM-unrelated copper transporter genes. 56
Fig 4: *In silico* analysis of *MtCopMd1*, *MtOliMd1* and *MtABCG3*. 57
Fig 5: Mycorrhized *M. truncatula* roots expressing a *MtCopMd1-gusAint* fusion. 59
Fig 6: Mycorrhized *M. truncatula* roots expressing a *MtOliMd1-gusAint* fusion. 60
Fig 7: Mycorrhized *M. truncatula* roots expressing a *MtABCG3-gusAint* fusion. 61
Fig 8: Relative expression of *MtOliMd1*, *MtABCG3*, and selected AM marker genes in mycorrhized amiRNA and control roots of *M. truncatula*. 62
Fig 9: AM-phenotype of amiRNA:*MtOliMd1*, amiRNA:*MtABCG3*, and amiRNA:*gusAint* roots of *M. truncatula*. 64
Fig 10: Relative expression of *MtAMT2;4* and selected AM marker genes in mycorrhized RNAi:*MtAMT2;4* and RNAi:*gusAint* roots of *M. truncatula* under nitrogen limitation. 66
Fig 11: Relative expression of selected membrane transporter genes in mycorrhized RNAi:*MtAMT2;4* and RNAi:*gusAint* roots of *M. truncatula* under nitrogen limitation. 67
Fig 12: *In vitro* transcribed *MtAMT2;4*-mRNA. 68
Fig 13: The pH-dependence of steady state currents in *MtAMT2;4* transfected and

control <i>X. laevis</i> oocytes with and without NH ₄ ⁺ .	69
Fig 14: GFP localization of plasma membrane, Golgi apparatus, and endoplasmic reticulum in mycorrhized <i>M. truncatula</i> roots.	70
Fig 15: Localization of the endoplasmic reticulum in mycorrhized <i>M. truncatula</i> roots.	71
Fig 16: Localization of MtAMT2;4-mGFP6 and additional fluorescence marker proteins in mycorrhized <i>M. truncatula</i> roots.	73
Fig 17: Induction of selected AM-induced membrane transporters genes in mycorrhized <i>M. truncatula</i> control roots vs. roots affected in the expression of key AM-related genes.	74
Fig 18: Hypothetical working mode of the ABC-transporter MtABCG3.	79
Fig 19: Hypothetical working mode of the putative ammonium transporter MtAMT2;4.	80
S1 Fig: Representative currents and voltage-pulse protocol of a MtAMT2;4-transfected <i>X. laevis</i> oocyte supplied with NH ₄ ⁺ .	86
S2 Fig: <i>In silico</i> analyses of the putative ammonium transporter MtAMT2;4.	86
S3 Fig: Translational fusion of MtAMT2;4, an oligopeptide linker and mGFP6.	87
 CHAPTER III	
Fig 1: Sequence analyses of AM-dependent defensins MtDefMd1-4 and AM-unrelated defensins.	100
Fig 2: Protein charge of MtDefMd1-4 and other defensin-like plant proteins in the pH range of 0 to 14.	102
Fig 3: Relative expression of <i>MtDefMd1-4</i> and selected AM marker genes in <i>M. truncatula</i> roots in a time course of mycorrhization and under different phosphate and nitrogen regimes.	104
Fig 4: Histochemical localization of <i>MtDefMd1</i> and <i>MtDefMd2</i> promoter activities.	105
Fig 5: Relative expression of <i>MtDefMd</i> and selected AM-marker genes in mycorrhized <i>M. truncatula</i> A17 wild type and <i>ram1-1</i> roots.	107
Fig 6: Expression of <i>MtDefMd</i> - and AM-induced EXOCYST genes in mycorrhized <i>M. truncatula</i> control and mutant roots.	108
Fig 7: Relative expression of <i>MtDefMd</i> and selected AM marker genes in mycorrhized RNAi:MtDefMd1/2 and RNAi: <i>gusAint</i> control roots of <i>M. truncatula</i> .	110
Fig 8: Relative expression of <i>MtDefMd1</i> and selected AM marker genes in mycorrhized <i>MtDefMd1</i> -overexpression and pPt4: <i>gusAint</i> -expressing control roots of <i>M. truncatula</i> .	111
Fig 9: Relative expression of <i>MtABCG3</i> in mycorrhized <i>MtDefMd1</i> -overexpression and pPt4: <i>gusAint</i> -expressing control roots of <i>M. truncatula</i> .	112
Fig 10: Relative expression of selected EXOCYST genes in mycorrhized <i>MtDefMd1</i> -overexpression and pPt4: <i>gusAint</i> -expressing control roots of <i>M. truncatula</i> .	113
Fig 11: Lipid staining of mycorrhized <i>M. truncatula</i> pUbi: <i>MtDefMd1</i> -overexpression and pUbi: <i>gusAint</i> control roots	114
Fig 12: Size distribution of arbuscules in mycorrhized <i>M. truncatula</i> <i>MtDefMd1</i> -overexpression, <i>MtDefMd1/2</i> -knockdown, and pPt4: <i>gusAint</i> control roots.	115
Fig 13: WGA-Alexa Fluor 488-stainings of arbuscules in mycorrhized <i>M. truncatula</i> pUbi:MtDefMd1-, pPt4:MtDefMd1- and pPt4: <i>gusAint</i> control roots.	117
Fig 14: Nodules of <i>M. truncatula</i> <i>MtDefMd1</i> -overexpression, <i>MtDefMd1/2</i> -knockdown, and pPt4: <i>gusAint</i> control roots.	119
Fig 15: Morphology of bacteroids in nodules of <i>M. truncatula</i> <i>MtDefMd1</i> -overexpression and pPt4: <i>gusAint</i> control roots.	120
Fig 16: Localization of MtDefMd1-mGFP6 and additional fluorescence marker proteins in mycorrhized <i>M. truncatula</i> roots.	123
Fig 17: Proposed time course of MtDefMd protein presence in relation to AM markers	

in <i>M. truncatula</i> roots after inoculation with <i>R. irregularis</i> .	127
Fig 18: Hypothetical modes of action of MtDefMd1.	129
S1 Fig: Localization of MtDefMd1-mGFP6 in mycorrhized <i>M. truncatula</i> roots expressing a multi-fluorophore reporter construct and a tonoplast marker.	139
 <u>GENERAL DISCUSSION</u>	
Fig 4: Proposed localization of AM-related membrane transporters during PAM biogenesis during the AM symbiosis of <i>M. truncatula</i> and <i>R. irregularis</i> .	143
Fig 5: Proposed localization of AM-related membrane proteins during PAM biogenesis and degradation in the AM symbiosis of <i>M. truncatula</i> and <i>R. irregularis</i> .	145
 <u>GENERAL MATERIALS AND METHODS</u>	
S1 Fig: The vectors p35S-mGFP6neu and pBIN:ER-rk.	164
S2 Fig: Cloning strategy of vectors for the localization and co localization of MtDefMd1.	164

List of Tables

GENERAL INTRODUCTION

Table 1:	Selected AM-dependent membrane transporter genes.	7
-----------------	---	---

CHAPTER I

Table 1:	pH of Seramis® after cultivating <i>M. truncatula</i> plants inoculated with <i>R. irregularis</i> for three weeks under different phosphate and nitrogen regimes.	24
Table 2:	AMF root colonization of <i>M. truncatula</i> inoculated with 1000 <i>R. irregularis</i> spores.	28
S1 Table:	Monitoring of plant dry mass from mycorrhized plants fertilized with different P and N supplies.	37
S2 Table:	All to all comparison of plant dry mass from mycorrhized plants fertilized with different P and N supplies.	37
S3 Table:	Primers used in real-time RT-PCR experiments.	37

CHAPTER II

Table 1:	PCR primers for the amplification of promoter sequences from the <i>M. truncatula</i> genome.	45
Table 2:	CLC cloner settings to calculate the secondary structure of RNA sequences.	46
Table 3:	Strategy for the creation of amiRNAs via overlapping mutation PCR.	47
Table 4:	amiRNA Primers for overlapping mutation PCR.	47
Table 5:	Primers used in real-time RT-PCR experiments.	47
Table 6:	Primers for the cloning of mGFP6 fusion constructs.	48
Table 7:	Primer for the heterologous expression of <i>M. truncatula</i> membrane transporters in <i>X. laevis</i> oocytes.	51
Table 8:	PCR program for the amplification of the CDS of AM dependent membrane transporter genes of <i>M. truncatula</i> .	51
Table 9:	Media for TEV-clamp measurements of <i>MtAMT2;4</i> transfected and control oocytes of <i>X. laevis</i> .	53

CHAPTER III

Table 1:	Candidates for MtdefMd1 interactors from yeast two-hybrid library screening.	103
S1 Table:	Primers used in real-time RT-PCR experiments.	136
S2 Table:	Properties and cleavage sites of the MtDefMd signal peptides predicted by <i>SignalP</i> .	136
S3 Table:	Correlation of <i>MtDefMd</i> and AM marker gene expression in the course of mycorrhization.	136
S4 Table:	Percentage of colonized and arbuscule-containing areas in mycorrhized <i>Medicago truncatula</i> MtDefMd1-overexpression (pPt4:MtDefMd1, pUbi:MtDefMd1) and pPt4:gusAint roots.	136
S5 Table:	Percentage of colonized and arbuscule-containing areas in mycorrhized <i>Medicago truncatula</i> MtDefMd1/2-knock-down (RNAi:MtDefMd1/2) and RNAi:gusAint roots.	137
S6 Table:	Underlying data points for the size distribution of arbuscules in mycorrhized <i>Medicago truncatula</i> MtDefMd1-overexpression (pPt4:MtDefMd1, pUbi:MtDefMd1), MtDefMd1/2-knockdown (RNAi:MtDefMd1/2), and pPT4:gusAint roots.	137

GENERAL MATERIALS AND METHODS

Table 1:	Standard PCR reaction.	152
-----------------	------------------------	-----

Table 2:	Standard PCR program.	153
Table 3:	Antibiotics for the selective cultivation of bacteria strains.	156
Table 4:	Enzymes and buffers for cloning and PCR used in this thesis.	159
Table 5:	Commercial kits used in this thesis.	159
Table 6:	Chemicals used in this thesis.	160
Table 7:	Desposables used in this thesis.	161
Table 8:	Technical devices used in this thesis.	162
Table 9:	Software used in this thesis.	163
Table 10:	Internet tools used in this thesis.	163
S1 table:	Bacterial and yeast clones.	165

Abbreviations

°C	degree celcius
µg	microgramm
µl	microliter
µM	micromolar
a.	appresorium
ABC	ATP-binding cassette
AM	arbuscular mycorrhiza
AMF	arbuscular mycorrhiza fungi
amiRNA	artificial micro RNA
Ap	ampicillin
Appr.	approximatively
Arb	arbuscule
ATP	adenosine triphosphate
b	birdfoot
BAC	bacterial artificial chromosome
BLAST	basic local alignment search tool
Bp	base pairs
BSA	bovine serum albumine
C	carbon
Ca	calcium
CDS	codon determing sequence
CFP	cyan fluorescent protein
Cm	centimeter
COs	chitooligosaccharides
CP	cytoplasm
Ctr	copper transporter
Cu	copper
cv.	cultivar
DCL1	dicer like protein 1
DDO	double dropout medium
Dm	dry matter
DMSO	dimethylsulfoxide
DNA	desoxyribonucleic acid
Dpi	days post inoculation
dsRed	discosoma Red
DTT	dithiothreitol
<i>e. g.</i>	exemplii gratia
EDTA	ethylene-diamine-tetra-acetate
Eh	extraradical hyphae
ER	endoplasmatic reticulum
<i>et al.</i>	et alii
F	fungus
Fe	ferrum
FM	fungal mass
g	gramm
GPAT	glycerole phosphate-O-acyltransferase
GUS	β-glucuronidase
H	hyphae
h/d	hours per day
i	infection
ID	identifier

Ih	intraradical hyphae
IPTG	isopropyle- β -D-thiogalactopyranoside
LB	left border
LDCV	Large dense core vesicle
K	potassium
Km	Kanamycin
LCOs	lipo-chitooligosaccharides
M	molar
m	milli
m(Cherry/GFP)	monomeric
mb	megabases
MFS	major facilitator superfamily
Mg	magnesium
miRNA	micro RNA
ml	milliliter
mM	millimolar
Mn	manganese
MOPS	3-Morpholinopropane-1-sulfonic acid
mRNA	messenger RNA
Myc-factor	factor for mycorrhization
Myk-	not mycorrhized
Myk+	mycorrhized
n	number of biological replicates
N	nitrogen
NBDs	nucleotide binding domains
NCR	nodule cysteine-rich
Ng	nanogramm
nm	nanometer
nmdg	N-Methyl-D-glucamine
Nod-factor	factor for nodulation
OLI	oligopeptide linker
p	promoter
P	phosphate
PA	Penassay
PAD	premature arbuscle degeneration
PAM	periarbuscular membrane
PAS	periarbuscular space
PBS	physiologically buffered saline
PCR	polymerase chain reaction
pH	pondus hydrogenii
PHT	phosphate transporter
PIP	phosphatidylinositol 4,5-bisphosphate
PIT	pre-infection threat
PM	plasmamembrane
POT	proton-dependent oligopeptide transporter
PPA	pre-penetration apparatus
PTGS	post transcriptional gene silencing
PTR	peptide transporter
QDO	quadruple dropout media
RAM1	reduced arbuscular mycorrhization 1
RB	right border
RFP	red fluorescent protein
RISC	RNA induced gene silencing complex

RNA	ribonucleic acids
RNAi	RNA interference
rpm	rounds per minute
RT	reverse transcription
s	spores
SD	single dropout
Se	seramis particle
sec	seconds
Spec	Spectomycin
Sm	Streptomycine
SYM	common symbiotic signaling
t	time
TA	Tris acetate
TCM	Tris calcium magnesium
TEV	two-electrode voltage
TF	transcription factor
TM	transmembrane
TP	tonoplast
TY	tryptone yeast
U	units
UTR	untranslated region
UTRs	untranslated regions
v	vacuole
Vs	versus
w/v	weight per volume
WGA	wheat germ agglutinin
Wt	wild type
YPDA	yeast peptone dextrose adenine hemisulfate
Zn	zinc
β-MAG	β-monoacyl glycerole

Curriculum Vitae

First name: Uhe
Last name: Marian
Date of birth: 25.09.1987
Place of birth: Göttingen
Nationality: German

Schooling:

1994-1998	<i>Grundschule Herberhausen</i> 37075 Göttingen
1998-2000	<i>Orientierungsstufe Nord</i> 37077 Göttingen
2000-2007	<i>Hainberg Gymnasium</i> (graduation: Abitur) 37075 Göttingen
07.02.05-18.02.05	Participation in an internship in the <i>Göttinger Experimentallabor für junge Leute e.V.</i> Unit of biology
02.07.07-31.03.08	Zivildienst at the <i>Seminar für Ur- und Frühgeschichte</i> of the <i>Georg August Universität Göttingen</i> (11 weeks excavation of a slavic settlement in Meetschow, germany)

Academic studies:

01.10.2008-30.09.2011	B.Sc. studies of Plant Biotechnology at the <i>Leibniz Universität Hannover</i> (graduation: Bachelor of Science, Plant Biotechnology) <u>Title of the B. Sc. thesis:</u> Establishment and first characterization of microsatellite markers for the cabbage aphid (<i>Brevicoryne brassicae</i> (L.))
01.10.2011-30.09.2013	M.Sc. studies of Plant Biotechnology at the <i>Leibniz Universität Hannover</i> (graduation: Master of Science, Plant Biotechnology) <u>Title of the M. Sc. thesis:</u> Functional analysis of membrane transporter genes in the arbuscular mycorrhiza symbiosis of <i>Medicago truncatula</i>

Since 10/2013 doctoral researcher at the Institute of Plant Genetics, Unit IV-Plant Genomics at Leibniz Universität Hannover, Hanover, Germany

Scientific Publications

Uhe M, Hogekamp C, Hartmann RM, Hohnjec N, and Küster H. The mycorrhiza-dependent defensin MtDefMd1 of *Medicago truncatula* acts during the late restructuring stages of arbuscule-containing cells. (2018) PLOS ONE 13(1): e0191841. <https://doi.org/10.1371/journal.pone.0191841>

Poster presentations

- 02.09.2015-03.09.2015: IMMM; 2nd International Molecular Mycorrhiza Meeting
Cambridge United Kingdom; poster “Functional analysis of arbuscular mycorrhiza-related membrane transporter genes of *Medicago truncatula* in the context of different nutrient regimes”
- 30.09.2015-02.10.2015: GRK1798: Doctoral student’s conference II
Goßlar, Germany; poster “Functional analysis of arbuscular mycorrhiza-related membrane transporter genes of *Medicago truncatula* in the context of different nutrient regimes”
- 14.09.2016-16.09.2016: GRK1798: Doctoral student’s conference III
Bad Salzdetfurth, Germany; poster “The role of defensins in the arbuscular mycorrhiza (AM) symbiosis of *Medicago truncatula*”

Acknowledgements

In this section I would like to thank everyone, who supported me during the studies presented in this Thesis.

Special thanks go to Prof. Dr. Helge Küster, who has given me the possibility to do a doctorate with him and his group and for providing me with an interesting and challenging project. I feel gratitude for his valuable advice that helped me to keep the focus and motivation. It was a joy to find a “story” in all these experiments! Sincere thanks to Prof. Manfred K. Schenk for taking an interest in the cultivation of *Medicago* plants and Prof. Thomas Debener for helpful input during the GRK *jour fixe* and to both for being referees of this Thesis.

I am thankful to Dr. Natalija Hohnjec, for helpful advice, especially in microscopy and how to improve presentation skills, as well as the coordination of a laboratory with many people and projects. I wish to thank the Deutsche Forschungsgemeinschaft (<http://www.dfg.de>) for financial support in frame of GRK1798 "Signaling at the Plant-Soil Interface".

Many thanks to Dr. Claudia Hogeckamp and Rico M. Hartmann, who supported me with data from Affymetrix GeneChip hybridizations and were engaged in many conversations, especially during the *jour fixe* of the group. I don't want to miss what I learned via debating our projects and ideas!

Natascha Köppens provided excellent technical assistance, was irreplaceable in planning practical courses and organizing all things that are or should be routine work in the laboratory. I must give kudos to her, due to her patience, foresight, competence and many kind words!

In addition, I wish to thank all members of the GRK1798: “Signaling at the Plant-Soil-Interface” for interesting discussions, which led to new ideas and perspectives for the setup and interpretation of experiments. Especially those members, who participated during our social events, I would like to thank for their wise counsel and sympathetic ear. Here, again, I must mention Rico M. Hartmann, who shared an office with me and while being witness of successful experiments and the other ones became a valued companion!

Furthermore, the whole team of the *Unit IV.: Plant Genomics* from the *Institute of Plant Genetics* contributed to make the days in the laboratory and office inspiring, fruit- and successful.

Finally, I would like to thank Laurine, my parents and Felix, for love, support, and motivation as well as for help during my desperate attempts to convert drawings into vector graphics.